INVESTIGATIONS ON THE MECHANICAL JOINTS PREPARED FROM ELECTRON BEAM CURED CARBON EPOXY NANOCOMPOSITE LAMINATES

Thesis

Submitted for the partial fulfillment of the Degree

of

Doctor of Philosophy

By

Mohit Kumar
(Registration No.: 901708013)

Under the guidance of

Dr. Jaswinder Singh Saini
Associate Professor
Department of Mechanical Engineering,
Thapar Institute of Engineering &
Technology (Deemed to be University),
Patiala

Dr. Haripada Bhunia
Professor
Department of Chemical Engineering,
Thapar Institute of Engineering &
Technology (Deemed to be University),
Patiala

THAPAR INSTITUTE
OF ENGINEERING & TECHNOLOGY
(Deemed to be University)

Patiala-147004, Punjab (India)
www.thapar.edu

August 2021

Dedicated

to

my

Daughter

“Paavni”

Certificate

This is to certify that the thesis entitled **"Investigations on the mechanical joints prepared from electron beam cured carbon epoxy nanocomposite laminates"** being submitted by Mr. Mohit Kumar to Department of Mechanical Engineering, Thapar Institute of Engineering & Technology (Deemed to be University), Patiala for the award of degree of Doctor of Philosophy, is a record of bonafide research work carried out by him under our guidance and supervision and has fulfilled the requirements for the submission of this thesis, which to our knowledge has reached the requisite standard.

The results embodied in the thesis have not been submitted in part or full to any other University or Institute for the award of any degree or diploma.

Dr. Jaswinder Singh Saini
Associate Professor
Department of Mechanical Engineering,
Thapar Institute of Engineering &
Technology (Deemed to be University),
Patiala

Dr. Haripada Bhunia
Professor
Department of Chemical Engineering,
Thapar Institute of Engineering &
Technology (Deemed to be University),
Patiala

Acknowledgments

I would like to thank most sincerely my supervisors, Dr. Jaswinder Singh Saini, Associate Professor, Department of Mechanical Engineering and Dr. Haripada Bhunia, Professor, Department of Chemical Engineering, Thapar Institute of Engineering & Technology (Deemed to be University), for providing me such a valuable research opportunity and for their countless guidance, knowledge and motivation during the course of my research. I learned a lot from them over the course of this Ph.D. work. Their goal-oriented style of work, passion towards research, work ethics, has been very inspiring for me. Their daily practice of following up on recent scientific literature is something that I also tried to adopt and greatly benefitted. I really appreciate their unconditional support and encouragement towards doing high-caliber research. It has been a great honor to work under their guidance.

I am extremely thankful to Prof. Prakash Gopalan, Director, Thapar Institute of Engineering & Technology (Deemed to be University), Prof. R. Siddique, Dean of Research & Sponsored Projects, Thapar Institute of Engineering & Technology (Deemed to be University) and Dr. T. P. Singh, Head, Department of Mechanical Engineering, Thapar Institute of Engineering & Technology (Deemed to be University) for extending the opportunity to undertake this doctoral research.

I would like to profoundly thank my doctoral committee members, Dr. Neeraj Grover and Dr. Bikramjit Sharma, Department of Mechanical Engineering and Prof. O. P. Pandey, School of Physics and Material Science, Thapar Institute of Engineering & Technology (Deemed to be University) for their immense help and guiding me towards the right direction. I am grateful to Prof. P. K. Bajpai, Distinguished Professor (Retired), Department of Chemical Engineering, Thapar Institute of Engineering & Technology (Deemed to be University) for his expert advice in various stages of my research work and also during writing of my thesis. My heartful thanks to the staff members of the Department of Mechanical Engineering and Department of Chemical Engineering, Thapar Institute of Engineering & Technology (Deemed to be University) for their valuable contribution, spiritual and moral support.

My special thanks to Dr. Kulwinder Singh, former research fellow, Thapar Institute of Engineering and Technology, who patiently and in a very dedicated way offered undivided attention and advice.

My endless thanks go to my research colleagues, Dr. Ankit Sharma, Mr. Mukul Chugh, Mr. Saudagar Dhongre, Mr. Gautam Khanna, Mr. Amit Pandey, Mr. Sunil Sable, Mr. Nirmal Singh, Mr. Shubham Choudhary, Mr. Sandeep Nain and Dr. Abhinav Jain, for their valuable contribution, spiritual and moral support at various stages of my work.

My deepest gratitude goes to my beloved parents, Mr. Brij Bhushan Dhiman, Mrs. Sunita Dhiman, my father-in-law, Mr. Amarjeet Dhiman and my mother-in-law, Mrs. Usha Dhiman, my brother, Mr. Varun Kumar, my brother's wife, Mrs. Megha Dhiman, my brother-in-law, Mr. Rajat Dhiman and my sister-in-law, Ms. Vandana Dhiman, who have always supported me through highs and lows of life. They have touched my life in many ways. My last word is reserved for my love, Mrs. Babita Dhiman, for her true companionship.

I gratefully acknowledge the financial support given by DAE-BRNS project (Sanction No. 35/14/10/2017-BRNS with RTAC), Bhabha Atomic Research Centre (BARC), Trombay, Mumbai (India).

I am really thankful to Dr. Subhendu Ray Chowdhury, Scientific Officer, Isotope and Radiation Application Division (IRAD), BARC, Trombay, Mumbai, for his valuable contribution and technical support.

Finally, I wish to thank the 'ALMIGHTY' God for his sufficiency.

Mohit Kumar

Abstract

In many development sectors, the fuel efficiency and harmful emissions from machines into the environment are the major concerns. Furthermore, these machines are made of conventional metallic materials that are susceptible to corrosion. To tackle these problems, various industries and researchers are focusing on the use of alternative lightweight materials that replace the old conventional materials to increase the strength and efficiency of the product. Therefore, a huge consideration is given to the lightweight fiber reinforced polymer (FRP) composite materials due to its high strength and stiffness to their weight ratios and good corrosion resistance properties.

The curing process plays a key role in preparation of these composite materials. The thermal curing process is the recognized manufacturing technology for curing of FRP composites, which consists of several hours of material heating at high temperatures, mostly under pressure and in the presence of highly toxic amine-based hardeners, but now the industries are focusing on the alternative methods such as electron beam (EB) curing process that have evidenced a huge transformation in the field of FRP composites.

In actual working conditions, the application of FRPs requires joining of materials with each other or with metallic or non-metallic components. Two types of joints *i.e.*, adhesive joints and mechanical joints are used for joining of FRPs. Adhesive joints being permanent in nature fails to operate in the same manner after the joint is opened. However, mechanical joints are preferred due to their ease of assembly and detachability. The mechanical joints seem to be simple, but they are much more than that because of stress concentration due to drilled holes. Improper design of a joint may lead to a failure of the whole structure. So, it is necessary to investigate the behavior of joints to achieve the maximum load-carrying capacity.

In numerous applications of marine and civil sectors, the FRP composites and their mechanical joints have concerns about their long-term durability under harsh environmental surroundings, such as ultraviolet (UV) radiation, moisture, elevated temperature, alkalinity, fire, etc. The main objective of the present work is to investigate the performance of EB cured carbon/epoxy composite joints under different geometric parameters and different aging environmental conditions to evaluate the bearing failure loads of the composite joints. Addition of multi-wall carbon nanotubes (MWCNTs) nanofiller into the epoxy, improved the performance of mechanical joints prepared from carbon/epoxy composite laminates. The carbon/epoxy composite laminates were prepared using EB curing process and thermal

curing process by incorporating 0.1 to 0.5 wt.% of MWCNTs. The optimum wt. % of MWCNTs in the composite material was found to be 0.3 wt.% showing maximum strength properties for both curing processes. Further, investigations were carried out on neat and optimized 0.3 wt.% of MWCNTs added composite joints prepared using both the curing processes. The single pin joint configurations were prepared using geometric combinations of width to diameter (W/D) ratio and edge to diameter (E/D) ratio, both varying from 2 to 5. Incorporating MWCNTs have shown positive contribution to failure loads and failure modes of the pin joint composite specimens. The failure of the pin joint is much simpler than the bolted joints where the lateral constraints are involved in terms of compressive forces. The numerically predicted ultimate failure loads were compared with the experimental obtained results, which were within 10% of acceptable difference, providing good correlation between each other.

Knowing the contribution of the MWCNTs into the pinned joint, the study was extended to bolted joints to analyze their durability under different environmental aging conditions. The composite bolted joint specimens were designed as per ASTM D5961 standard having geometric parameters *i.e.,* W/D and E/D ratios fixed to 6 and 5, respectively. The bolt torques of 0, 2 and 4 Nm were used. The performance of bolted joints was analyzed under hygrothermal aging conditions and accelerated weathering aging conditions. For hygrothermal aging, three different water immersion temperatures *i.e.*, 25 ^{o}C, 45 ^{o}C and 65 ^{o}C were used for duration of 10, 20 and 30 days. The water absorption studies were conducted as per ASTM D5229 standard. The statistical investigations were performed using the central composite design on different control factors *i.e.,* temperature, duration, bolt torque and material. The immersion of composite bolted joints into water at elevated temperatures (45 ^{o}C and 65 ^{o}C), for 30 days significantly reduces the performance of composite material. The elevated temperature for prolonged duration contributes to inducing the water intake kinetics. The neat composite specimens were more susceptible to the water absorption, especially at higher water temperatures. Incorporating MWCNTs nanofiller, lowered the water absorption rate and thus increased strength retention ability. This increase corresponds to the tortuosity effect which forces water molecules to follow prolonged paths and reduces moisture absorption rate. For accelerated weathering aging, combined cyclic exposure with 8 h of UV at 60 ^{o}C and 4 h of condensation at 50 ^{o}C (at relative humidity of 100% in condensation cycle) was given to the composite specimens as per ASTM G154, for duration of 250, 500, 750 and 1000 h. Upto 250 h of aging exposure, a slight increase in strength of the joints was observed whereas after 250 h of aging exposures, strength of the

joints decreased significantly. The MWCNTs added composite specimens hold the strength retention ability due to increased interfacial area and UV resistant properties that counters the aging effect. The bolt torques contributed in a positive way for unaged specimens. The increased bolt torques enables stress distribution over a wide area, which enhanced the failure loads and stiffness of the bolted joints. But under both the aging conditions, specimen exposure for long durations showed less bolt torque efficiency in neat composite specimens. Moreover, incorporating MWCNTs in the specimens shows good bolt torque effectiveness even at higher exposure duration, under similar conditions. The progressive damage analysis with characteristic curve method was used to predict the ultimate failure loads of bolted joints exposed to hygrothermal aging and accelerated aging conditions. The numerically predicted results have shown good correlation with the experimental ones.

Figure 1 shows the schematic of overall thesis work.

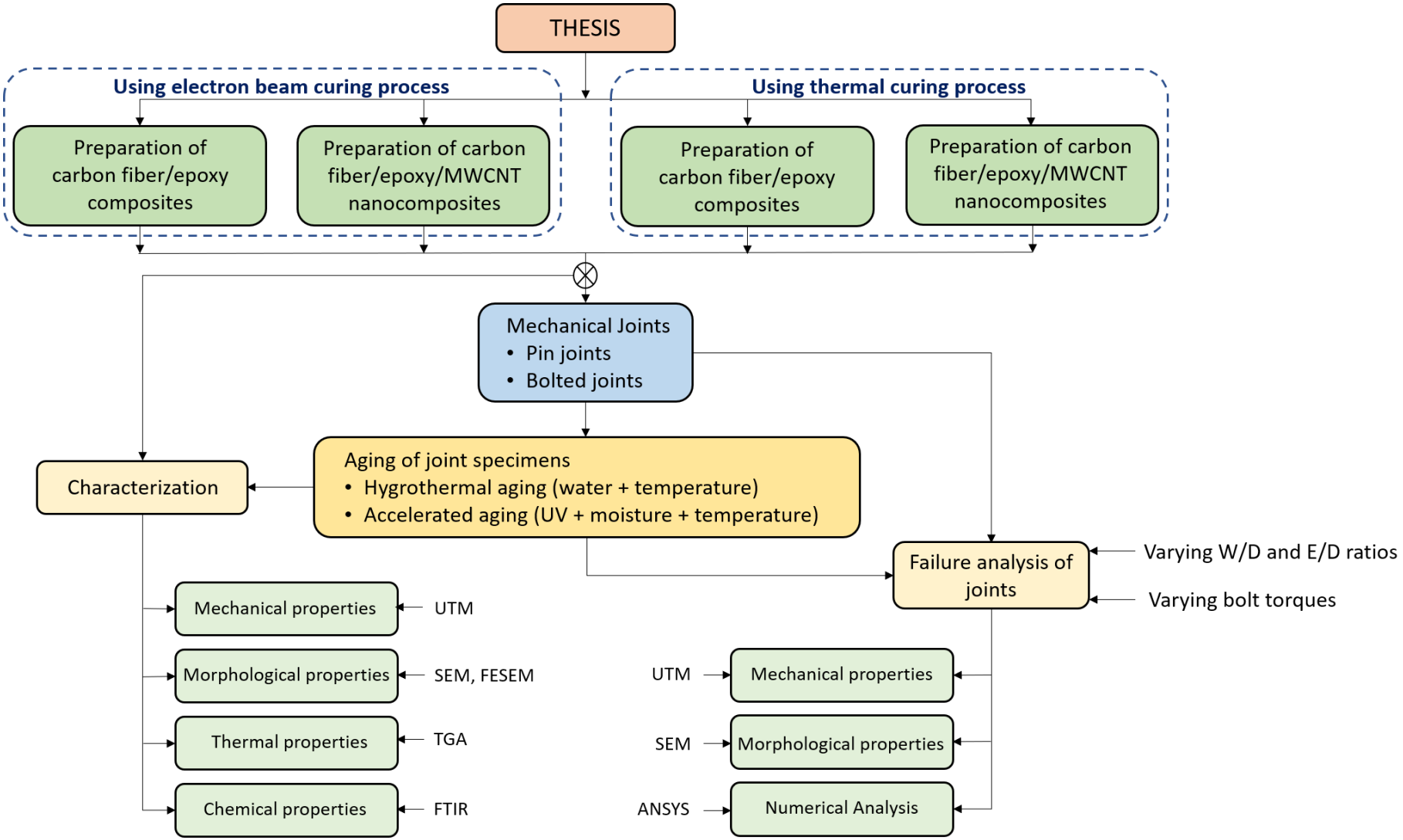

Fig. 1 Flowchart of overall thesis work

Table of Contents

Certificate ..... **i**

Acknowledgments ..... **iii**

Abstract ..... **v**

Table of Contents ..... **ix**

List of Figures ..... **xiii**

List of Tables ..... **xxi**

List of Symbols ..... **xxiii**

List of Abbreviations ..... **xxv**

Chapter 1 Introduction and Literature Review **1**

1.1 Components of FRP composites 1

1.1.1 Classification of fibers and its materials 2

1.1.2 Polymer matrix 2

1.2 Manufacturing of FRP composite material 3

1.2.1 Manufacturing techniques 3

1.2.2 Curing process 5

1.3 Nanofiller addition in FRP composite materials 5

1.4 Applications of FRP composite materials 6

1.5 Joints in FRP composite material 7

1.5.1 Mechanical joints 7

1.5.2 Adhesive joints 7

1.5.3 Benefits of mechanical joints over adhesive joints 8

1.6 Design of mechanical joints 8

1.6.1 Pin joints 8

1.6.2 Bolted joints 8

1.6.3 Modes of failure 9

1.6.4 Strength parameters 10

1.7 Impact of aging on FRP composite materials 11

1.8 Literature review 11

1.8.1 Radiation curing of FRP composites 12

1.8.2 Effect of different parameters on the performance of FRP based mechanical joints 15

1.8.3 Aging effect on the FRP composites and their mechanical joints 19

1.8.4 Conclusion from the literature review 24

1.9 Motivation and objectives 24

1.10 Thesis overview 25
Chapter 2 Materials and Methods 29
2.1 Materials 29
2.2 Methods 31
2.2.1 Preparation of electron beam (EB) cured composite laminates 31
2.2.2 Preparation of thermally cured composite laminates 33
2.2.3 Preparation of mechanical joints 34
2.2.4 Environmental aging 35
2.3 Characterization 36
2.3.1 Morphological properties 36
2.3.2 Thermal properties 37
2.3.3 Chemical properties 37
2.3.4 Mechanical properties 37
2.4 Performance evaluation of joint specimens 37
2.5 Numerical analysis 39
2.6 Closure 41
Chapter 3 Optimization of MWCNTs Nanofiller Content 43
3.1 Optimization of MWCNTs content 43
3.2 Characterization of composite laminates at optimum wt.% of MWCNTs 47
3.3 Closure 47
Chapter 4 Investigations on Single Pin Joint Composites 49
4.1 Single pin joint configurations 49
4.2 Testing of pin joints 49
4.3 Numerical analysis 50
4.4 Results and discussion 53
4.4.1 Joints prepared from EB cured composites 54
4.4.2 Joints prepared from thermally cured composites 61
4.5 Closure 68
Chapter 5 Performance of Bolted Joints under Hygrothermal Aging Environment 69
5.1 Hygrothermal aging 69
5.1.1 Water diffusion behavior 69
5.1.2 Bolted joints under hygrothermal conditioning 71
5.2 Results and discussion 72
5.2.1 Bolted joints prepared from EB cured composites 72
5.2.2 Bolted joints prepared from thermally cured composites 93

5.3 Numerical Analysis 103
5.3.1 Loads and boundary conditions 104
5.4 Closure 107
Chapter 6 Performance of Bolted Joints under Accelerated Aging Environment 109
6.1 Accelerated weathering conditions 109
6.1.1 Bolted joint under accelerated aging conditions 109
6.2 Results and discussion 110
6.2.1 Bolted joints prepared from EB cured composites 110
6.2.2 Bolted joints prepared from thermally cured composites 128
6.3 Numerical analysis 135
6.3.1 Loads and boundary conditions 135
6.4 Closure 138
Chapter 7 Conclusions and Recommendations for Future Work 139
7.1 Conclusions 139
7.2 Recommendations for future work 141
References 143
List of Publications 157

List of Figures

Figure No.	Title	Page No.
Figure 1	Flowchart of overall thesis work	viii
Figure 1.1	Compression molding [12]	4
Figure 1.2	Vacuum-assisted resin transfer molding (VARTM) [12]	4
Figure 1.3	Classification of Nanofillers [58]	6
Figure 1.4	Modes of failure in FRP composites [68]	10
Figure 1.5	Bending strength of the composite plate [98]	13
Figure 1.6	Tan δ curves from DMTA analysis [41]	14
Figure 2.1	Setup for 4 MeV pulsed horizontal EB accelerator machine	33
Figure 2.2	Manufacturing process of carbon/epoxy nanocomposites	34
Figure 2.3	The geometry of single hole pin joint configuration	35
Figure 2.4	Test setups for analysis of failure loads (a) UTM machine and (b) specimen in steel fixture	38
Figure 2.5	Schematic design of composite specimen and fixture	39
Figure 2.6	UTM machine setup along with fixture assembly	40
Figure 3.1	Tensile properties of EB cured carbon/epoxy nanocomposite	44
Figure 3.2	Dispersion behavior of MWCNTs with sedimentation experiment	46
Figure 3.3	FESEM images of composite (a) Neat, (b) 0.1 wt.% MWCNTs, (c) 0.3 wt.% MWCNTs and (d) 0.5 wt.% MWCNTs configurations	46
Figure 4.1	Algorithm for the progressive damage analysis of composite pin joints [215]	51
Figure 4.2	Wireframed mesh around the pin hole showing side edge and free edge	52
Figure 4.3	Convergence study on the failure load	53
Figure 4.4	Load vs. displacement graphs for different joint configurations of EB cured neat carbon/epoxy composite laminates under tensile test	54

Figure 4.5	Load vs. displacement graphs for different joint configurations of EB cured 0.3 wt.% of MWCNTs added carbon/epoxy composite laminates under tensile test	55
Figure 4.6	Actual images of failure modes of EB cured joint carbon/epoxy composites for (a) neat and (b) MWCNTs added configuration	57
Figure 4.7	Ultimate failure loads for EB cured neat and MWCNTs added composite joint specimens at (a) W/D=2, (b) W/D=3, (c) W/D=4 and (d) W/D=5	59
Figure 4.8	Net-tension mode of failure in EB cured neat composite joint for W/D=2 and E/D=4 at applied load of (a) 20%, (b) 40%, (c) 60%, (d) 80% and (e) 100%	60
Figure 4.9	Shearing mode of failure in EB cured neat composite joint for W/D=3 and E/D=2 at applied load of (a) 20%, (b) 40%, (c) 60%, (d) 80% and (e) 100%	60
Figure 4.10	Bearing mode of failure in EB cured MWCNTs added composite joint for W/D=5 and E/D=5 at applied load of (a) 20%, (b) 40%, (c) 60%, (d) 80% and (e) 100%	61
Figure 4.11	Comparison of failure loads for EB cured neat and MWCNTs added composite specimens	62
Figure 4.12	Load vs. displacement graphs for different joint configurations of neat carbon/epoxy composite laminates under tensile test	63
Figure 4.13	Load vs. displacement graphs for different joint configurations of 0.3 wt.% of MWCNTs added carbon/epoxy composite laminates under tensile test	64
Figure 4.14	Comparison of ultimate Failure loads of thermal cured neat and MWCNTs joint specimens for (a) W/D=2, (b) W/D=3, (c) W/D=4 and (d) W/D=5	65
Figure 4.15	Net-tension mode of failure in neat composite joint for W/D=2 and E/D=4 at applied load of (a) 20%, (b) 40%, (c) 60%, (d) 80% and (e) 100%	66

Figure 4.16	Shearing mode of failure in neat composite joint for W/D=3 and E/D=2 at applied load of (a) 20%, (b) 40%, (c) 60%, (d) 80% and (e) 100%	66
Figure 4.17	Bearing mode of failure in MWCNTs added composite joint for W/D=5 and E/D=5 at applied load of (a) 20%, (b) 40%, (c) 60%, (d) 80% and (e) 100%	67
Figure 4.18	Comparison of numerical and experimental results of ultimate failure loads of neat and MWCNTs added composite specimens	68
Figure 5.1	Water absorption vs. square root of time plot of FRP composite [223]	71
Figure 5.2	Water absorption behavior in EB cured neat and MWCNTs added composite specimens at (a) 25 ^{o}C, (b) 45 ^{o}C and (c) 65 ^{o}C	73
Figure 5.3	Tensile stress vs. tensile strain for EB cured unaged and aged specimens (a) Neat and (b) MWCNTs added configurations	74
Figure 5.4	Flexural stress vs. flexural strain for EB cured unaged and aged specimens (a) Neat and (b) MWCNTs added configurations	75
Figure 5.5	Strength retentions of hygrothermally aged EB cured composite specimens of neat configuration at (a) 25 ^{o}C, (b) 45 ^{o}C and (c) 65 ^{o}C and MWCNTs added configuration at (d) 25 ^{o}C, (e) 45 ^{o}C and (f) 65 ^{o}C	76
Figure 5.6	The damage mechanism in EB cured neat and MWCNTs added composite specimens at 25 ^{o}C, 45 ^{o}C and 65 ^{o}C after 30 days of aging	78
Figure 5.7	SEM micrographs of the surface of neat composite specimens (a) unaged and (b) aged at 65 ^{o}C for 30 days and MWCNTs added composite specimens (c) unaged and (d) aged at 65 ^{o}C for 30 days	79
Figure 5.8	SEM micrographs obtained from after mechanical characterization of neat composite specimens (a),(b)	81

	unaged, (c),(d) aged at 25 ^{o}C, (e),(f) aged at 45 ^{o}C and (g),(h) aged at 65 ^{o}C for 30 days and 0.3 wt.%, MWCNTs added composite specimens (m),(n) unaged, (o),(p) aged at 25 ^{o}C, (q),(r) aged at 45 ^{o}C and (s),(t) aged at 65 ^{o}C for 30 days	
Figure 5.9	Load vs. displacement curves of unaged EB cured composite joint specimens (a) neat and (b) 0.3 wt.% of MWCNTs added configuration	83
Figure 5.10	Load vs. displacement graphs for hygrothermally aged EB cured neat composite bolted joint specimens at 25 ^{o}C, 45 ^{o}C and 65 ^{o}C	84
Figure 5.11	Load vs. displacement graphs for hygrothermally aged EB cured 0.3 wt.% of MWCNTs added composite bolted joint specimens at 25 ^{o}C, 45 ^{o}C and 65 ^{o}C	85
Figure 5.12	Actual images of neat composite bolted joint specimens at 65^{o}C for 30 days at (a) 0 Nm (b) 2 Nm and (c) 4 Nm bolt torques	86
Figure 5.13	Ultimate failure loads of unaged and aged EB cured joint specimens at different bolt torques	86
Figure 5.14	Surface plots indicating ultimate failure loads for EB cured (a) neat composite joints (b) MWCNTs added composite joints for 10, 20 and 30 days of aging	92
Figure 5.15	Water absorption behavior in thermally cured nanocomposites at (a) 25 ^{o}C, (b) 45 ^{o}C and (c) 65 ^{o}C for 30 days	94
Figure 5.16	Tensile and flexural properties of thermally cured composite specimens, unaged and aged, at different conditions	95
Figure 5.17	Mechanical strength retention of thermally cured nanocomposite specimens under hygrothermal conditions at (a) 25 ^{o}C, (b) 45 ^{o}C and (c) 65 ^{o}C	97
Figure 5.18	SEM images obtained after mechanical characterization of thermally cured neat composite specimens (a) unaged, (b) aged at 25 ^{o}C, (c) aged at 45 ^{o}C and (d) aged at 65 ^{o}C for 30 days and 0.3 wt.% of MWCNTs added composite specimens	99

(e) unaged, (f) aged at 25 ^{o}C, (g) aged at 45 ^{o}C and (h) aged at 65 ^{o}C for 30 days

Figure 5.19 Load vs. displacement graphs for hygrothermally aged thermally cured neat composite joint specimens at 25 ^{o}C, 45 ^{o}C and 65 ^{o}C 100

Figure 5.20 Load vs. displacement graphs for hygrothermally aged thermally cured MWCNTs added composite joint specimens at 25 ^{o}C, 45 ^{o}C and 65 ^{o}C 101

Figure 5.21 Bar graphs showing ultimate failure loads of thermally cured nanocomposites at different hygrothermal aging conditions 101

Figure 5.22 Characteristic curve 103

Figure 5.23 Loads and boundary conditions in the composite bolted joint specimens 105

Figure 5.24 The meshing of composite bolted joint specimen 105

Figure 5.25 Progressive damage contour plots of composite bolted joint specimen with bolt torque of 4 Nm at (a) 20%, (b) 40%, (c) 60%, (d) 80% and (e) 100% of applied load 106

Figure 5.26 Damage plots obtained at 4 Nm bolt torque for neat configuration (a) numerical and (b) experimental 107

Figure 5.27 Numerically predicted ultimate failure loads obtained after different hygrothermal aging conditions 107

Figure 6.1 ATR-FTIR spectra of neat configurations showing changes in (a) hydroxyl region and (b) carbonyl region for unaged and accelerated aged specimens 110

Figure 6.2 ATR-FTIR spectrums of 0.3 wt.% of MWCNTs added configurations showing changes in (a) hydroxyl region and (b) carbonyl region for unaged and accelerated aged specimens 111

Figure 6.3 TGA thermograms of neat composite samples before and after accelerated aging 112

Figure 6.4 TGA thermograms of 0.3 wt.% of MWCNTs added composite samples before and after accelerated aging 113

Figure 6.5	Strength and modulus properties of EB cured neat and MWCNTs added nanocomposites (a) tensile, (b) compressive and (c) shear	115
Figure 6.6	Strength retentions of EB cured neat and MWCNTs added nanocomposites (a) tensile strength, (b) compressive strength and (c) shear strength	116
Figure 6.7	Surface morphology of neat composite specimens (a) unaged, (b) after 1000 h of accelerated aging and MWCNTs added composite specimens (c) unaged and (d) after 1000 h of accelerated aging	117
Figure 6.8	SEM micrographs obtained from tensile fracture specimens of neat composite specimens (a),(b) unaged and (c),(d) aged for 1000 h and MWCNTs added composite specimens (e),(f) unaged, (g),(h) aged for 1000 h	118
Figure 6.9	Load vs. displacement graphs for EB cured neat composite bolted joint specimens (a) unaged, (b) 250 h, (c) 500 h, (d) 750 h and (e) 1000 h of accelerated environmental aging	120
Figure 6.10	Load vs. displacement graphs for EB cured MWCNTs added composite bolted joint specimens (a) unaged, (b) 250 h, (c) 500 h, (d) 750 h and (e) 1000 h of accelerated environmental aging	122
Figure 6.11	Bar graphs showing ultimate failure loads of EB cured unaged and aged joint specimens at different bolt torques (a) neat and (b) MWCNTs added configurations	123
Figure 6.12	Surface plots indicating ultimate failure loads for (a) neat composite joints (b) MWCNTs added composite joints	126
Figure 6.13	ATR-FTIR spectra of thermally cured neat composite specimens, unaged and aged	127
Figure 6.14	ATR-FTIR spectra of thermally cured MWCNTs added composite specimens, unaged and aged	128
Figure 6.15	Mechanical strength retention of thermally cured unaged and aged composite specimens for 0, 250, 500, 750 and 1000 h (a) tensile, (b) compressive and (c) shear strength	130

Figure 6.16	SEM micrographs obtained from tensile fracture specimens of neat composite specimens (a) unaged and (b) aged for 1000 h and MWCNTs added composite specimens (c) unaged, (d) aged for 1000 h	131
Figure 6.17	Load vs. displacement graphs for thermally cured neat composite joint specimens (a) unaged, (b) aged for 250 h, (c) aged for 500 h, (d) aged for 750 h and (e) aged for 1000 h	132
Figure 6.18	Load vs. displacement graphs for thermally cured MWCNTs added composite joint specimens (a) unaged, (b) aged for 250 h, (c) aged for 500 h, (d) aged for 750 h and (e) aged for 1000 h	133
Figure 6.19	Ultimate failure loads at different bolt torques (a) neat composite joints and (b) MWCNTs added composite joints	133
Figure 6.20	Progressive damage contour plots of unaged neat composite bolted joint specimen with bolt torque of 0 Nm at (a) 20%, (b) 40%, (c) 60%, (d) 80% and (e) 100% of applied load	135
Figure 6.21	Progressive damage contour plots of unaged MWCNTs added composite bolted joint specimen with bolt torque of 4 Nm at (a) 20%, (b) 40%, (c) 60%, (d) 80% and (e) 100% of applied load	135
Figure 6.22	Numerical and experimentally obtained damage plots for unaged neat bolted joint configuration at (a) 0 Nm and (b) 4 Nm	136
Figure 6.23	Numerically predicted ultimate failure loads under accelerated aging for 0, 250, 500, 750 and 1000 h (a) neat composites and (b) MWCNTs added composites at different bolt torques	136

List of Tables

Table No.	Title	Page No.
Table 1.1	Applications of FRP composite materials	7
Table 2.1	Physical and mechanical properties of carbon fiber (provided by the supplier)	29
Table 2.2	Physical properties of the epoxy resin (provided by the supplier)	29
Table 2.3	Processing properties of the epoxy resin (provided by the supplier)	30
Table 2.4	Mechanical properties of the epoxy composite (provided by the supplier)	30
Table 2.5	Typical properties of the MWCNTs nanofillers (provided by supplier)	31
Table 2.6	Specifications of the different parts of the fixture	40
Table 3.1	Mechanical properties of EB cured carbon fiber/epoxy composite laminates	45
Table 3.2	Comparison of mechanical properties of nanocomposites	48
Table 4.1	Joint parameters with W/D and E/D ratios	50
Table 4.2	Hashin damage failure criterion and associated degradation rule [214]	52
Table 4.3	Experimentally obtained failure modes and failure loads for EB cured carbon fiber/epoxy composite pin joints	58
Table 4.4	Experimentally obtained failure modes and failure loads for thermal cured carbon fiber/epoxy composite pin joints	64
Table 5.1	Water absorption and diffusion coefficient of EB cured composite specimens	73
Table 5.2	Mechanical properties of EB cured composite specimens under hygrothermal aging	75
Table 5.3	Ultimate failure loads of EB cured bolted joint specimens at different hygrothermal aging conditions	87
Table 5.4	Control parameters	88

Table 5.5	Sample runs with accordance to central composite design in statistical analysis	89
Table 5.6	Analysis of Variance	90
Table 5.7	Water absorption percent and diffusion coefficient of nanocomposite materials	94
Table 5.8	Mechanical properties of thermally cured nanocomposite specimens under aging conditions	96
Table 5.9	Ultimate failure loads of thermally cured bolted joint specimens at different hygrothermal aging conditions	102
Table 6.1	TGA results of neat and 0.3 wt.% of MWCNTs added composite samples before and after accelerated aging	113
Table 6.2	ANOVA table	124
Table 6.3	Validation test for bolted joint configurations	125
Table 6.4	Mechanical properties of thermally cured composite specimens under accelerated aging conditions	129

List of Symbols

A_C	Longitudinal compressive strength
A_T	Longitudinal tensile strength
B_C	Transverse compressive failure strength
B_T	Transverse tensile strength
D	Diameter of the hole
D_Z	Diffusion coefficient
E	Edge distance from the free edge of specimen
E_1	Longitudinal modulus
E_2	Transverse modulus
F_t	Failure strength in net tension
F_s	Failure strength in shearing
F_b	Failure strength in bearing
G_{12}	Shear modulus
L	Length of the specimen
M_t	Water gain (%) at time t
P_{max}	Maximum load
R_{oc}	Characteristic length in compression
R_{ot}	Characteristic length in tension
S	In-plane shear strength
t	Thickness of the specimen
T_g	Glass transition temperature
W	Width of the specimen
W_o	Mass (g) of the initial reference specimen
W_t	Specimen mass (g) at time t
wt.%	Weight percentage

Greek Symbols

ν_{12}	Poisson ratio
Θ_f	Failure angle
σ_b	Bearing stress
σ_i	Stress components in the longitudinal direction
σ_t	Tensile stress
τ_s	Shear stress

List of Abbreviations

ANOVA	Analysis of variance
ASTM	American society for testing and materials
B	Bearing
DGEBA	Di glycidyl ether of bisphenol-A
EB	Electron beam
FEM	Finite element method
FESEM	Field emission scanning electron microscopy
FI	Failure Index
FRP	Fiber reinforced polymer
FRPs	Fiber reinforced polymers
FTIR	Fourier transform infrared spectroscopy
gsm	Gram per m^2
h	hours
MWCNTs	Multi-walled carbon nanotubes
N	Net-tension
PMCs	Polymer matrix composites
S	Shearing
SEM	Scanning electron microscopy
TGA	Thermogravimetric analysis
UTM	Universal testing machine
VARTM	Vacuum assisted resin transfer molding
XRD	X-Ray Diffraction

Chapter 1
Introduction and Literature Review

From the last few decades, the changing environmental conditions have a severe impact on the existence of natural resources [1]. The major concern is the high use of petroleum products in the development sectors [2]. Now, many industries started working on the usage of electric-based products. The lightweight materials have been developed that replace the old conventional materials to increase the strength and efficiency of the product [3]. Consequently, a huge consideration is given to the lightweight fibrous composite materials by the researchers and industries because of their high strength and stiffness, to their weight ratios [4, 5]. These fibrous composite materials have a wide range of applications in aerospace, civil structures, automobiles and marine sectors [6-10]. Usually, the manufacturing of fiber reinforced polymer (FRP) composites, consists of a polymer matrix and fiber reinforcement. Fiber reinforcements are preferred, as the strength of any material is much higher in fiber form than in bulk form [11]. FRP composite materials are orthotropic in nature, i.e., having different properties in different directions [11]. In these composites, matrix material surrounds and keep the fibers in the desired orientation and location whereas the fiber reinforcements contribute to enhance the physical and mechanical properties of the matrix material [12]. Matrix material also acts as a shield for fibers against environmental surroundings. FRP composite materials have shown huge advantages over conventional materials in terms of low thermal expansion, good dimensional stability, erosion and wear resistance, enhanced fatigue life, lightweight, high strength properties, corrosion resistance, etc. [12-16]. Inspite of that, combined effect of environmental conditions may affect the performance of FRP composites [17-19]. The combination of water, temperature, ultraviolet rays and humidity are responsible for generation of internal stresses in the material [20-23]. Thus, these conditions must be avoided to protect the composite surface.

1.1 Components of FRP composites

Basically, FRP composites consist of two primary constituents *i.e.*, matrix and the fiber reinforcement [11]. The matrix part holds the fibers well in position and helps to protect against environmental effects. The fibers are the load-carrying agent that enhances the strength properties of the matrix part [12]. The different kinds of fiber reinforcements and polymer matrix are discussed in the following subsections.

1.1.1 Classification of fibers and its materials

The fibers in the composite materials are the main strength builders on which the whole structural component is supported. The fibers reinforced in the matrix can be classified depending upon their fiber length [12].

***(a) Continuous fibers*:** Fibers that are continuously oriented in one direction are continuous fibers. These provide excellent directional tailoring properties and imparts high strength and modulus to the composite materials in the direction of fibers. Depending upon their fiber orientations these can be unidirectional, bidirectional and multidirectional.

(b) Discontinuous fibers: Fibers that impart isotropic properties i.e., no change in mechanical properties along the directions are the discontinuous fibers. Although the strength of these fibers is less than continuous fibers in a particular direction but can take load along any direction of the composite material.

(c) Hybrid fibers: The combination of continuous fibers and discontinuous fibers can be termed as hybrid fibers.

The above given fibers have no comparison within itself as these are used as per their required application area. The arrangement and orientation of fiber describe the structural behavior of FRP composites [24, 25]. Numerous fiber materials available for composites are primarily categorized as synthetic and natural fibers. Synthetic fibers mainly consists of glass fibers, carbon fibers, graphene fibers, basalt fibers, kevlar fibers and lot more [26-28]. Whereas, natural fibers consists of sisal, jute, hemp, rice, husk, coir, etc., [24].

1.1.2 Polymer matrix

The main function of the matrix is to protect and support the fibers and to deliver the distributing load and transferring the load between the fibers. This load transfer mechanism imparts shear stress in the matrix that resists the pulling out of the broken fibers [12]. The matrix in the composite materials can be metallic, organic, ceramic, or carbon, but the main emphasis of this section is on the polymer matrix. Since polymer matrix is light in weight, have low processing temperatures and have excellent corrosive resistant properties, these are widely used with glass and carbon fiber reinforcements [29].

Polymers are the long molecular chain or network of repeating monomer units that are bonded together using chemical reactions [30]. Polymer matrix act as a continuous phase

that holds the fiber in its place, with its properties influencing most of the degradative processes like chemical resistance, delamination, water absorption, etc., [31].

Generally, the polymer matrix is categorized in thermoset and thermoplastic polymers [32]. A three-dimensional cross-linked solid structure is obtained after the curing of thermoset polymers that claims solvent resistant properties and high thermal stability. Epoxies, polyesters, phenolics, vinyl esters and polyamides are some examples of thermoset polymers. Thermosets imparts good mechanical strength and low manufacturing cost. Thermoplastic polymers can be melted and reformed without altering its physical properties due to weak intermolecular bonds. The composites manufactured from thermoplastic polymers claim good impact resistance and damage tolerance but are less brittle than thermosets and required a large amount of processing energy and cost. Few examples of thermoplastic polymers are polyphenylene sulfide, polyether ether ketone, polycarbonates and polyetherimides.

1.2 Manufacturing of FRP composite material

Manufacturing of FRP composites consists of the preparation of fiber preforms and reinforcing these fibers with polymer matrix using different techniques. Here, fiber preforms signify weaving, braiding, stitching and knitting of fibers in a long sheet [33-35]. The hand layup technique is the special technique and the primary phase for the manufacturing of FRPs [36]. Under this process, the desired fiber preforms are placed in a mold and the matrix material is applied onto the fibers through brush or roller. Rollers ensure the interaction between the successive layers of fibers and the matrix by forcing the matrix part into the fiber reinforcement. The combination of uncured matrix material and fibers is known as prepregs. These prepared composite prepregs are finally cured using different curing processes [36].

1.2.1 Manufacturing techniques

Manufacturing techniques are the primary step in the preparation of composite materials. Different techniques such as filament winding, compression molding, vacuum-assisted resin transfer molding (VARTM), pultrusion and injection molding are used for composite material preparation. Filament winding is a technique to wind the fiber on the mandrel after passing it through liquid resin and then curing. This technique can be used to produce pressure vessels, power and transmission poles, aircraft fuselages, pipes, etc. The compression molding operation begins with the hand layup technique to form prepregs

inside the open molds followed by compression of these prepregs under high temperature and pressure. Application of compression molding can be found in automotive industries which include, leaf springs, rod wheels and bumpers. A schematic diagram of the manufacturing of the composite part using compression molding is shown in Fig. 1.1 [12].

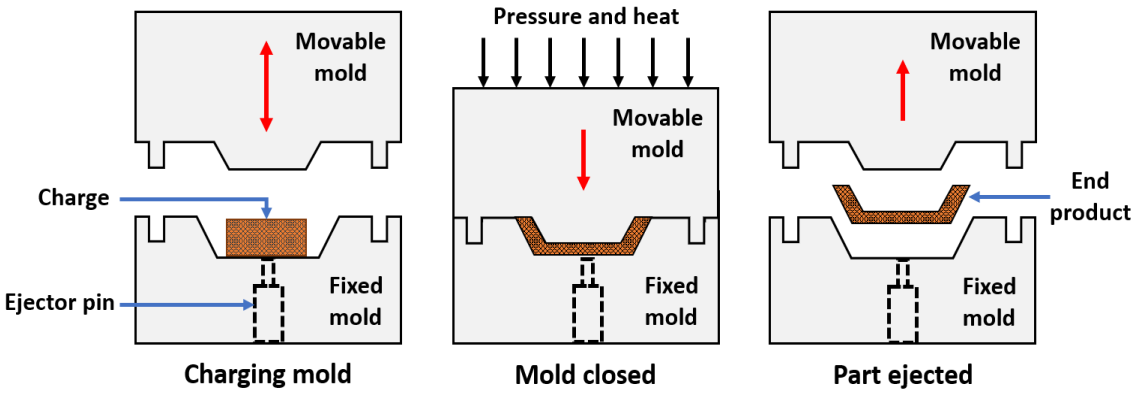

Fig. 1.1 Compression molding [12]

In VARTM technique, fiber preforms are placed on the molds and resin is transferred through perforated tubes over the fibers under vacuum. This technique leaves no traces of excess air in the composite that makes it popular in many applications like wind turbine blades and boat hulls. Figure 1.2 [12] shows the VARTM process for the preparation of a composite laminate.

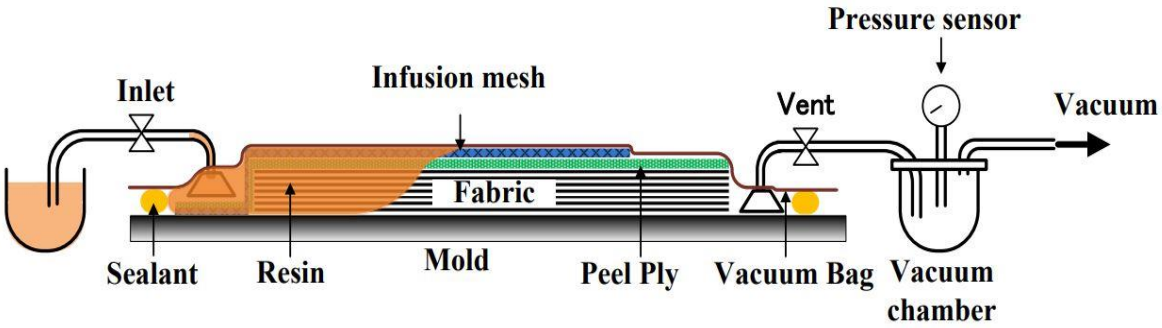

Fig. 1.2 Vacuum-assisted resin transfer molding (VARTM) [12]

In pultrusion process, the stand of continuous fibers is pulled through the resin bath and then cured in a heating die. A uniform cross-section and with relatively long lengths allow this technique to produce beams, flat sheets, solid and hollow tubes, etc. Injection molding is generally used to produce thermoplastic based composite products in very little time.

1.2.2 Curing process

According to the curing mechanism, the curing of FRP composite material can be done by two different processes as follows [37].

1.2.2.1 Thermal curing process

The thermal curing process is the most widely used method for curing of polymer composites. This curing process involves the application of heat combined with any manufacturing technique. According to their heating mechanism, thermal heating techniques can be classified in conduction, convection, and radiation heating. Thermal heating sources for the thermal curing process can include laser, infrared, microwave, hot gas, oven, hot shoe, induction, autoclave, ultrasonic, and resistance heating [38-40]. Although thermal curing provides enormous strength, stiffness, and dimensional stability to the composite structures, but several hours of material heating at high temperatures, mostly in the presence of pressure and highly toxic amine-based hardeners limits the use of thermal curing process. There is a need of alternative method that can cure composite material in less curing times at room temperature and with no use of toxic hardeners.

1.2.2.2 Radiation curing process

Radiation curing is the fastest growing technology in the field of polymer composites [41]. This curing process is based on the ionization of radiation-sensitive polymers that require high energy electromagnetic radiations such as electron beam (EB), X-rays, gamma rays, or ultraviolet (UV) rays. As the thermal curing system involves a two-component system, resin and hardener for crosslinking or curing, the radiation curing system does not require hardener for initiation of curing mechanism. The radiation curing method provides unique technological superiority which involves resin stability, energy efficiency, low manufacturing costs, high controllability, environment friendly nature, fast curing time, low energy consumption, room temperature curing, high curing efficiency, fast and ease to manufacture complex products [42-49]. Automobile, aerospace, marine sectors are promising areas where radiation curing is practiced.

1.3 Nanofiller addition in FRP composite materials

The performance of the FRP composites can be enhanced by incorporating nanofillers in the FRPs. The fundamental properties of nanocomposites like charge capacity, melting temperature, color and magnetic properties can be modified without disturbing its chemical

composition [50]. The size of the nanofiller is significantly reduced at the nanoscale level which leads to improvement in the surface area of the nanofillers. The addition of nanofillers in the polymer matrix enhances the mechanical, thermal and barrier properties because of effective stress transfer between the stiff nanofillers and soft polymer matrix through refined polymer/nanofiller interface and improved interfacial bond strength [51-56]. The property of a high specific surface area of nanofillers due to its nano dimensions helps in the formation of the large interfacial area in the nanocomposites. Thus, supports reducing the interfacial stress concentration and later enables the transfer of stresses from the polymer to the nanofillers [57]. This allows the nanocomposite materials to withstand higher loads and further increases its properties.

The nanofillers can be classified as organic and inorganic nanofillers such as clay (e.g., Montmorillonite (MMT)), natural antimicrobial agents (e.g., nisin, grape seed extract), natural biopolymers (e.g., chitosan), metal (e.g., aluminium, titanium), metal oxides (e.g., TiO_2, SiO_2) and carbon nanotubes (e.g., single-walled, double-walled, multi-walled). Figure 1.3 represents the classification of nanofiller that are used in making nanocomposites [58].

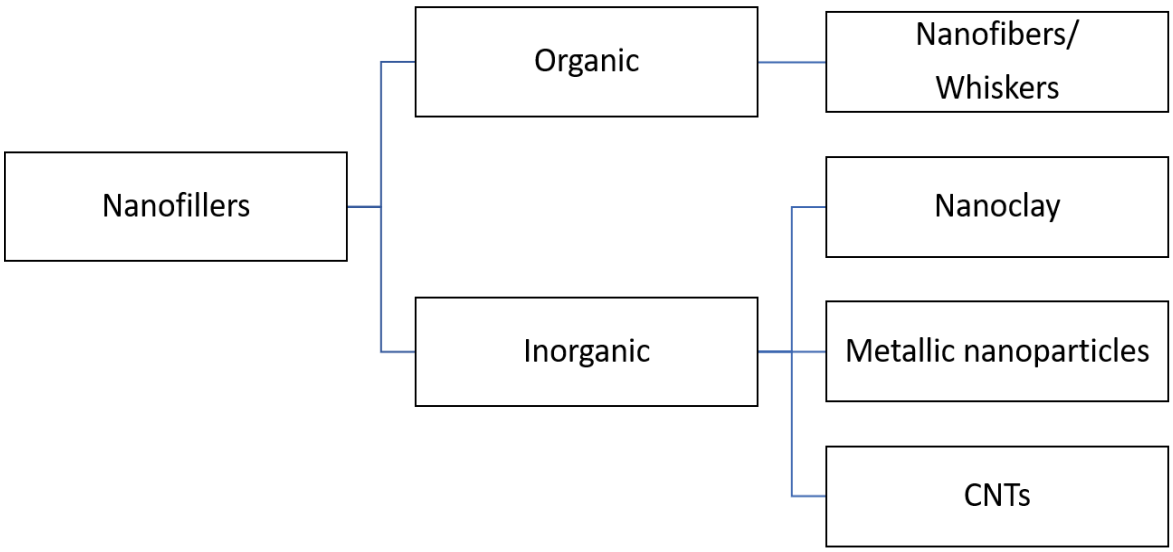

Fig. 1.3 Classification of nanofillers [58]

1.4 Applications of FRP composite materials

The FRP composites have potentially been used in the number of sectors such as automobile, aircraft, marine, civil, space and sports. Its applications also range in industrial products (i.e., tanks, power transmission shafts, step ladders), in medical industries (i.e., bone plates

for physically challenged, implants) and in furniture manufacturing. Table 1.1 shows few applications of FRP composite materials.

Table 1.1 Applications of FRP composite materials

Engineering sector	Applications
Aircraft [4]	• F-111 Wing pivot fitting • Vought A-7 speed brake • Lockheed L-1011 vertical fin • Boeing 777
Automobile [8]	• Springs and driveshafts in cars • Body of sports car, etc.
Space [6]	• Hubble space telescope • Tubes of interplanetary satellites
Commercial [7]	• Columns of bridges • Wind turbines, etc.
Marine [9]	• Fishing and sail boats • Yachts, etc.
Sports [59]	• Archery bows • Hockey sticks • Fishing rods, etc.

1.5 Joints in FRP composite material

In actual working conditions, the applications of FRPs requires joining of materials with each other or with metallic or non-metallic components. Another reason is that the manufacturing of large structural components is not always conceivable. Thus, it is suitable to join smaller units to assemble a large structural component. The joining methods are broadly classified into two categories depending upon the structural applications [60-62].

1.5.1 Mechanical joints

These are the semi-permanent or temporary joints that are used to join the structural component because of its ease in assembly and detachability [60]. The bolts, pins and rivets are the few examples of mechanical joints. These joints benefit the structural component in its maintenance and repair. Drilling of holes is the main source of stress concentration in the composite material which is the setback in mechanical joints [63].

1.5.2 Adhesive joints

These are the permanent joints that use adhesives between the two adherent surfaces. Some common adhesives are silicones, epoxy, phenolics, cyanoacrylates and methyl acrylate.

These joints provide improved damage tolerance and lower fabrication cost [61]. Machining operations like drilling are not required in these joints but have lower mechanical strengths than mechanical joints. Cohesive and adhesive damage are the two kinds of failure that occurs in adhesive joints [64].

1.5.3 Benefits of mechanical joints over adhesive joints

Some applications in the automobile and aerospace industries require frequent maintenance and quality checks. In that case, adhesive bonds being permanent in nature fails to operate in the same manner after the joint is opened. These circumstances limit the use of adhesive joints in many structural components that requires regular maintenance. Whereas, mechanical joints are primarily chosen by the industries due to their ease in assembly and disassembly. Also, mechanical joints deliver good mechanical and thermal properties, low maintenance costs and easy repair as compared to the adhesive joints [60].

1.6 Design of mechanical joints

The failure of mechanical joints may be due to the composite failure or fastener failure. To analyze the actual failure in the composite material, the fasteners used are normally stronger than its constituent material. The two primary mechanical joints i.e., pin joints and bolted joints are usually used to investigate the failure behavior in the composite material.

1.6.1 Pin joints

In pin joints, a metallic cylindrical pin is inserted into the drilled hole of the composite material. These types of joints allow each component part to rotate at a point of joint connection. The applied force can cause failure in the composite material as pin moves in the direction of the applied force. No clamping forces are used in the pin joints so the stress concentration is accumulated in the narrow contact area which is in contact with the pin [65, 66].

1.6.2 Bolted joints

Bolted joints require fasteners and washers to assemble the big composite structural component. In comparison to pin joints, the addition of out of place compressive forces with in-plane forces in the bolted joints lowers the delamination effect and also improves the joint strength as clamping forces also come into action. This clamping force is generated through washers which reduces stress concentration around the hole and distribute it over a larger area [67]. Based on external forces acting on the joint, bolted joints can be classified as

tension joints and shear joints. In tension joints, the line of action of the externally applied forces is parallel to the bolt axes whereas, in shear joints, the line of action of the externally applied forces is perpendicular to the bolt axes. The application, which requires leakage prevention in two clamped members, uses tensile joints whereas assembly of different structural components requires shear joints.

1.6.3 Modes of failure

The design of the mechanical joint is a highly critical issue to investigate the failure around the hole. The basic modes of failure in single pin/bolted composite joints are net-tension, shearing and bearing modes, shown in Fig. 1.4 [68]. Net-tension and shearing modes are catastrophic in nature that implies joint failure occurs immediately without any warning. These failure modes arise due to excessive tensile and shear stresses. However, bearing failure mode is progressive in nature and is related to compressive failure [67].

(a) Net-tension mode: In this mode of failure, the material fails immediately without any warning in catastrophic nature across the width of the specimen. One of the reasons for failure in net-tension is the smaller width to diameter (W/D) ratio [68]. The failure strength (F_t) in net-tension mode can be evaluated using Eq. (1.1).

$$F_t = (W - D) \times t \times \sigma_t \tag{1.1}$$

Where, σ_t is the tensile stress, W, D and t are the width, hole diameter and thickness of the specimen.

(b) Shearing mode: This mode also fails catastrophically but along the longitudinal edges of the specimens towards the free edge. This type of failure occurs due to excessive shear stresses [69]. The strength (F_s) in shearing mode can be evaluated using Eq. (1.2).

$$F_s = 2 \times E \times t \times \tau_s \tag{1.2}$$

Where, τ_s is the shear stress, t is the thickness and E is the edge distance from the free edge to the centre of the hole.

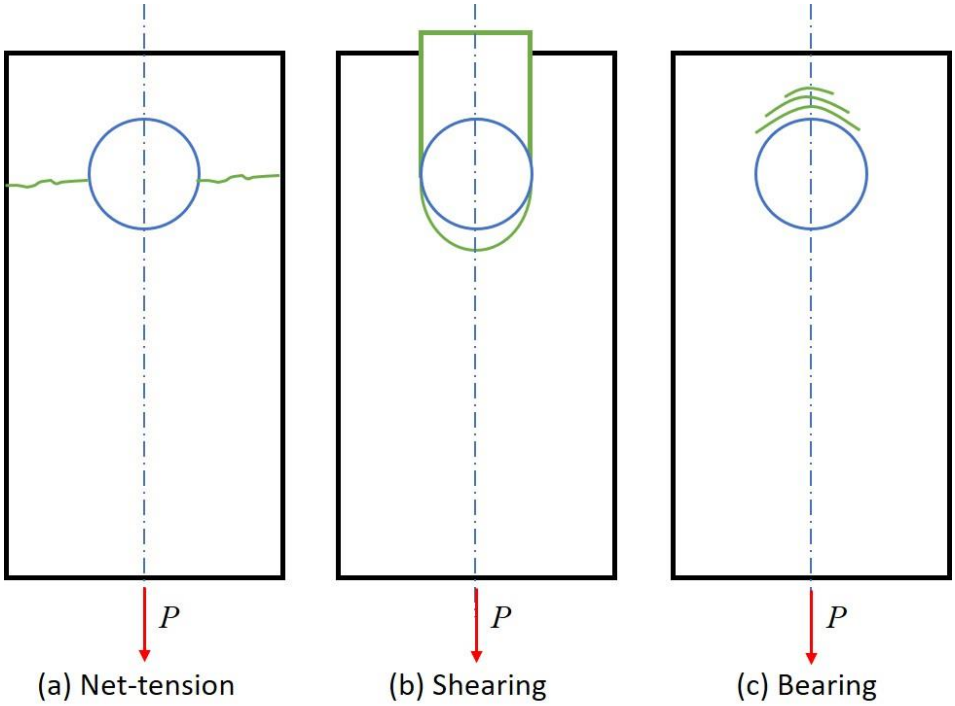

Fig. 1.4 Modes of failure in FRP composites [68]

(c) Bearing mode: This failure mode is progressive in nature and occurs due to the compressive stresses exerted by the fasteners or the pin. This failure is progressive towards the free edge in the direction of the applied load. This failure gives the maximum failure loads in the FRP composites [70]. The strength (F_b) in bearing mode can be evaluated using Eq. (1.3).

$$F_b = D \times t \times \sigma_b \tag{1.3}$$

Where, σ_b is the bearing stress, D and t are the hole diameter and thickness of the specimen, respectively.

1.6.4 Strength parameters

In joints, the primary focus is on the strength of the joints that control the composite failure. The factors that affect the strength of the joints are as follows [71]:

(a) Material: It comprises of type of matrix material, fiber material along with its arrangements and stacking sequence of the composite laminate.

(b) Geometry: The geometry comprises the length, width and thickness of the composite laminate. It also includes the size and location of the hole in the composite laminate.

(c) Fasteners: It consists of the types of fasteners, the size of the fasteners and its clearance with the hole diameter.

(d) Design: It comprises the application of the joints depending upon the loading type, loading direction, type of joint (single lap, double lap, etc.), the geometry of joint (pitch, width, edge distance and hole pattern) and the environmental conditions.

1.7 Impact of aging on FRP composite materials

In several applications such as civil and marine structures, FRP composite materials are exposed to different aging environments that involve moisture and temperature. Therefore, the durability and performance of composite structures under these environments must be analyzed. The degradation of FRP composite material is dependent on the stability of the fiber/polymer interface and its constituent phases [18]. The combined effect of temperature and moisture for short- or long-term durations is responsible for chemical and physical changes in the fiber/matrix interface. The common consequences of moisture absorption includes deterioration of the mechanical strength, reduction of glass transition temperature, swelling of polymer and increased viscoelasticity [19, 72, 73].

Among different studies, it was also recognized that by incorporating hydrophobic nanofiller into the polymer matrix, the moisture diffusion rate gets reduced. These nanofillers act as a mechanical barrier against the seepage of water through polymer matrix as the tortuosity effect increases the water diffusion path for water molecules in composite materials. Also, incorporating nanofillers in the composite material ease to reduce the water permeability by hindering the tranquility of polymeric chains surrounding the nanofiller [20, 21].

1.8 Literature review

In recent years, different researchers in the field of FRP composite materials and their mechanical joints have reported a substantial amount of work. These composites found their applications in many industrial sectors which require mechanical joints to fabricate a big structural component. Various parameters such as types of material, geometric parameters and size of fasteners used in the joints affect the strength of mechanical joints in a composite structural component. This chapter discusses the investigations carried out on the different curing processes and the factors, that affect the performance of FRP composites and their mechanical joints. The literature review is broadly classified into three categories:

- Radiation curing of FRP composites.
- Effect of different parameters on the performance of FRP based mechanical joints.
- Aging effect on the FRP composites and their mechanical joints.

1.8.1 Radiation curing of FRP composites

From past decades, thermal curing is the recognized manufacturing technology for curing polymer-based composites, which consists of several hours of material heating at high temperatures, mostly at high pressure in the presence of highly toxic amine-based hardeners [74, 75]. To overcome these drawbacks an alternative method, radiation curing has gained prodigious interest and evidenced a huge transformation in the field of polymer matrix composites.

Radiation cured polymer composites are used in many industrial applications of aerospace, automobile, transportation and energy sectors [6-9]. Various out-of-autoclave curing processes like electron beam (EB) curing, gamma-ray curing, X-ray curing and ultraviolet (UV) curing have been put forward for curing of polymer composites [76-80]. The penetration depth of X-rays is larger, but the dose rate is lower as compared to that of EB curing process, resulting in curing time about 60 times longer than EB curing process. Further, gamma rays can be very effective but with serious irradiation hazards. Ultraviolet light curing is applicable in transparent composites but it can hardly cure black composites. Amongst all, EB curing emerges as an innovative technology that has shown significant properties in the polymer matrix composites due to its high controllability, reduced thermal stresses, environmental friendly, fast curing, low energy consumption, room temperature curing, low cost, better material handling and high curing efficiency in comparison to other radiation and thermal curing processes [42, 47, 81-85].

In polymer matrix composites, the EB curing process uses high energy electron beams (4-15 MeV) and low energy electron beams (below 300 keV) that initiate the polymerization and crosslinking in the polymers. In the late 1970s, the Aerospeticle French-based company was the first who introduced the concept of electron beam curing of polymer composites [85]. Many researchers from Canada, United States, Japan, China and Europe have reported plenty of research findings in this field. A lot of investigations were conducted by Singh and Saunders [42, 44, 49, 79] on the effect of EB curing on the epoxy acrylate composites, fiber and its sizing. Beziers *et al.* [45] worked on the filament wound EB cured epoxy acrylates and bismaleimide composites, since 1970s. The EB curing of acrylate-based composites under irradiation undergoes a free radical mechanism and are not able to match the properties of advanced composites due to high moisture absorption and high shrinkage. Therefore, a suitable resin system was required for composite applications. Criverllo *et al.* [86] had developed the epoxy resin which undergoes cationic polymerization using cationic

initiators such as onium salts. Due to the excellent properties and processing characteristics of epoxy resins, these are widely used in polymer matrix composites [87]. Different varieties of epoxy resins have shown excellent radiation reactivity and became the prime resin matrix in EB curable composites [87-89]. From 1994 to 1997, the Department of Energy and Defense along with other industrial agencies have signed the Cooperative Research and Development Agreement (CRADA) which was potentially working for EB curing of polymer matrix composite technology. Various developments and optimization processes of polymer matrix composites have been carried out within the CRADA to meet the performance of thermally cured composites [90-92]. With the positive aspects of research and development in the EB cured cationic polymer systems, these systems were potentially applied in the curing of FRP composites [88, 93-97]. Different researchers have worked upon the polymer matrix composites and FRP composites that has been cured by EB curing process.

Zsigmond *et al*. [98] examined the mechanical properties of the EB cured carbon fiber/vinyl ester composite plates. The improved adhesion between fiber and the matrix was observed, as related to the conventional chemical crosslinking. It was found that the EB cured composite plates showed better interlaminar shear strength (ILSS), bending strength and modulus of elasticity. The bending strength of the composite plate is shown in Fig. 1.5.

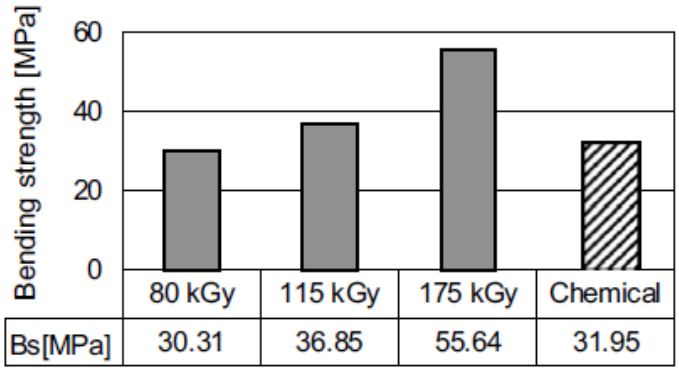

Fig. 1.5 Bending strength of the composite plate [98]

In polymer composites, not all polymers (such as Bisphenol A diglycidyl ether-based epoxy resins) can be cured by the radiation beam curing process, so it required a cationic initiator to initiate a cationic polymerization mechanism [86, 99]. The excellent properties and characteristics of the epoxy resin system facilitate its usage in EB curable composites [85, 100].

Nishitsuji *et al.* [101] made the use of commercial epoxy resins and cationic initiators for preparing radiation cured composite material with similar or better results than thermally cured composites. The composite specimens were cured at 150 kGy of total irradiation dose within few minutes in radiation curing while it takes around 20 hours for thermal curing. Sui *et al.* [102] studied the influence of cationic initiator, EB irradiation dose, molecular weight and chemical construction on the thermomechanical properties of cured bisphenol A and phenolic epoxy resin samples. The radiation dose used in the work was 50, 150, 250 and 300 kGy. Raghavan [103] evaluated the influence of process parameters (*i.e.*, dose and dose rate) on the mechanical properties, evolution of cure and residual stresses. It was found that a shorter dose rate and prolonged exposure ensured a higher degree of cure.

Over potential benefits of EB curing, few researchers found that the degree of cure by EB radiations was not 100% and cured composites had low mechanical properties due to crosslinking inhomogeneity [41, 104, 105]. This issue was generally fixed by post curing treatment after a total irradiation dose of 150-250 kGy [106-108].

Pitarresi *et al.* [104] examined the performance of carbon/epoxy composites on short beam shear test with EB cured, thermally cured and EB cured followed by post curing. It found that post curing helps in achieving the mechanical properties equivalent to the thermal curing process. Similarly, dynamic mechanical thermal analysis (DMTA) on EB cured carbon/epoxy composites was carried by Spadaro et al. [41] to determine the degree of cross-linking. The results of DMTA curves pointed towards the non-uniformity in the cross-linking degree of the EB cured samples with a wide range of relaxation temperature. The post thermal curing had given a more uniform cross-linking structure as shown by the narrow peaks in the loss tangent curves shown in Fig. 1.6.

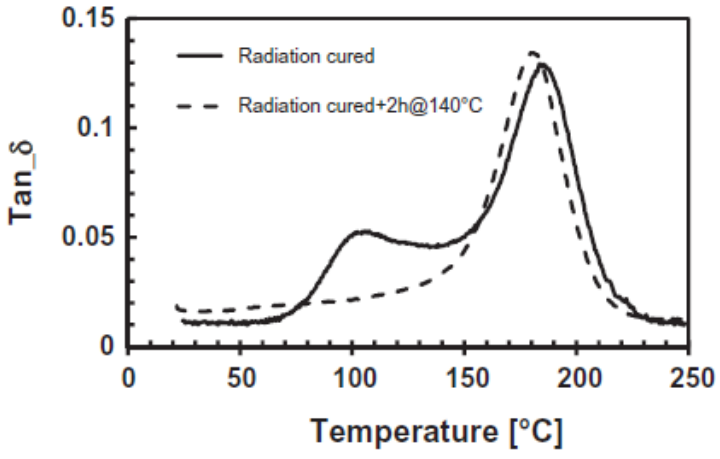

Fig. 1.6 Tan δ curves from DMTA analysis [41]

1.8.2 Effect of different parameters on the performance of FRP based mechanical joints

The applications of FRPs require the joining of materials with each other or with metallic or non-metallic components as manufacturing of large structural components is not always conceivable. So, mechanical joints are widely chosen by the industries for assembling composite part belonging to primary structures. The performance of these mechanical joints depends upon the different parameters that include the type of fibers and their material, ply orientation, joint design, fasteners, bolt preloads and most importantly on the geometry of the joint. Various investigations are reported on the different parameters to improve the performance of mechanical joints.

Quinn and Matthews [109] studied the effect of stacking sequence on the bearing strength of glass/epoxy composite pin joints. A stacking sequence of eight layers, two each at 0^o, 90^o and $\pm 45^o$ were used. It was estimated that the bearing strength increased by placing a 90^o layer (normal to the applied load) at or next to the surface. The ultimate failure loads showed dependency on the stacking sequence. Okutan and Karakuzu [110] investigated the effect of geometric parameters on the net-tension, shearing and bearing strengths of glass/epoxy composite pinned joints. Two different ply orientations such as $[90/\pm45]_s$ and $[0/\pm45]_s$ were used with 20 different geometric combinations. The effect of joint geometry prepared from unidirectional and woven composite laminates, on the failure loads and failure modes was studied experimentally and numerically by Ahn *et al.* [65]. The Tsai-Wu and Yamada-Sun failure criterion were applied for the prediction of failure on the characteristic curve. VirSingh *et al*. [111] used three dimensional finite element approach to evaluate elasto-plastic material properties of the particle reinforced composites. Aluko [112] presented the analytical method for the prediction of failure in the composite pin joints using the characteristic curve method. Similarly, Irisarri *et al.* [113] presented a modified finite element model for carbon/epoxy composite joints based on a progressive damage failure approach and found good agreement with the experimental data. Another experimental and numerical study on pin joints was conducted by Turan *et al.* [114] to estimate the failure modes and failure load in the single pin joints prepared from unidirectional carbon/epoxy composite laminates. The effect of joint geometry and fiber orientation was studied. Numerical simulations were performed on the ANSYS software using Hashin failure criteria. Olmedo *et al.* [115] developed the model that combined the characteristic curve

model for damage prediction and a mass-spring model for joint stiffness reproduction in each ply of pin joint composites.

A progressive damage analysis was performed by Bakhshan *et al.* [116] using ABAQUS software, on the pin-hole composite plate under tensile loading. The Hashin and Yamada-Sun failure criteria along with Camanho's material degradation model were studied to investigate the effect of failure criteria in composites. Khashaba *et al.* [117] established the progressive damage model (PDM) to predict the failure loads in glass/epoxy composite pinned joints using the Riccio degradation rule and Hashin failure criteria.

Some researchers worked on the performance of multi-hole pin joint composites. Karakuzu *et al.* [118-120] examined the bearing strength and failure modes using different geometric parameters in single pin loaded glass/vinyl ester composites, followed by the double pin loaded in series and parallel in glass/vinyl ester composites. In another study, Aktas *et al.* [121] used Yamada sun failure criteria to calculate the failure modes and bearing strength in glass/epoxy composites loaded with double serial pin joints. It was concluded that maximum bearing load was attained at $W/D \geq 4$ and $E/D \geq 4$. Pisano *et al.* [122] used carbon/epoxy composite multi-pin joints to evaluate the fastening failure loads with a kinematic approach of limit analysis.

Some investigations were carried out on the bolted joints and their associated bolt tightening toques that exerts a lateral compressive force on the composite laminate and thus distributes the stress within the contact region at the initial stage of loading. Sen *et al.* [123] studied the effect of bolt torque on the bearing strength and failure modes of glass/epoxy composite bolted joints. Three different bolt tightening torques of 0, 3 and 6 Nm were taken. The geometric parameters, W/D and E/D ratios were varied from 2 to 5 and 1 to 5, respectively. It was found that the bearing strength was increased with an increase in bolt torques and geometric values. In another investigation, an experimental study was performed by Othman and Jadee [124] on the effect of different reinforcements, W/D ratio and E/D ratio on the glass-reinforced composite bolted joints. Four different reinforcements were prepared, consisting of the chopped strand (600 g/m^2), plain weave (800 g/m^2 and 290 g/m^2) and 2/2 twill weave (600 g/m^2). A bearing test was performed as per ASTM D5961 standard to determine the specific bearing strength. Giannopoulos *et al.* [125] investigated the effect of bolt preloads on the fatigue life and strength of the FRP composites bolted joints. Optical microscopy was used to study the damage initiation and final failure manifestation. The three-bolt torque levels of 0, 5 and 10 Nm were used. To predict the failure loads of bolted joints, the effect of clamping force was studied by Choi *et al.* [126]. The prediction was

done using the Tsai-Wu criteria combined with the characteristic length method. Mandal and Chakrabarti [127] presented a novel 3D FEM model to predict the failure load of FRP multi-bolt composite joints subjected to different bolt preloads and different bolt diameters. The progressive damage algorithms were integrated into the ABAQUS using user-subroutine UMAT instead of commonly used user-subroutine USDFLD.

Another important aspect in the mechanical joints is the effect of clearance at the pin/bolt hole interface, interference fit, washer size and metal inserts. Murthy *et al*. [128] performed the numerical analysis on clearance fit with a smaller diameter pin inserted into the hole. It was found that contact status did not change with load levels when clearance was zero and it became a case of the linear problem. But when a smaller diameter pin was inserted into the hole, it became a case of non-linear problem due to changing partial contact regions. The experimental study was carried out by Zhai *et al*. [129] on the effect of bolt-hole clearance and bolt torque on single-lap, single-bolt and countersunk composite joints prepared from carbon/epoxy composite laminates. The joint stiffness, bearing stress and bearing strength was estimated using ASTM D5961. In another investigation, Khashaba *et al.* [130] investigated the influence of tightening torque (0, 5, 10 and 15 Nm) and washer outer diameter (14, 18, 22 and 27 mm) of glass/epoxy composite bolted joints. The results showed that under the same tightening torque, the joint stiffness increased with decreasing washer size. The maximum strength was obtained at bolted joint with 18 mm washer size and an applied torque of 15 Nm. The bolted joint with hand tightening torque (0 Nm) had the lowest joint stiffness, which showed an unstable development of internal damage. Kim and Kim [131] examined the effect of interference fit on the bearing strength of carbon/epoxy composite pin joint. Five different combinations *i.e.*, one transition fit and four interference fits (0.2, 0.4, 0.6 and 1%) were used in the pin-hole. It was concluded that the interference fit can improve the joint stiffness under both the static and dynamic bearing load conditions. The concept of inserting a metallic insert in the vicinity of a hole of graphene epoxy bolted joint was given by Nilsson [132]. The addition of a metallic insert reduced the stress concentration around the hole and hence provided improved failure loads. The adhesive strength and stiffness of the metallic insert controlled the failure loads of the joint.

In another study, to overcome the inefficiencies of hole clearance and bolt pre-defined tensions, Mara *et al.* [133] utilized metallic inserts in the hole of single shear bolted joint. The influence of metallic inserts on the bolt tension relaxation, joint stiffness and load-bearing behavior of joints was analyzed experimentally and numerically. The results showed that the metallic insert minimized the bolt tension relaxation, helped in utilizing the load that

was lost in friction initially and increased joint stiffness. Singh *et al.* [134] used metallic inserts incorporated in the glass/epoxy composite pin joint laminates with varying geometric combinations of W/D and E/D ratios to evaluate the bearing strength. Metallic inserts improved the stress distribution near the hole and thus further increased the bearing strength. The enormous improvements in the performance of FRP composites were reported with the addition of nanofillers [135, 136]. The high specific surface area of nanofillers helps in the formation of the large interfacial area in the composite materials and thus improves mechanical strength [57, 137-139]. A few researches were carried out to investigate the influence of nanofiller addition on the behavior of mechanical joints. Asi [140] experimentally investigated the effect of Al_2O_3 nanofillers on the bearing strength, failure loads and failure modes of glass/epoxy composite pin joints. The Al_2O_3 added in pin joint specimens were 7.5, 10 and 15 wt.%. An increase in Al_2O_3 content in the matrix improved the bearing strength of the composites. The addition of 10 wt.% of Al_2O_3 showed the highest bearing strength at W/D = 4 and E/D = 4. Further addition of Al_2O_3 content reduced the bearing strength in the composite joints. In another work, Singh *et al.* [141] incorporated nanoclay into the glass/epoxy composites to study the load-bearing capacity and failure loads and failure modes of pin joints. W/D and E/D ratios were varied from 1 to 5. For failure modes prediction, Tsai-wu failure criteria along with Progressive damage analysis (PDA) and characteristic curve method was used. Nanoclay in glass/epoxy composite laminates showed higher bearing strength than laminates without nanoclay content. Sekhon *et al.* [142] used two different nanofillers, TiO_2 and nanoclay in the glass/epoxy composite pin joints to investigate the bearing strength. The maximum bearing strength was obtained at 2 wt.% of TiO_2 and 3 wt.% of nanoclay. Singh *et al.* [143] investigated the bearing strength and failure modes of pin joints with the addition of nanoclay as a filler material. The effect of different geometric parameters (E/D and W/D) and the ply orientations were also studied for single hole pinned joints prepared from glass-epoxy nanocomposite laminates. The layups with [0°/90°/0°] stacking sequence demonstrated 10–12% higher bearing strength than the layups with [0°/45°/0°] orientation. It was found that the failure modes were dependent on the geometry of the joint. In another investigation, Tuzemen *et al.* [144] estimated the bearing strength of bolted carbon/epoxy nanocomposites after incorporating nanoclay, carbon nanotubes (CNT) and a hybrid of both the fillers. Four different specimens were prepared, neat, 4 wt.% nanoclay, 0.3 wt.% CNT and the hybrid with 4 wt.% nanoclay and 0.3 wt.% CNT. The results exhibited 5.2%, 3.9% and 0.8% improvement in bearing strength by addition of nanoclay, CNT and the hybrid nanoparticles.

1.8.3 Aging effect on the FRP composites and their mechanical joints

In several applications of civil, aerospace and marine sectors, FRP made composite structures and their mechanical joints are prolongedly exposed to the hygrothermal aging environment which involves moisture and high temperature [145, 146]. One of the primary causes of FRP composite degradation is moisture absorption, which results in the epoxy swelling, hydrolysis of resin, microcracking and debonding of the fiber/matrix interface [147-149]. The absorbed water molecules can be of bound and free water type in which free water is gathered in the voids present inside the epoxy or at fiber/matrix interface and bound water is usually bonded with the hydroxyl group of epoxy [150, 151]. The moisture absorbed in the composites weakens its thermal, mechanical, electrical, physical and chemical properties. The plasticization and swelling in epoxy are attributed to the physical changes and chain scission while hydrolysis relates to chemical changes [152, 153]. The FRP composite degradation is dependent on the stability of the fiber/polymer interface and its constituent phases [18]. But swelling reduces the interfacial bond strength, which affects the mechanical properties of the composites. Overall, the consequences of moisture absorption are to deteriorate the mechanical strength, reduce glass transition temperature, swelling of the polymer and increased viscoelasticity of FRP composites [19, 72, 73]. Therefore, under hygrothermal conditions, strength retention property of the composite structure is a big challenge for the industries and researchers. Many researchers have contributed to investigate the severe effect of hygrothermal aging conditions on the FRP composite materials.

Alessi et al. [154] investigated the hygrothermal aging behavior in the carbon/epoxy composite at 30 ^{o}C and 70 ^{o}C and exposure time of 4 weeks and 8 weeks, respectively. The water uptake behavior, dynamic mechanical thermal analysis (DMTA) and fracture toughness studies were conducted on the composite materials. In the case of higher aging temperature, composites evidenced a higher water uptake, which results in more degradation/plasticization effect of the matrix at matrix/fiber interface. DMTA evidenced the lowering of glass transition temperature (T_g) due to the onset of plasticization effect on composites. High temperature favors the strong matrix/fiber degradation and reduction of stick-slip crack growth mechanism. The durability studies were conducted by Hong et al. [155] on the pultruded carbon fiber reinforced polymer (CFRP) composite plates. The specimens were immersed into water at different temperatures of 23 ^{o}C, 40 ^{o}C and 60 ^{o}C for evaluation of water uptake and mechanical properties. The mechanical properties of CFRP

composites along with resin matrix and fiber/resin adhesion were investigated. The diffusion of water was more in CFRP composites than in neat resin matrix. Fiber/matrix adhesion was susceptible to water immersions at higher temperatures. The flexural behavior of the pultruded FRPs under fresh water and artificial seawater environments at 40 ^{o}C, 60 ^{o}C and 80 ^{o}C was examined by Xin *et al.* [156]. The specimens were exposed to the hygrothermal conditions for 5000 h. The Arrhenius relationships and Phillips equations were used for the prediction of the long-term hygrothermal effect on the flexural properties. Experimental results revealed that the reduction in flexural properties increased when temperature changed from 40 ^{o}C to 80 ^{o}C. The predicted results showed a good correlation with experimental results expected for 80 ^{o}C, where predicted values showed less reduction in flexural properties at the end of aging duration.

Above all consequences, one probable solution to reduced moisture diffusion and improvement in interfacial properties is by incorporating hydrophobic nanofiller into the polymer matrix. These nanofillers act as a mechanical barrier against the seepage of water through the polymer matrix as the tortuosity effect increases the water diffusion path for water molecules in composite materials. Also, incorporating nanofillers in the composite material ease to reduce the water permeability by hindering the tranquility of polymeric chains surrounding the nanofiller [20, 21]. The hygrothermal aging and water absorption studies were performed on organomontmorillonite (OMMT)/polyamide 6/polypropylene (PA6/PP) composites with and without malleated PP, by Chow *et al.* [157]. The three different temperatures of 30 ^{o}C, 60 ^{o}C and 90 ^{o}C were used for immersion of specimens into water and weights were recorded periodically, to investigate the water absorption behavior. It was found that the kinetics of water absorption obeys Fickian law and moisture diffusion and diffusion coefficient were strongly dependent upon immersion temperatures, OMMT loading and MAH-g-PP concentration. Firdosh *et al.* [158] predicted the long-term durability of glass/vinyl ester composites with 0-5 wt.% added nanoclay, based on experimentally obtained tensile strength properties under hygrothermal environment, using Arrhenius rate model. The exposure time at 30 ^{o}C, 50 ^{o}C and 60 ^{o}C for 75 days and at a relative humidity of 95% was used. For higher filler content, the diffusivity was reduced to nearly 50% compared to the diffusivity of neat epoxy resin [159]. The effect of TiO_2 nanofiller on the water absorption mechanics of glass/polymer composites was studied by Nayak *et al.* [160]. Under hygrothermal conditions at 70 ^{o}C for 30 days, the addition of 0.1 wt.% of TiO_2 showed enhanced flexural strength and interlaminar strength by 19% and 18% and reduced moisture diffusion coefficient by 9% compared to neat glass/polymer

composites. Prusty *et al.* [161] elucidate the influence of hygrothermal aging on the degradation behavior of multi walled carbon nanotubes (MWCNTs) added glass/epoxy nanocomposites. It was examined that at lower aging temperatures, the moisture diffusion was significantly suppressed by MWCNTs addition as compared to higher aging temperatures due to the generation of thermal stresses at the MWCNTs/polymer interface. Gonzalez *et al.* [162] explained the consequences of distilled water and seawater aging on the low impact behavior of glass/polymer composites with the addition of MWCNTs as a nanofiller. The specimens made from two different polymers (i.e., epoxy and vinyl ester) were hygrothermally aged at 60 ^{o}C for 2000 h. The results showed that epoxy-based composites performed well under hygrothermal conditions. Also, MWCNTs addition showed significant improvement in the impact strength with no change in the moisture absorption behavior. In another investigation on seawater exposure, Lee *et al.* [163] studied the tensile and fracture behavior of MWCNTs added epoxy composites. Three different specimens (unmodified, oxidized and silane MWCNTs) with 0.1 wt.% content were prepared. Silane modified specimens showed higher tensile strength and modulus properties than unmodified and oxidized MWCNTs specimens, irrespective of moisture absorption. After seawater exposure, no significant change was seen in fracture toughness of silane and oxidized specimens whereas unmodified specimens showed lower fracture toughness.

Another source of FRP deterioration is UV radiation, which is attributed to the physical and chemical changes in the constituent resin because of the series of complex processes characterizing UV radiation and oxygen [164-166]. UV radiation may also lead to photochemical degradation that is initiated by the interaction of light photons with the polymeric molecular chain. At elevated temperatures, the degradation in FRP composites begins when the glass transition temperature of the resin material is reached [167]. From investigations, it was noted that the combined action of UV radiation, moisture and elevated temperature accelerates the degradation of polymeric materials.

The study on the effect of UV radiation and condensation on carbon fiber-epoxy composites was conducted by Kumar *et al.* [23]. It was revealed that combined environmental factors operate in a synergetic way that causes substantial loss of the epoxy matrix, resulting in the reduction of tensile strength by 29% after 1000 h of aging. Mouzakis *et al.* [168] fabricated an accelerated weathering chamber to investigate the consequence of temperature, UV and humidity on polyester/ glass fiber reinforced composites. SEM images revealed some microcracks on the surface of the specimens after aging. The dynamic mechanical analysis (DMA) technique confirmed interfacial degradation in glass/polyester composites at high

temperatures. Stewart and Douglas [169] explored the performance of FRP composites under accelerated aging conditions and found that the loss of mechanical properties was due to the degradation of the epoxy matrix. The epoxy swelling, plasticization, hydrolysis and chain scission reactions are the main mechanism responsible for the degradation of tensile, flexural and fracture toughness properties. Similarly, Yan *et al.* [170] studied the combined effect of UV radiation and water spraying on mechanical properties of flax fabric reinforced epoxy composite after 1500 h of aging. The test results showed a 29.9%, 34.9%, 10% and 10.2% reduction in tensile strength, tensile modulus, flexural strength and modulus properties, respectively. The cyclic exposure of UV and condensation at elevated temperature was examined by Batista *et al.* [171] on the polyphenylene sulfide (PPS)/carbon fiber composites. The results revealed that UV exposure for a short duration increases the compressive strength, while long duration promoted deterioration in the strength properties. Nicholas *et al.* [172] assessed the accelerated aging effect on the microstructure and the impact behavior of glass/polyurethane composite. The sample were exposed for 250, 500, 750 and 1000 h in the accelerated weathering environment. The results revealed that there was no significant change in the impact properties and the material showed resistance to the UV radiations. The color change was observed with an increase in aging duration. Barbosa *et al.* [173] explored the consequence of temperature and humidity with controlled UV exposure on the carbon/epoxy composites. Interlaminar shear strength, Fourier transform infrared spectroscopy (FTIR), dynamic mechanical analysis (DMA), compressive strength and SEM characterizations were used to evaluate the material changes. The material changes were observed by chemical alterations, weight loss, surface degradation and increased crack density. Panaitescu *et al.* [174] conducted the accelerated aging for automotive parts made of glass/polyurethane composites. The combined effect of high temperatures and liquid immersions produced a significant impact on the material in terms of delamination and chemical alterations. Bazli *et al.* [175] evaluated the mechanical properties of glass/polymer pultruded profiles under similar conditions of UV radiation, moisture and elevated temperature for 1000, 1500, 2000 and 3000 h of aging. The result showed a decrease in the mechanical properties with aging. However, the rate of reduction was slightly lower during 1000 h, rapidly increased during 1000-2000 h and again slowed down during 2000-3000 h. The maximum reduction in tensile, bending and compression strength was 28%, 34% and 23% after 3000 h of exposure time.

Woo *et al.* [176, 177] studied the degradation phenomenon of epoxy/organoclay nanocomposites due to combined exposure of humidity and UV radiations for 300 h.

Organoclay based nanocomposites showed better resistance towards the deteriorating effect of combined exposure than the neat composites. Chang and Chow [178] used an accelerated weathering test to study the effect of UV exposure on flexural properties and fracture toughness of glass/epoxy/organo-montmorillonite (OMMT) nanocomposites for 100 h. Similarly, Chiang *et al.* [179] investigated the flexural and interlaminar properties of carbon/epoxy composite laminates containing different wt.% (0.25, 0.50, 0.75 and 1) of graphene nanoplatelet (GNP)/nano-carbon aerogel (NCA) under the effect of different environmental aging conditions. Awad *et al.* [180] illustrated the influence of accelerated weathering on the morphological, mechanical, chemical and thermal properties of MWCNTs/epoxy nanocomposites for different exposure time.

A lot of work has been conducted on the performance of PMCs and FRPs under different environmental conditions, whereas very less work is reported on the performance of joints under these conditions.

Zhang and Rowland [181] studied the effect of extreme temperatures on damage progression in CFRP composite pin joints. A novel finite element-based framework was developed that implemented progressive damage method along with Hashin damage criteria in the model. At three selected ambient temperatures of -55 ^{o}C, 20 ^{o}C and 82 ^{o}C and three selected relaxation temperatures of 20 ^{o}C, 60 ^{o}C and 100 ^{o}C, the double shear pin joint test was modelled. Extreme temperatures showed lower joint strength than room temperature models and increasing relaxation temperatures showed a reduction in joint strength. An experimental failure analysis was conducted by Soykok *et al.* [182] to examine the effects of the thermal condition and tightening torque on the failure behavior of glass/epoxy composite lap joints. The specimens were exposed to 40-80 ^{o}C temperature levels, during the tensile test. It was concluded that with an increase in the temperature levels, the load carrying capacity of joints decreased gradually. Maximum decrease of 55% and 70% was found at 70 ^{o}C and 80 ^{o}C, respectively, due to heat damage to the resin matrix. The joint strength was estimated at 0 and 6 Nm torque levels and found positive effect of tightening torque even at elevated temperatures. In another investigation Soykok *et al.* [183] studied the behavior of glass/epoxy composite lap joints under hot water immersion. The specimens were immersed in hot water at 50 ^{o}C, 70 ^{o}C and 90 ^{o}C for 1 and 2 weeks. From tensile test results, it was concluded that failure behavior of joint strictly dependent on the temperature and water immersion duration. Jojibabu et al. [184] carried out the hygrothermal conditioning of neat epoxy and different carbon nanofiller added epoxy composites to measure the strength and durability of adhesive joints. It was found that the addition of

nanofillers lowers the water absorption rate as compared to pure epoxy composites. Fang *et al.* [185] investigated the combined effects of seawater aging and fatigue loading on the bearing performance and failure mechanism of CFRP/CFRP single lap bolted joints. The bolted joints were prepared with an interference fit size of 1.15% and immersed in the artificial seawater solution for 7 months. The bearing failure morphology was analyzed by SEM images. The experimental results showed an exponential decrease in ultimate bearing loads with an increase in aging time. Moreover, there was shearing fracture failure in bearing zones that increased with aging time.

1.8.4 Conclusion from the literature review

The work done by different researchers on FRP composites and their mechanical joints can be concluded as follows:

(i) The advantages of the EB curing process in terms of high controllability, reduced thermal stresses, environmentally friendly, fast curing, low energy consumption, room temperature curing, low cost, better material handling and high curing efficiency, makes it possible to use it for curing of FRP composites.

(ii) The post curing technique after EB curing helped in increasing the degree of cure in composite materials and facilitated in achieving properties equivalent to thermal curing.

(iii) The performance of mechanical joints was significantly affected by the geometric parameters such as E/D and W/D ratios. The bearing strength and failure loads of joints increased with increasing E/D and W/D ratios.

(iv) The tremendous improvement was reported by incorporating nanofillers in the PMCs and FRP composites and their mechanical joints.

(v) Bolt tightening torques and metal inserts improved the joint efficiency and ultimate failure loads.

(vi) Significant degradation occurred in FRP composites and their joints when subjected to harsh environmental conditions such as moisture, elevated temperatures, UV radiations, seawater, or a combination of these conditions. Although the addition of nanofillers restricts the degradation rate in the composites.

1.9 Motivation and objectives

From the last few decades, many researchers have shown a huge interest in the field of FRP composite material over traditional metallic materials due to their high strength and stiffness

to weight ratios. Further, the development of nanocomposite in FRPs provides great strength and barrier properties to the structural components. The properties of the FRP composite materials also depend upon the curing process.

For the curing of these composites, different thermal and radiation curing methods can be used. Different researchers have revealed the advantages of using the radiation curing process over the thermal curing. These advantages include lesser curing time, ease in manufacturing complex composite structures and less energy required, to name a few. Several studies investigated the strength of mechanical joints using different parameters i.e., stacking sequence, width to diameter (W/D) ratio, edge to diameter (E/D) ratio, ply orientation, material properties, interference fits, preload, etc. The improvement in strength properties of FRP composites was reported with the addition of nanofillers, at room temperature. In real-time, there are a large number of application areas that work under the aging environment that affects the performance of FRP nanocomposites. Different studies have been carried out to investigate the combined effect of the aging environment (e.g., hygrothermal aging, accelerated weathering aging) on the mechanical properties of FRP nanocomposites. Very few researchers contributed towards the effect of aging on mechanical joints with the addition of nanofillers. Moreover, less work is reported on the mechanical joints prepared from the radiation cured FRP composites. So, the purpose of the present study is to enhance the performance of mechanical joints using different geometric parameters along with the addition of MWCNTs as nanofiller. The performance of the mechanical joints is analyzed both in unaged and aged conditions i.e., moisture, temperature, ultraviolet radiations, etc.

The specific objectives of the present work are:

- Preparation and characterization of electron beam cured carbon fiber/epoxy reinforced composite laminates with CNTs as a nano material.
- Experimental analysis of mechanical joints prepared from electron beam cured laminates with different parameters.
- Aging of the mechanical joints prepared from electron beam cured laminates.
- Numerical analysis for the prediction of strength of joints under aging process.

1.10 Thesis overview

The different curing processes (EB curing process and thermal curing process) have been used for the preparation of the laminates. The wt. % of MWCNTs in epoxy was optimized to maximize the mechanical properties of FRP nanocomposites. With the optimized wt. % of MWCNTs, the mechanical joints were studied to investigate the effect of geometric

parameters, nanofiller and bolt preload. The performance of the mechanical joints was analyzed under both unaged and aging/weathering conditions. This thesis includes the following eight chapters.

Chapter 1 (Introduction and Literature Review) discusses the basics of FRP composite materials, its classification, manufacturing techniques, curing processes and the advantages of EB curing as compared to thermal curing. It explains the need for mechanical joints in the structural components and their mode of failures. It discusses the different parameters that produce an impact on the performance of mechanical joints in the FRPs. The impact of severe aging conditions on the structural part and its joints have been discussed. It also describes the benefits of using nanofillers in the FRP composite material.
The second part of this chapter broadly reviews the available literature on the performance of FRP composite and their mechanical joints are broadly reviewed. It discusses the impact of radiation curing on the performance of FRP composites. The influence of geometric parameters and nanofillers on the mechanical and thermal properties of the FRPs is also discussed. The available literature also elucidates the consequence of aging on the FRP composites.

Chapter 2 (Materials and Methods) gives the details of procured materials and the experimental work conducted. The woven carbon fibers and DGEBA based epoxy resins were used for preparation of laminates. The cationic photoinitiator *i.e.,* bis(4-methylphenyl) iodonium hexafluoro-phosphate was used for cationic polymerization. The MWCNTs nanofiller was used for improvement in mechanical properties of the epoxy resin. The two different materials, neat and MWCNTs added carbon fiber/epoxy composites and their joints were prepared using different curing processes (EB curing process and thermal curing process). The testing procedures, characterization and performance evaluation of mechanical joints are described.

Chapter 3 (Optimization of MWCNTs Nanofiller content) presents the results on the mechanical properties of nanocomposites as a function of MWCNTs content in the composites. The optimum content of nanofiller was found to be 0.3 wt. %.

Chapter 4 (Investigations on Single Pin Joint Composites) deals with the performance improvement of single pin joint using MWCNTs nanofiller. The investigations were carried out on neat and optimized 0.3 wt. % of MWCNTs added composite materials prepared using EB curing as well as thermal curing process. The single pin joint configurations were

prepared using geometric combinations of width to diameter (W/D) ratio and edge to diameter (E/D) ratio, varying from 2 to 5. A positive contribution on failure loads and failure modes of the pin joint was seen by incorporating MWCNTs nanofiller. Use of MWCNTs showed the maximum improvement of 26.63% and 26.34% in the failure loads for EB cured and thermally cured pin joint composites, respectively. The numerical analysis was performed using Hashin damage criteria along with progressive damage analysis to compare the predicted failure loads with the experimental results. A good correlation was obtained between the numerical and experimental results.

Chapter 5 (Performance of Bolted Joints under Hygrothermal Aging Environment) is focused on the hygrothermal aging of the bolted joints prepared from carbon fiber/epoxy composites. The investigations were carried out on the neat and optimized 0.3 wt. % of MWCNTs added composite materials prepared using two different processes (thermal curing and EB curing). Incorporating MWCNTs nanofiller in the composite material eases to reduce the water permeability by hindering the tranquility of polymeric chains surrounding the nanofiller. The composite bolted joint specimens were designed as per ASTM D5961 standard having geometric parameters, width to diameter ratio (W/D) and edge to diameter ratio (E/D) fixed to 6 and 5, respectively. The bolt torque effect at different levels of 0, 2 and 4 Nm were also examined. To investigate the performance of joints under hygrothermal aging conditions, three different temperatures 25 ^{o}C, 45 ^{o}C and 65 ^{o}C for 10, 20 and 30 days duration were considered. Under aging conditions, the water absorption tendency was higher in neat composite specimens than in MWCNTs added composite specimens. Similarly, in the aging process, specimens made from MWCNTs nanofiller have shown good mechanical strength retention than neat composite specimens. A strong correlation between the water temperature, aging duration and the ultimate failure load of the joint was observed. With the increase in immersion time and water temperature, the ultimate failure load values decreased. The bolted joint with MWCNTs added configuration had shown higher ultimate failure loads retention than the joints with neat configuration. Progressive damage analysis was performed using characteristic curve method along with Hashin damage criteria. A good correlation was obtained between the experimental and numerical results.

Chapter 6 (Performance of Bolted Joints under Accelerated Aging Environment) deals with the accelerated aging of bolted joints prepared from carbon fiber/epoxy composite laminates. The studies were performed on the composite materials prepared using two

different curing processes. To investigate the performance of joints under accelerated aging conditions, the combined cyclic exposure of UV radiations, moisture and temperature were given to the composite specimens for 0, 250, 500, 750 and 1000 hours. Upto 250 hours of exposure to UV radiation, moisture and temperature, the material evidenced a slight increase in mechanical strength and modulus properties due to relative stiffening effect and reaction of unreacted cationic photoinitiator molecules under UV radiation. However, after exposure for more than 250 hours, the reduction in the strength and modulus properties began which directed towards the initiation of degradation in the material due to moisture absorption and the photo-oxidation reactions. The specimens made from MWCNTs nanofiller have shown good mechanical strength retention than neat composite specimens. The ultimate failure load values of the bolted joints were affected due to accelerated weathering conditions. The exposure of 1000 hours significantly degraded the failure loads of the bolted joints. The bolted joint with MWCNTs added configuration have shown higher ultimate failure loads retention than the joints with neat configuration. Progressive damage analysis was performed using characteristic curve method along with Hashin damage criteria. A good correlation was obtained between the experimental and numerical results.

C**hapter 7 (Conclusions and Recommendation for Future Work)** summarizes the conclusions drawn from the present work and also gives recommendations for future research.

Chapter 2
Materials and Methods

In this chapter, the materials used, different curing methods to prepare the fiber reinforced polymer (FRP) composite laminates along with their characterization/ testing procedures and performance evaluation of the joints are described.

2.1 Materials

A polyacrylonitrile (PAN) based, 200 gsm woven carbon fiber was used as reinforcement in the present work. The carbon fiber was procured from the CFW Enterprises Pvt Ltd, New Delhi, India. The woven carbon fiber has advantages of high strength and stiffness to the weight ratios, temperature and corrosion resistance properties and low density which make them favorable over other fiber materials [27, 186]. The physical and mechanical properties of the carbon fiber provided by supplier are summarized in Table 2.1. The diglycidyl ether bisphenol A (DGEBA) based thermoset epoxy resin (L-12), anhydride hardener (K-12) and accelerator (K-13) were used as a matrix and were supplied by Atul Industries, Gujarat, India. The properties of the epoxy resin system given by supplier are shown in Table 2.2 to 2.4.

Table 2.1 Physical and mechanical properties of carbon fiber (provided by the supplier)

Property	**Value**	**Test method**
Density (g/cm^3)	1.8	TY-030B-02
Tensile strength (MPa)	4000	TY-030B-01
Tensile modulus (GPa)	240	TY-030B-01
Elongation at break (%)	1.7	TY-030B-01
Areal weight (g/m^2)	200	ASTM D3801
Poisson ratio	0.3	-
Filament diameter (μm)	7	-

Table 2.2 Physical properties of the epoxy resin (provided by the supplier)

Property	**Epoxy (L-12)**	**Hardener (K-12)**	**Accelerator (K-13)**
Density (g/cm^3)	1.1–1.2	1.15–1.25	0.88–0.92
Viscosity (mPa.s)	9000–12000	150–230	<10

Table 2.3 Processing properties of the epoxy resin (provided by the supplier)

Property	**Mixing ratio (by wt.) *(Resin: Hardener : Accelerator)***	**Initial mix viscosity**	**Pot life of mix (< 5 kg)**	**Gel time**
Condition	-	@ 40°C	@ 80°C	@ 80°C
Unit	w/w	cP	Minutes	Minutes
Value	100: 100: 0.1–2	450	60	150

Table 2.4 Mechanical properties of the epoxy composite (provided by the supplier)

Property	**Value**
Density (g/cm^3)	1.1–1.2
Tensile strength (MPa)	70–90
Tensile modulus (GPa)	3.2–3.5
Elongation at break (%)	2–4
Compressive strength (MPa)	190–210
Flexural strength (MPa)	100–120
Impact strength (kJ/m^2)	4–7

A cationic photoinitiator of iodonium salt, bis(4-methylphenyl) iodonium hexafluoro-phosphate, was procured from Sigma-Aldrich, Missouri, United States, which on reaction with EB rays decomposes into protonic acid H^+ and further reacts with the oxygen atom of the epoxy group. The purity and melting point of bis(4-methylphenyl) iodonium hexafluorophosphate were 98% and 180 ^oC, respectively. The NC 7000 series, multiwalled carbon nanotubes (MWCNTs) were used as nanofillers for improvement in mechanical properties of the epoxy resin. This nanofiller was procured from Nanocyl, Belgium. The MWCNTs were chosen as nanofiller due to its hydrophobic nature, low cost and density, high surface area and excellent mechanical properties [187]. Typical properties of the MWCNTs are given in Table 2.5. A high purity solvent ($(CH_3)_2CO$) acetone of ACS reagent grade and quality level of 200, was procured from Sigma-Aldrich, USA. It is used to help in the homogenization of epoxy and MWCNTs particles. The alloy steel fasteners manufactured by commercially available 'Unbrako' brand having diameter of 4 mm (M4) size was used in the present work. The tensile load carrying capacity and tensile strength of these fasteners were 11.4 kN and 1300 MPa, respectively, as quoted by the supplier. For the proper tightening of bolt-nut assembly, lock nut was used. The washer of size 2D+3 mm

was also used to distribute the load. The lock nut and the washer used in the present work were of the same material as the shoulder bolts and the nuts.

Table 2.5 Typical properties of the MWCNTs nanofiller (provided by the supplier)

Property	Value	Method of measurement
Average length (μm)	1.5	Transmission electron microscopy (TEM)
Average diameter (nm)	9.5	Transmission electron microscopy (TEM)
Carbon purity (%)	90	Thermogravimetric analysis (TGA)
Surface area (m^2/g)	250–300	BET surface area analysis
Volume resistivity (ohm.cm)	10^{-4}	Internal test method (resistivity on powder)

2.2 Methods

In the present work, two different curing methods were used for the preparation of carbon fiber reinforced epoxy composite laminates with and without the addition of MWCNTs nanofiller. Firstly, it was the radiation curing method using electron beam (EB) accelerator setup at room temperature and secondly, it was the thermal curing method using compression molding machine at high temperature.

2.2.1 Preparation of electron beam (EB) cured composite laminates

The preparation of EB cured composite laminates involved three stages; the hand layup technique, exposure to EB radiations and post curing of irradiated composite material. The two different materials, neat carbon fiber/epoxy composite laminates and the MWCNTs added carbon fiber/epoxy composite laminates were prepared using this technique.

2.2.1.1 Preparation of MWCNTs/epoxy resin solution

Generally, the MWCNTs nanofiller is available in the agglomerated form to reduce the net surface energy. So, for deagglomeration of the MWCNTs nanofiller, the high purity acetone is used for suspending the nanoparticles.

The desired wt.% of MWCNTs was dispersed in 120 ml of acetone, then mechanically stirred at 6000 rpm for 30 minutes with digital homogenizer using Pro 25D model (Pro scientific Inc., Oxford, USA), followed by 60 minutes of sonication using probe sonicator (model Q-700, Q-Sonica, New town, USA). Homogenization is a high-speed shear mixing

process which is used to disperse one phase/ingredient (MWCNTs) into a main continuous phase (epoxy resin) which is normally immiscible with hand mixing. The role of sonicator is to disperse the agglomerates that are present even after the process of homogenization. The probe sonicator uses sound waves that agitates the particles in the solution. Sonication process is done at pulse on-off time of 50 seconds. The sedimentation experiment was performed to ensure the dispersion behavior of MWCNTs [188]. The 2 wt. % of cationic photoinitiator, bis(4-methylphenyl) iodonium hexafluoro-phosphate (in the white powder form) was completely dissolved in the acetone (using sonication process) and then poured into preweighted amount of epoxy resin. Thereafter, MWCNTs/acetone suspension was poured into the epoxy/initiator mixture and stirred at 60 ^{o}C and 9000 rpm till complete evaporation of the acetone. The complete removal of acetone was ensured by weighing the mixture before and after the process. This epoxy/MWCNTs/initiator mixture was finally sonicated for 30 minutes. The final prepared epoxy/MWCNTs/initiator mixture is evenly permeated onto the carbon fabric layers using hand layup technique.

2.2.1.2 Preparation of EB cured carbon fiber/epoxy nanocomposite laminates

The required size of carbon fabric laminas was cut from the carbon fabric roll. The final prepared epoxy/MWCNTs/initiator mixture was applied onto these carbon fabric laminas through roller/brush for preparing the composite laminate using a hand layup technique. Rollers ensure the interaction between the successive layers of carbon fibers and the mixture by forcing the matrix part into the fiber reinforcement. The stacking sequence of $[0/90]_6$ was used so as to obtain the similar results in transverse as well as in longitudinal directions. For good surface finish and uniform thickness, the prepared laminates were kept inside the aluminium molds (releasing gel used so that laminate do not get stick to it) with the constant pressure applied through clamps on the sides of mold. Lastly, to initiate the EB curing process, the mold was placed on the conveyor belt, under electron accelerated gun of 4 MeV pulsed horizontal accelerator machine, located at Bhabha Atomic Research Centre (BARC), Mumbai, India (shown in Fig. 2.1). During the process, the pulse current, frequency and conveyor speed was maintained at 100 mA, 10 Hz and 3 cm/sec, at a dose rate of 10 kGy/pass with total irradiation dose of 240 kGy. After EB irradiation, the prepared laminates were post cured at 100 ^{o}C for 2 h. The final thickness of EB cured carbon fiber/epoxy/MWCNTs nanocomposite laminate obtained was 2 ± 0.2 mm. The same manufacturing technique was used for the fabrication of EB cured neat carbon fiber/epoxy composite laminates. For assessment of void content in the EB cured composite laminates,

the acid digestion test was performed as per ASTM D3171 standard. Void content was found to be 1.32% for neat composites and 0.96% for MWCNTs added composite specimens.

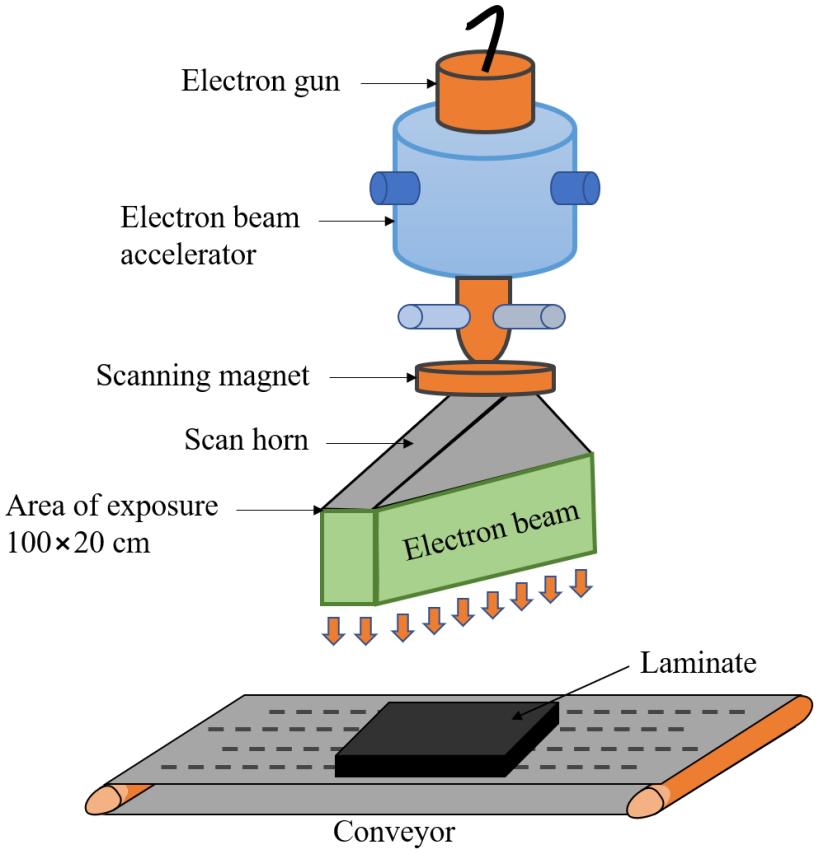

Fig. 2.1 Setup for 4 MeV pulsed horizontal EB accelerator machine

2.2.2 Preparation of thermally cured composite laminates

The preparation of composites begins with the cutting of bidirectional woven carbon fabric laminas from the fabric roll to the required dimensions. After the cutting process of carbon fabric laminas, the matrix part was prepared. The desired wt.% of MWCNTs was dispersed in 120 ml of acetone, mechanically stirred at 6000 rpm for 30 minutes, followed by 60 minutes of sonication process. This MWCNTs/acetone suspension was poured into the preweighed amount of epoxy resin and stirred at 60 ^{o}C and 9000 rpm till the complete evaporation of acetone was ensured. The epoxy/MWCNTs suspension was again sonicated for 30 minutes and then as per supplier's recommendations preweighted amount of hardener and accelerator were poured into the suspension and stirred for 10 minutes at 9000 rpm. The final prepared suspension was used along with the bidirectional woven carbon fabric for preparing the composite laminate using a hand layup technique. Stacking sequence of 0^{o} and 90^{o} was used to obtain similar results in transverse and longitudinal directions for the

required thickness of the laminate. For gel formation, the laminates were cured for 24-48 hours at room temperature and then finally cured using compression molding at 150 ^{o}C and 3.5 MPa pressure for 45 minutes. The final thickness of cured carbon fiber/epoxy/MWCNTs nanocomposite laminate obtained was 2 ± 0.2 mm. The same process of hand layup technique followed by compression molding was used for the fabrication of neat carbon fiber/epoxy composite laminates.

The prepared laminates of neat and MWCNTs configurations were inspected for the void contents. The acid digestion test as per ASTM D3171 was done using sulfuric acid to check the void content in the manufactured composite specimens. By using a physical fiber density and resin density provided by the suppliers, the void contents for composite specimens were determined. Void content was found to be 0.68% for neat composites and 0.54% for MWCNTs added composite specimens. The complete fabrication process of a composite laminate is shown in Fig. 2.2.

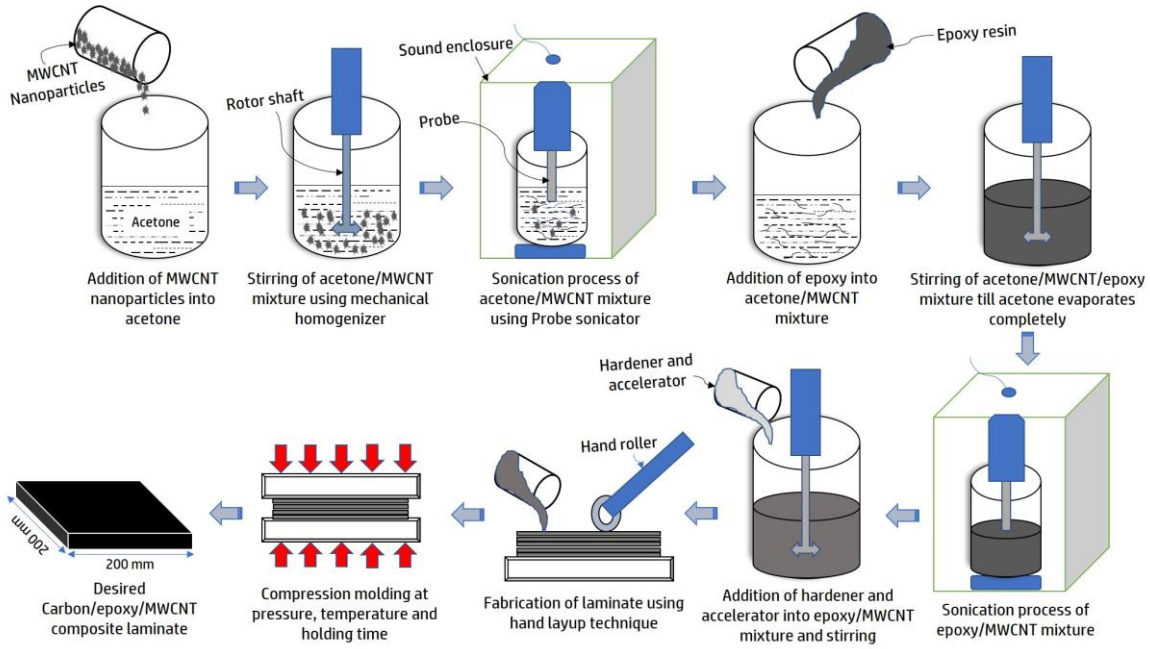

Fig. 2.2 Manufacturing process of carbon fiber/epoxy nanocomposites

2.2.3 Preparation of mechanical joints

The mechanical joints were prepared from carbon fiber/epoxy composite laminates with neat and MWCNTs added configurations. The following sub-sections describe the preparation of two types of mechanical joints; pin joints and bolted joints, for which the performance assessment was carried out.

2.2.3.1 Pin joints

The single pin joint composite specimens were prepared from the neat and MWCNTs added carbon fiber/epoxy composite laminates using different geometric combinations of width to diameter (W/D) ratio and edge to diameter (E/D) ratio, both varying from 2 to 5. The single pin joint configuration consists of a rigid pin inserted into the carbon fiber/epoxy composite specimens having a length (L), thickness (t), width (W), edge distance (E) and hole diameter (D=4 mm), as shown in Fig. 2.3.

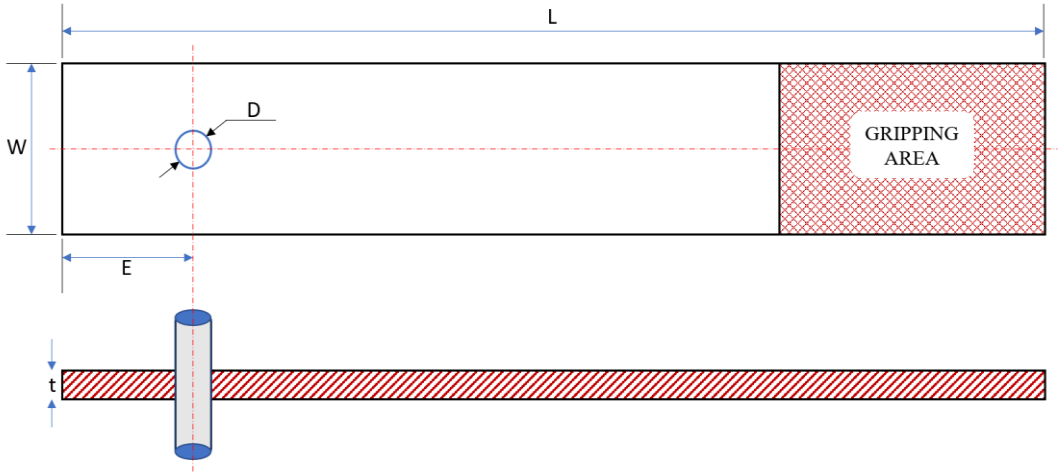

Fig. 2.3 The geometry of single hole pin joint configuration

2.2.3.2 Bolted joints

The bolted joint composite specimens were prepared from the neat and MWCNTs added carbon fiber/epoxy composite laminates as per ASTM D5961 standard having geometric parameters of W/D ratio and E/D ratio fixed to 6 and 5, respectively. The hole diameter used to insert the M4 size bolt was fixed to 4 mm. The bolt torques of different levels (0, 2 and 4 Nm) were used.

2.2.4 Environmental aging

In many engineering applications, the FRP composites and their joints have concerns about the long-term durability under harsh environmental conditions, such as ultraviolet (UV) radiation, moisture, elevated temperature, alkalinity and fire [189-191]. To analyse the detrimental effects of different environmental conditions, the different aging tests were performed on the composite laminates and their joints prepared in the present work.

2.2.4.1 Hygrothermal aging

The prepared composite laminates and their joints were aged under given hygrothermal condition as per ASTM D5229 standard. Before the immersion of specimens into the temperature-controlled digital water bath, these were dried at 80 ^{o}C for 4 hours. Three different temperatures, 25 ^{o}C, 45 ^{o}C and 65 ^{o}C were used in the digital water bath, model MSW-273(SL), MAC for duration of 30 days. The water absorption behavior was studied to estimate the maximum water gain and diffusion coefficient after aging process.

2.2.4.2 Accelerated weathering aging

The prepared composite laminates and their joints were exposed to accelerated weathering conditions to study the effect of cyclic exposure of UV and condensation with temperature on their physical and mechanical properties. The tests were conducted as per the ASTM G154 standard, in the accelerated weathering chamber (QUV basic model, Q-Lab Corporation, USA). The QUV chamber replicates the damage caused due to sunlight, rain and precipitation by exposing composite laminates and their joints at accelerated weathering conditions. In QUV chamber, UV radiations are illuminated using eight fluorescent UV-A lamps having solar radiation wavelengths of 340 nm at an irradiance of 0.68 W/m^2. The cyclic exposure of 8 h of UV at 60 ^{o}C and 4 h of condensation at 50 ^{o}C were given to the composite materials for 1000 h. The relative humidity was maintained at 100% in the environmental chamber at higher temperatures. For the given accelerated environmental conditions, the composite laminates and their joints were exposed for 0, 250, 500, 750 and 1000 h of aging.

2.3 Characterization

The different techniques used for the characterization of prepared composite laminates and their joints have been given in the following subsections.

2.3.1 Morphological properties

2.3.1.1 Scanning electron microscopy (SEM)

The structural morphology of the composite specimens was analysed using SEM (JEOL 6200 Scanning Electron Microscope, JEOL Pty. Ltd. USA) at an accelerated voltage of 20 kV. Before visualization, the specimens were prepared by gold coating using MP-19020NCTR Neocoater to prevent the charging problem of material.

2.3.1.2 Field emission scanning electron microscopy (FESEM)

FESEM images were taken on Zeiss Sigma model, Germany, to check the dispersion of MWCNTs in the epoxy matrix and existence of agglomerates. The FESEM images were taken at 60.00 kX magnification.

2.3.2 Thermal properties

The thermogravimetric analyser (TA Instruments TGA Q-500 series, USA) was used to determine the thermal stability of the composite specimens. The samples of 5-10 mg were placed in an aluminium pan and then heated from 30 to 600 ^{o}C at a rate of 10 ^{o}C/min.

2.3.3 Chemical properties

The chemical structure changes in specimens before and after the aging process were examined by Fourier transform infrared (FTIR) spectroscopy on Perkin Elmer Spectrum spectrometer using attenuated total reflectance (ATR) mode. The FTIR test was conducted on prepared specimens after 0, 250, 500, 750 and 1000 h of aging time. The range and resolution of spectra were taken as 400 to 4000 cm^{-1} and 2 cm^{-1}, respectively.

2.3.4 Mechanical properties

The tensile, flexural, compression and shear properties of manufactured composite laminates were evaluated using ASTM D3039, D790, D695 and D732 standards, respectively, before and after the aging under different conditions. Five specimens for each configuration were tested on the Zwick-Roell make universal testing machine (UTM) of 100 kN capacity. The crosshead speeds of 2, 2, 1.3 and 2 mm/min were used for tensile, flexural, compression and shear testing, respectively. The performance of joints was evaluated on the Zwick Roell make universal testing machine (UTM) having a capacity of 10 kN at a crosshead speed of 2 mm/min.

2.4 Performance evaluation of joint specimens

The failure analysis was done to evaluate the performance of pin joint and bolted joint composite specimens. In pin joint composite specimens, prepared with neat and MWCNTs added configurations, the failure loads and failure modes were estimated under the effect of different geometric parameters *i.e.,* W/D and E/D ratios from 2 to 5, respectively. The failure loads of pin joint composite specimens were evaluated under tensile loading on Zwick Roell make UTM machine with a capacity of 10 kN and crosshead speed of 2 mm/min. The testing setup used for pin joint composite specimens is shown in Fig. 2.4.

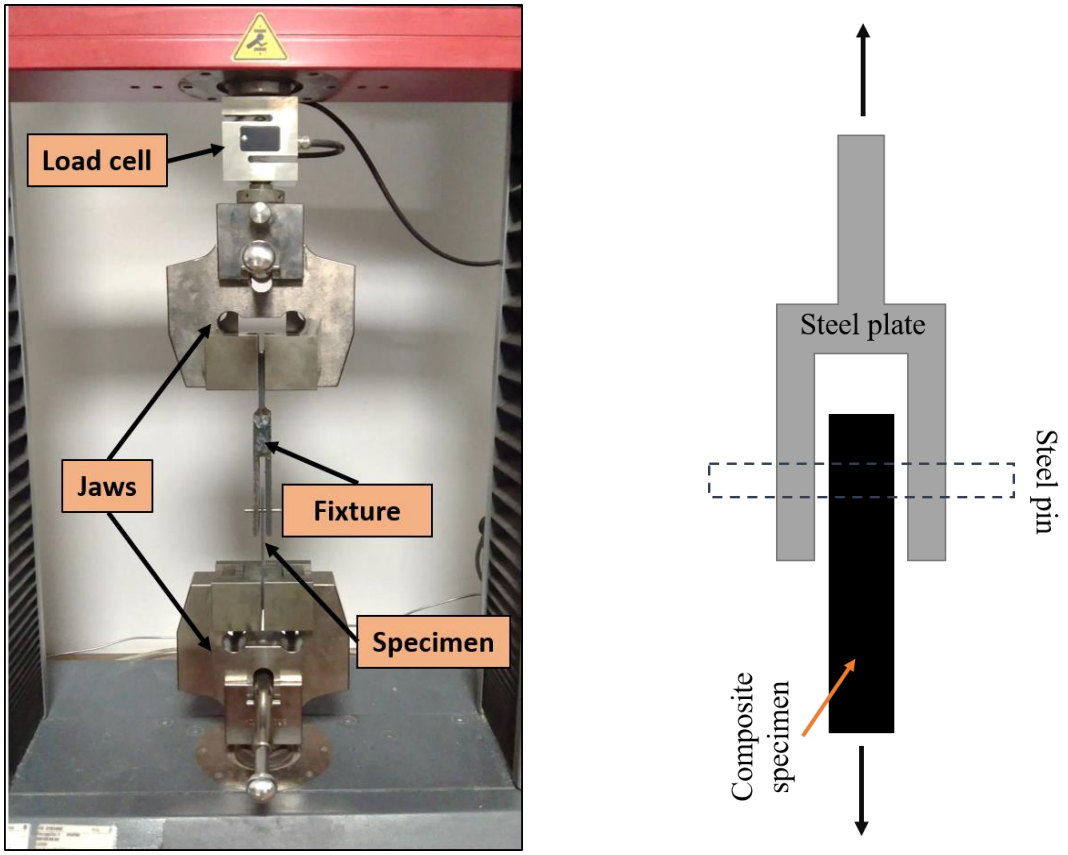

Fig. 2.4 Test setups for analysis of failure loads (a) UTM machine and (b) specimen in steel fixture

The failure of the pin joint is much simpler than the bolted joints where the lateral constraints are involved in terms of compressive forces. In many engineering applications like civil, aircraft and marine sectors, bolted joints are susceptible to the aging environment. To outspread the scope of the mechanical joints, failure analysis was done for performance evaluation of the bolted joints under different aging environmental conditions. The tests were performed on the bolted joint composite specimens, before and after the aging process. The unaged and aged joint composite specimens were clamped into the fixture through fasteners as shown in Fig. 2.5 and given a tightening bolt torque using a calibrated torque wrench having a variable torque and a least count of 0.5 Nm. The fabricated fixture consists of steel plates, M4 size shoulder bolts and washers. The material properties and dimensions of different components of the fixture are given in Table 2.6. Three different bolt tightening torques (0, 2 and 4 Nm) were used for the composite joints before testing. The bolt torques of 0, 2 and 4 Nm correspond to 0, 2500 and 5000 N preload values. Through testing, the maximum torque limit was found to be 9 Nm which produces a bearing stress of 149.2 MPa

under the washer, having an outside diameter of 2D+3 mm. To avoid unwanted damage to the laminate surface, the maximum torque limit was not exceeded beyond 9 Nm.

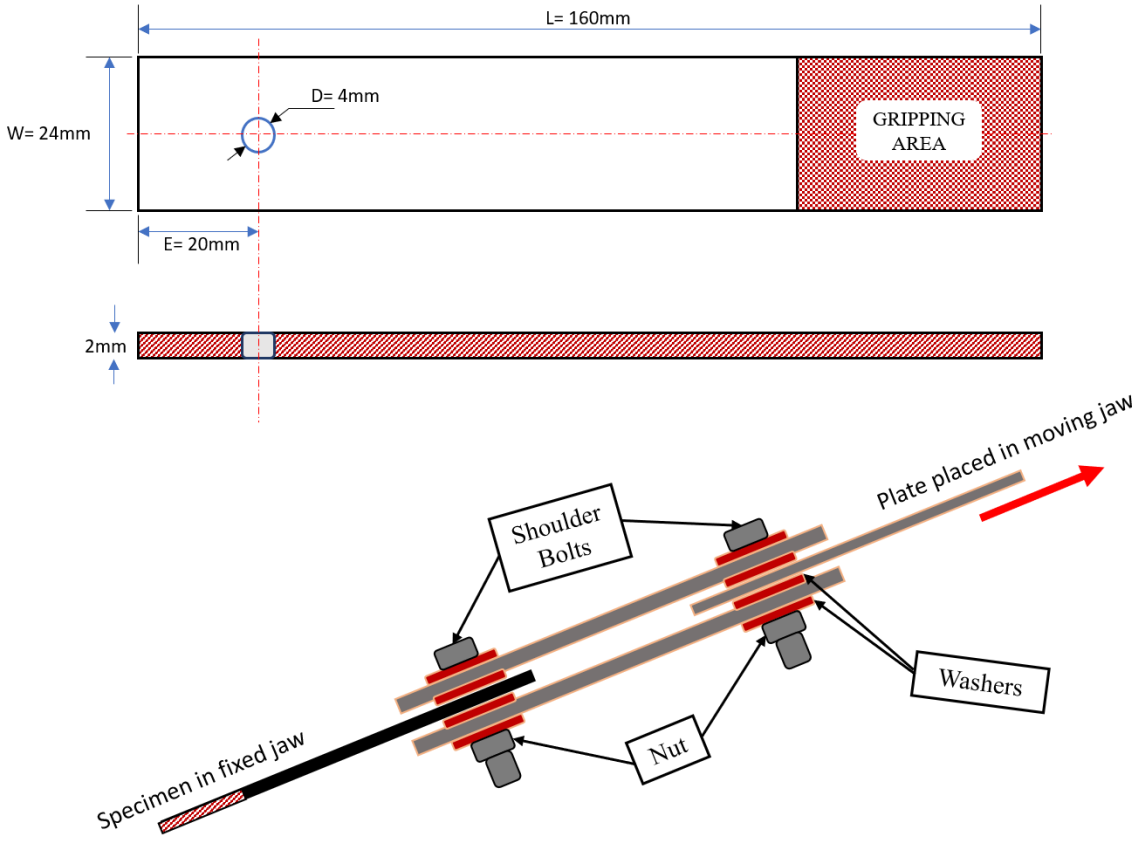

Fig. 2.5 Schematic design of composite specimen and fixture

Finally, the complete assembly (joint specimens along with fixture) was clamped in the Zwick Roell make UTM machine having a capacity of 10 kN and tested under tensile load with a crosshead speed of 2 mm/min. The UTM setup along with the fixture and specimen is shown in Fig. 2.6.

2.5 Numerical analysis

In the present work, a ANSYS software was utilized to perform numerical analysis on the joint composite specimens. The progressive damage analysis was conducted using Hashin damage criteria along with characteristic curve method for prediction of failure. The models for joint composite specimens were designed in geometry section of static structural module. The properties of the composite laminates obtained through characterization were added in the design module.

Table 2.6 Specifications of the different parts of the fixture

Components	**Dimension/Size (mm)**	**Material properties**
Steel plates	Length = 120 Width = 24 Thickness = 5	*Stainless steel (SS 304):* Density= 8 g/cm^3 Tensile strength= 515-750 MPa Tensile modulus= 193 GPa Yield strength= 205 MPa
Bolts	M4, Diameter = 4	*Alloy steel:* Tensile strength= 19,0000 psi Yield strength= 17,0000 psi
Washers	Internal diameter = 4.3 External diameter = 9 Thickness = 0.8	*Stainless steel (SS 304):* Density= 8 g/cm^3 Tensile strength= 515-750 MPa Tensile modulus= 193 GPa Yield strength= 205 MPa

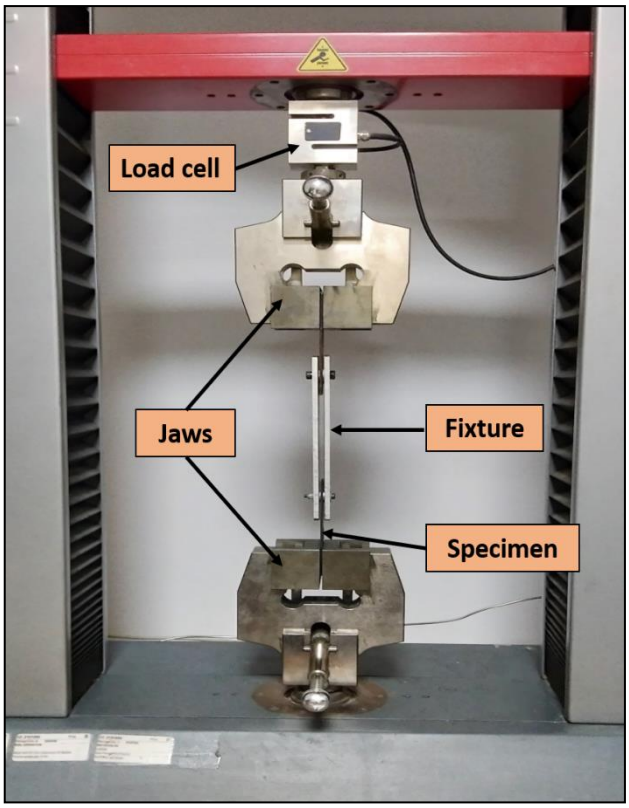

Fig. 2.6 UTM machine setup along with fixture assembly

2.6 Closure

The present chapter gave the details of materials used, different curing methods for preparation of composite laminates and their respective characterization/testing procedures. The composite laminates were prepared using thermal curing process and EB curing process with and without the addition of MWCNTs nanofiller. The evaluation procedure of mechanical joint was discussed under the effect of different geometric parameters and under different environmental aging conditions.

In the next chapter, the optimization of MWCNTs nanofiller content in the carbon fiber/epoxy composite laminates was studied.

Chapter 3
Optimization of MWCNTs Nanofiller Content

The addition of nanofillers in the FRP composite enhances the mechanical properties due to effective stress transfer between the stiff nanofillers and soft polymer matrix through refined polymer/nanofiller interface and improved interfacial bond strength [51-54]. In the present work, the MWCNTs nanofiller was added into the carbon fiber/epoxy composites prepared from two different curing processes. The optimization of wt.% of MWCNTs in the composites was carried out to reduce the overall manufacturing cost and time.

3.1 Optimization of MWCNTs content

The amount of MWCNTs, varying from 0 to 0.5 wt.%, was added into the epoxy resin and composite laminates were prepared using the methods described in section 2.2. From the prepared composite laminates, the tensile specimens were prepared as per ASTM D3039 standard. The tensile test has been performed on the Zwick Roell UTM machine of 100 kN load cell at crosshead speed of 2 mm/min. Five specimens of each configuration were tested and the average results of tensile properties are plotted in Fig. 3.1.

The tensile strength of nanocomposite specimens increased up to 0.3 wt.% of MWCNTs and decreased thereafter, as can be seen in Fig. 3.1. With the addition of 0.3 wt. % of MWCNTs, the tensile strength of the composite specimen increased by 15.43% as compared to that of neat composite specimen. The improved interfacial bonding initiates the effective stress shifting between MWCNTs and the polymer matrix that helps in increasing the average tensile strength of MWCNTs added composite specimens. The nano dimension of MWCNTs facilitates a high specific surface area that supports the formation of a large interfacial region in composite materials. Large epoxy/MWCNTs interfacial area reduces the interfacial stress concentration and allows stress transfer from the matrix to the MWCNTs [57]. This enables MWCNTs modified composites to sustain higher stress, hence increases its strength. Also, the addition of MWCNTs produces a bridging effect at the epoxy matrix/fiber interface which gives a higher frictional coefficient. Further, beyond 0.3 wt. % of MWCNTs content, the reduction in tensile strength indicates towards the ability of MWCNTs to form agglomerates which continues to grow as stress concentration sites and also affects the specific surface area.

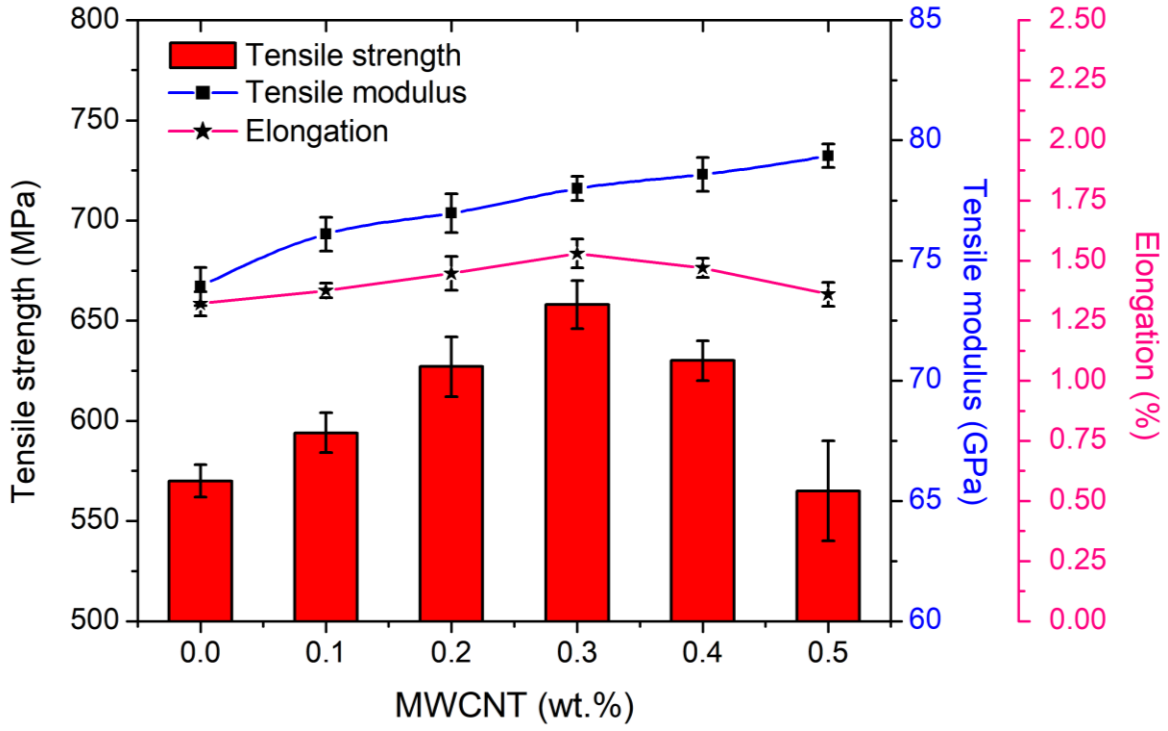

Fig. 3.1 Tensile properties of EB cured carbon fiber/epoxy nanocomposite

The tensile modulus property (from Fig. 3.1) reveals that the modulus values continue to increase with addition of MWCNTs from 0 to 0.5 wt.%. The improvement in tensile modulus attributed to the enhancement of stiffness properties and effective stress transfer between the stiff MWCNTs and epoxy matrix [57].

The percentage elongation (tensile strain at break) also increased by 15.90% with 0.3 wt.% addition of MWCNTs in the composite specimen (Fig. 3.1). The presence of MWCNTs nanofiller ahead of the crack-tip in the carbon/epoxy composites hampers the crack propagation rate. At the same time, the crack bridging by MWCNTs and nanotubes pull out may have also enhanced the toughness of the material [192]. These are the prime factors for enhancing the toughness of 0.3 wt.% of MWCNTs added composites as confirmed from percentage elongation in Fig. 3.1. Hence 0.3 wt. % of MWCNTs addition in the carbon fiber/epoxy composites not only makes it stiffer, stronger but also toughens the material, broadening its area of application. In support of tensile results, the compressive strength, shear strength and flexural strength of the composite material were also evaluated as per ASTM standards D790, D695 and D732, respectively and are summarized in Table 3.1.

To ensure the dispersion behavior of MWCNTs in acetone solvent, sedimentation experiment was performed [188] in vials, as shown in Fig. 3.2. The dispersion behavior is demonstrated with the addition of 0.3 wt. % of MWCNTs in acetone. Figure 3.2 (a) shows

the addition of 0.3 wt.% of MWCNTs to acetone, which is settled at the bottom in entangled form without homogenization and sonication process. After the process of homogenization (at 6000 rpm for 30 minutes) followed by ultrasonication (for 60 min) used in the present work, the MWCNTs was completely homogenized into the acetone which is shown in Fig. 3.2 (b). To ensure the homogenized dispersion, the sample was placed into vials and subsequently left standing for 48 hours. In Fig. 3.2 (c), uniform and stable black dispersion are clearly visible that shows there is no change in the dispersion behavior of the mixture even after 48 hours.

Table 3.1 Mechanical properties of EB cured carbon fiber/epoxy composite laminates

Properties	**Symbol (Units)**	**Neat**	**With MWCNTs (wt.%)**				
			0.1	0.2	0.3	0.4	0.5
Tensile modulus (longitudinal)	E_1 (GPa)	73.92 ± 0.80	76.10 ± 0.70	76.97 ± 0.80	78.00 ± 0.50	78.58 ± 0.70	79.36 ± 0.50
Tensile modulus (transverse)	E_2 (GPa)	73.92 ± 0.80	76.10 ± 0.70	76.97 ± 0.80	78.00 ± 0.50	78.58 ± 0.70	79.36 ± 0.50
Tensile strength (longitudinal)	A_T (MPa)	570 ± 13	594 ± 10	627 ± 15	658 ± 12	630 ± 10	565 ± 25
Tensile strength (transverse)	B_T (MPa)	570 ± 13	594 ± 10	627 ± 15	658 ± 12	630 ± 10	565 ± 25
Compressive strength (longitudinal)	A_C (MPa)	287 ± 12	309 ± 07	327 ± 08	345 ± 09	330 ± 12	297 ± 16
Compressive strength (transverse)	B_C (MPa)	287 ± 12	309 ± 07	327 ± 08	345 ± 09	330 ± 12	297 ± 16
Shear strength	S (MPa)	113 ± 04	123 ± 05	131 ± 03	140 ± 05	122 ± 04	107 ± 07
Flexural strength (longitudinal)	A_F (MPa)	820 ± 10	865 ± 13	910 ± 15	970 ± 15	890 ± 20	830 ± 18
Flexural strength (transverse)	B_F (MPa)	820 ± 10	865 ± 13	910 ± 15	970 ± 15	890 ± 20	830 ± 18

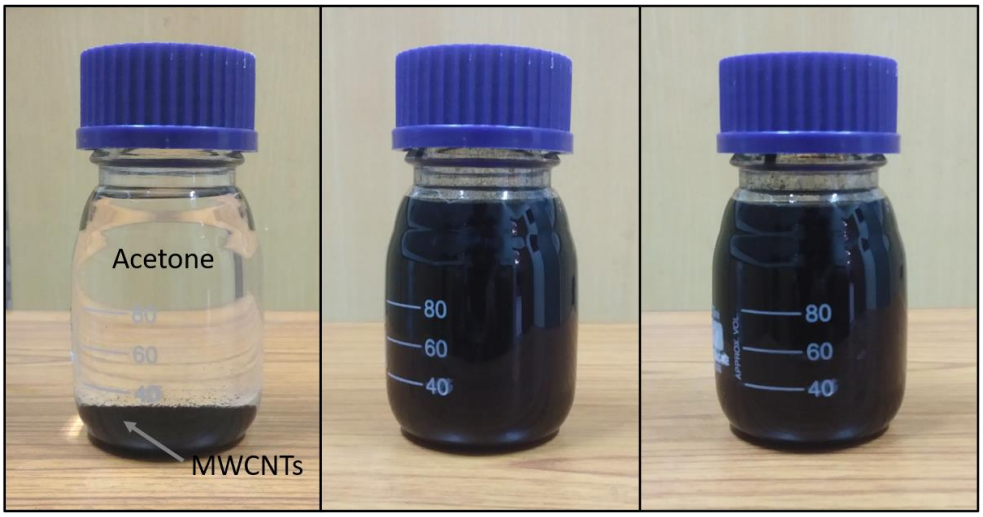

(a) Without homogenization and sonication

(b) Just after homogenization and sonication

(c) 48 h after homogenization and sonication

Fig. 3.2 Dispersion behavior of MWCNTs with sedimentation experiment

Figure 3.3 shows the FESEM images of the MWCNTs content in the composite materials. The MWCNTs nanofiller are shown in Fig. 3.3 (a)-(d). As can be seen from Fig. 3.3 (c) that the uniform distribution of MWCNTs can be seen in composite with 0.3 wt.% of MWCNTs which justifies its highest tensile strength.

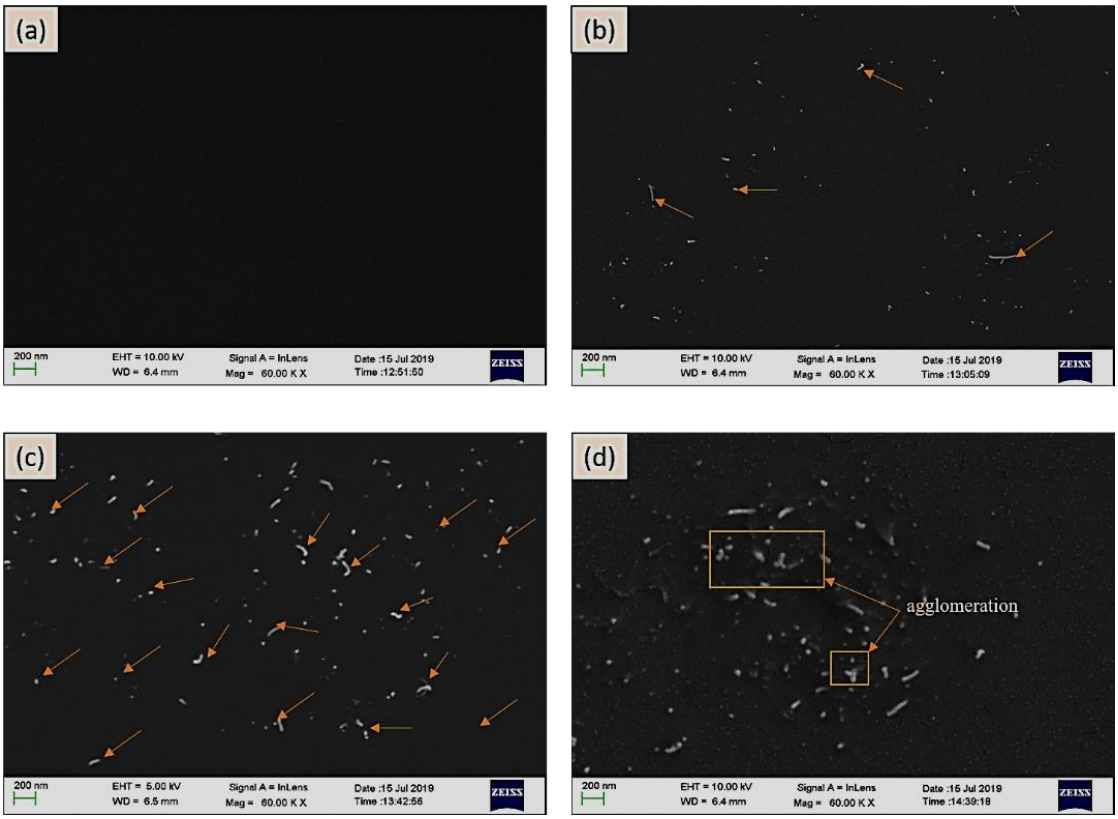

Fig. 3.3 FESEM images of composite (a) Neat, (b) 0.1 wt.% MWCNTs, (c) 0.3 wt.% MWCNTs and (d) 0.5 wt.% MWCNTs configurations

Agglomerates can be seen in the composite specimens with 0.5 wt.% of MWCNTs. So, considering the effect of adding 0.3 wt.% of MWCNTs in the epoxy matrix, studies were conducted on laminates prepared with the addition of 0.3 wt.% of MWCNTs.

3.2 Characterization of composite laminates at optimum wt.% of MWCNTs

The mechanical properties were evaluated for the specimens prepared from thermally cured composite laminates, EB cured (without post curing) composite laminates and EB cured (followed by post curing) composite laminates (Table 3.2). The thermally cured composite specimens have shown the highest mechanical properties.

In EB cured composite specimens, the degree of cure was not achieved upto 100% due to the occurrence vitrification. Because of vitrification, diffusion of the dissociated photoinitiator fragments and polymer chain became increasingly difficult with increase in dose causing a reduction in degree of cure [103]. Furthermore, the increased mechanical properties of EB cured (followed by post curing) composite specimens attributed to improved crosslinking between the epoxy matrix, fibers and the MWCNTs nanofiller [41]. Inspite of that, the advantages of EB curing such as less curing time, environment friendly nature (no hardener), processing complex structure, high controllability, implementation in mass production etc. [88], interestingly consents to further investigations on EB cured (followed by post curing) composite laminates.

3.3 Closure

This chapter presented the results on the mechanical properties of the composite laminate with the addition of MWCNTs content varying from 0.1 to 0.5 wt.%. The optimum content of nanofiller was found to be 0.3 wt. %.

In the next chapter, the effect of different geometric parameters was studied on the single hole pin joint prepared from EB cured (followed by post curing) composite laminate with neat and 0.3 wt.% of MWCNTs added specimens.

Table 3.2 Comparison of mechanical properties of nanocomposites

Properties	**Symbol *(Units)***	**Thermally cured (± SD) ***		**EB cured (without post curing) (± SD) ***		**EB cured (followed by post curing) (± SD) ***	
		Neat	**0.3 wt.% of MWCNTs**	**Neat**	**0.3 wt.% of MWCNTs**	**Neat**	**0.3 wt.% of MWCNTs**
Tensile modulus (longitudinal)	E_1 *(GPa)*	77.85 ± 0.70	81.67 ± 0.50	68.26 ± 0.70	72.10 ± 0.50	73.12 ± 0.80	78.00 ± 0.50
Tensile modulus (transverse)	E_2 *(GPa)*	77.85 ± 0.70	81.67 ± 0.05	68.26 ± 0.70	72.10 ± 0.50	73.12 ± 0.80	78.00 ± 0.50
Tensile strength (longitudinal)	A_T *(MPa)*	606 ± 10	680 ± 08	535 ± 15	632 ± 14	570 ± 13	658 ± 12
Tensile strength (transverse)	B_T *(MPa)*	606 ± 10	680 ± 08	535 ± 15	632 ± 14	570 ± 13	658 ± 12
Compressive strength (longitudinal)	A_C *(MPa)*	315 ± 15	371 ± 15	250 ± 11	324 ± 12	287 ± 12	345 ± 09
Compressive strength (transverse)	B_C *(MPa)*	315 ± 15	371 ± 15	250 ± 11	324 ± 12	287 ± 12	345 ± 09
Shear strength	S *(MPa)*	125 ± 05	153 ± 06	100 ± 06	129 ± 07	113 ± 04	140 ± 05
Flexural strength (longitudinal)	A_F *(MPa)*	878 ± 09	1022 ± 08	760 ± 12	910 ± 10	820 ± 10	970 ± 15
Flexural strength (transverse)	B_F *(MPa)*	878 ± 09	1022 ± 08	760 ± 12	910 ± 10	820 ± 10	970 ± 15
Elongation	*%*	1.36 ± 0.04	1.44 ± 0.03	1.10 ± 0.01	1.34 ± 0.01	1.32 ± 0.05	1.53 ± 0.06
Total curing time	*h, mins*	34 h – 40 h		4 mins – 40 mins		2 h, 4 mins – 2 h, 40 mins	

***SD = Standard deviation**

Chapter 4
Investigations on Single Pin Joint Composites

In any structural component made of FRP composites, the joints are the weakest portion of that component. So, it is necessary to investigate the behavior of joints to achieve the maximum load-carrying capacity. The studies have been performed on the pin joints prepared from carbon fiber/epoxy composite laminates for improvement in failure loads and failure modes by incorporating MWCNTs nanofiller. The investigations were carried out on neat and optimized 0.3 wt.% of MWCNTs added composite materials prepared using two different processes *i.e.,* thermal curing and EB curing process. The single pin joint configurations were prepared using geometric combinations of width to diameter (W/D) ratio and edge to diameter (E/D) ratio, both varying from 2 to 5. The numerical analysis was performed using Hashin damage criteria [193] along with progressive damage analysis to compare the predicted failure loads with the experimental results.

4.1 Single pin joint configurations

In the present work, the single pin joint configuration consisted of a rigid pin inserted into the carbon/epoxy composite specimens having a length (L), thickness (t), width (W) and hole diameter (D=4 mm), as shown in Fig. 2.3.

The circular hole of 4 mm diameter was positioned along the centreline from the free edge at edge length, E. A uniformly distributed and gradually increasing load was given to the composite specimen and a stationary pin counter this load. No bending stresses occurred due to tensile loading as the load was in the longitudinal direction of the specimen and the plate was geometrically symmetric from both sides of the hole.

The geometrical parameters, W/D and E/D ratios, were varied from 2 to 5, in the neat and 0.3 wt.% of MWCNTs added composite joint specimens. The specimens were prepared using EB curing and thermal curing processes. The different combinations of geometric parameters are given in Table 4.1.

4.2 Testing of pin joints

The influence of different geometric parameters along with the addition of MWCNTs on the bearing performance of pin joint specimens was evaluated under tensile loading on Zwick Roell make UTM machine with a capacity of 10 kN. The testing setup used for evaluating the failure loads of the pin joints is shown in Fig. 2.4. While testing the joint, the test setup was calibrated and considered symmetric for applied load with no out of plane forces.

Table 4.1. Joint parameters with W/D and E/D ratios

S.No.	Hole diameter, D (mm)	Ratios		W (mm)	E (mm)
		W/D	E/D		
1	4	2	2	8	8
2	4	2	3	8	12
3	4	2	4	8	16
4	4	2	5	8	20
5	4	3	2	12	8
6	4	3	3	12	12
7	4	3	4	12	16
8	4	3	5	12	20
9	4	4	2	16	8
10	4	4	3	16	12
11	4	4	4	16	16
12	4	4	5	16	20
13	4	5	2	20	8
14	4	5	3	20	12
15	4	5	4	20	16
16	4	5	5	20	20

To initiate the test, the rigid pin was inserted into the drilled hole and the load was applied onto it through a steel fixture gripped in the movable upper jaw of the UTM machine. The other end of the joint specimen was gripped in the fixed lower jaw of the UTM machine. The load vs. displacement curves were obtained with a crosshead speed of 2 mm/min that applied a gradually increasing load with gear arrangements and electric motor with no backlash. The force values were derived from the load cell and displacement values were obtained from crosshead travel. Five specimens of each joint configurations were tested and evaluated for their average ultimate failure loads.

4.3 Numerical analysis

In the fibrous composite material, the structural component goes through several local damages before it loses its complete mechanical strength. The ultimate failure in the composite material is considered as the complete loss in the different segments of the composite material. The progressive damage analysis using Hashin damage criteria was applied for the prediction of damage evolution and damage initiation. Ansys software was utilized to design a model of the desired joint configuration. The initial values of mechanical

properties for the material were taken as given in Table 3.2. The designed numerical model comprises of three important stages: analysis of stress, failure criteria and the degradation rules. These were combined to generate a progressive damage model which is given by the algorithm [194] shown in Fig. 4.1.

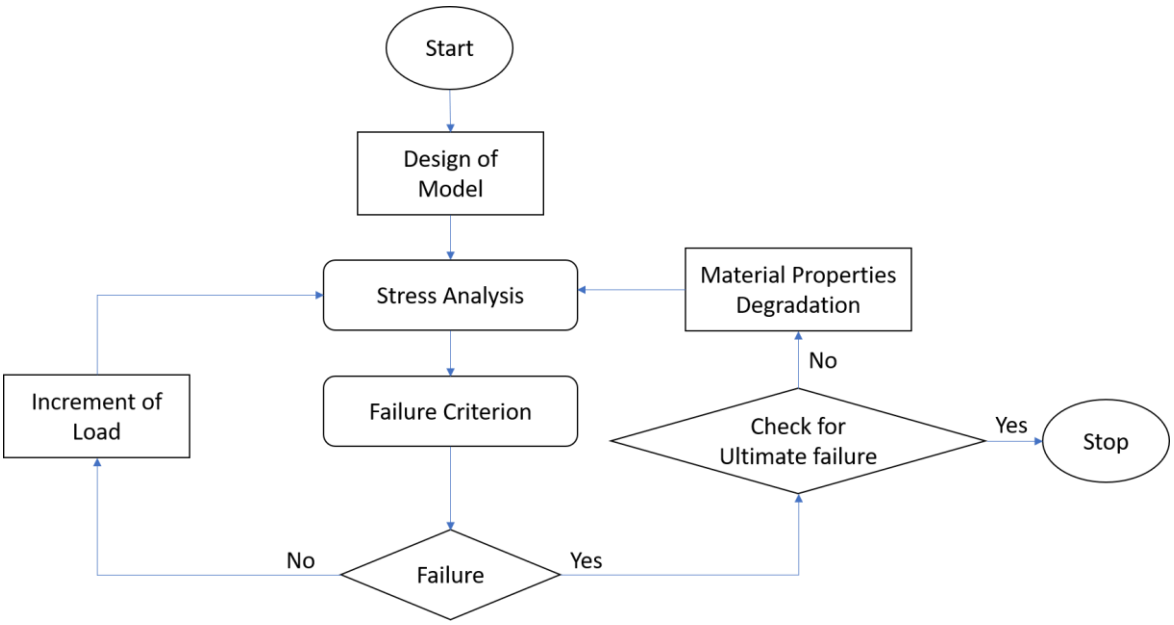

Fig. 4.1 Algorithm for the progressive damage analysis of composite pin joints [194]

The appropriate boundary conditions and gradually increasing bearing force was applied to the modelled specimen. This applied load increases gradually until the first damage occurred in the specimen. Later on, the property of the damaged composite material degrades according to the damage evolution law. According to this law, the load transferred to other elements of the specimen may or may not show the specific increment in the bearing load. The increase in load shows the load-bearing capacity of that element in the specimen and the decrease shows that further damage occurred in the other element. This iteration proceeds further until the failure index (FI) value exceeds 1 which signifies the complete rapture of the material.

The different joint configurations (with varying W/D and E/D ratios) of neat and MWCNTs added composite materials were made in ANSYS modeler and then imported to ANSYS ACP Pre-module where ply definition was given to the composite specimen. In the design, twelve layers of woven carbon fiber were stacked together and simulated.

To conduct a progressive damage analysis in the composite joints, the Hashin failure criterion was used. The material properties of that element are degraded where the failure mechanism occurs [195]. The Hashin damage criterion works upon the four failure

equations for fiber and the matrix. Table 4.2 shows the failure criterion and their corresponding equations along with the reduced material properties.

Table 4.2 Hashin damage failure criterion and associated degradation rule [193]

Failure criterion	**Equations**	**Reduced material properties**
Tensile failure in fiber ($\sigma_1 \geq 0$)	$\left(\frac{\sigma_1}{A_t}\right)^2 + \left(\frac{\tau_{12}}{S}\right)^2 = 1$	$E_1, \upsilon_{12}, \upsilon_{21} \rightarrow 0$
Compression failure in fiber ($\sigma_1 < 0$)	$\frac{\sigma_1}{A_c} = 1$	$E_1, \upsilon_{12}, \upsilon_{21} \rightarrow 0$
Tensile failure in matrix ($\sigma_2 \geq 0$)	$\left(\frac{\sigma_2}{B_t}\right)^2 + \left(\frac{\tau_{12}}{S}\right)^2 = 1$	$E_2, G_{12}, \upsilon_{12}, \upsilon_{21} \rightarrow 0$
Compression failure in matrix ($\sigma_2 < 0$)	$\left(\frac{\sigma_2}{2S}\right)^2 + \left(\frac{\tau_{12}}{S}\right)^2 + \left[\left(\frac{B_c}{2S}\right)^2 - 1\right]\frac{\sigma_2}{B_c} = 1$	$E_2, G_{12}, \upsilon_{12}, \upsilon_{21} \rightarrow 0$

Here, σ_1 and σ_2 are the stress values in longitudinal and transverse directions, S is the in-plane shear stress, A_t and A_c are the stress limits in tension and compression along the longitudinal direction, B_t and B_c are the stresses in tension and compression along the transverse direction. The present work uses the bidirectional carbon fabric with the same value of stress in longitudinal and transverse direction. So, $A_t = B_t$ and $A_c = B_c$.

The modelled specimen representing the wireframed mesh around the pin hole and the boundary conditions are shown in Fig. 4.2. The mesh density plays an important role in numerical analysis to predict the results. So, on each joint configuration, convergence studies have been done to minimize the effect of mesh density.

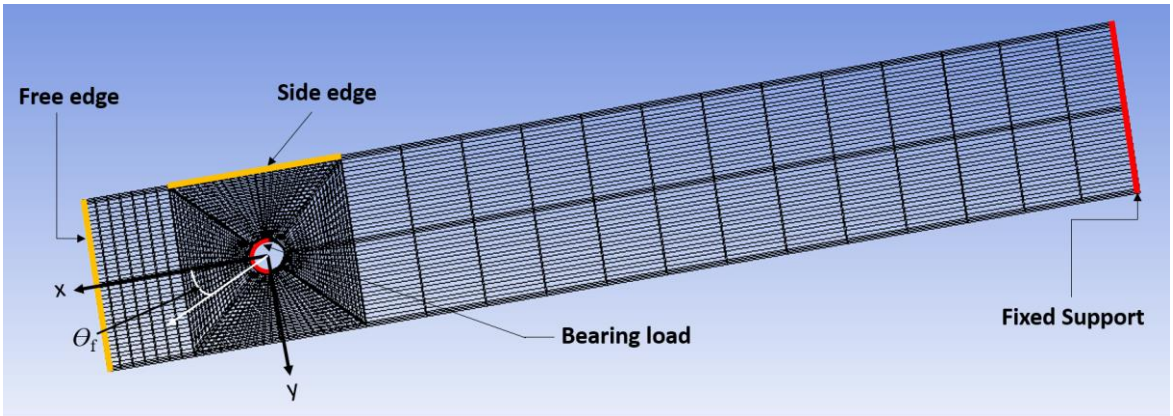

Fig. 4.2 Wireframed mesh around the pin hole showing side edge and free edge.

The results of convergence study from one joint configuration given in Fig. 4.3 show that the error was reduced to less than 2% with variation in the mesh density. In Fig. 4.3, numerically predicted failure load is the quantity utilized to calculate the error. The error is the difference between the previously predicted failure load and the new predicted failure load by increasing the number of elements. The number of elements is increased till the difference between the previously predicted failure load and the new predicted failure load (i.e., error) is approximately less than 2%.

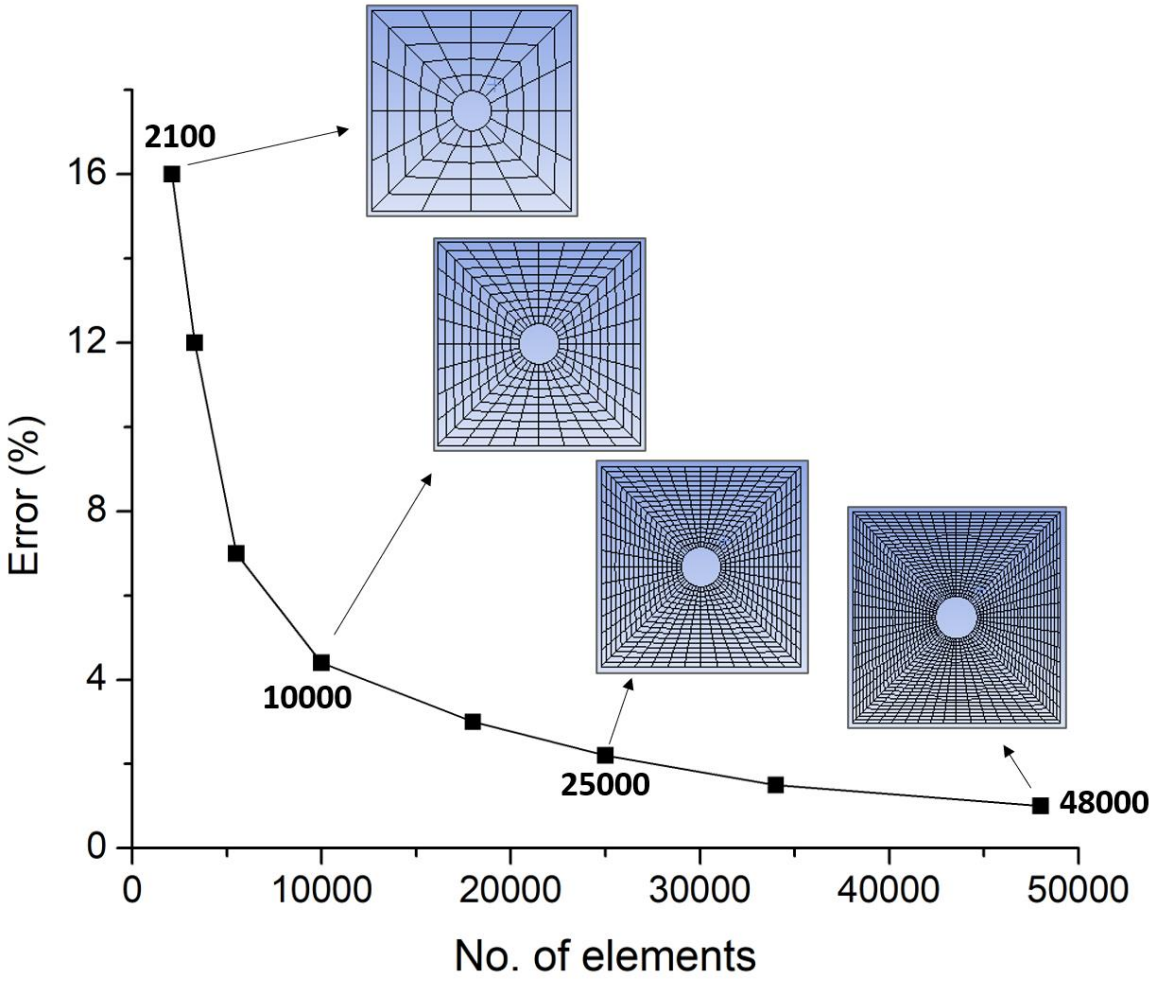

Fig. 4.3 Convergence study on the failure load

4.4 Results and discussion

The following section describes the experimental and numerical results of the pin joint specimens prepared from EB cured and thermal cured composite laminates.

4.4.1 Joints prepared from EB cured composites

4.4.1.1 Experimental results

The failure loads of single pin joint configuration using different geometric parameters for EB cured neat and MWCNTs added carbon fiber/epoxy composite laminates are shown in Fig. 4.4 and 4.5. Five specimens of each joint configuration were tested and average results were plotted in Fig. 4.4 and 4.5.

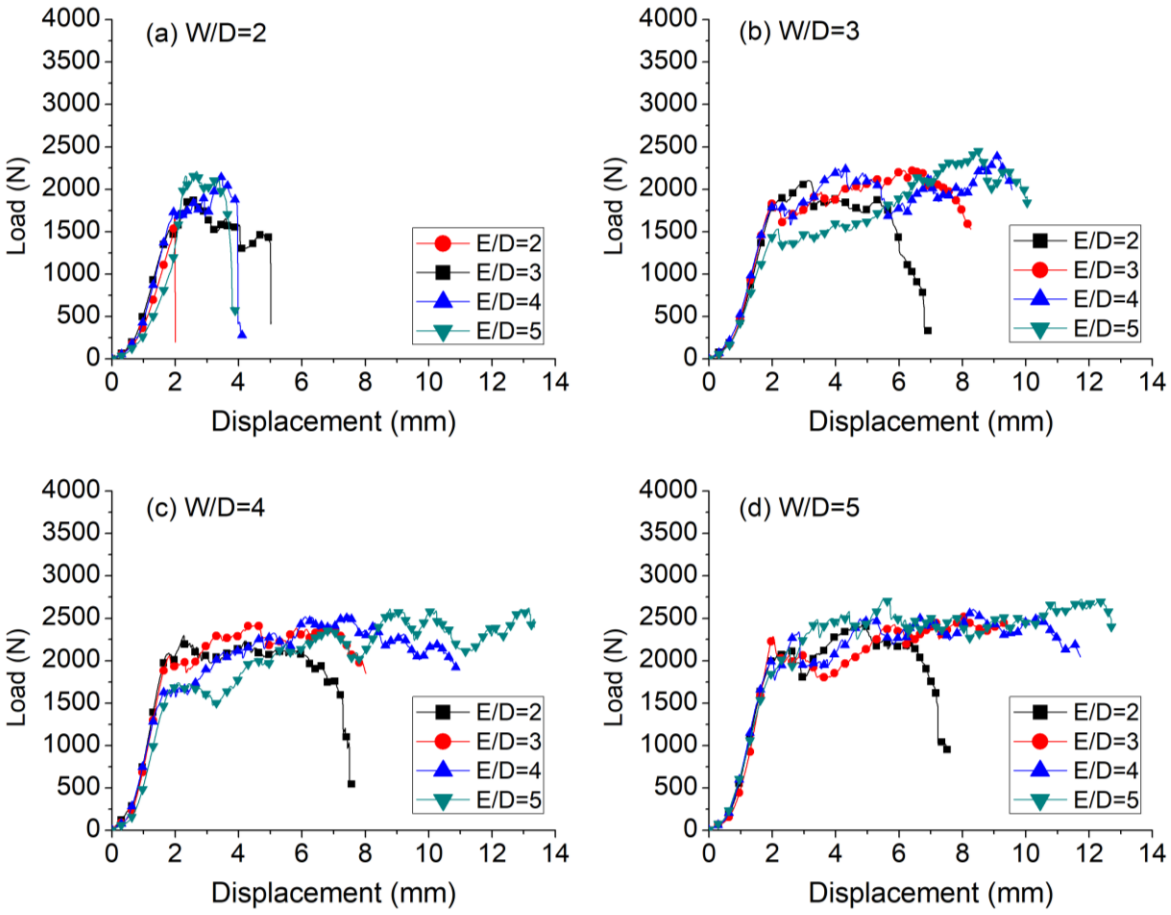

Fig. 4.4 Load vs. displacement graphs for different joint configurations of EB cured neat carbon/epoxy composite laminates under tensile test

Mainly three types of failure modes exist in the failure phenomenon *i.e.*, bearing, shearing and net-tension failure modes [143]. The occurrence of a failure in net-tension and shearing modes is a catastrophic type of failure. Whereas, the bearing mode of failure is not immediate and it follows the progressive damage failure.

From Fig. 4.4 and 4.5, it was observed that the mode of failure depended on the W/D and E/D ratios. By selecting the proper geometrical parameter values, the net-tension and shearing failure modes can be evaded. The bearing (B), shearing (S) and net-tension (N)

modes of failure are easily predicted through load vs. displacement graphs of the composite specimens. The mode of failure which occurs as a sudden reduction in the graph values is a net-tension mode of failure. If the graph shows the dropping of the curve in a zig-zag manner then it represents the shearing mode of failure. However, if the graph shows the curve going forward in a zig-zag manner then it represents the bearing mode of failure.

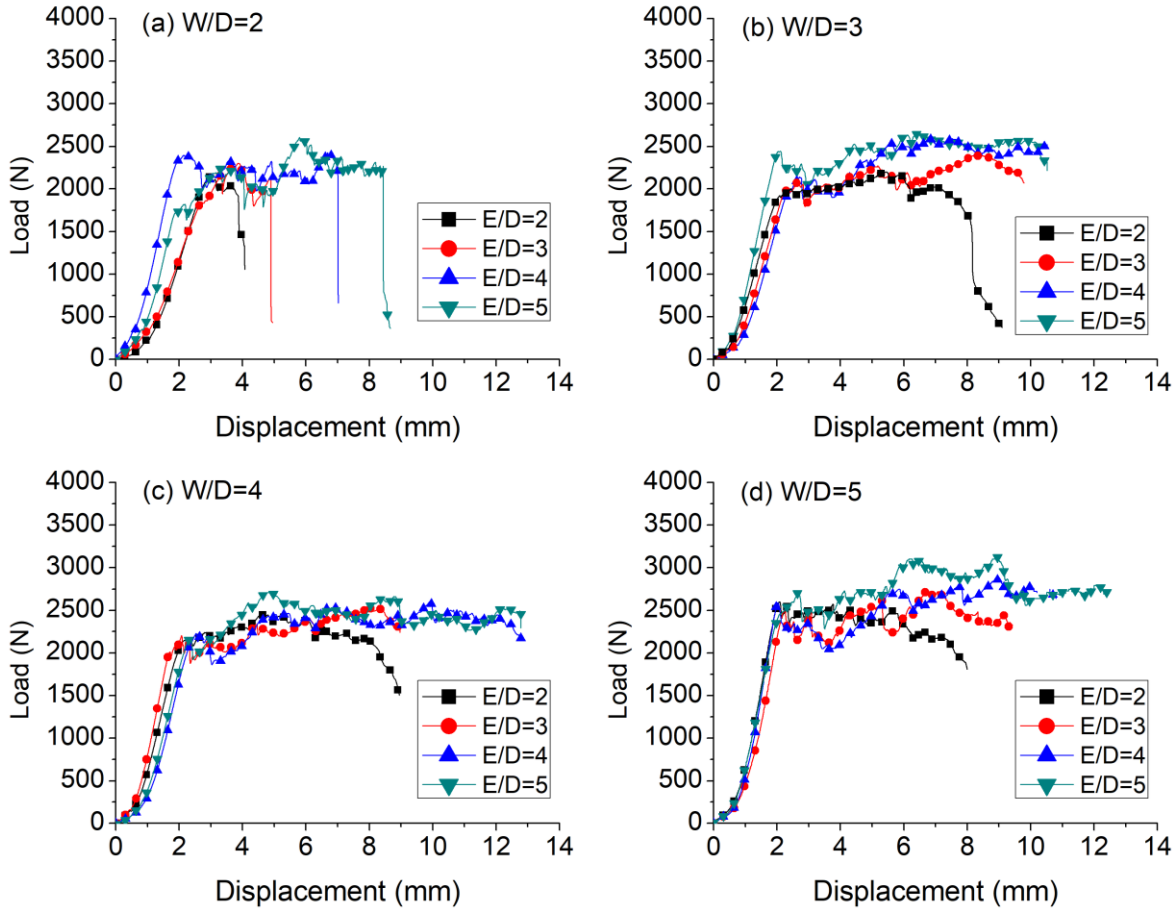

Fig. 4.5 Load vs. displacement graphs for different joint configurations of EB cured 0.3 wt.% of MWCNTs added carbon/epoxy composite laminates under tensile test

The trends in Fig. 4.4 and 4.5 show that at lower W/D and E/D ratios, catastrophic and premature shear mode of failure has occurred. These modes of failure are caused by excessive tensile and shear stresses present at the hole surface area and due to the small margin between the pinhole and side edges. Net-tension and shearing failure modes needs to be avoided by proper design due to their catastrophic failure characteristic. Therefore, the ideal W/D and E/D ratios must be selected to overcome the sudden failures in the pin joints. For higher values of W/D and E/D ratios, the progressive bearing failure mode occurred. Bearing failure mode was caused by compressive stresses that occur due to accumulated delamination damage and micromechanical buckling in the laminate [196].

For neat configuration specimens (Fig. 4.4) it was found that the bearing failure mode occurred for W/D ≥ 3 and E/D ≥ 3, which is desirable for application aspects. This happened because the margin among the pin hole and side edge was very small for W/D=2. So, it failed under net-tension and shear failure modes. Though improvement in failure modes was observed with the addition of MWCNTs in comparison to neat joint specimens as the net-tension and shear failure modes changed to mixed failure modes *i.e.*, bearing followed by net-tension and bearing followed by shearing, at E/D ≥ 3, W/D=2 and W/D≥ 3, E/D=2. These mixed failure modes are enhanced modes than the net-tension and shear failure modes.

Figure 4.5 shows the trends obtained for the MWCNTs added carbon fiber/epoxy composite specimens. It was observed that the value of failure loads for different joint geometries in MWCNTs added specimens were on the higher side than that in neat specimens (Fig. 4.4). The reason being, MWCNTs act as mechanical interlocks between the epoxy matrix and carbon fiber which produces high friction coefficient. The actual images of failed joint specimens after the tensile testing are shown in Fig. 4.6 and their corresponding modes of failure are outlined in Table 4.3.

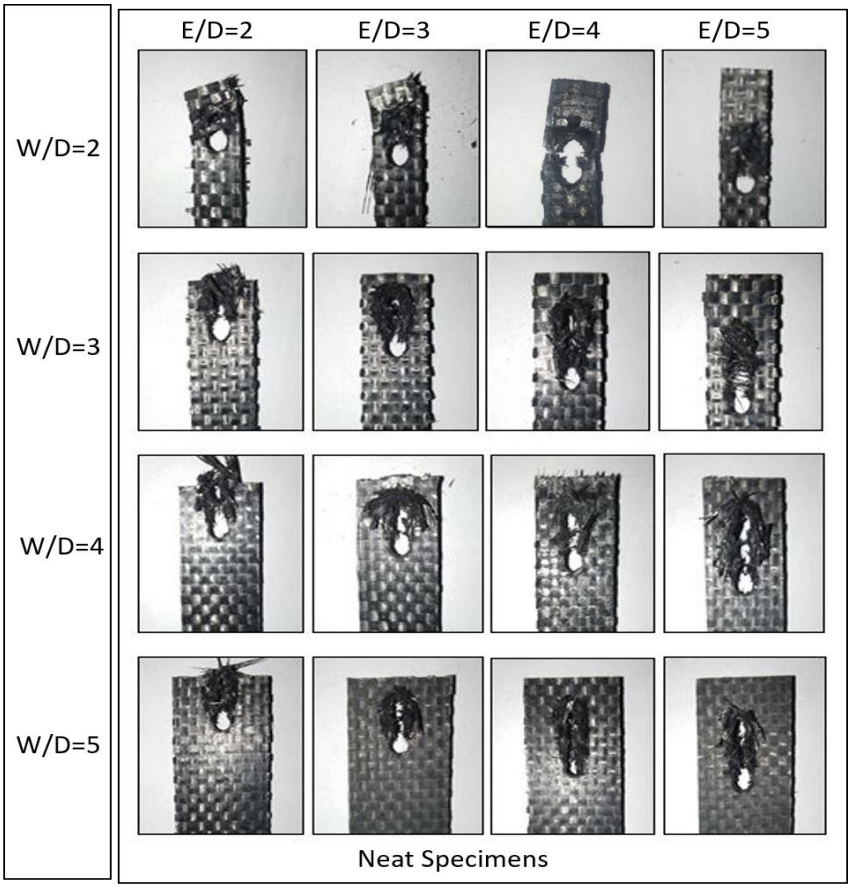

(a)

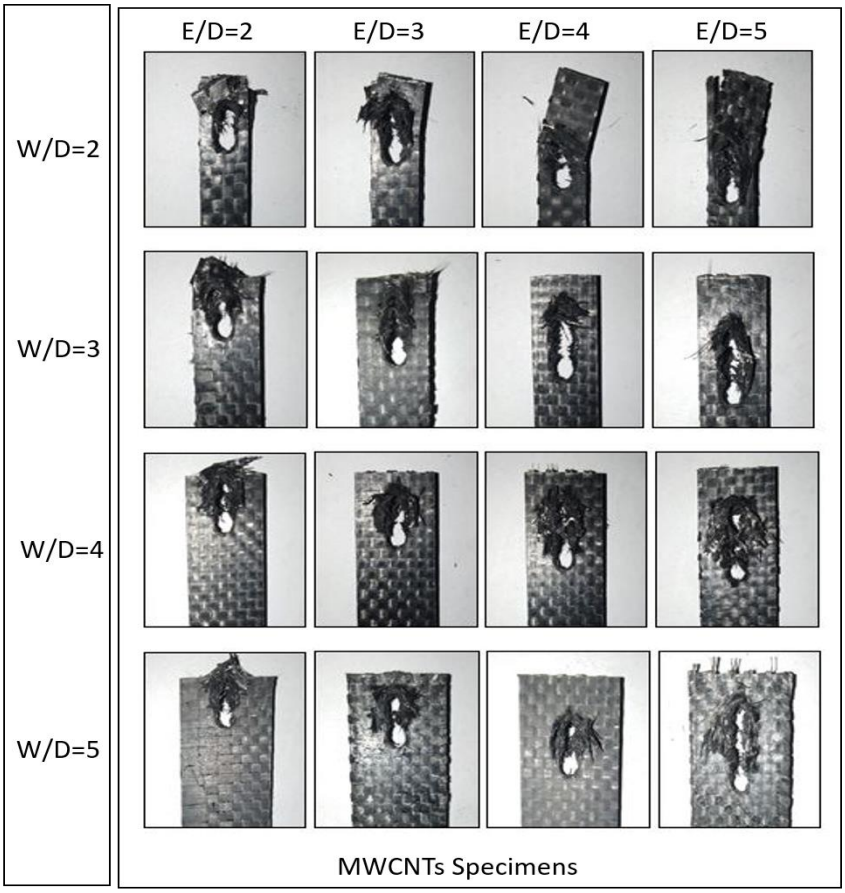

(b)

Fig. 4.6 Actual images of failure modes of EB cured joint carbon fiber/epoxy composites for (a) neat and (b) MWCNTs added configuration

The comparison of the ultimate failure loads for neat and MWCNTs added composite joints at different geometric parameters are shown in Fig. 4.7. It was observed that with increasing W/D and E/D ratios, the ultimate failure load values increased.

The maximum improvement in ultimate failure load of 26.6% was found in pin joint specimen configured at W/D= 2 and E/D= 2 (failure under net-tension mode), with the addition of MWCNTs. The ultimate failure load was increased up to 14.3% in pin joint specimen configured at W/D=5 and E/D=5 (failure under bearing mode) with the addition of MWCNTs. The enhancement of failure loads by the addition of MWCNTs into the matrix is due to the increased interfacial bond strength and the efficient stress transfer between the stiff MWCNTs and soft polymer matrix through refined polymer/MWCNTs interface, which helps in achieving higher failure loads.

Table 4.3 Experimentally obtained failure modes and failure loads for EB cured carbon fiber/epoxy composite pin joints

S.No.	Hole diameter D (mm)	W/D ratio	E/D ratio	Composite materials			
				Neat		MWCNTs	
				Failure mode	***Failure load (N)***	***Failure mode***	***Failure load (N)***
1	4	2	2	N	1690	N	2140
2	4		3	N	1900	B→N	2300
3	4		4	N	2150	B→N	2420
4	4		5	B→N	2210	B→N	2600
5	4	3	2	S	2100	B→S	2200
6	4		3	B	2250	B	2400
7	4		4	B	2390	B	2590
8	4		5	B	2450	B	2650
9	4	4	2	S	2300	B→S	2450
10	4		3	B	2430	B	2530
11	4		4	B	2540	B	2600
12	4		5	B	2620	B	2710
13	4	5	2	S	2430	B→S	2600
14	4		3	B	2520	B	2730
15	4		4	B	2610	B	2870
16	4		5	B	2730	B	3120

4.4.1.2 Numerical results

For the numerical prediction of failure modes and failure loads, a progressive damage analysis was performed with the use of Hashin failure criteria on the collective damage of all the layers of the pin joint specimen. In each joint specimen, a ramped bearing load was applied onto the hole edge in the longitudinal direction, as shown in Fig. 4.2.

The failure modes were estimated based on Θ_f, the angle of the first failure node. The bearing mode is considered if Θ_f lies between 0^o to 15^o, the shearing mode is considered if Θ_f lies between 30^o to 60^o and the net-tension mode is considered if Θ_f lies between 75^o to 90^o. The net-tension, shearing and bearing modes of failure from EB cured composite specimens for random joint configurations are shown in Fig. 4.8, 4.9 and 4.10. These figures concentrate on the hole with the free edge and the side edge for demonstrating different types of failure modes without showing the full length of joints. The cumulative damage in all layers of the composite specimen is shown in these figures. As given by Hashin failure criteria, some of the elements failed due to matrix compression, while some failed due to fiber tension. The

higher mesh density makes it difficult to mention the type of failure in each of the individual elements.

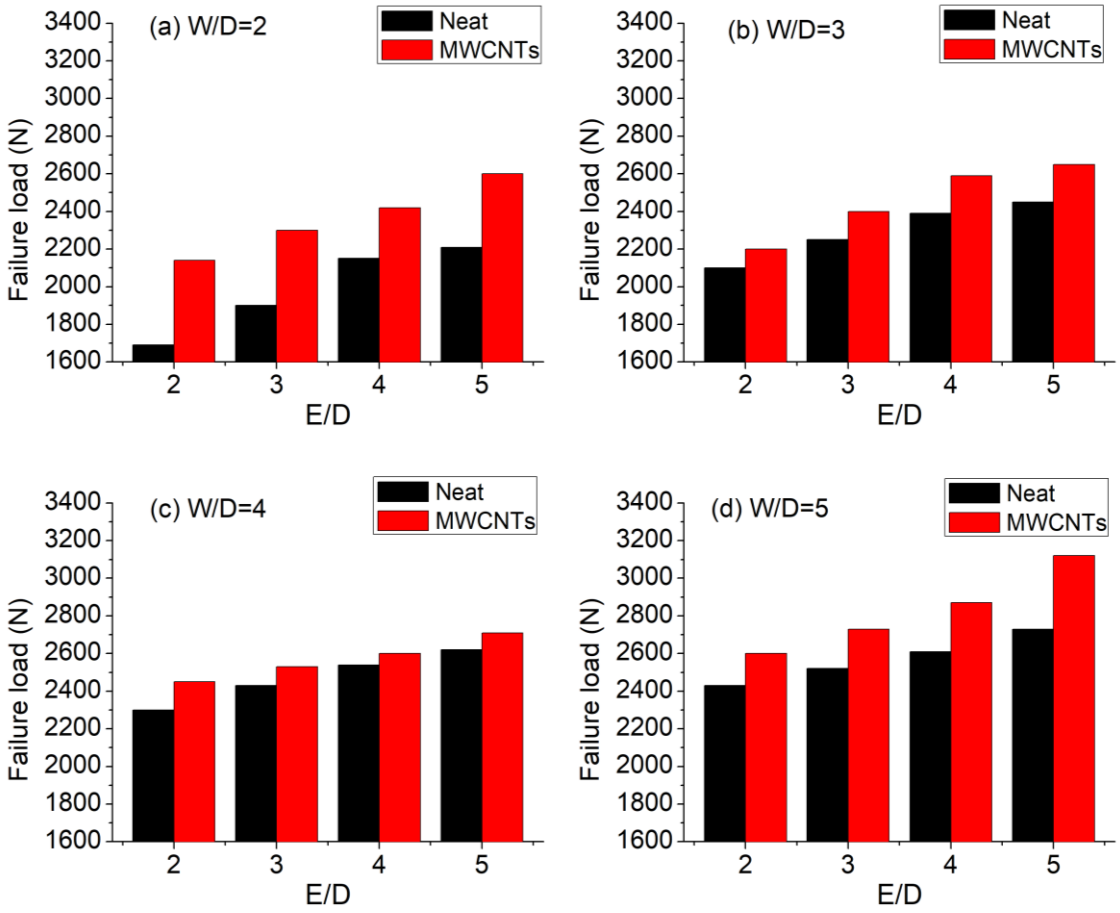

Fig. 4.7 Ultimate failure loads for EB cured neat and MWCNTs added composite joint specimens at (a) W/D=2, (b) W/D=3, (c) W/D=4 and (d) W/D=5

The joint configuration with geometric parameters of W/D=2 and E/D=4 for neat composite specimen showing the net-tension mode of failure under tensile loading of 3300 N is presented in Fig. 4.8. It can be visualized that the failure progresses firstly near the hole boundary and further spreads in the direction of side edges as the load is increased, resulting the failure in net-tension mode.

The shearing mode of failure occurred for joint configuration with the selected geometric combination of W/D =3 and E/D =2 for neat composite specimen under tensile loading of 3200 N is shown in Fig. 4.9. It can be seen that the damage progresses towards the free edge of the pin joint as the free edge distance is smaller than the side edge from the hole which confirms the shearing mode of failure in the pin joint.

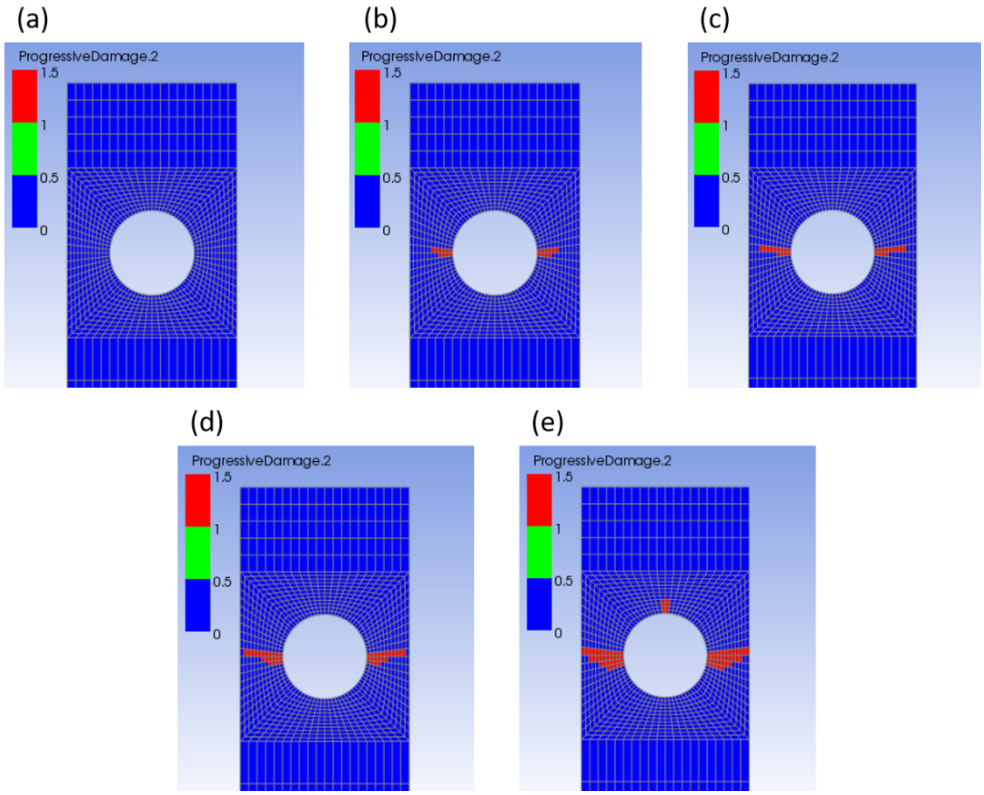

Fig 4.8 Net-tension mode of failure in EB cured neat composite joint for W/D=2 and E/D=4 at applied load of (a) 20%, (b) 40%, (c) 60%, (d) 80% and (e) 100%

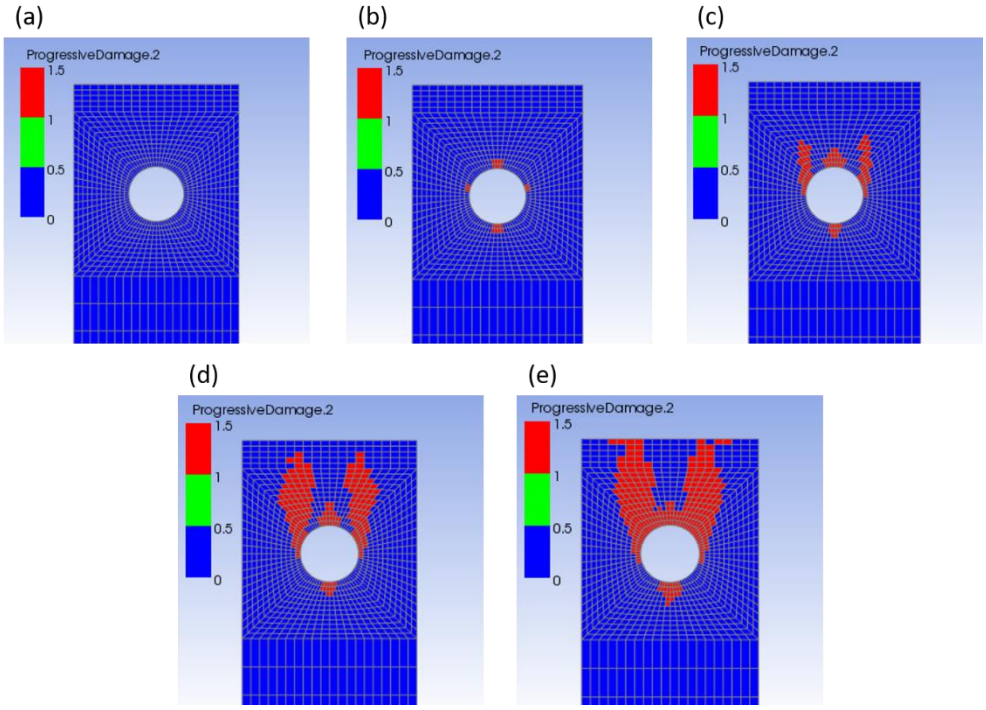

Fig. 4.9 Shearing mode of failure in EB cured neat composite joint for W/D=3 and E/D=2 at applied load of (a) 20%, (b) 40%, (c) 60%, (d) 80% and (e) 100%

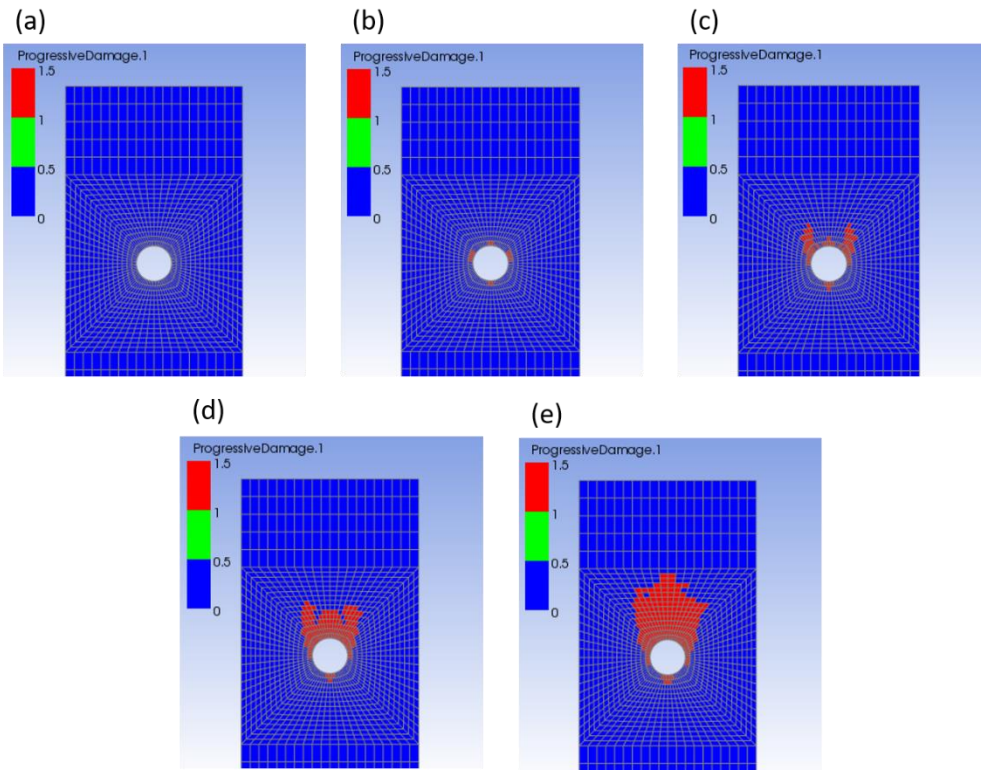

Fig. 4.10 Bearing mode of failure in EB cured MWCNTs added composite joint for W/D=5 and E/D=5 at applied load of (a) 20%, (b) 40%, (c) 60%, (d) 80% and (e) 100%

The experimental results confirmed the bearing mode of failure with increment in W/D and E/D ratios. A similar bearing mode of failure is obtained from the failure analysis for joint configuration with geometric combinations of W/D =5 and E/D =5 for neat composite specimen under tensile loading of 4200 N as shown in Fig. 4.10. The numerically predicted ultimate failure loads with different geometric parameters are plotted in Figure 4.11. Comparing the experimental values of ultimate failure loads with the numerical values, it was observed that the prediction through failure analysis is within 9% of the acceptable difference, which shows the good agreement among the obtained results.

4.4.2 Joints prepared from thermally cured composites

4.4.2.1 Experimental results

Under similar geometric combinations (as used for EB cured composites), the pin joint specimens which were prepared using thermal cured process were tested and results were plotted in Fig. 4.12 and 4.13. In Fig. 4.12, the load vs. displacement graphs of neat composite joint specimens is shown for different W/D and E/D ratios. Similarly, Fig. 4.13 shows the load vs. displacement graphs of MWCNTs composite joint specimens for different W/D and

E/D ratios. These results revealed that the thermal cured composite joint specimens showed higher ultimate failure loads than the EB cured composite joint specimens.

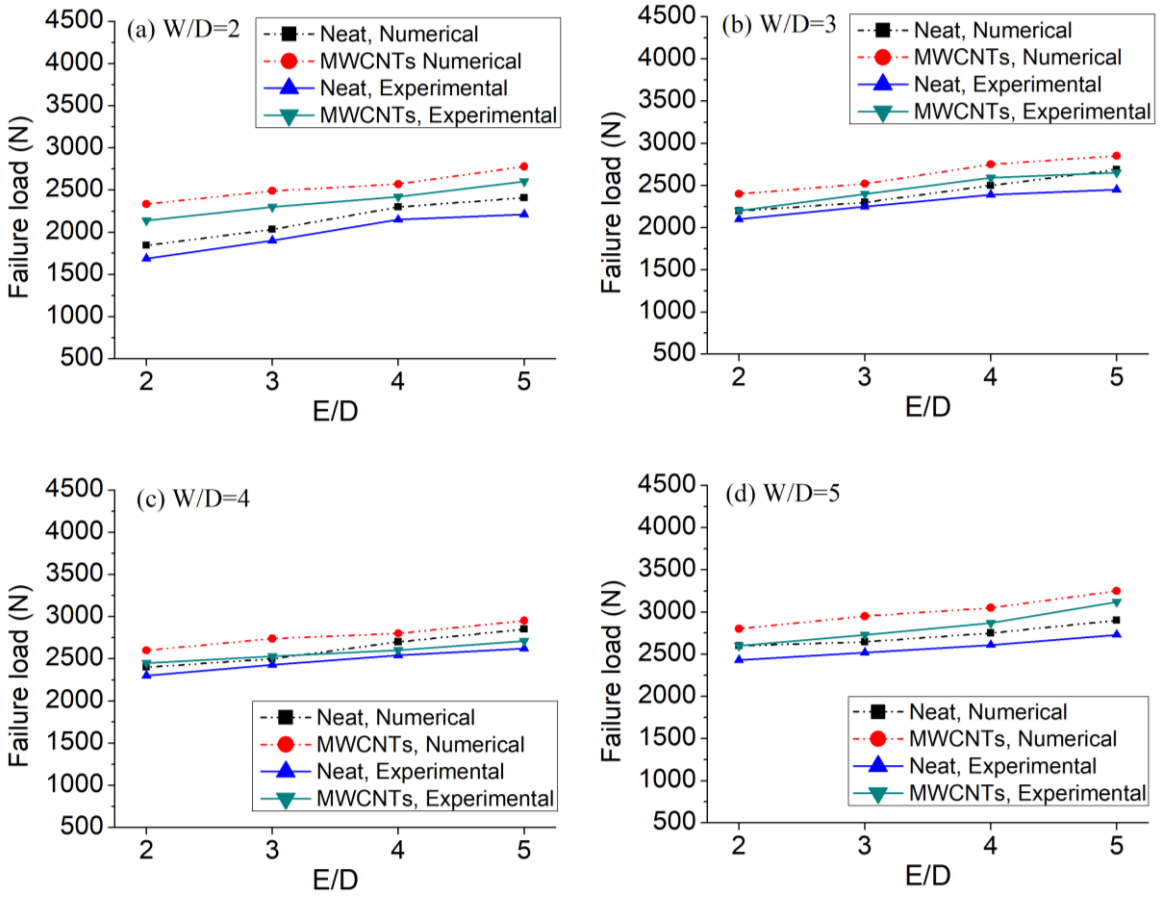

Fig. 4.11 Comparison of failure loads for EB cured neat and MWCNTs added composite specimens

The thermal cured joint specimens had also undergone bearing, shearing and net-tension failure modes. From neat joint specimens in Fig. 4.12, it was found that the bearing failure modes occurred for W/D ≥ 3 and E/D ≥ 3, which were similar to EB cured joint specimens. The improvement in failure modes was observed with the addition of MWCNTs in comparison to neat joint specimens as the net-tension and shear failure modes changed to mixed failure modes *i.e.*, bearing followed by net-tension and bearing followed by shearing, at E/D ≥ 2, W/D=2 and W/D≥ 3, E/D=2.

The different modes of failure obtained for thermally cured neat and MWCNTs added joint specimens are outlined in Table 4.4.

Figure 4.14 shows the comparison of experimentally obtained ultimate failure loads for neat and MWCNTs added composites at different geometric parameters. The maximum improvement in ultimate failure load of 26.34% was found in pin joint specimen configured

at W/D= 2 and E/D= 2 (failure under net-tension mode), with the addition of MWCNTs. The ultimate failure load was increased up to 15.3% in pin joint specimen configured at W/D=5 and E/D=5 (failure under bearing mode) with the addition of MWCNTs.

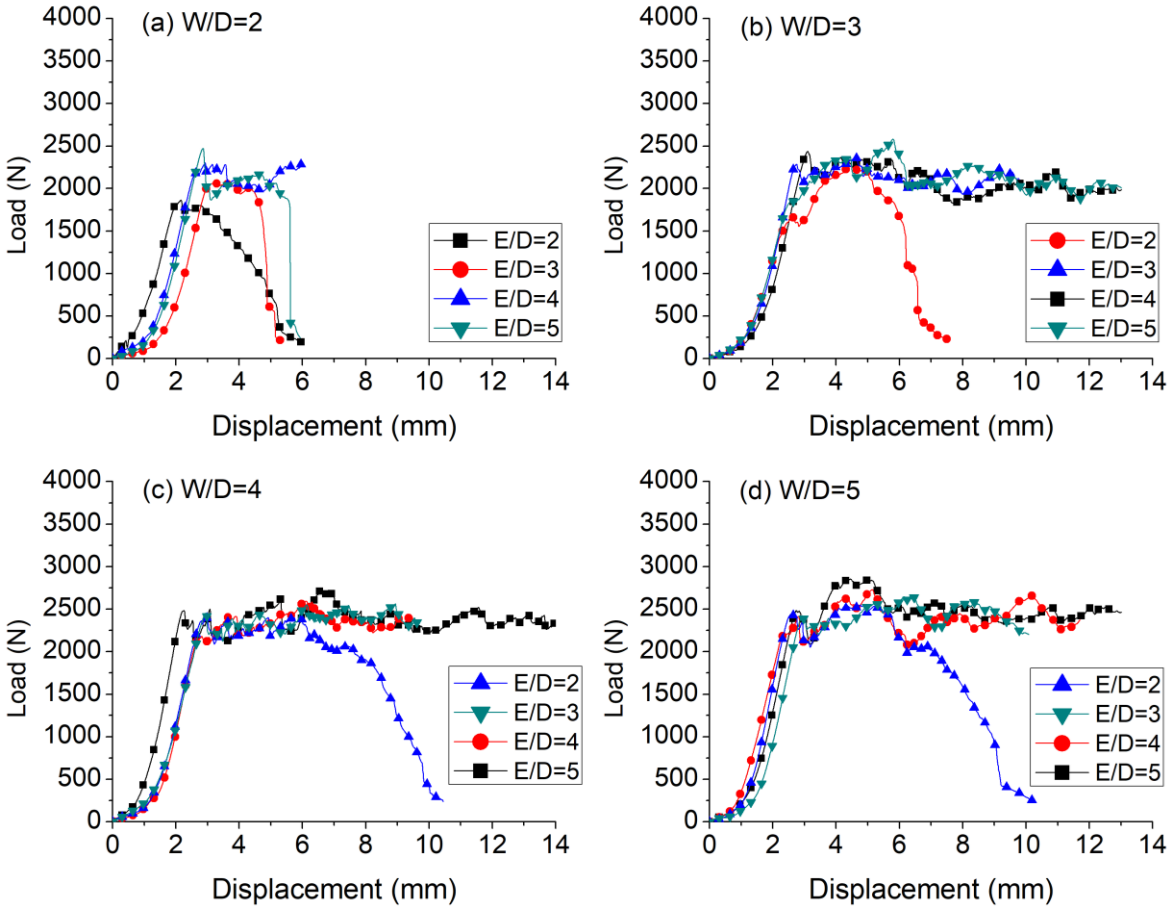

Fig. 4.12 Load vs. displacement graphs for different joint configurations of neat carbon fiber/epoxy composite laminates under tensile test

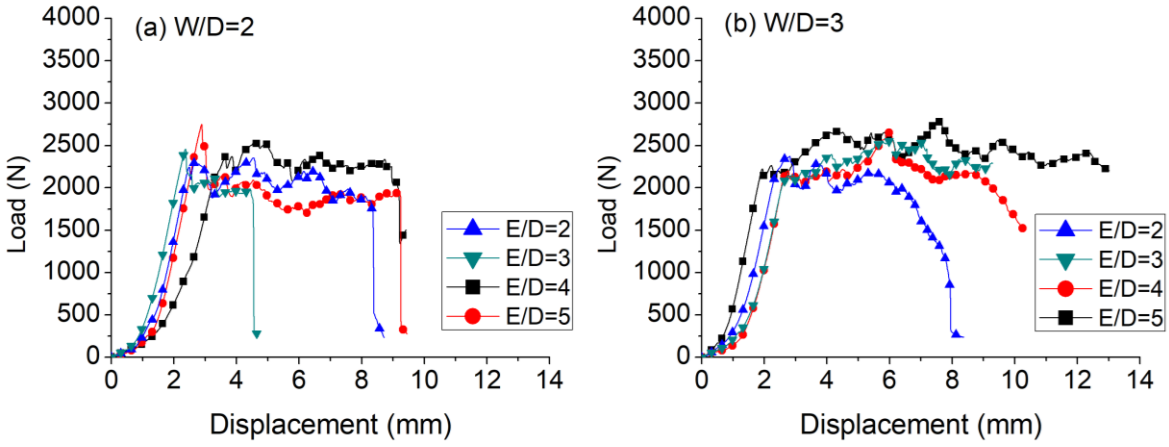

Continued…

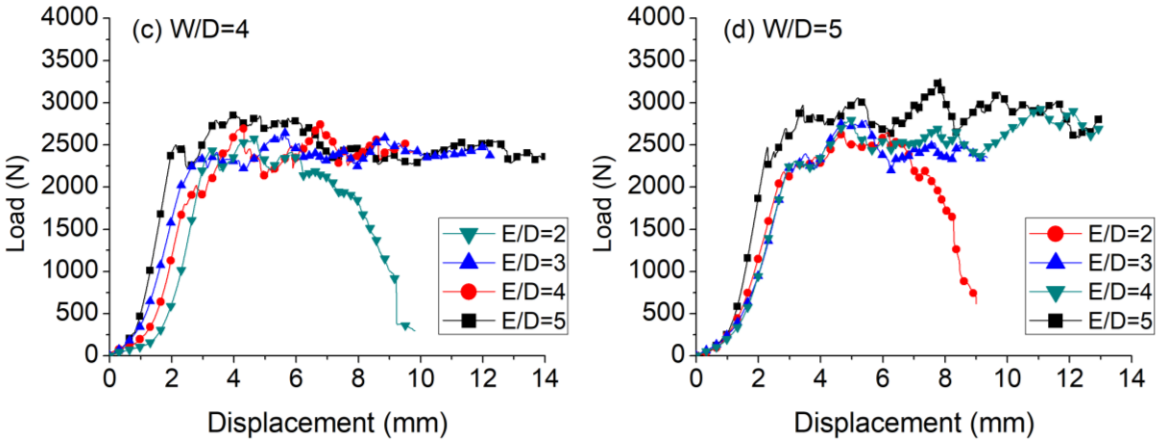

Fig. 4.13 Load vs. displacement graphs for different joint configurations of 0.3 wt.% of MWCNTs added carbon fiber/epoxy composite laminates under tensile test

Table 4.4 Experimentally obtained failure modes and failure loads for thermal cured carbon fiber/epoxy composite pin joints

S.No.	Hole diameter D (mm)	W/D ratio	E/D ratio	Composite materials			
				Neat		MWCNTs	
				Failure mode	*Failure load (N)*	*Failure mode*	*Failure load (N)*
1	4	2	2	S	1860	N	2350
2	4		3	N	2080	B→N	2460
3	4		4	N	2340	B→N	2540
4	4		5	N	2470	B→N	2750
5	4	3	2	S	2260	B→S	2370
6	4		3	B	2370	B	2570
7	4		4	B	2430	B	2660
8	4		5	B	2580	B	2790
9	4	4	2	B→S	2400	B→S	2580
10	4		3	B	2570	B	2640
11	4		4	B	2600	B	2750
12	4		5	B	2720	B	2870
13	4	5	2	B→S	2550	B→S	2650
14	4		3	B	2670	B	2790
15	4		4	B	2760	B	2930
16	4		5	B	2850	B	3286

4.4.2.2 Numerical results

The numerically predicted modes of failure *i.e.*, net-tension, shearing and bearing modes from composite specimens for different joint configurations are shown in Fig. 4.15, 4.16 and 4.17, respectively. The joint configuration with geometric parameters of W/D = 2 and

E/D = 4 for neat composite specimen showing the net-tension mode of failure under tensile loading of 4000 N is presented in Fig. 4.15. It can be visualized that the failure progresses initially near the hole boundary and further spreads in the direction of side edges as the load is increased, justifying the failure in net-tension mode. The shearing mode of failure occurred for joint configuration with a selected geometric combination of W/D = 3 and E/D = 2 for neat composite specimen under tensile loading of 3800 N as shown in Fig. 4.16. It can be visualized that the damage progresses towards the free edge of the pin joint as the free edge distance is smaller than the side edge from the hole confirming the shearing mode of failure in the pin joint. The experimental results confirmed the bearing mode of failure with increase in W/D and E/D ratios.

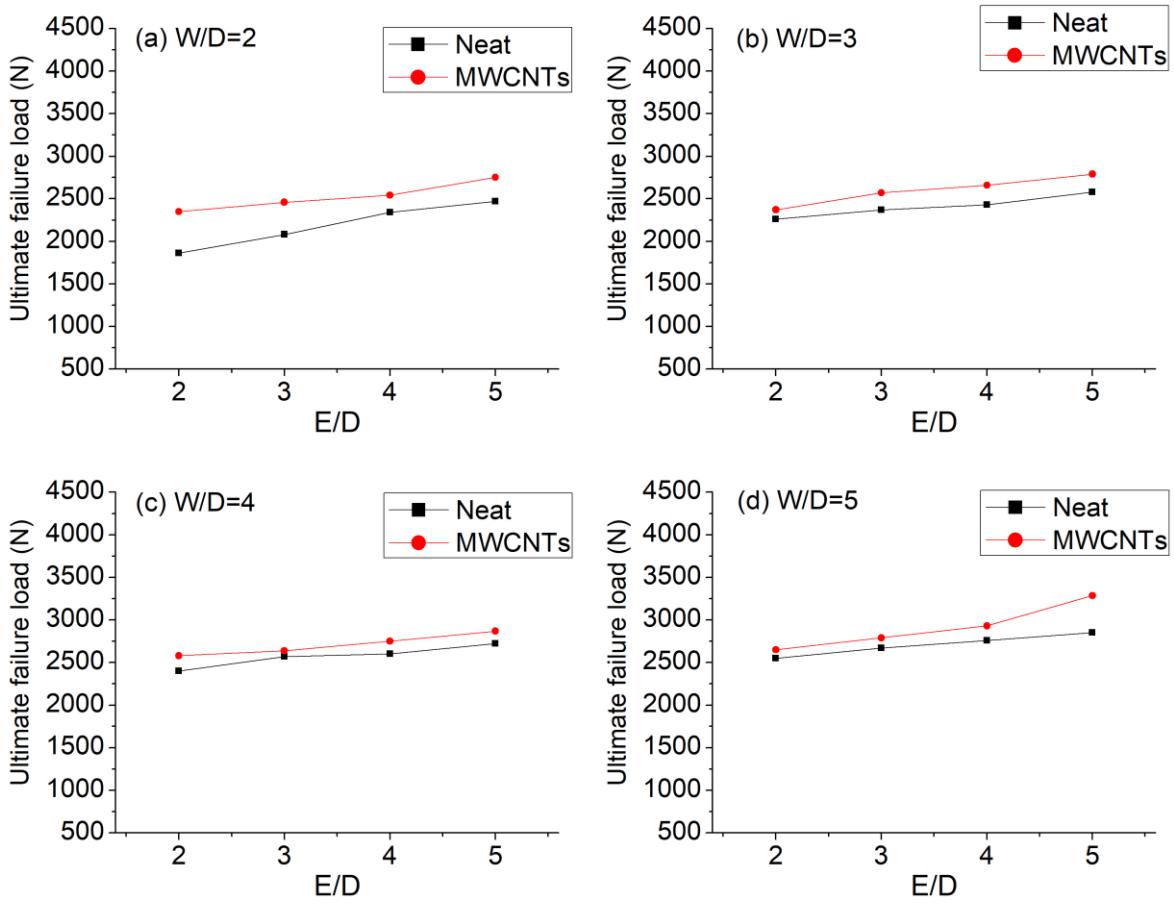

Fig. 4.14 Comparison of ultimate failure loads of thermal cured neat and MWCNTs joint specimens for (a) W/D = 2, (b) W/D = 3, (c) W/D = 4 and (d) W/D = 5

Similarly, the bearing mode of failure is obtained from the failure analysis for joint configuration with geometric combinations of W/D = 5 and E/D = 5 for MWCNTs added composite specimen under tensile loading of 5500 N as seen in Fig. 4.17.

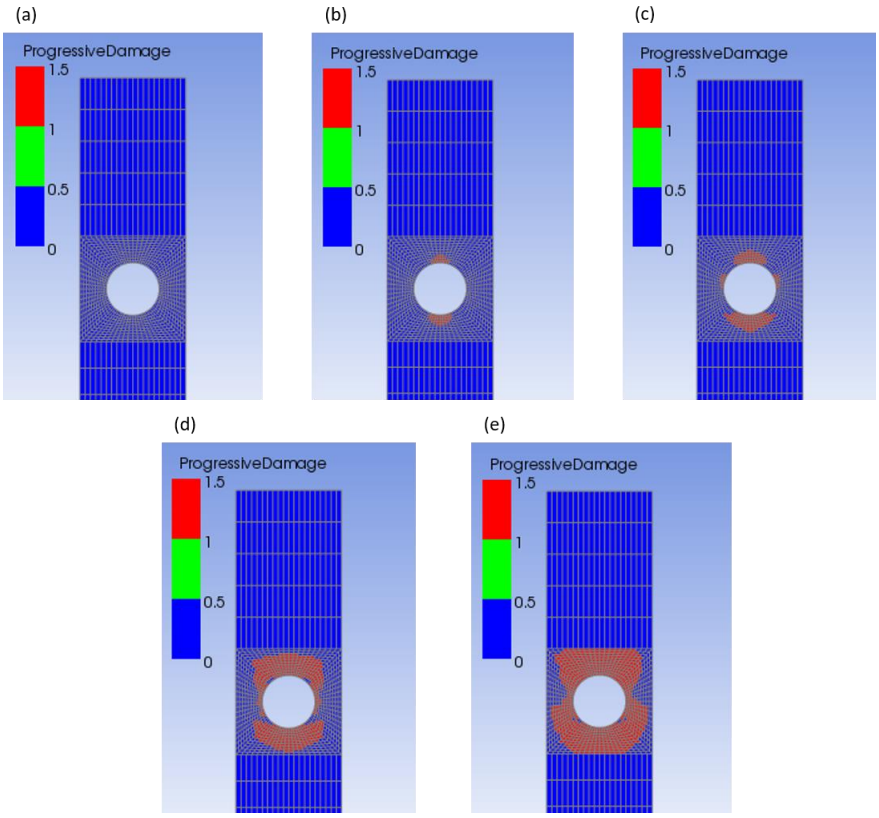

Fig. 4.15 Net-tension mode of failure in neat composite joint for W/D = 2 and E/D = 4 at applied load of (a) 20%, (b) 40%, (c) 60%, (d) 80% and (e) 100%

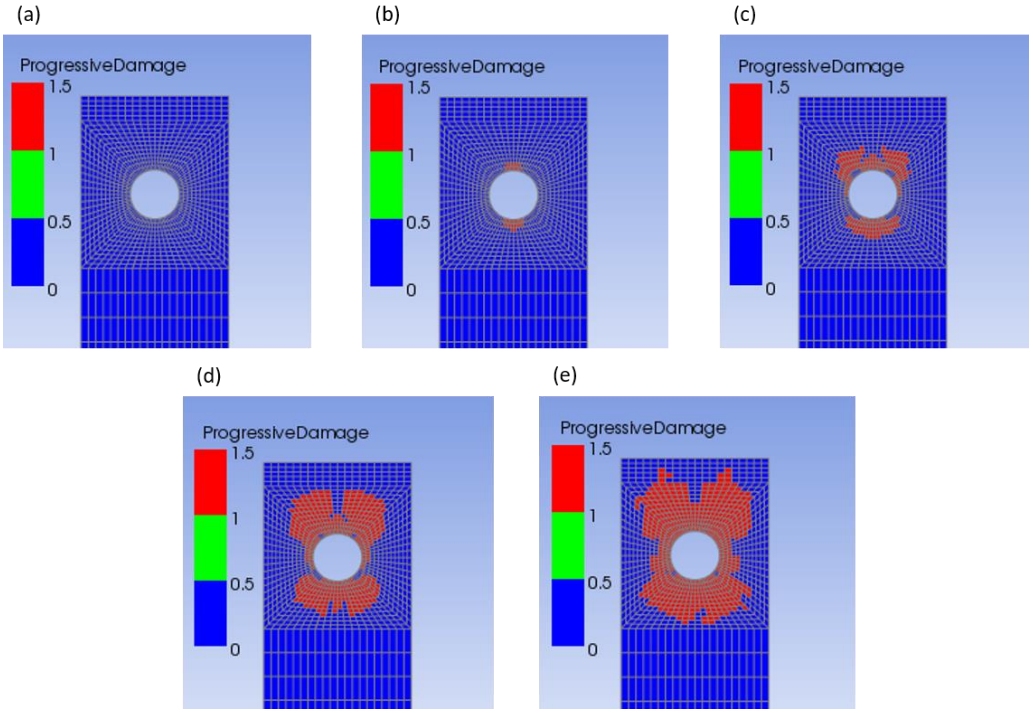

Fig. 4.16 Shearing mode of failure in neat composite joint for W/D = 3 and E/D = 2 at applied load of (a) 20%, (b) 40%, (c) 60%, (d) 80% and (e) 100%

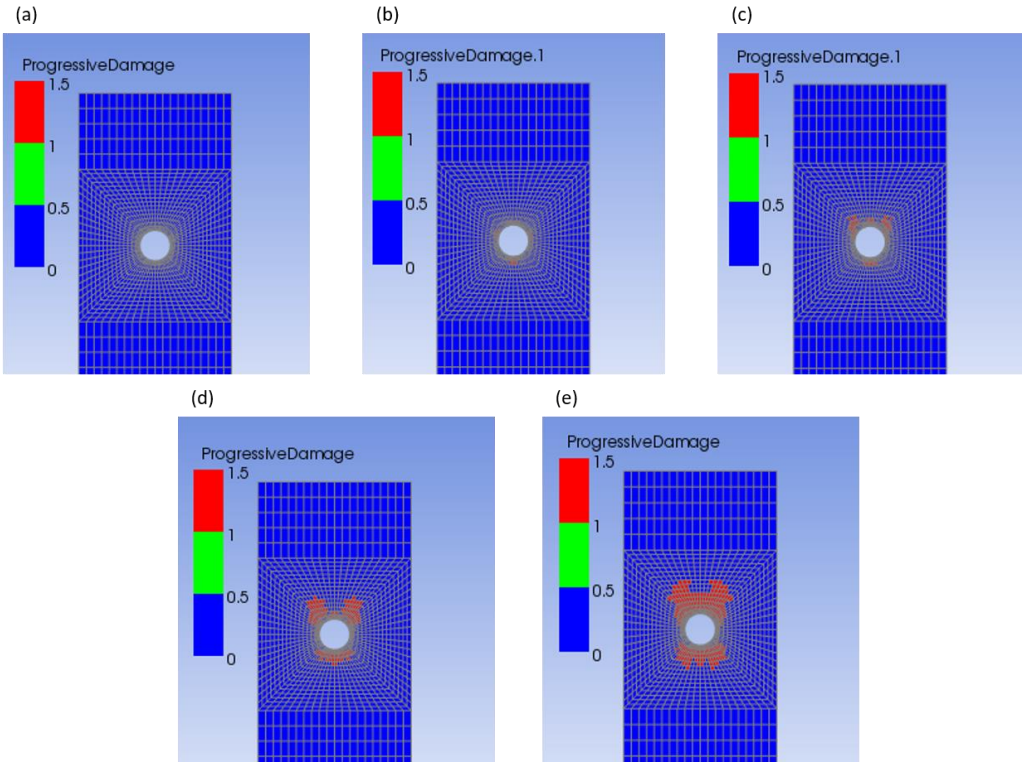

Fig. 4.17 Bearing mode of failure in MWCNTs added composite joint for W/D = 5 and E/D = 5 at applied load (a) 20%, (b) 40%, (c) 60%, (d) 80% and (e) 100%

The ultimate failure loads, numerically predicted and compared with experimental results for different geometric parameters, are plotted in Fig. 4.18. Comparing the experimental values of ultimate failure loads with the numerical values, it is observed that prediction through failure analysis is within 10% of the acceptable difference, which shows the good agreement among the obtained results.

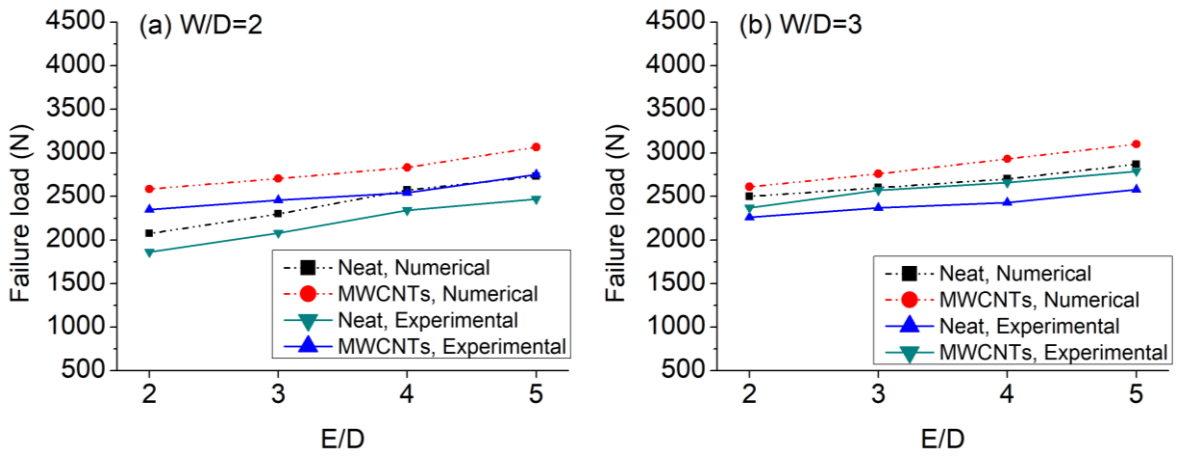

Continued…

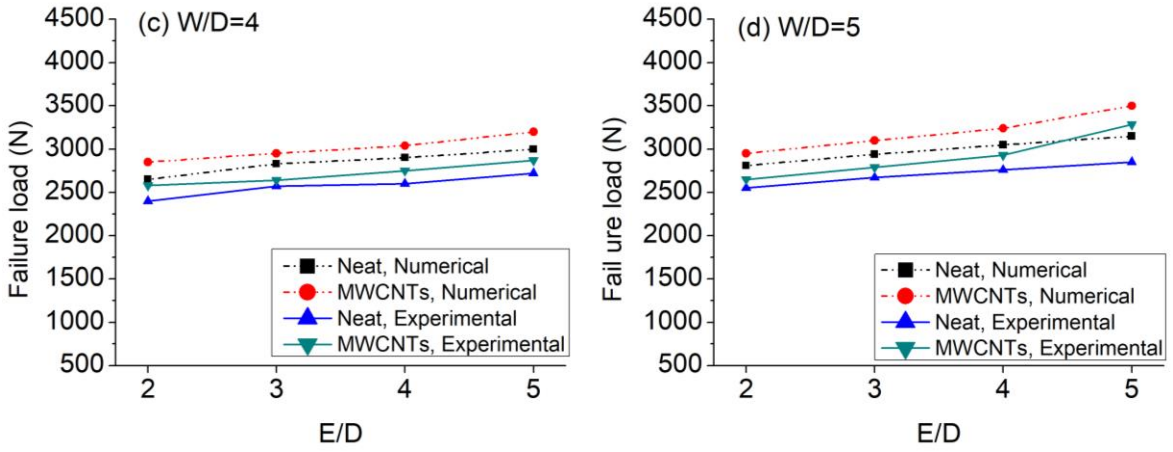

Fig. 4.18 Comparison of numerical and experimental results of ultimate failure loads of neat and MWCNTs added composite specimens

4.5 Closure

This chapter explained the effect of different geometric parameters (i.e., W/D and E/D ratios) on the failure loads and failure modes of EB cured mechanical pin joints. The investigations were carried out on neat and optimized 0.3 wt. % of MWCNTs added carbon fiber/epoxy composite materials prepared using two different processes *i.e.*, EB curing and thermal curing process. A positive contribution to failure loads and failure modes of the pin joint was seen by incorporating MWCNTs nanofiller. Using MWCNTs showed the maximum improvement of 26.63% and 26.34% in the failure loads for EB cured and thermally cured pin joint composites, respectively.

The present chapter was mainly concentrated on the performance of pin joints to analyze their failure characteristics. The failure of the pin joint is much simpler than the bolted joints where the lateral constraints are involved in terms of compressive forces. Many engineering applications *i.e.*, civil, aircraft and marine sectors, make use of bolted joints and are susceptible to the aging environment. To outspread the scope of the mechanical joint, the further chapters are concentrated on the performance analysis of the bolted joints under aging environmental conditions.

Chapter 5
Performance of Bolted Joints under Hygrothermal Aging Environment

In several applications of civil, aerospace and marine sectors, bolted joints in composite structures are exposed to the hygrothermal aging environment which involves moisture and high temperature. These conditions affect the strength retention ability of the bolted joints. So, it is extremely important to study the performance characteristics of prepared materials and their joints under hygrothermal conditions. The present chapter is focused on the hygrothermal aging of the bolted joints prepared from carbon fiber/epoxy composites. The investigations were carried out on the neat and optimized 0.3 wt.% of MWCNTs added composite materials prepared using two different processes *i.e.,* EB curing and thermal curing process. Incorporating MWCNTs nanofiller in the composite material ease to reduce the water permeability by hindering the tranquility of polymeric chains surrounding the nanofiller [20, 21]. The composite bolted joint specimens were designed as per ASTM D5961 standard having geometric parameters *i.e.,* width to diameter ratio (W/D) and edge to diameter ratio (E/D) fixed to 6 and 5, respectively. The effect of bolt torque at different levels *i.e.,* 0, 2 and 4 Nm were also investigated.

5.1 Hygrothermal aging

For hygrothermal aging, EB cured and thermally cured composite specimens of neat and 0.3 wt.% of MWCNTs added configurations were conditioned at three different temperatures, 25 ^{o}C, 45 ^{o}C and 65 ^{o}C for 30 days.

5.1.1 Water diffusion behavior

The specimens of neat and 0.3 wt.% of MWCNTs added configurations were prepared from the composite laminates and were hygrothermally conditioned as per ASTM D5229 standard. Before immersing the specimens into the water bath, these were dried at 80 ^{o}C for 4 hours. According to ASTM D5229 standard, the maximum recommended test temperature (in ^{o}C) for polymer matrix materials is 70^{o}C. Accordingly, different water temperatures, 25^{o}C, 45^{o}C and 65^{o}C, which are within the range of the maximum recommended temperature, were used in the present work. The same temperature ranges have also been reported by different researchers in the literature [155, 158, 197, 198]. Moreover, after 30

days of conditioning, the water absorption rate tends to be constant [199-201]. Therefore, 30 days was considered for the aging time in the present work.

At different intervals of time, the specimens were taken out from the water bath, dried using tissue paper and then the weight was recorded by high precision weighing machine, with an accuracy of 0.0001 g. It was assumed that the desorption did not take place during the weight measurements. Five specimens of each configuration were conditioned. The mass gain of neat and MWCNTs added composite specimens was obtained using Eq. (5.1).

$$\mathrm{M_t} = \frac{\mathrm{W_t} - \mathrm{W_o}}{\mathrm{W_o}} \times 100 \tag{5.1}$$

Where, $\mathrm{M_t}$ is the water gain (%) at time t, $\mathrm{W_t}$ is the present specimen mass (g) at time t and $\mathrm{W_o}$ is the reference specimen mass (g). A standard water absorption behavior of FRP composite material can be seen in Fig. 5.1 [202]. The water absorption in polymers takes place linearly and follows Fickian diffusion law in the initial phase. In the middle phase, absorption becomes nearly saturated and finally, it increases further due to degradation and micro-cracks generation in the epoxy matrix and fiber/matrix interface through capillary action.

The diffusion coefficient of water into the nanocomposites in the Fickian diffusion region was computed using Eq. (5.2).

$$\mathrm{D_z} = \pi \left(\frac{h}{4 \times \mathrm{M_m}}\right)^2 \left(\frac{d\mathrm{M}}{d\sqrt{t}}\right)^2 \tag{5.2}$$

Where, $\mathrm{D_z}$ is the diffusion coefficient, h is the thickness of specimen, t is the time duration and $\mathrm{M_m}$ is the situation water absorption. Here, $\mathrm{D_z}$ accounts for diffusion in one dimension *i.e.*, diffusion takes place through the edge. The novel diffusion coefficient which is based on water diffusion through sides and thickness of the composite specimen is given by Eq. (5.3). [203]

$$D = \frac{\mathrm{D_z}}{\left[1 + \frac{h}{l} + \frac{h}{w}\right]^2} \tag{5.3}$$

Where, h, l *and* w are the thickness, length and width of the composite specimen, respectively.

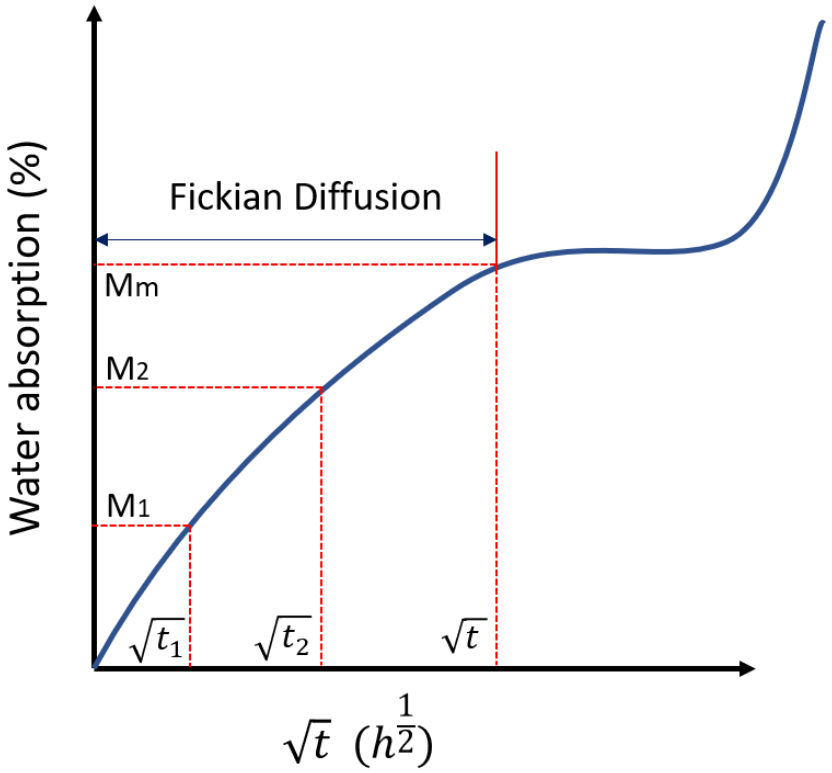

Fig. 5.1 Water absorption vs. square root of time plot of FRP composite [202]

5.1.2 Bolted joints under hygrothermal conditioning

In the present investigation, the performance of bolted joints prepared from carbon fiber/ epoxy composite laminates was analyzed under hygrothermal aging conditions. As per the ASTM standard D5961, the bolted joints specimens of neat and 0.3 wt.% of MWCNTs added configuration were prepared from the composite laminates to identify the bearing responses. This standard used geometric parameters *i.e.*, edge to diameter ratio (E/D) and width to diameter ratio (W/D) as 5 and 6, respectively. The hole diameter used to insert the M4 size bolt was fixed to 4 mm. The prepared joint specimens were immersed in water bath, at three different temperatures, 25 ^{o}C, 45 ^{o}C and 65 ^{o}C, for 10, 20 and 30 days.

After hygrothermal conditioning, these joint specimens of carbon fiber/epoxy nanocomposite were clamped into the fixture through fasteners as shown in Fig. 2.5 and given a tightening bolt torque using a calibrated torque wrench having variable torque and a least count of 0.5 Nm. The fabricated fixture consists of steel plates, M4 size shoulder bolts and washers. The material properties and dimensions of different components of the fixture are given in Table 2.6. Three different bolt tightening torques of 0, 2 and 4 Nm, were used for the composite joints before testing.

Finally, the complete assembly (joint specimens along with the fixture) was clamped in the Zwick Roell make UTM machine of 10 kN capacity and tested under tensile load. The UTM setup along with the fixture and specimen is shown in Fig. 2.6. The gradually increasing load was countered by the bolt placed at the center of the drilled hole. No bending moment in the composite specimen was observed due to symmetrical boundary conditions and the design of the joint along the centerline.

5.2 Results and discussion

The following section provides the results on the performance of joints after hygrothermal conditioning of the bolted joint specimens prepared from EB cured and thermal cured composite laminates.

5.2.1 Bolted joints prepared from EB cured composites

5.2.1.1 Water diffusion behavior

The water diffusion behavior of the EB cured composite specimens at different hygrothermal conditions of 25 ^{o}C, 45 ^{o}C and 65 ^{o}C is shown in Fig. 5.2. It was found that the hygrothermal aging for lower water temperature (25 ^{o}C) had less impact on the water absorption rate. But at higher water temperatures, increased segmental movement of the polymeric chain helps in enhancing the water absorption rate. It was observed that the aging temperature contributes to inducing the water intake kinetics. The neat composite specimens were more susceptible to water absorption, especially at higher water temperatures. The reason being at elevated temperatures, the extensive crosslinking leads to embrittlement that creates microcracks in the epoxy matrix and at the fiber/matrix interface and results in more absorption of water due to capillary action [204]. The induced thermal stresses were also another reason for microcrack formations [205].

It was observed that incorporating 0.3 wt.% of MWCNTs in the composite specimens lowers the water absorption rate as compared to neat composite specimens. The reduction in absorption rate is attributed to the fact that the formation of good MWCNTs/polymer interfacial bonding and excellent barrier properties lowers the tendency to absorb water through capillary action. The high aspect ratio of the MWCNTs tends to generate the tortuosity effect that forces water molecules to follow prolonged paths [187].

Further, the suppression in water absorption can be explained by the free volume concept in the epoxy system. The homogenized distribution of MWCNTs helps in accumulating the free volume sites which further resists the water absorption phenomenon. The Eqs. (5.2)

and (5.3) were used to calculate the water diffusion coefficient for neat and 0.3 wt.% of MWCNTs added composite specimens. The results obtained in terms of the diffusion coefficient and water absorption in the specimens at 25 °C, 45 °C and 65 °C for 30 days are summarized in Table 5.1.

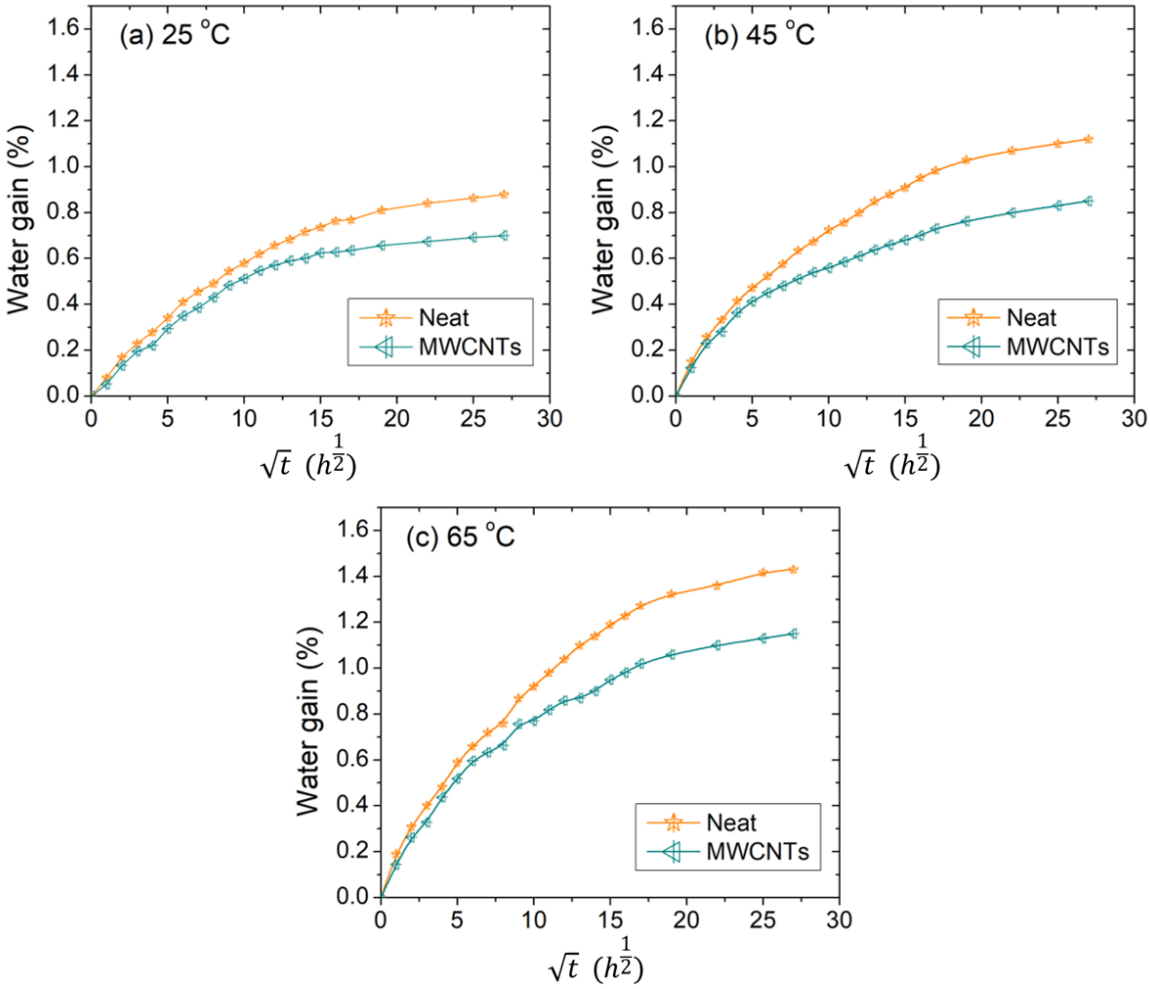

Fig. 5.2 Water absorption behavior in EB cured neat and MWCNTs added composite specimens at (a) 25 °C, (b) 45 °C and (c) 65 °C

Table 5.1 Water absorption and diffusion coefficient of EB cured composite specimens

Material	Temperature (°C)	Maximum water absorption (M_m) (%)	Diffusion coefficient (D) (10^{-8} cm^2/s)
Neat	25	0.88	3.98
MWCNTs	25	0.70	2.83
Neat	45	1.12	5.01
MWCNTs	45	0.85	3.64
Neat	65	1.43	6.20
MWCNTs	65	1.09	4.82

From Table 5.1, it is found that incorporating MWCNTs in the composite specimens reduces water absorption rate and corrected diffusion coefficient by 20.5% and 28.9% at 25 ^{o}C and 23.7% and 22.3% at 65 ^{o}C. The results show that at higher water temperatures, the efficiency of MWCNTs to sustain water absorption was slightly reduced in comparison to lower water temperature aging. This is due to the generation of thermal stresses which leads to microcracks [205].

5.2.1.2 Assessment of mechanical properties

The stress-strain curves for tensile and flexural properties of neat and 0.3 wt.% of MWCNTs added composite specimens before and after 30 days of aging are shown in Fig. 5.3 and 5.4. The stress-strain curves revealed that after hygrothermal conditioning of 30 days at 65^{o}C, the reduction in tensile strength, tensile modulus, flexural strength and flexural modulus were 12.63%, 16.43%, 19.51% and 20.12%, respectively for neat composites. Correspondingly, for MWCNTs added composites, reduction in these properties was 6.83%, 8.32%, 8.04% and 9.21%, respectively. The reduction in modulus properties implies the reduced stiffness of the material after the water molecules occupies the free space of the composite specimens at higher temperatures. The absorbed water at higher temperatures causes swelling in the epoxy matrix and generates thermal stresses which degrades the material.

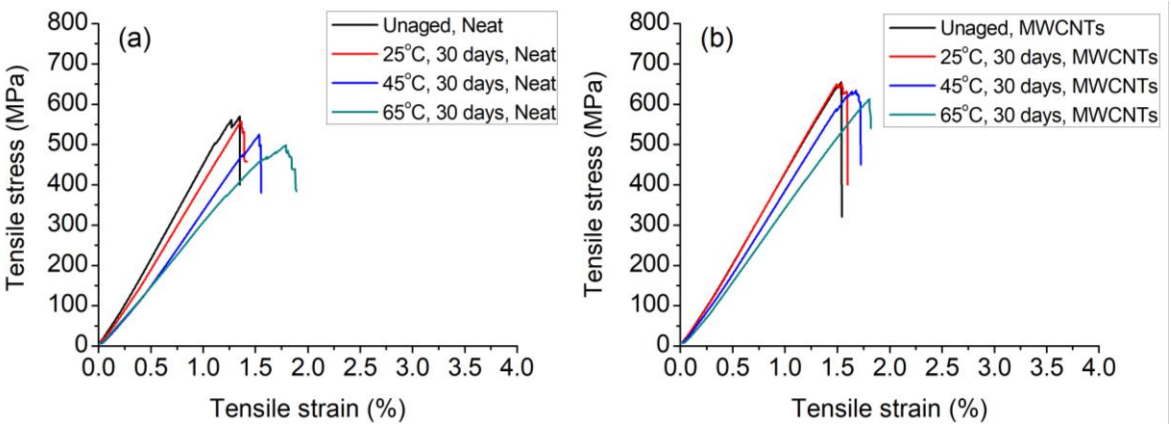

Fig. 5.3 Tensile stress vs. tensile strain for EB cured unaged and aged specimens (a) Neat and (b) MWCNTs added configurations

Figures 5.3 and 5.4 also show the tensile and flexural strains (percentage of elongation at break) for neat and MWCNTs added composite specimens. After hygrothermal conditioning at higher temperatures, the strain values get enhanced due to the plasticization effect. The strain rate was higher in neat composite specimens than in the MWCNTs added composite

specimens. The graphs in Fig. 5.3 also shows that all the composite specimens had brittle failure. Table 5.2 shows the average tensile and flexural strength of composite specimens after hygrothermal aging.

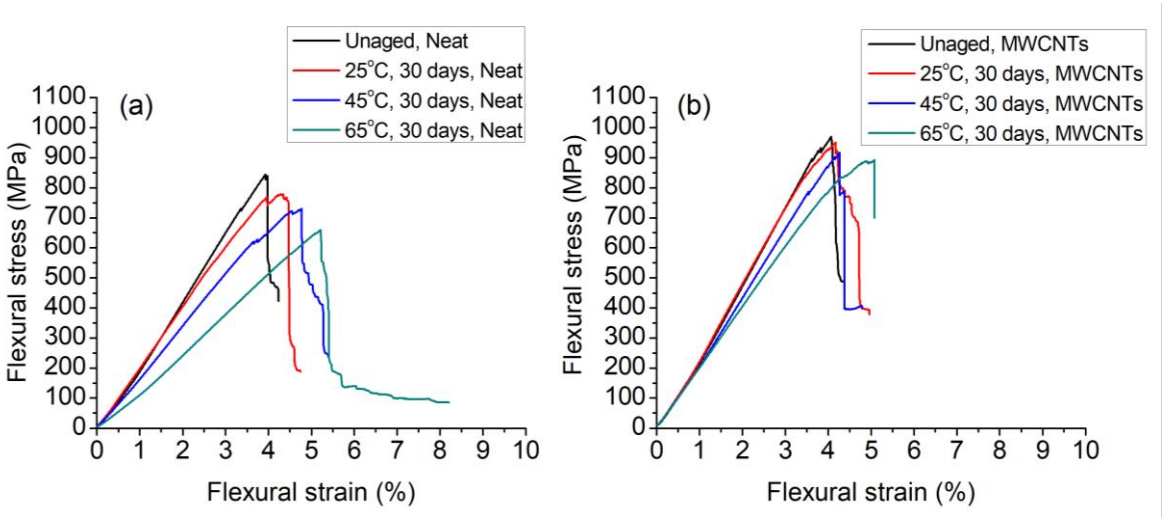

Fig. 5.4 Flexural stress vs. flexural strain for EB cured unaged and aged specimens (a) Neat and (b) MWCNTs added configurations

Table 5.2 Mechanical properties of EB cured composite specimens after hygrothermal aging

S. No.	Temperature (ºC)	Duration (days)	Tensile strength (MPa) (SD*)		Flexural strength (MPa) (SD*)	
			Neat	MWCNTs	Neat	MWCNTs
1	Unaged	0	570 ± 13	658 ± 12	820 ± 10	970 ± 15
2	25	10	568 ± 08	657 ± 10	808 ± 12	965 ± 11
3	25	20	562 ± 06	653 ± 10	796 ± 09	957 ± 10
4	25	30	556 ± 07	650 ± 08	779 ± 09	951 ± 10
5	45	10	560 ± 07	651 ± 09	795 ± 10	954 ± 09
6	45	20	545 ± 10	646 ± 08	763 ± 12	934 ± 09
7	45	30	524 ± 11	634 ± 10	730 ± 12	917 ± 08
8	65	10	549 ± 12	646 ± 12	779 ± 10	941 ± 10
9	65	20	523 ± 09	632 ± 06	730 ± 08	922 ± 10
10	65	30	498 ± 10	613 ± 07	660 ± 09	892 ± 11

*** SD = Standard deviation**

The tensile and flexural strength retention plots are shown in Fig. 5.5. A significant reduction in tensile and flexural strength was observed in the composite specimens with the

increase in water temperature and duration. The swelling of the epoxy matrix due to water absorption leads to the weakening of the interfacial bonding between the matrix and the fiber and hence reduced mechanical strength.

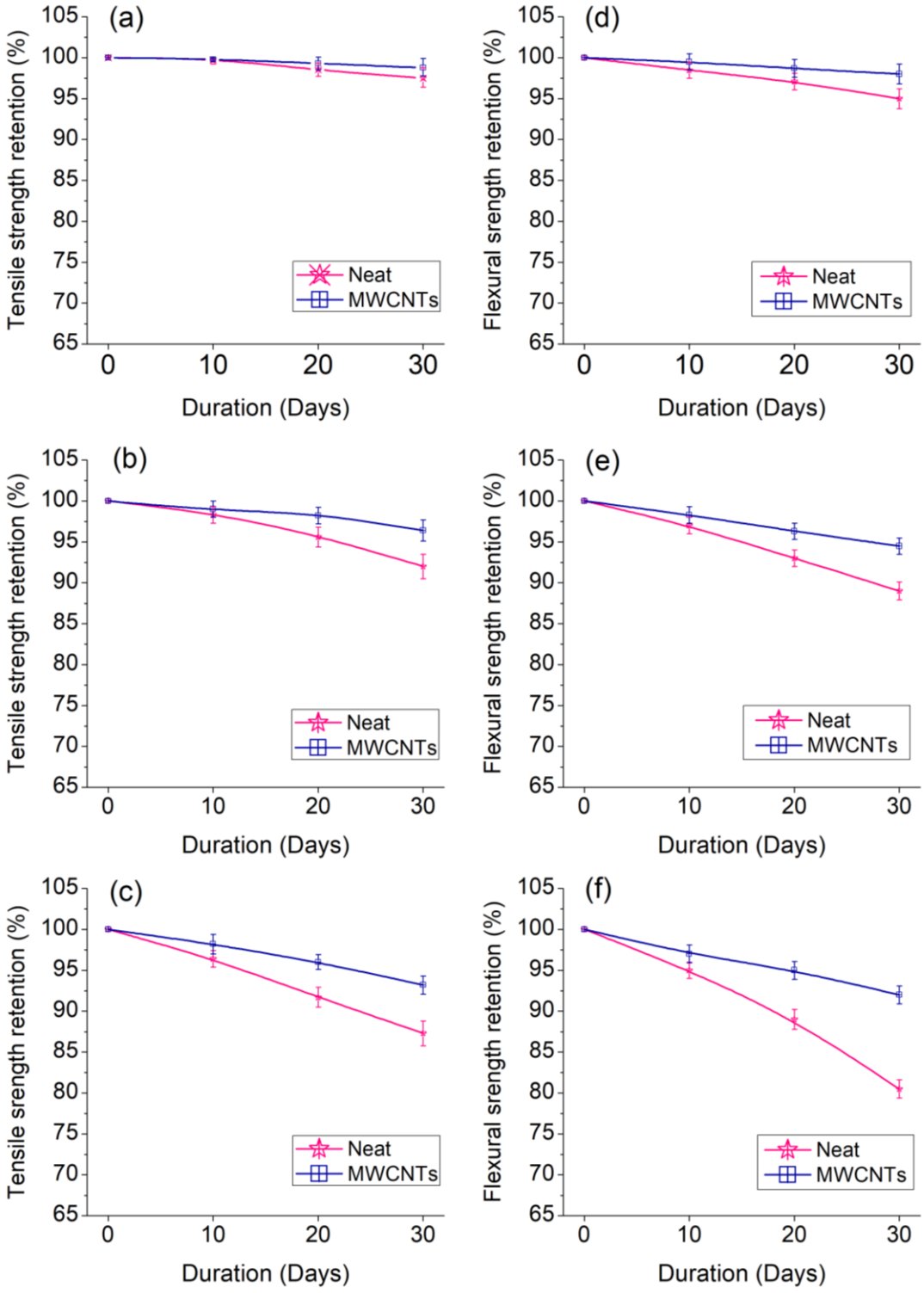

Fig. 5.5 Strength retentions of hygrothermally aged EB cured composite specimens of neat configuration at (a) 25 ^{o}C, (b) 45 ^{o}C and (c) 65 ^{o}C and MWCNTs added configuration at (d) 25 ^{o}C, (e) 45 ^{o}C and (f) 65 ^{o}C

The absorbed water molecules can be bound and free water types in which free water was gathered in the voids present inside the epoxy or at fiber/matrix interface and bound water was usually attached with the hydroxyl group of epoxies. At higher water temperatures, the absorbed water present inside the voids and bonded with an epoxy group was responsible for the uneven epoxy swelling which results in microcracks. Also upon redrying, the space vacated by the water molecules creates micro-cavities that act as stress concentration points which lead to the initiation of cracks in the epoxy matrix and are further responsible for the decrease in the mechanical performance of composites [206]. It was observed that water absorption and composite degradation have a strong correlation with each other. The tensile and flexural strength retentions have faced significant reduction after hygrothermal aging as water absorption and diffusion increased (as confirmed from water absorption studies) at higher water temperatures, which encouraged degradation phenomenon. From Fig. 5.5 (a)-(f), it is seen that at lower water temperature aging (25 ^{o}C), the strength retention rate is better as compared to the higher water temperature aging (65 ^{o}C).

The addition of MWCNTs in the composite specimen results in a higher strength retention rate, as more steep slopes (showing the rate of degradation) can be seen in the neat composite specimens as compared to the MWCNTs added composite specimens. MWCNTs added composite specimens showed less degradation than the neat composite specimens. This was due to the high aspect ratio of the MWCNTs that tends to generate the tortuosity effect which forces the water molecules to follow prolonged paths. Also, the formation of good MWCNTs/polymer interfacial bonding and excellent barrier properties tend to restrict the interfacial debonding [161]. The percentage tensile strength retentions for neat composite specimens at water temperature of 25 ^{o}C, 45 ^{o}C and 65 ^{o}C were 97.5%, 92% and 87.3% after 30 days. Correspondingly, for MWCNTs added composite specimens the percentage tensile strength retentions were 98.8%, 96.4% and 93.2%, respectively. The percentage flexural strength retention for neat composite specimens at water temperature of 25 ^{o}C, 45 ^{o}C and 65 ^{o}C were 95%, 89% and 80.5% after 30 days. Correspondingly, for MWCNTs added composite specimens the percentage flexural strength retentions were 98%, 96.3% and 92%, respectively.

The damage mechanism of EB cured neat and MWCNTs composite specimens under different aging conditions are shown in Fig. 5.6. It can be seen that even after 30 days of water aging at 25 ^{o}C, there was a strong interfacial bonding between the epoxy matrix and the fibers in both neat and MWCNTs added specimen.

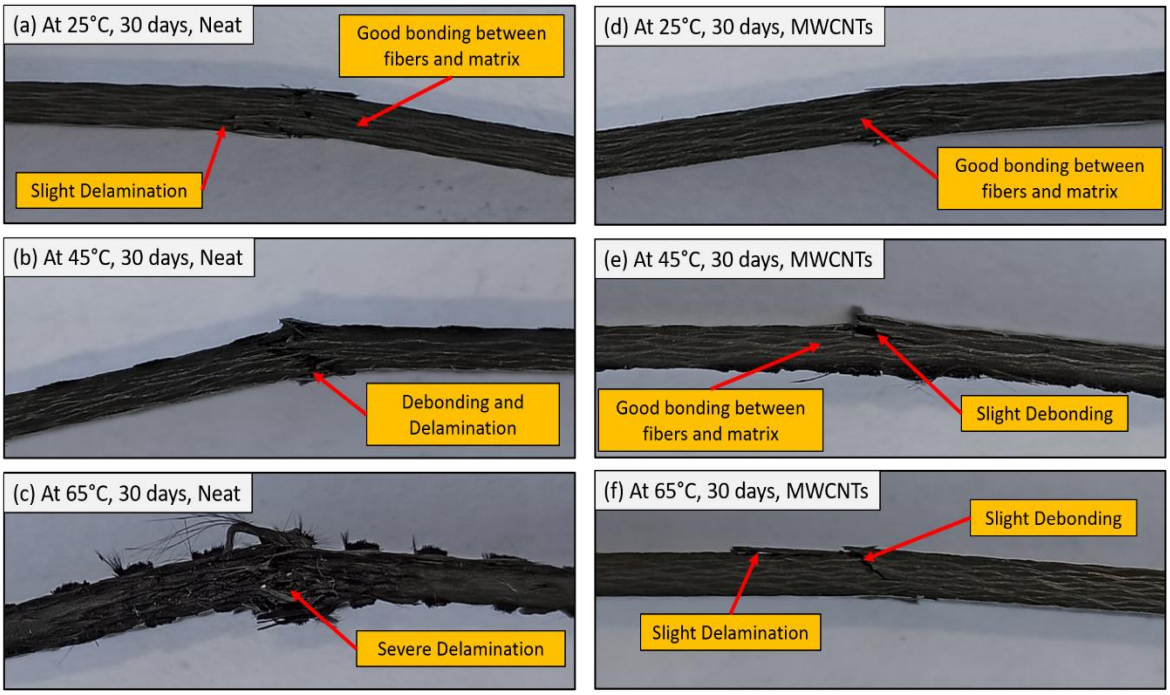

Fig. 5.6 The damage mechanism in EB cured neat and MWCNTs added composite specimens at 25 ^{o}C, 45 ^{o}C and 65 ^{o}C after 30 days of aging

The aging at 45 ^{o}C of water temperature reveals that water absorption in the composites leads to delamination between the composite plies and debonding between the fibers and the epoxy matrix in the neat composite specimen as subjected to flexural loading. On the other hand, good interfacial bonding was observed in the MWCNTs added specimens with slight debonding at 45 ^{o}C of water temperature. The severe damage in terms of delamination was observed at 65 ^{o}C of water temperature for a neat specimen as shown in Fig. 5.6 (c). Moreover, slight delamination and debonding between the fiber and epoxy matrix can be seen in MWCNTs added specimen in Fig. 5.6 (f), showing good resistance to degradation.

5.2.1.3 SEM analysis

The SEM micrographs of the EB cured composite specimens at different hygrothermal aging conditions are shown in Fig. 5.7 and 5.8. The SEM micrographs from Fig. 5.7 illustrates the surface degradation of the neat and MWCNTs added composite specimens for the unaged and aged at 65 ^{o}C for 30 days. It can be seen that the neat specimens are prone to severe epoxy degradation at higher water temperature (65 ^{o}C) than MWCNTs specimens showing less damage at the surface.

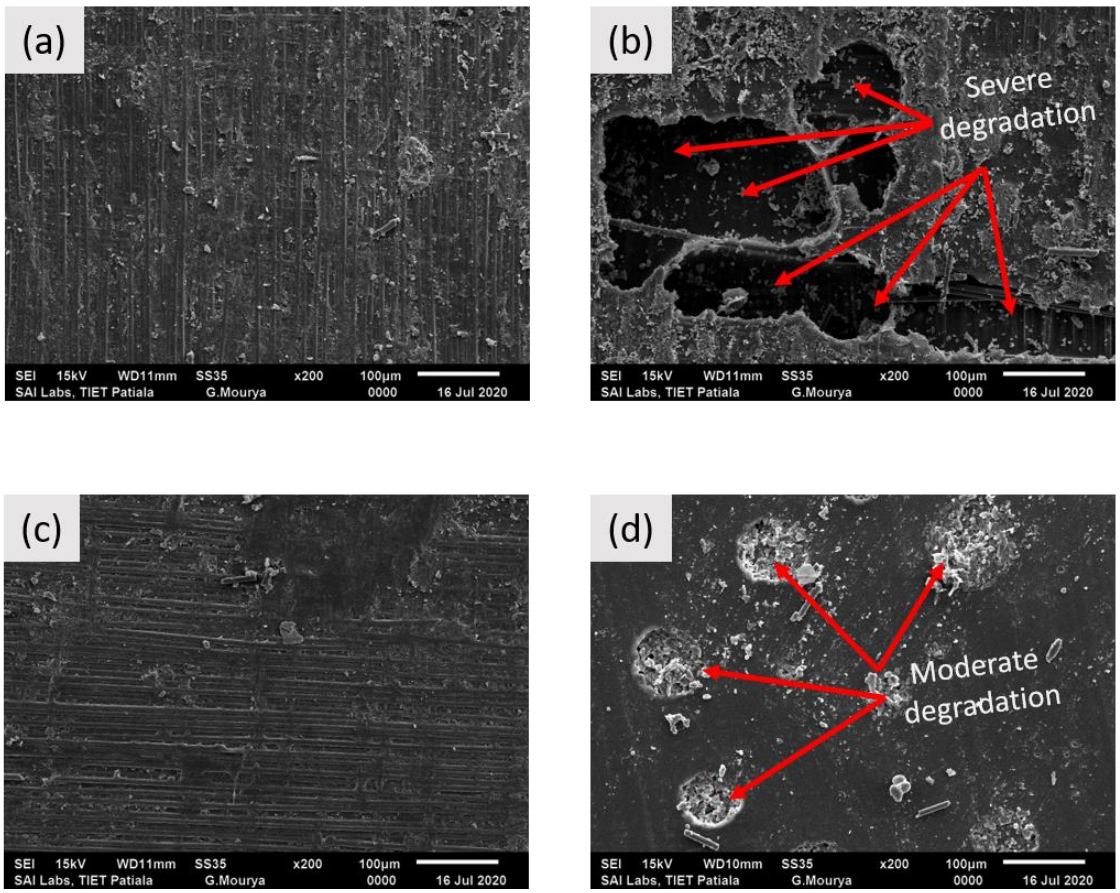

Fig. 5.7 SEM micrographs of the surface of neat composite specimens (a) unaged and (b) aged at 65 ^{o}C for 30 days and MWCNTs added composite specimens (c) unaged and (d) aged at 65 ^{o}C for 30 days

The SEM micrographs given in Fig. 5.8 show the fractured surface of the composite specimens for unaged and aged composites at 25 ^{o}C, 45 ^{o}C and 65 ^{o}C for 30 days. The excellent interfacial bonding between the fiber and the epoxy matrix was observed for unaged neat and MWCNTs composite specimens (Fig. 5.8 (a,b) and (m,n)) and fibers that pulled out were well coated with resin. Even after specimens fracture, fibers firmly placed at their positions show the good adhesion properties of the epoxy matrix. In Fig. 5.8 (c,d) and (o,p), for the water aging at 25 ^{o}C, no significant degradation was observed at the fiber/matrix interface for neat and MWCNTs composites even after 30 days as compared to unaged composites, confirming that the impact of aging was very low on mechanical properties.

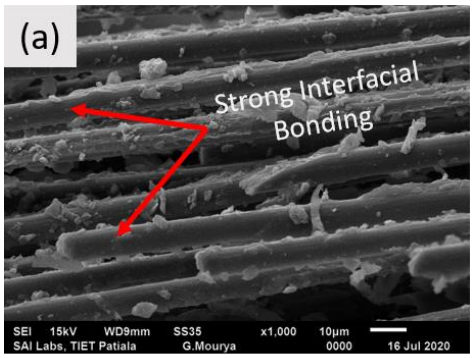
(a)
Strong Interfacial Bonding
SEI 15kV WD9mm SS35 x1,000 10µm
SAI Labs, TIET Patiala G.Mourya 0000 16 Jul 2020

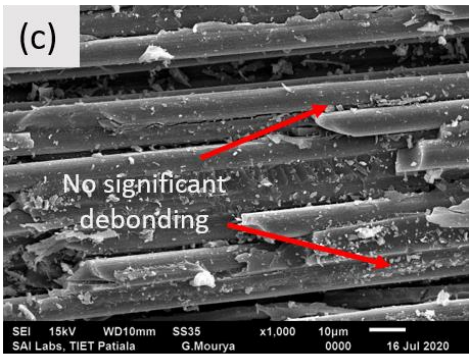
(c)
No significant debonding
SEI 15kV WD10mm SS35 x1,000 10µm
SAI Labs, TIET Patiala G.Mourya 0000 16 Jul 2020

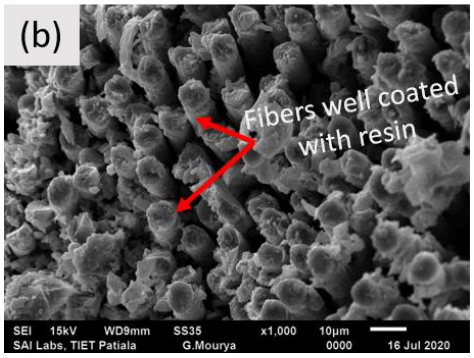
(b)
Fibers well coated with resin
SEI 15kV WD9mm SS35 x1,000 10µm
SAI Labs, TIET Patiala G.Mourya 0000 16 Jul 2020

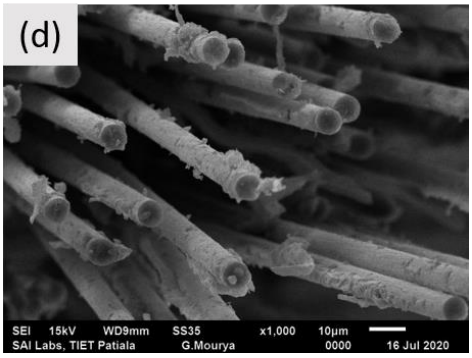
(d)
SEI 15kV WD9mm SS35 x1,000 10µm
SAI Labs, TIET Patiala G.Mourya 0000 16 Jul 2020

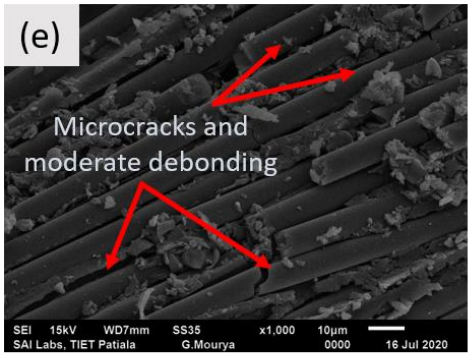
(e)
Microcracks and moderate debonding
SEI 15kV WD7mm SS35 x1,000 10µm
SAI Labs, TIET Patiala G.Mourya 0000 16 Jul 2020

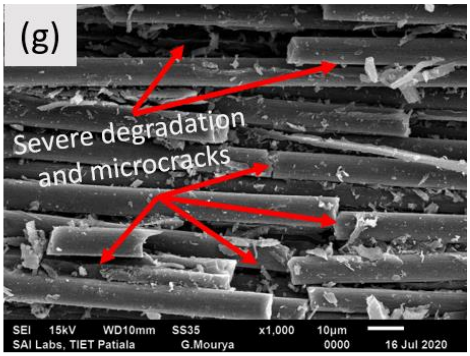
(g)
Severe degradation and microcracks
SEI 15kV WD10mm SS35 x1,000 10µm
SAI Labs, TIET Patiala G.Mourya 0000 16 Jul 2020

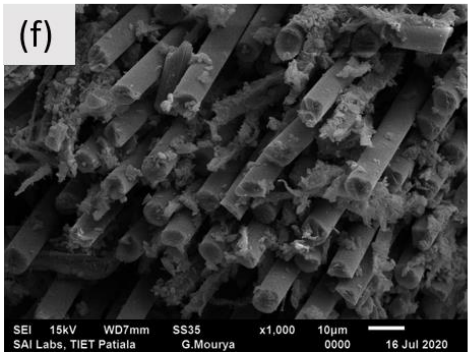
(f)
SEI 15kV WD7mm SS35 x1,000 10µm
SAI Labs, TIET Patiala G.Mourya 0000 16 Jul 2020

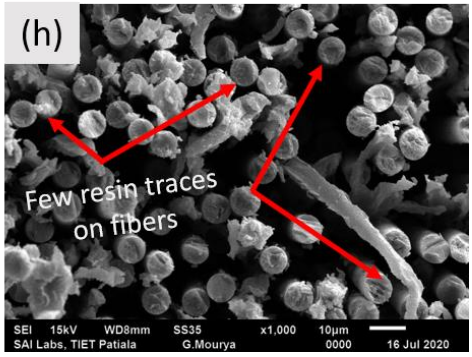
(h)
Few resin traces on fibers
SEI 15kV WD8mm SS35 x1,000 10µm
SAI Labs, TIET Patiala G.Mourya 0000 16 Jul 2020

Continued…

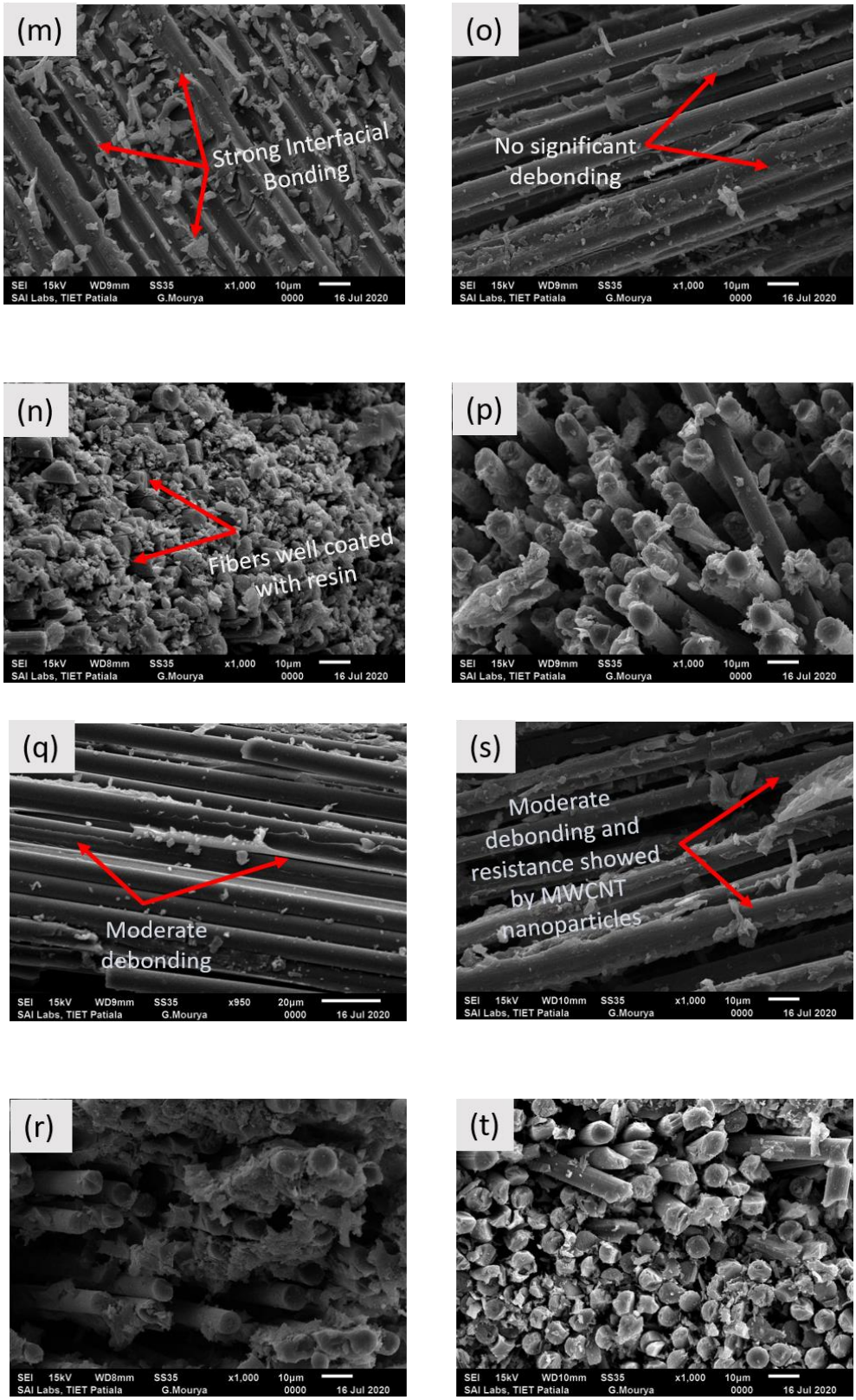

Fig. 5.8 SEM micrographs obtained after mechanical characterization of neat composite specimens (a),(b) unaged, (c),(d) aged at 25 ^{o}C, (e),(f) aged at 45 ^{o}C and (g),(h) aged at 65 ^{o}C for 30 days and 0.3 wt.%, MWCNTs added composite specimens (m),(n) unaged, (o),(p) aged at 25 ^{o}C, (q),(r) aged at 45 ^{o}C and (s),(t) aged at 65 ^{o}C for 30 days

Aging at 45 ^{o}C and 65 ^{o}C for 30 days, the impact of water temperature and duration was severe in neat composite specimens as compared to MWCNTs added composite specimens as shown in Fig. 5.8 ((e,f) and (g,h)) and ((q,r) and (s,t)). In neat composites (Fig. 5.8 (g,h)), at 65 ^{o}C after 30 days, the increased crosslinking leads to embrittlement and creates microcracks which result in debonding at the fiber/matrix interface. Further, these microcracks result in more water absorption and accelerate the degradation rate. The uneven epoxy swelling due to water absorption also contributes to the severe degradation of the composites [152]. After 30 days at 65 ^{o}C water temperature, the surface morphology of pulled out fibers changes from wavelike to relatively smooth. Although, incorporating MWCNTs produces a tortuosity effect which forces water molecules to follow prolonged paths and reduces water absorption rate. Moreover, the hydrophobic nature of MWCNTs acts as a mechanical blockage to water diffusibility, as an outcome helps to counter the deterioration of nanocomposites under hygrothermal aging conditions. Besides this, MWCNTs have a high specific surface area, that helps in improving the interfacial properties to counter the aging effect [57].

5.2.1.4 Performance of bolted joints under hygrothermal aging condition

Figure 5.9 shows the tensile testing results for unaged EB cured composite bolted joint specimens for neat and 0.3 wt.% of MWCNTs added configurations, respectively at varying bolt torques. As can be seen from Fig. 5.9 (a-b) that the curves for bearing response start with a linear movement and after reaching the first failure load, it continues moving in a zig-zag pattern showing the bearing mode of failure. The highest peak of a curve in the graphs is taken as the ultimate failure load for a particular condition.

In bolted joints, the bearing failure occurs in stages as the damage spreads into the composite specimen. A set of shear cracks are generated in each stage in 0 Nm (hand tightening) bolt torque through washers due to the accumulation of damage in individual piles of the composite bolted joint specimens. These shear cracks followed propagation towards the outer surface of the specimen as lateral constraints prevent the inward growth of shear cracks which opposes delamination. Moreover, these lateral constraints support damaged material that continues to withstand an additional ultimate failure load even after substantial damage had accumulated under the washers. The accumulation and propagation of damage continued into the composite bolted joint specimen as the ultimate failure load increased. Proceeding from the first set, the second set of shear cracks was formed. This shear crack growth mechanism continued until the damage propagated beyond the washers. At this

stage, due to the absence of lateral supports, joints lose their capacity to withstand higher loads. At higher bolt torques (2 and 4 Nm) in the bolted joints, the shear crack formation may be hindered as the transverse expansion of damaged material was restrained. However, under lateral constraints, bolt torques do not alter the nature of the bearing failure mechanism but hinder the damaged material from the formation of visible shear cracks. Hence, the increase in the ultimate failure load in bolted joints for higher bolt torques can attribute to the frictional forces between the washers and the specimens [67].

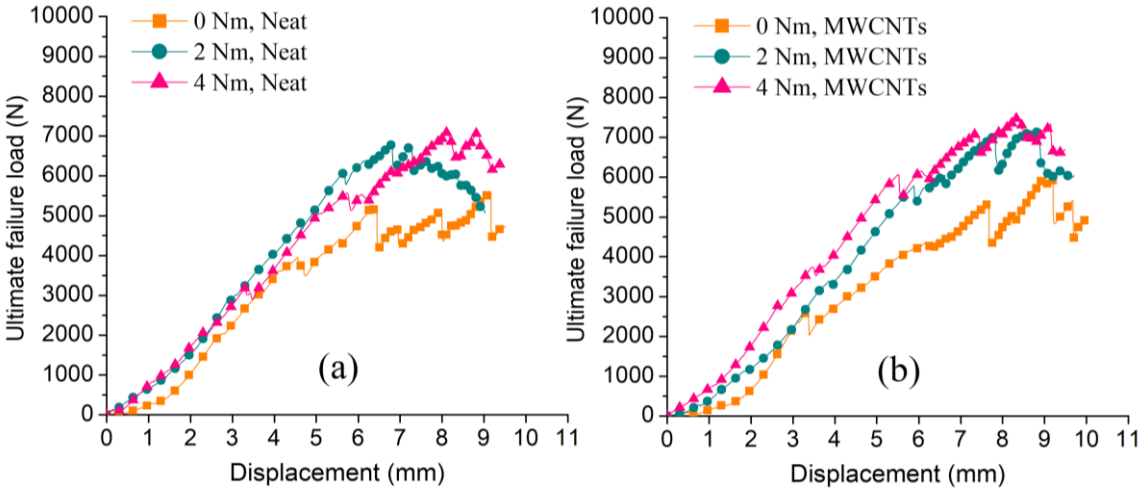

Fig. 5.9 Load vs. displacement curves of unaged EB cured composite joint specimens (a) neat and (b) 0.3 wt.% of MWCNTs added configuration

Figures 5.10 and 5.11 shows the tensile results of hygrothermal aged composite bolted joint specimens for neat and 0.3 wt.% of MWCNTs added configurations, respectively, at different conditions. It can be seen from Fig. 5.10 that with the increase in water temperature and aging time, there is a drop in the ultimate failure loads, as the water absorption phenomenon has subsequently progressed at higher aging conditions which are further responsible for the degradation of epoxy matrix and fiber/epoxy interface. It was observed that while varying bolt torque from 0 to 2 Nm and 2 to 4 Nm, the slope of the curves shows increasing trends. This is due to the increased lateral compressive forces through washers that increases the joint stiffness. But at higher water temperature (65 ^{o}C) as the aging time progresses, the slope of the curves decreases and varying bolt torques become less effective than at low temperature (25 ^{o}C). The plasticization and swelling in the epoxy matrix due to water absorption decreases the joint stiffness at higher water temperatures and prolonged duration. The slope of the curves in Fig. 5.11 shows that the MWCNTs added joint specimens are less affected by the different aging conditions as compared to the neat joint

specimens. The hydrophobic nature of MWCNTs resists the water absorption up to some extent and also produces a bridging effect between the fibers and the epoxy matrix that maintains the joint stiffness.

The actual images of the tested bolted joint specimens at different bolt torque levels (0, 2 and 4 Nm) aged at 65 ^{o}C for 30 days, are shown in Fig. 5.12. It can be seen from the images that all the specimens failed under bearing mode. In Fig. 5.12 (a) the failure occurred in the narrow zone at 0 Nm (hand tightening torque) whereas in Fig. 5.12 (b) and (c) the failure occurred in the wider zone due to higher lateral constraints which increased the joint stiffness and further promoted higher bearing failure loads.

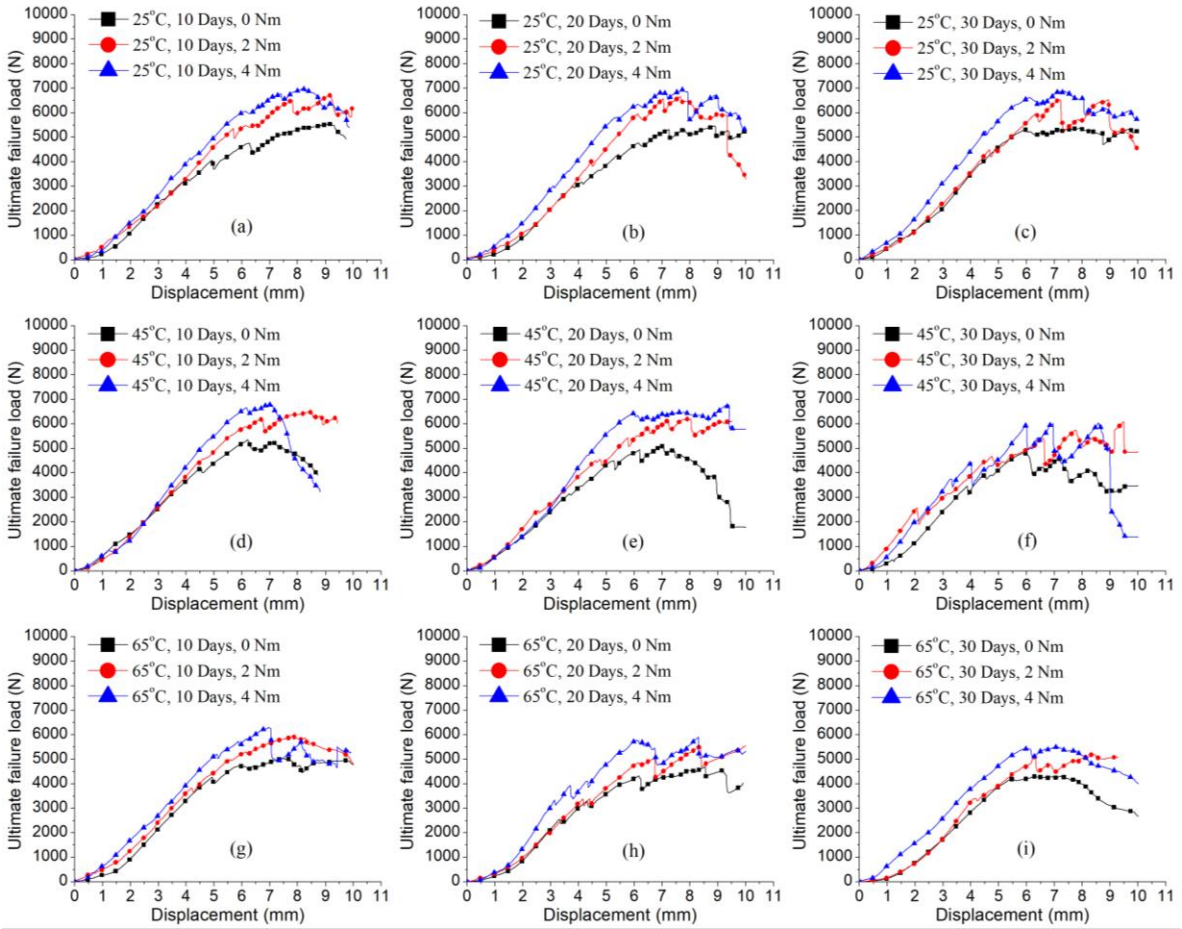

Fig. 5.10 Load vs. displacement graphs for hygrothermally aged EB cured neat composite bolted joint specimens at 25 ^{o}C, 45 ^{o}C and 65 ^{o}C

The comparison of neat and MWCNTs added composite bolted joint specimens, unaged and hygrothermal aged, at different bolt torques are plotted in Fig. 5.13. Table 5.3 shows the ultimate failure loads of EB cured bolted joint specimens at different hygrothermal aging conditions. It was observed that ultimate failure loads are more in MWCNTs joint specimens

as compared to neat joint specimens. The formation of good MWCNTs/polymer interfacial bonding and excellent barrier properties tends to restrict the interfacial debonding under hygrothermal aging conditions which helps in increasing the ultimate failure loads whereas, in neat joint specimens, the combined effect of water and temperature for a prolonged duration on composite specimens have shown a deteriorating effect on the ultimate failure loads. It was found that when temperature and duration increases from 25 ^{o}C to 65 ^{o}C and 0 to 30 days, the ultimate failure loads decreases significantly.

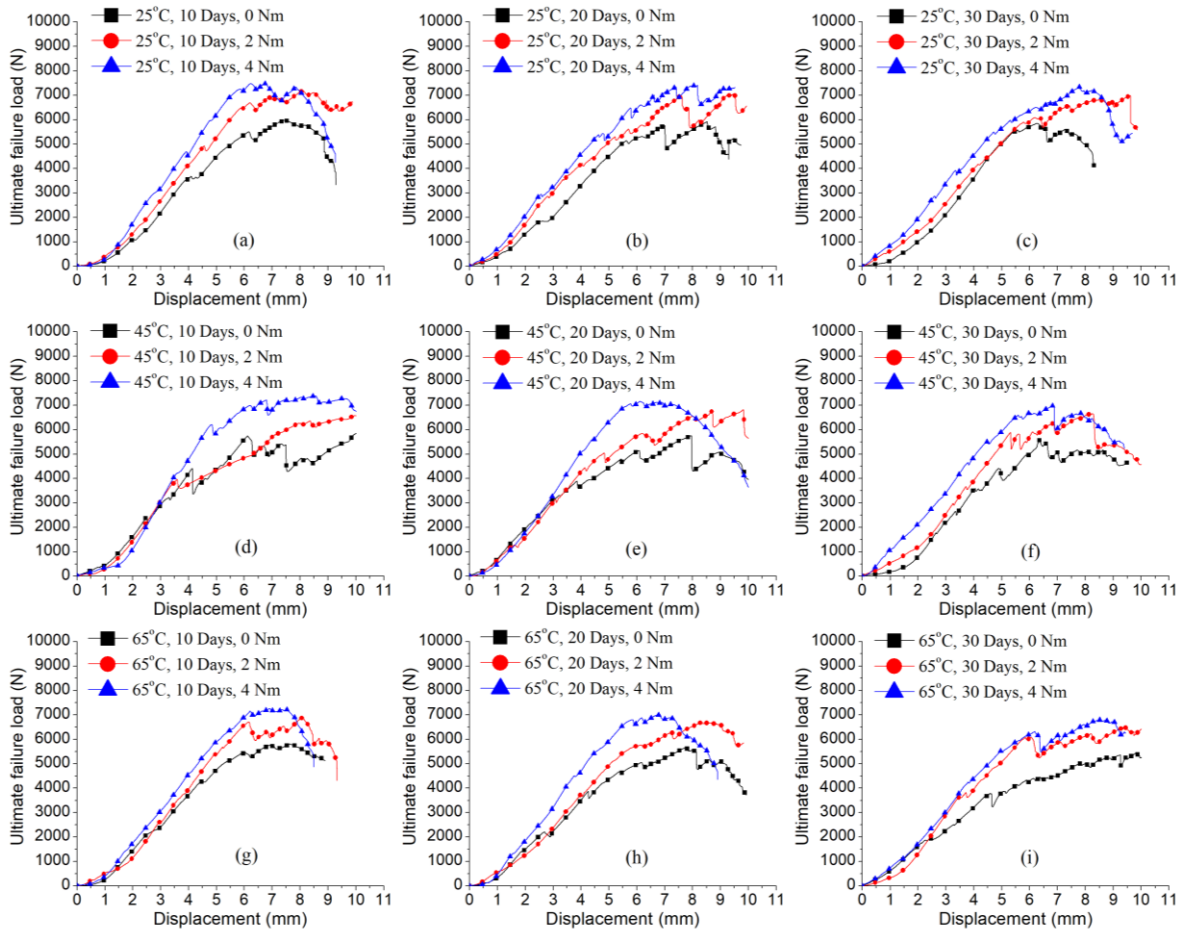

Fig. 5.11 Load vs. displacement graphs for hygrothermally aged EB cured 0.3 wt.% of MWCNTs added composite bolted joint specimens at 25 ^{o}C, 45 ^{o}C and 65 ^{o}C

From Fig. 5.13 (a and d), the negligible impact on ultimate failure load was observed in neat and MWCNTs composite bolted joints specimens for unaged and aged at 25 ^{o}C, even after 30 days. The moderate change in ultimate failure loads was observed at a water temperature of 45 ^{o}C and 65 ^{o}C for shorter durations.

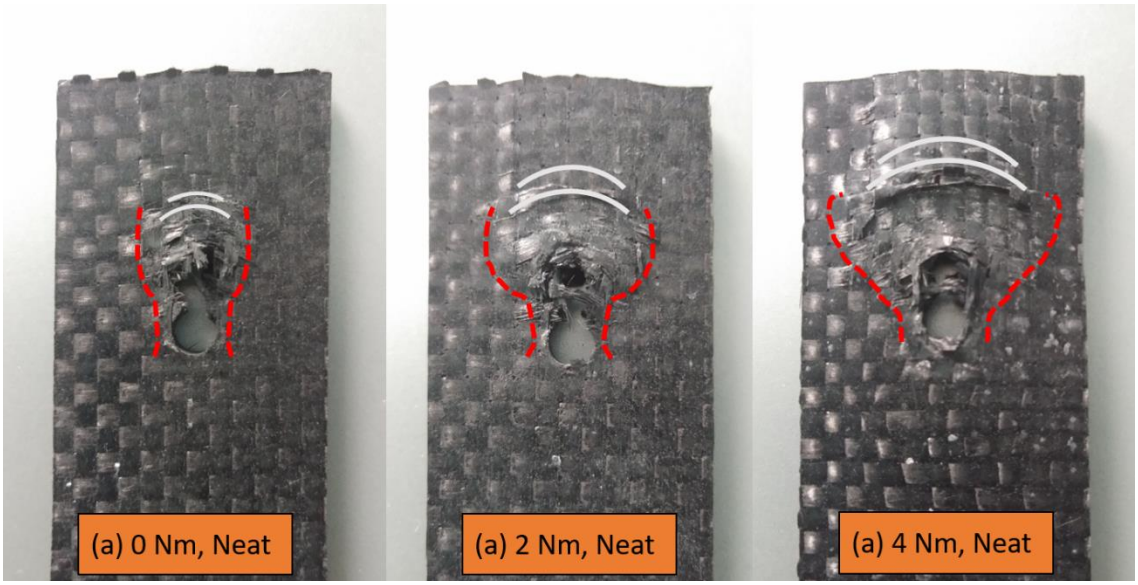

Fig. 5.12 Actual images of neat composite bolted joint specimens at 65ºC for 30 days at (a) 0 Nm (b) 2 Nm and (c) 4 Nm bolt torques

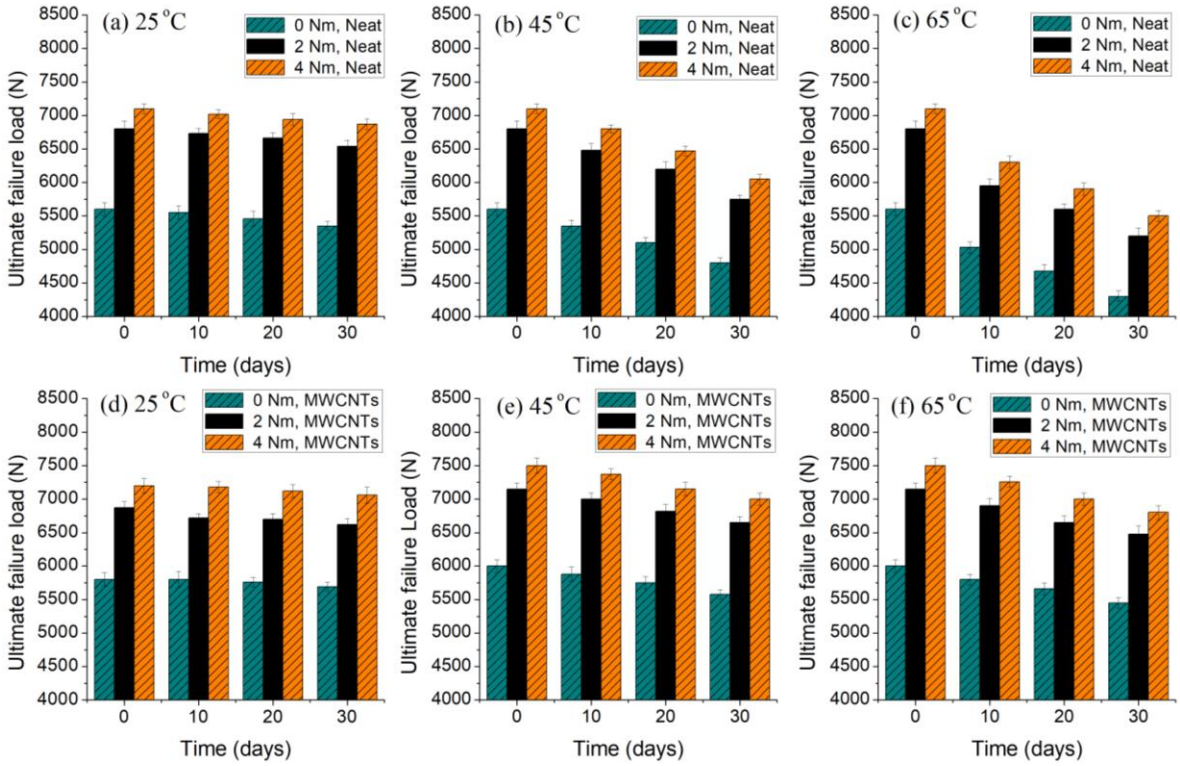

Fig. 5.13 Ultimate failure loads of unaged and aged EB cured joint specimens at different bolt torques

But as time progresses, the degradation rate became more severe in the composite bolted joint specimens after 30 days of aging. This degradation behavior was related to the water

absorption phenomenon, which is less at a water temperature of 25 ^{o}C. At higher water temperatures, increased segmental movement of the polymeric chain helps in enhancing the water absorption rate [204] and resulting in the reduction of the performance of composite bolted joints.

Table 5.3 Ultimate failure loads of EB cured bolted joint specimens at different hygrothermal aging conditions

Sr. No.	Factor			Material			
				Neat		with MWCNTs	
	Temperature (°C)	Time (Weeks)	Torque (Nm)	Failure load (N)	% reduction	Failure load (N)	% reduction
1	Unaged		0	5600	-	6000	-
2	Unaged		2	6800	-	7150	-
3	Unaged		4	7100	-	7500	-
4	25	10	0	5550	0.89	5970	0.50
5	25	20	0	5460	2.50	5920	1.33
6	25	30	0	5350	4.46	5850	2.50
7	25	10	2	6730	1.03	7150	0
8	25	20	2	6660	2.06	7070	1.12
9	25	30	2	6540	3.82	6970	2.52
10	25	10	4	7020	1.13	7480	0.27
11	25	20	4	6940	2.25	7410	1.2
12	25	30	4	6870	3.24	7350	2.00
13	45	10	0	5350	4.46	5880	2.00
14	45	20	0	5100	8.93	5750	4.17
15	45	30	0	4800	14.29	5580	7.00
16	45	10	2	6480	4.71	7000	2.10
17	45	20	2	6200	8.82	6820	4.62
18	45	30	2	5750	15.44	6650	6.99
19	45	10	4	6800	4.23	7370	1.73
20	45	20	4	6470	8.87	7150	4.67
21	45	30	4	6050	14.79	7000	6.67
22	65	10	0	5030	10.18	5800	3.33
23	65	20	0	4680	16.43	5660	5.67
24	65	30	0	4300	23.21	5450	9.17
25	65	10	2	5950	12.50	6900	3.50
26	65	20	2	5600	17.65	6650	6.99
27	65	30	2	5200	23.53	6480	9.37
28	65	10	4	6300	11.27	7260	3.20
29	65	20	4	5900	16.90	7000	6.67
30	65	30	4	5500	22.54	6800	9.33

From these results, it can be seen that in neat configurations, the water absorption rate is higher which results in epoxy swelling and creating microcracks at the fiber/matrix interface

which contributes to severe degradation of the joints with respect to time duration. Whereas incorporating nanofiller (0.3 wt.% of MWCNTs) in the joint specimens lowers the water absorption rate even at the higher temperature. Thus, the ultimate failure load values in MWCNTs composites were on the higher side as compared to neat composite bolted joint configurations. The reduction in absorption rate is attributed to the fact that the barrier properties, tortuosity effect and interfacial bonding between fiber and epoxy are stronger in MWCNTs added composite bolted joints that lowers the tendency to absorb water through capillary action [161, 187].

The ultimate failure loads for MWCNTs joint configuration as seen in Fig. 5.13 (d)-(f), are less affected by water temperature and duration at higher torques in comparison to neat configurations (Fig. 5.13 (a)-(c)). The reason being MWCNTs act as a mechanical interlock between fiber/epoxy interface and epoxy matrix that supports the structural integrity of the composites under hygrothermal conditions [162]. The overall percent reduction in ultimate failure loads for neat composite bolted joints at 0 Nm bolt torque were 4.5%, 14.3% and 23.2% at 25 ^{o}C, 45 ^{o}C and 65 ^{o}C, respectively after 30 days. Whereas the percent reduction for MWCNTs added composite bolted joints were 2.5%, 7.0% and 9.2% at 25 ^{o}C, 45 ^{o}C and 65 ^{o}C, respectively, after 30 days.

5.2.1.5 Statistical Analysis

Response surface methodology (RSM) technique has been applied on the EB cured bolted composite joint using a central composite design to optimize the output response which has a dependency on the different control parameters. In the present work, failure load is taken as an output response for three continuous and one categorical control parameter as shown in Table 5.4. Continuous factors consist of duration (P), torque (Q) and temperature (R) while the material (M) is specified under the categorical factor. Using RSM statistical approach, 40 runs were conducted for analysis which are shown in Table 5.5. The experimental data obtained through analysis of variance (ANOVA) is given in Table 5.6.

Table 5.4 Control parameters

Factors		**Levels**		
		1	**2**	**3**
Continuous	Duration, P (days)	10	20	30
	Torque, Q (Nm)	0	2	4
	Temperature, R (^{o}C)	25	45	65
Categorical	Material, M	Neat	MWCNTs	--

Table 5.5 Sample runs with accordance to central composite design in statistical analysis

S.No.	Duration, P	Torque, Q	Temperature, R	Material, M	Failure loads
1	10	4	65	Neat	6300
2	10	4	65	MWCNTs	7260
3	20	2	45	MWCNTs	6820
4	30	4	25	MWCNTs	7350
5	30	4	25	Neat	6870
6	10	0	25	Neat	5550
7	10	0	25	MWCNTs	5970
8	30	0	65	MWCNTs	5450
9	20	2	45	MWCNTs	6720
10	20	2	45	Neat	6200
11	20	2	45	Neat	6290
12	30	0	65	Neat	4300
13	10	0	65	Neat	5030
14	10	4	25	Neat	7020
15	30	4	65	MWCNTs	6800
16	20	2	45	Neat	6100
17	20	2	45	Neat	6150
18	30	0	25	Neat	5350
19	30	0	25	MWCNTs	5850
20	20	2	45	MWCNTs	6820
21	10	4	25	MWCNTs	6300
22	20	2	45	MWCNTs	6750
23	10	0	65	MWCNTs	5800
24	30	4	65	Neat	5500
25	20	0	45	MWCNTs	5750
26	10	2	45	MWCNTs	7000
27	20	2	25	MWCNTs	7070
28	20	2	45	MWCNTs	6790
29	20	2	65	Neat	5600
30	20	4	45	MWCNTs	7150
31	20	2	45	Neat	6100
32	20	4	45	Neat	6470
33	20	2	45	Neat	6120
34	10	2	45	Neat	6480
35	30	2	45	Neat	5750
36	20	2	45	MWCNTs	6750
37	20	2	25	Neat	6660
38	30	2	45	MWCNTs	6650
39	20	0	45	Neat	5100
40	20	2	65	MWCNTs	6650

Table 5.6 Analysis of Variance

Source	DF	Adj SS	Adj MS	F-Value	P-Value	Contribution (%)
Model	13	17677786	1359830	52.09	0.0001	96.30
Linear	4	14160065	3540016	135.60	0.0001	77.13
Duration, P	1	403280	403280	15.45	0.0010	2.20
Torque, Q	1	8281845	8281845	317.23	0.0001	45.11
Temperature, R	1	1404500	1404500	53.80	0.0001	7.65
Material, M	1	4070440	4070440	155.92	0.0001	22.17
Square	3	1732591	577530	22.12	0.0001	9.43
$P \times P$	1	6825	6825	0.26	0.6130	0.03
$Q \times Q$	1	826828	826828	31.67	0.0001	4.51
$R \times R$	1	575	575	0.02	0.8830	0.01
2-way Interaction	6	1785130	297522	11.40	0.0001	9.72
$P \times Q$	1	67600	67600	2.59	0.1200	0.36
$P \times R$	1	532900	532900	20.41	0.0001	2.90
$P \times M$	1	283220	283220	10.85	0.0030	1.54
$Q \times R$	1	13225	13225	0.51	0.4830	0.07
$Q \times M$	1	31205	31205	1.20	0.2840	0.17
$R \times M$	1	856980	856980	32.83	0.0001	4.66
Error	26	678774	26107			3.69
Lack of fit	16	642824	40177	11.18	0.0001	3.50
Pure error	10	35950	3595			0.19
Total	39	18356560				

ANOVA is a collection of statistical data used to verify the differences in means among the different groups. It can be seen from Table 5.6 (p-value < α at 95% confidence interval) that factors P, Q, R, M and their respective interactions are the significant terms for output response i.e., failure loads. Therefore, these are taken as the input factors for the output response. The R^2 value is determined to examine the correctness of the statistical model. The R^2 value is a statistical measure of the closeness of the data to the fitted regression line. The closer the value of R^2 to 100%, the closer is the statistically predicted values to the experimental values, the model is significant and suitable [207, 208].

For the present model, the R^2 value is 0.9630 i.e., the model predicted value is 96.30% closer to the experimental values of the failure loads. The measure of deviation from the mean values is termed as the coefficient of variation (CV), which illustrates the reliability of the experiments. From the literature, it was found that the CV of less than 10% gives better reliability [208]. In the present work, the CV was less than 5%, showing that the failure load response model is highly reliable. The impact of control parameters i.e., temperature,

duration (time), torque and material on failure load was analytically found to be 7.65%, 2.20%, 45.11% and 22.17%, respectively.

The regression equations (5.4) and (5.5) are used to predict the failure loads in neat and 0.3 wt.% of MWCNTs added composite laminate joints.

$$Failure\ load\ (Neat) = 5858 + (22.6 \times P) + (631.9 \times Q) - (4.5 \times R) - (0.352 \times P \times P) - (96.9 \times Q \times Q) - (0.026 \times R \times R) + (3.25 \times P \times Q) - (0.913 \times P \times R) + (0.72 \times Q \times R) \quad (5.4)$$

$$Failure\ load\ (MWCNTs) = 5167 + (46.4 \times P) + (592.4 \times Q) + (16.2 \times R) - (0.352 \times P \times P) - (96.9 \times Q \times Q) - (0.026 \times R \times R) + (3.25 \times P \times Q) - (0.913 \times P \times P) + (0.72 \times Q \times R) \quad (5.5)$$

The individual consequence of hygrothermal aging factors on ultimate failure loads for EB cured neat and 0.3 wt.% of MWCNT added composite joints were studied through surface plots (Fig. 5.14). The surface plots were obtained at different durations of 10, 20 and 30 days. It can be seen that the load-bearing capacity reduced with increase in aging durations. From Fig. 5.14 (a), it can be seen that the temperature and duration severely degrade the ultimate failure load in neat composite joints. At 25 ^{o}C, the time duration hardly affects the ultimate failure loads. But as the temperature rises from 25 ^{o}C to 65 ^{o}C, the ultimate failure load values decrease with respect to time due to debonding of fiber-matrix and epoxy swelling which reduces the performance of bolted joints. Debonding is the consequence of the different volumetric expansion of fiber and epoxy matrix due to moisture absorption that creates localized stresses in the material, which is more severe in accelerated aging conditions [209]. The addition of MWCNTs hinders the moisture absorption up to some extent and also maintains the fiber/matrix interfacial bonding of the composite material. Thus, addition of MWCNTs helps in improving the ultimate failure loads of the composite joints as shown in Fig. 5.14 (b). The bolt torque effect under hygrothermal aging conditions is also shown in Fig. 5.14, for neat and MWCNTs composite joints. It is observed that ultimate failure loads increase with the increase in bolt torque values for both neat and MWCNTs added composite joints. The bolt torque efficiency was slightly less in neat composite joints as compared to MWCNTs added composite joints due to severe degradation in the epoxy and its interface. In such conditions, even the applied torque was not capable of maintaining the joint stiffness and thus reduces the ultimate failure loads. The

addition of MWCNTs in the composites improves the bolt torque efficiency even at higher aging conditions in comparison to neat composites.

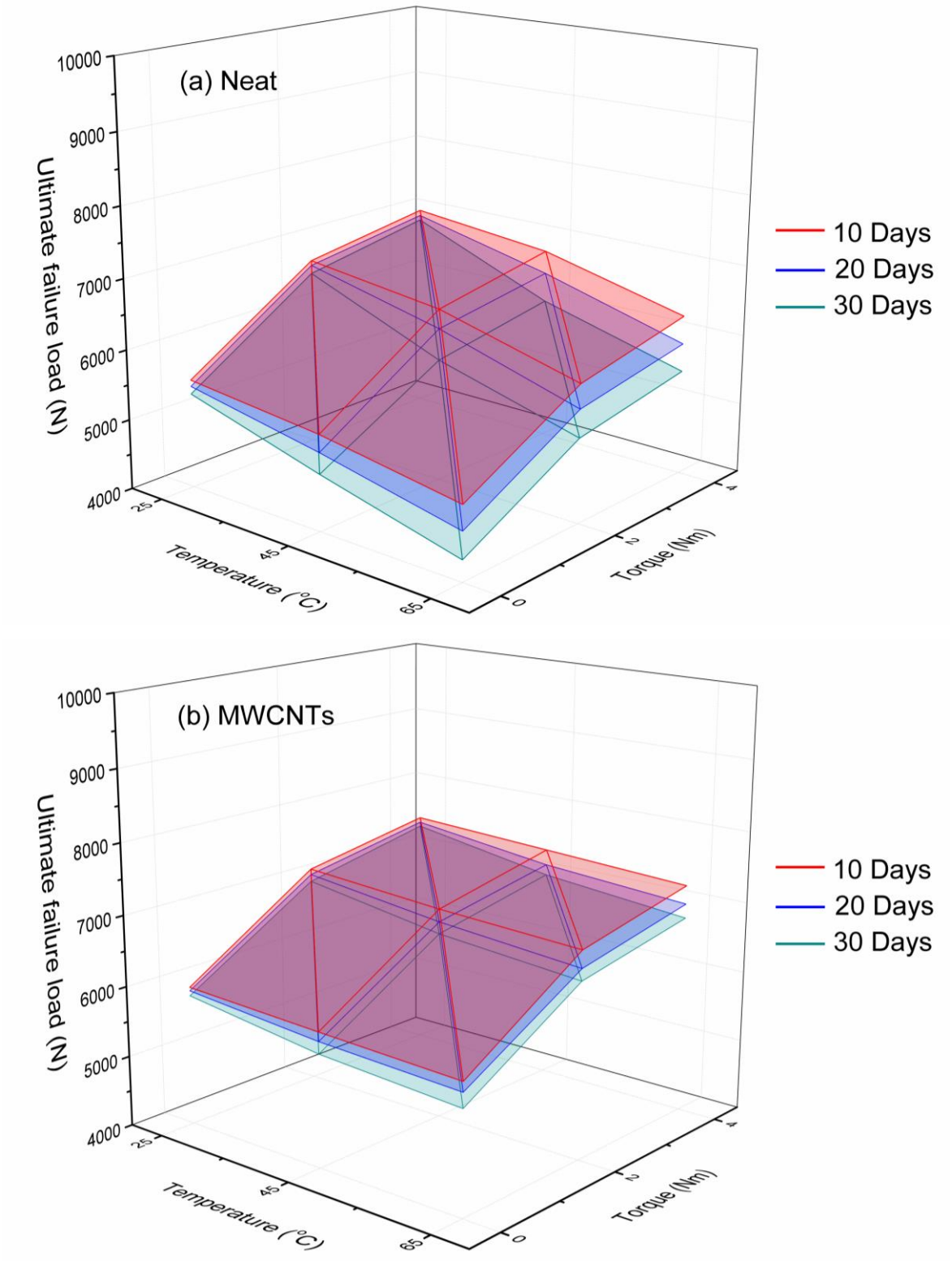

Fig. 5.14 Surface plots indicating ultimate failure loads for EB cured (a) neat composite joints (b) MWCNTs added composite joints for 10, 20 and 30 days of aging

It can be seen from Figs. 5.14 (a) and (b), that the gap between the different surface plots is lesser in MWCNTs added composite joints as compared to neat joints which signifies that the addition of MWCNTs improves the performance of the joints. The reason being MWCNTs act as a mechanical interlock between fiber/epoxy interface and epoxy matrix that supports the structural integrity of the composites under hygrothermal conditions [20, 21]. The statistical analysis also shows that the contribution of bolt torque was maximum as compared to the other factors since joint stiffness was maintained by the compressive forces generated through washers. The results show that after addition of MWCNTs nanofiller, bolt torques have proved to be a very effective aspect to sustain the structural integrity under hygrothermal aging conditions.

5.2.2 Bolted joints prepared from thermally cured composites

5.2.2.1 Water diffusion behavior

Under similar hygrothermal aging conditions as taken for EB cured composites, *i.e.,* aging at 25 ^{o}C, 45 ^{o}C and 65 ^{o}C for 30 days, the results from thermal cured neat and 0.3 wt.% of MWCNTs added composite specimens were obtained and plotted in Fig. 5.15. Table 5.7 shows the maximum water absorption percent and diffusion coefficient obtained for nanocomposite specimens. The results show that water diffusion in thermal cured composite specimens takes place in a similar manner as in EB cured composite specimens. No significant difference in the maximum water absorption (M_m) was seen between the thermal and EB cured composite specimens after immersion in water for 30 days, except for the neat specimen (thermally cured) at 65^{o}C which sustain 14.68% less water absorption as compared to the neat specimen (EB cured). This can be due to the higher void content present in the EB cured composites which acts as a free site for the accumulation of water molecules. Other factors like epoxy swelling, micro-cracks and thermal stresses at higher temperatures are responsible for the degradation and higher absorption in the composite specimen.

The results obtained from hygrothermal aged thermally cured composite specimens show that adding MWCNTs reduced water absorption rate and corrected diffusion coefficient by 19% and 26.9% at 25 ^{o}C and by 13.2% and 12.3% at 65 ^{o}C.

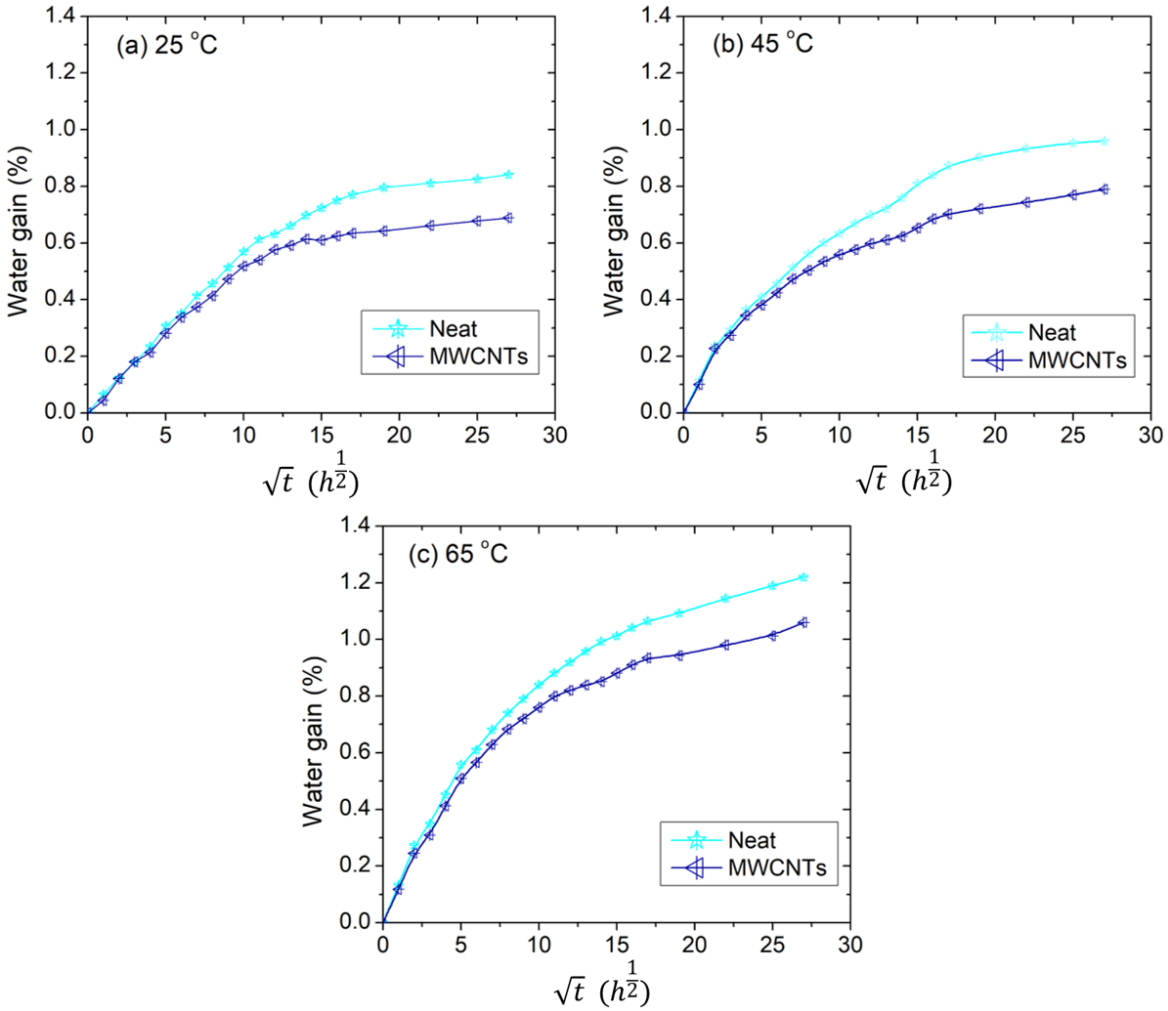

Fig. 5.15 Water absorption behavior in thermally cured nanocomposites at (a) 25 ºC, (b) 45 ºC and (c) 65 ºC for 30 days

Table 5.7 Water absorption percent and diffusion coefficient of nanocomposite materials

Material	**Temperature (ºC)**	**Water absorption, M_m (%)**	**Diffusion coefficient, D (10^{-8} cm^2/s)**
Neat	25	0.84	3.82
MWCNTs	25	0.68	2.79
Neat	45	0.96	4.15
MWCNTs	45	0.79	3.27
Neat	65	1.22	5.67
MWCNTs	65	1.06	4.77

5.2.2.2 Assessment of mechanical properties

The thermally cured neat and MWCNTs added composite specimens were tested at different hygrothermal conditions for tensile and flexural properties. The bar graphs of the tensile and flexural properties of the unaged and aged composite specimens at 25 ºC, 45 ºC and 65 ºC for different time durations are shown in Fig. 5.16.

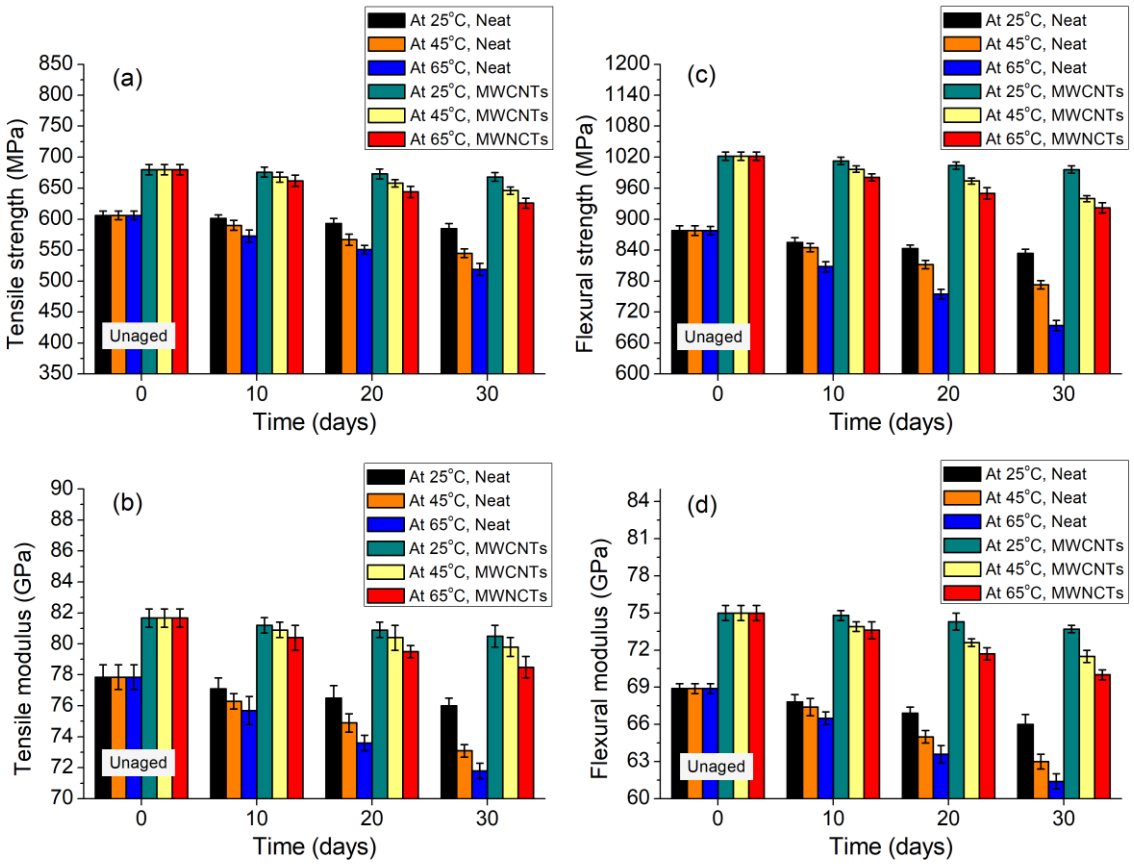

Fig. 5.16 Tensile and flexural properties of thermally cured composite specimens, unaged and aged at different conditions

It can be seen from Fig. 5.16 that the addition of MWCNTs resulted in the improvement in strength and modulus properties of unaged composite specimens. The tensile strength, tensile modulus, flexural strength and flexural modulus of MWCNTs composite specimens have increased by 12.2%, 4.9%, 16.4% and 8.9% respectively, as compared to neat composite specimens. The enhancement in strength and modulus properties is due to the reinforcing ability of the MWCNTs nanofiller [210]. After hygrothermal aging of the specimens at different conditions, the strength and modulus properties were drastically changed. At 25 ºC of water temperature, the strength and modulus properties have shown

negligible degradation in their properties even after 30 days of aging. However, at elevated water temperatures (45 ^{o}C and 65 ^{o}C), a significant reduction in strength and modulus properties were observed in the composite specimens as can be seen in Fig. 5.16. It was found that the degradation was more severe with the increase in aging time. The loss in strength and modulus properties of neat composite specimens were more than that of MWCNTs added composite specimens. After 30 days of aging at 65 ^{o}C of water temperature, the tensile strength, tensile modulus, flexural strength and flexural modulus contributed to the loss by 14.3%, 7.8%, 20.9% and 10.9%, respectively. Similar conditions of aging contributed to the loss of 7.9%, 3.9%, 9.7% and 6.6%, respectively in case of MWCNTs added composite specimens.

Table 5.8 shows the tensile and flexural strength for an average of five specimens of thermally cured composite specimens after hygrothermal aging with their respective percentage strength retentions (Fig. 5.17). The tensile and flexural strength retentions have faced significant reduction under hygrothermal conditioning at higher temperatures as water absorption increases which helps in the degradation phenomenon. These consequences were also examined by Abdel et al. [211] and Ellyin and Maser [212]. From Fig. 5.17, it can be seen that at a lower water temperature, the strength retention rate was higher as compared to that at the elevated water temperature. It can also be seen that the addition of MWCNTs in the composite specimens results in a higher strength retention rate as slope variations of MWCNTs added composite specimens are lower.

Table 5.8 Mechanical properties of thermally cured nanocomposite specimens under aging conditions

S. No.	Temperature (^{o}C)	Duration (days)	Tensile strength (MPa) (SD*)		Flexural strength (MPa) (SD*)	
			Neat	MWCNTs	Neat	MWCNTs
1	Unaged	0	606 (7)	680 (8)	878 (9)	1022 (8)
2	25	10	601 (6)	676 (8)	855 (9)	1013 (7)
3	25	20	593 (8)	673 (8)	843 (7)	1004 (7)
4	25	30	585 (8)	668 (7)	834 (8)	996 (7)
5	45	10	590 (8)	668 (8)	845 (8)	997 (6)
6	45	20	567 (9)	658 (6)	812 (8)	974 (6)
7	45	30	545 (7)	646 (6)	773 (8)	940 (6)
8	65	10	573 (10)	662 (9)	808 (10)	981 (7)
9	65	20	551 (7)	644 (9)	755 (9)	950 (11)
10	65	30	519 (10)	626 (8)	694 (10)	922 (10)

*** SD = Standard deviation**

It was observed that at 65 ^{o}C, after 30 days the tensile strength retention for neat and MWCNTs added composite specimens were 85.7% and 92%, respectively. Correspondingly, the flexural strength retention for neat and MWCNTs added composite specimens were 79% and 90.2%, respectively.

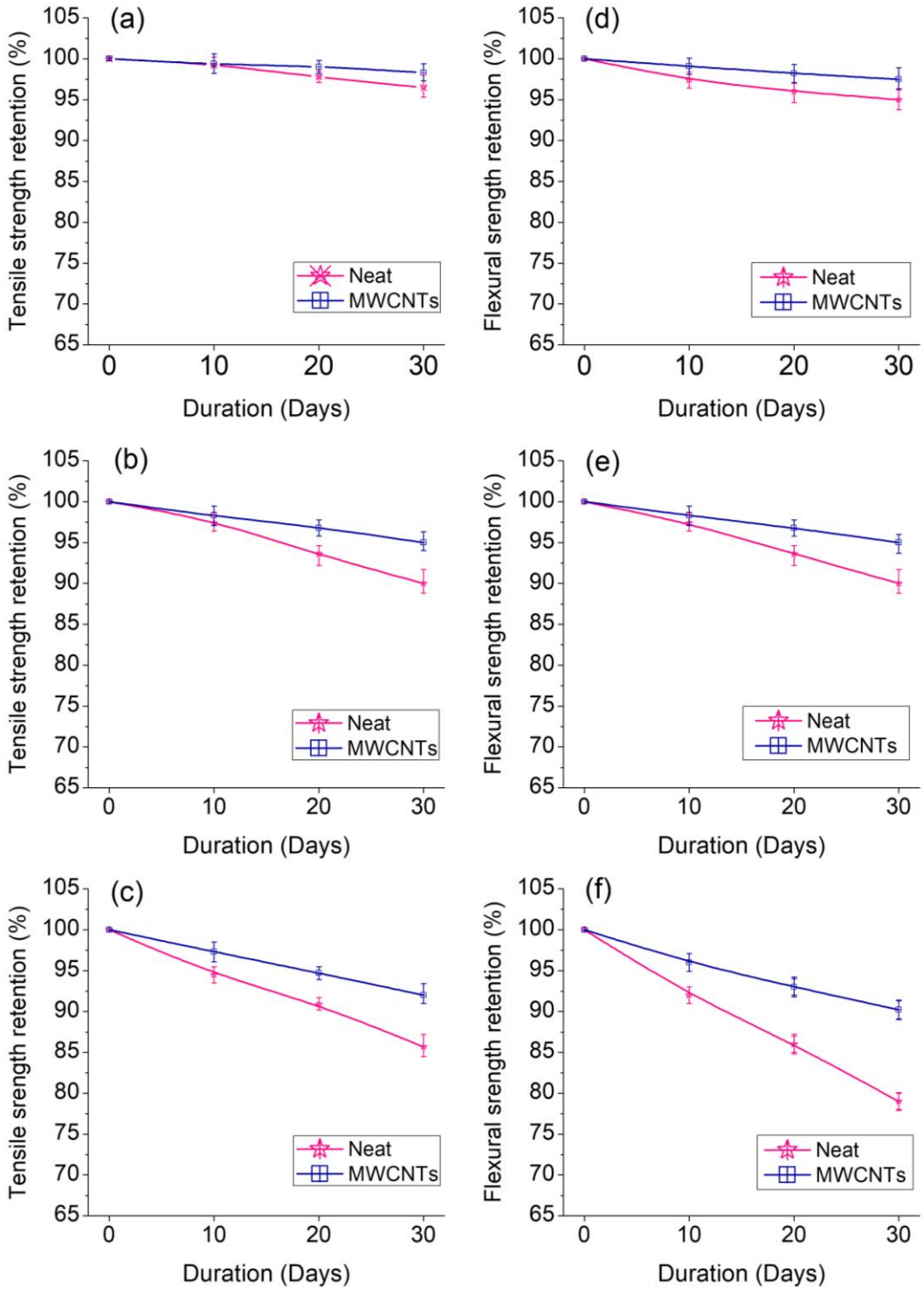

Fig. 5.17 Mechanical strength retention of thermally cured nanocomposite specimens under hygrothermal conditions at (a) 25 ^{o}C, (b) 45 ^{o}C and (c) 65 ^{o}C

5.2.2.3 SEM analysis

The SEM images of unaged and aged specimens at 25 ^{o}C, 45 ^{o}C and 65 ^{o}C for maximum duration of 30 days were analyzed for thermally cured neat and MWCNTs added composite specimens as shown in Fig. 5.18. The excellent interfacial bonding between the fiber and the epoxy matrix was observed for unaged composite specimens as can be seen in Fig 5.18 (a and e). Even after fracture of the specimen, fibers are firmly placed at their positions, showing the good adhesion properties of the epoxy matrix. In Fig. 5.18 (b and f), for the aging at 25 ^{o}C, there was no significant degradation observed at the fiber-matrix interface for neat and MWCNTs added composites even after 30 days as compared to unaged composites, which confirms that the impact of aging was very less on mechanical properties. At 45 ^{o}C and 65 ^{o}C for 30 days of aging, the impact of temperature and duration was severe in neat composite specimens as compared to MWCNTs added composite specimens as shown in Fig. 5.18 (c)-(d) and (g)-(h). In neat composites, at elevated temperatures, the water absorption rate is higher which results in epoxy swelling and creating microcracks and debonding at the fiber/matrix interface as can be seen in Fig. 5.18 (d), which contributes to the severe degradation of the composites with respect to time duration.

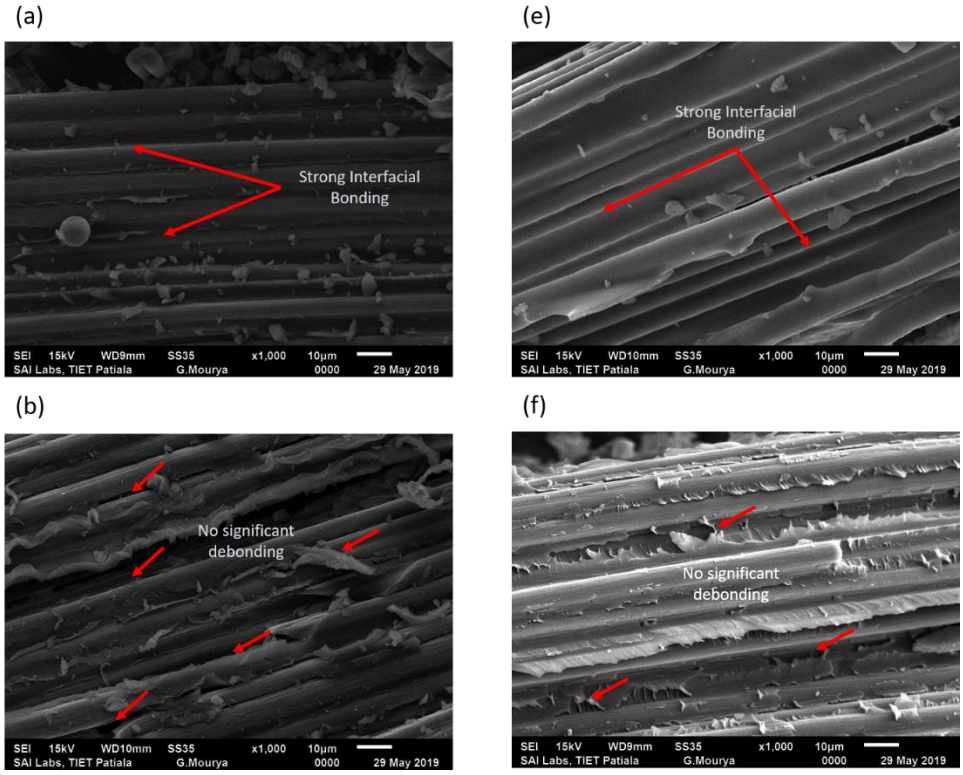

Continued…

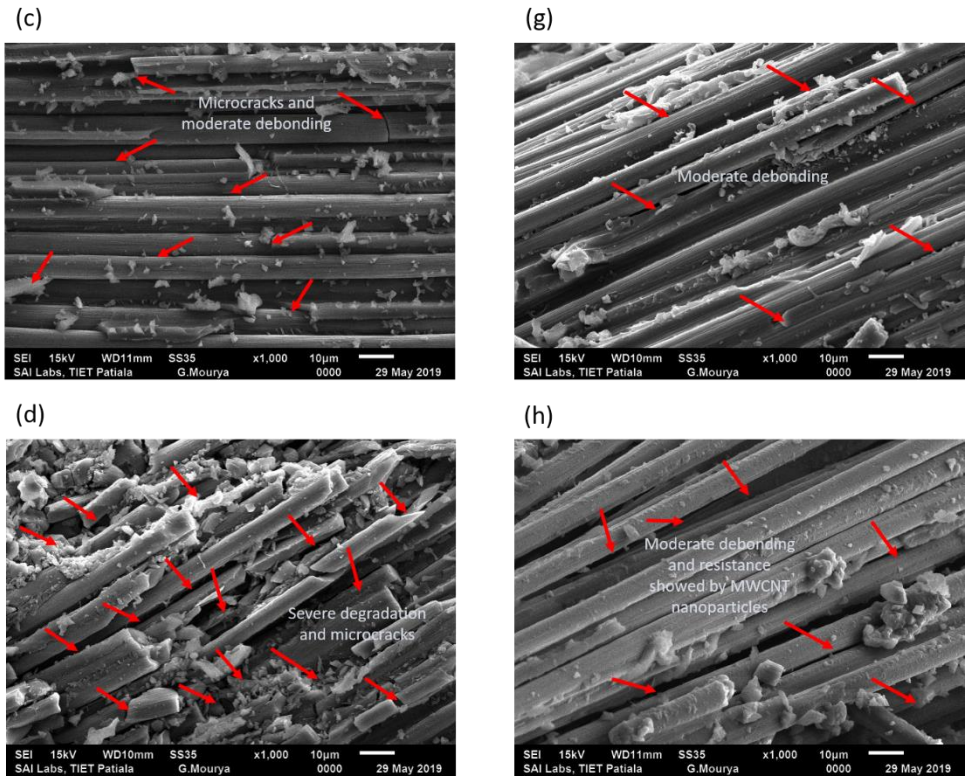

Fig. 5.18 SEM images obtained after mechanical characterization of thermally cured neat composite specimens (a) unaged, (b) aged at 25 ^{o}C, (c) aged at 45 ^{o}C and (d) aged at 65 ^{o}C for 30 days and 0.3 wt.% of MWCNTs added composite specimens (e) unaged, (f) aged at 25 ^{o}C, (g) aged at 45 ^{o}C and (h) aged at 65 ^{o}C for 30 days

5.2.2.4 Performance of bolted joints under hygrothermal aging conditions

Five joint specimens of each configuration after aging were tested and the average results are plotted in Figs. 5.19 and 5.20. The load vs. displacement curves for bearing response starts with a linear movement and after reaching the first failure load it continues moving in a zig-zag pattern showing the bearing mode of failure. The highest peak of the curve in the graphs is taken as the ultimate failure load.

Similar to EB cured joint specimens, the results showed that in the thermally cured joint specimen, joint stiffness increased with increasing bolt torques which further helped in the improvement of ultimate failure loads. Under aging conditions, ultimate failure loads decreased because the water absorption phenomenon was subsequently progressive at severe conditions which are further responsible for the degradation of epoxy matrix and fiber/epoxy interface.

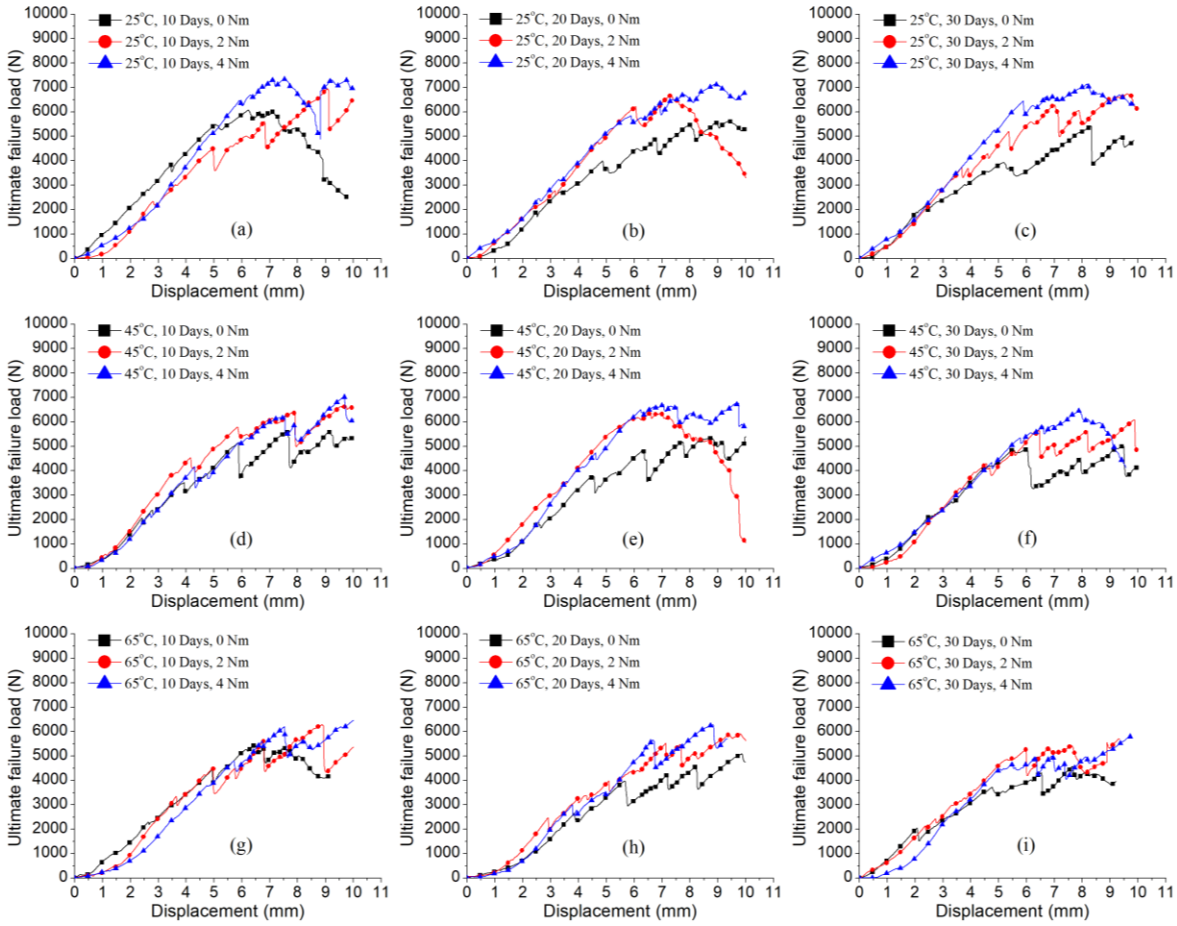

Fig. 5.19 Load vs. displacement graphs for hygrothermally aged thermally cured neat composite joint specimens at 25 ºC, 45 ºC and 65 ºC

The effect of aging conditions on ultimate failure load values of neat and 0.3 wt.% of MWCNTs added composite specimens are shown in Fig. 5.21 and Table 5.9. Comparing bar graphs in Fig. 5.21, for neat and MWCNTs composite joints, it is observed that ultimate failure loads are higher in MWCNTs added composite joints. It is found that when temperature and duration increase from 25 ºC to 65 ºC and 0 to 30 days, respectively, the ultimate failure loads decrease significantly. Figures 5.21(a) and (d) show that there was a lesser difference in neat and MWCNTs added composite joints for unaged and aged at 25 ºC, even after 30 days. The moderate degradation rate occurred for hygrothermal aging at 45 ºC and 65 ºC, the degradation rate was severe in the composite specimens after 30 days of aging. This degradation behavior was related to the water absorption phenomenon, which is less at 25 ºC.

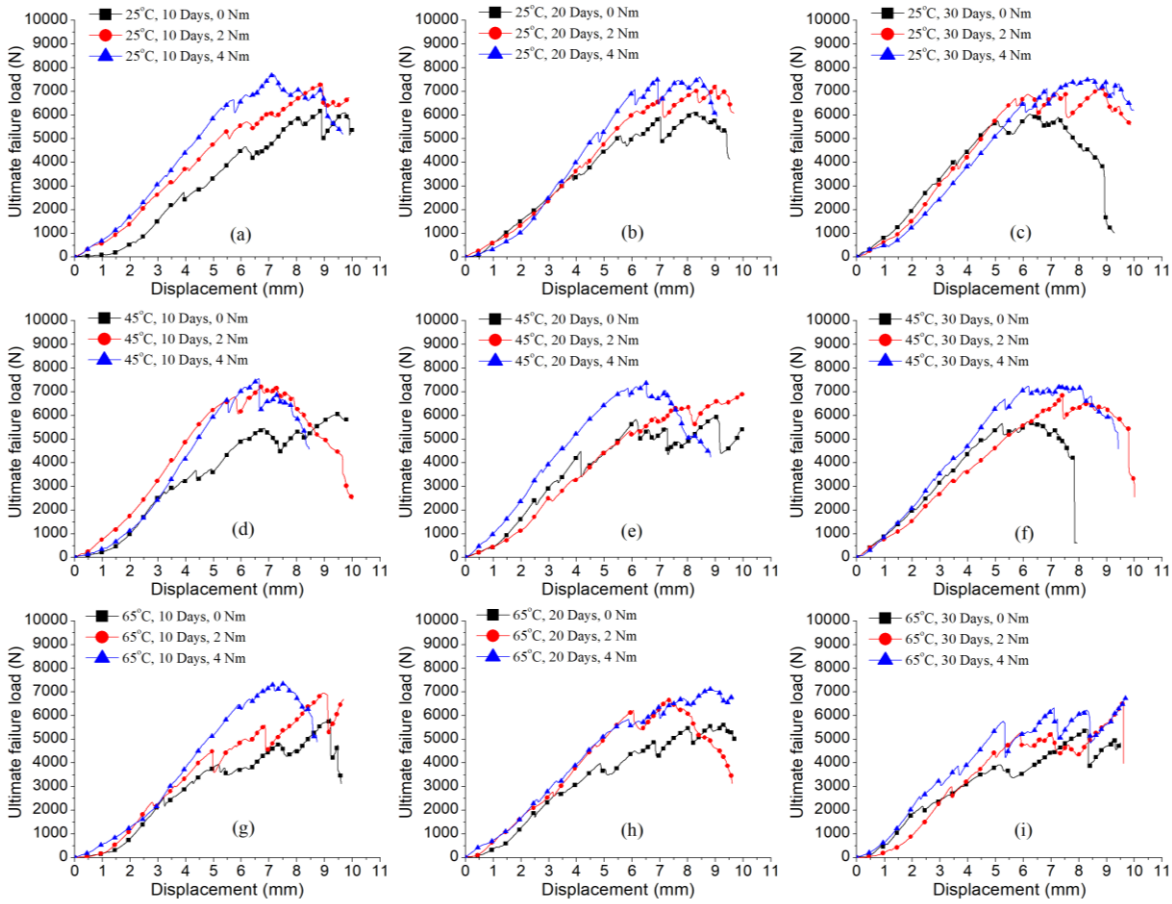

Fig. 5.20 Load vs. displacement graphs for hygrothermally aged thermally cured MWCNTs added composite joint specimens at 25 ºC, 45 ºC and 65 ºC

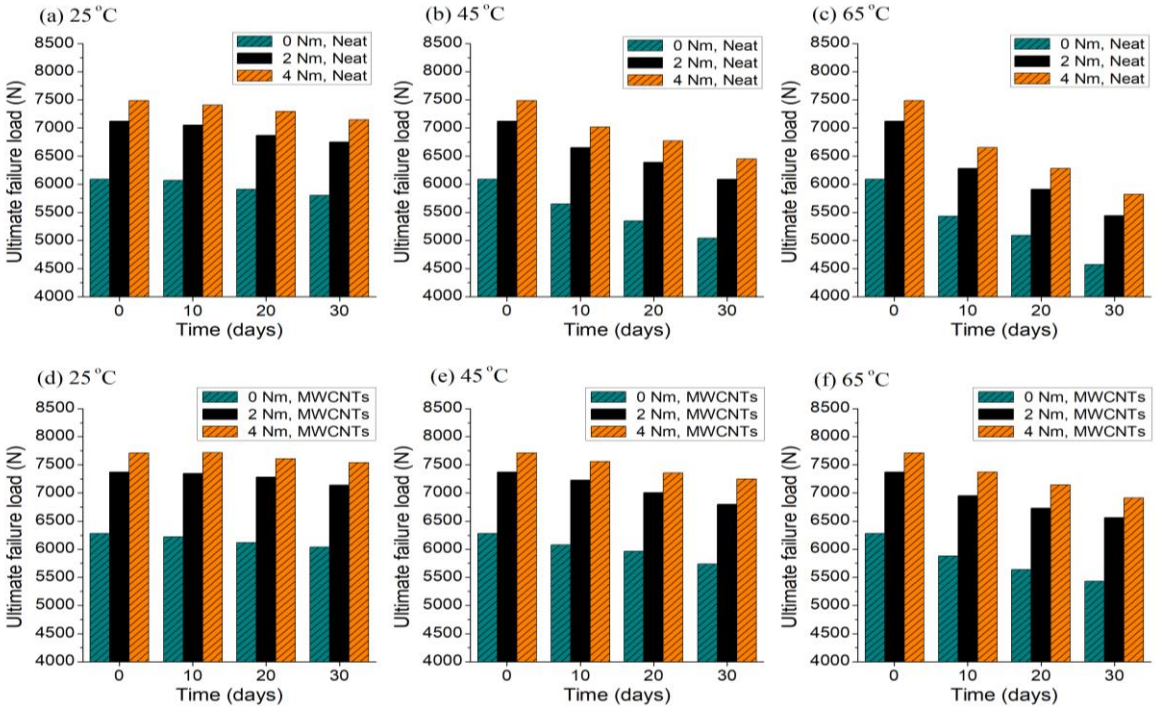

Fig. 5.21 Bar graphs showing ultimate failure loads of thermally cured nanocomposites at different hygrothermal aging conditions

Table 5.9 Ultimate failure loads of thermally cured bolted joint specimens at different hygrothermal aging conditions

S. No.	Factor			Material			
				Neat		with MWCNTs	
	Temperature (°C)	Time (Weeks)	Torque (Nm)	Failure load (N)	% reduction	Failure load (N)	% reduction
1	Unaged		0	6090	-	6280	-
2	Unaged		2	7120	-	7370	-
3	Unaged		4	7490	-	7710	-
4	25	10	0	6070	0.33	6260	0.32
5	25	20	0	5910	2.96	6120	2.55
6	25	30	0	5800	4.76	6040	3.82
7	25	10	2	7050	0.98	7350	0.27
8	25	20	2	6870	3.51	7280	1.22
9	25	30	2	6750	5.20	7140	3.12
10	25	10	4	7410	1.07	7710	0
11	25	20	4	7290	2.67	7610	1.30
12	25	30	4	7150	4.54	7540	2.20
13	45	10	0	5650	7.22	6080	3.18
14	45	20	0	5350	12.15	5960	5.10
15	45	30	0	5040	17.24	5740	8.60
16	45	10	2	6650	6.60	7230	1.90
17	45	20	2	6390	10.25	7010	4.88
18	45	30	2	6090	14.47	6800	7.73
19	45	10	4	7020	6.28	7560	1.95
20	45	20	4	6770	9.61	7360	4.54
21	45	30	4	6450	13.89	7250	5.97
22	65	10	0	5430	10.84	5880	6.37
23	65	20	0	5090	16.42	5640	10.19
24	65	30	0	4570	24.96	5430	13.54
25	65	10	2	6280	11.80	6950	5.70
26	65	20	2	5910	16.99	6730	8.68
27	65	30	2	5440	23.60	6560	10.99
28	65	10	4	6650	11.21	7370	4.41
29	65	20	4	6280	16.15	7150	7.26
30	65	30	4	5820	22.30	6910	10.38

The contribution of bolt torques can also be seen in Fig. 5.21, which reflects towards positive aspects of using bolt torque in hygrothermal conditions. The overall percent reduction in ultimate failure loads for neat joint configurations at 0 Nm bolt torque was 4.7%, 17.2% and 24.8% at 25 ^{o}C, 45 ^{o}C and 65 ^{o}C, respectively, for 30 days of aging. Whereas, the percent reduction in ultimate failure loads for MWCNTs added joint configurations was 3.8%, 8.5% and 13.5% at 25 ^{o}C, 45 ^{o}C and 65 ^{o}C, respectively, for 30 days of aging.

5.3 Numerical Analysis

The finite element analysis was carried out on the bolted joint using a structural analysis module in ANSYS software. In-situ properties of the EB cured composite specimen were considered for numerical analysis. The Hashin damage criteria along with progressive damage analysis have been utilized for failure analysis of the composite bolted joints. Generally, in the joint specimens, the drilled hole has a high-stress concentration around the hole boundary and may give premature results after evaluation of failure. So, to predict the real-time failure load in the composite bolted joint specimen, the characteristic curve method has been used [213]. A graphical representation of a characteristic curve is shown in Fig. 5.22. The characteristic curve radius (r_c) is given by Eq.(5.6).

$$r_c = \frac{D}{2} + R_{ot} + (R_{oc} - R_{ot})\cos\theta \tag{5.6}$$

where, D is the hole diameter, R_{oc} and R_{ot} are the compressive and tensile characteristic lengths, respectively.

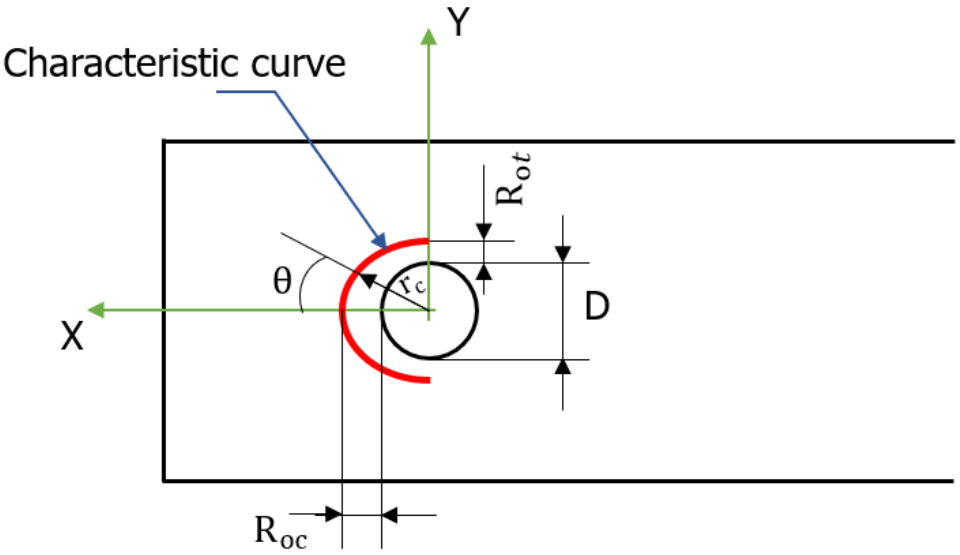

Fig. 5.22 Characteristic curve

The compressive and tensile characteristic lengths are obtained numerically by performing tensile and bearing tests on the open hole composite specimen using finite element analysis. The composite specimens were modelled with the bolted configuration for characteristic length calculations. The specimen was subjected to a symmetrical tensile load, P. The mean tensile strength, $(\sigma_t)_{mean}$ was obtained using Eq.(5.7)

$$(\sigma_t)_{mean} = \frac{P}{(W - D)t} \tag{5.7}$$

Where, W and t are the width and thickness of the composite specimen. While moving in the transverse direction, the distance from the hole edge to the point where equivalent stress is equal to the mean tensile strength is the tensile characteristic length, R_{ot}.

The hole specimen was subjected to the compressive load, P. The mean bearing strength, $(\sigma_b)_{mean}$ was obtained using Eq.(5.8)

$$(\sigma_b)_{mean} = \frac{P}{D \times t} \tag{5.8}$$

The distance from the hole edge to the point, where equivalent stress is equal to the mean bearing strength, is the compressive characteristic length, R_{oc}. In the present work, the numerically calculated values of compressive characteristic length, R_{oc} and tensile characteristic length, R_{ot} are 1.062 mm and 2.291 mm, respectively.

For damage progression in the bolted joint specimen, the Hashin damage criteria was implemented. Hashin damage criteria works upon the equations of fiber and the matrix failure in tensile and compressive loads, as shown in Table 4.2.

The maximum value among the fiber failure and matrix failure in tension and compression is termed as maximum failure index, FI_{max} which is used to determine the failure loads. Failure modes can be determined depending upon the failure location, θ of the bolted joint on the characteristic curve. The failure in the joint occurs when the value of the maximum failure index reaches the reference value on the characteristic curve. Eqs.(5.9) and (5.10) were used to determine the failure modes and failure loads in the bolted joint specimens.

$$\begin{aligned} &\text{Bearing: } 0^o \leq \theta \leq 15^o \\ &\text{Shearing: } 30^o \leq \theta \leq 60^o \\ &\text{Net-tension: } 75^o \leq \theta \leq 90^o \end{aligned} \tag{5.9}$$

The failure load of the bolted joint specimens is calculated using Eq.(5.10)

$$\text{Failure load} = \frac{P}{FI_{max}} \tag{5.10}$$

5.3.1 Loads and boundary conditions

The finite element analysis was performed on the composite bolted joint specimens clamped into the fixture with boundary conditions, applied loads and contact regions as shown in Fig. 5.23. An arbitrary tensile load, P is applied along the x-direction to the fixture while the composite bolted joint specimen was fixed at the end. To allow the working of bolt pretension (bolt torque), the motion is permitted in z-direction and constraint in x, y directions. In all contact regions, frictional contacts are used except the contact between the

bolt and nut which represents the locked condition and given bonded contact. It is assumed that the coefficient of friction remains unaffected after aging and is taken as constant in all joint specimens.

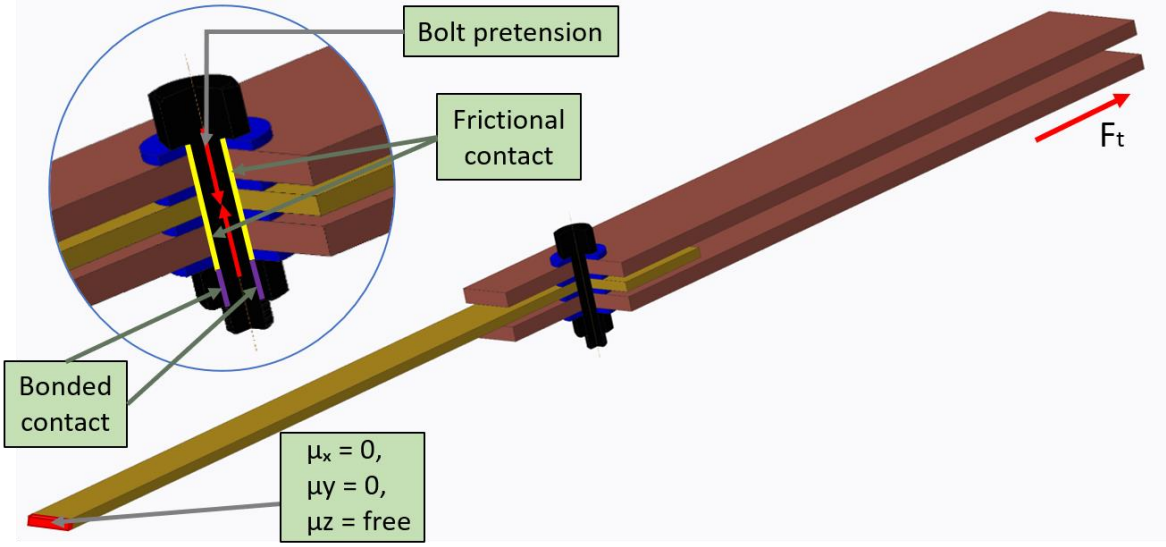

Fig. 5.23 Loads and boundary conditions in the composite bolted joint specimens

The meshing is done using the multizone mesh method with all quad elements. A refined mesh is used in the region around the hole boundary to increase the accuracy of results. The meshed composite bolted joint specimen with the fixture is shown in Fig. 5.24. The analysis has been done in two steps. Firstly, the bolt pretension is given to the joint specimen and secondly, the tensile load is applied while the given bolt pretension is locked.

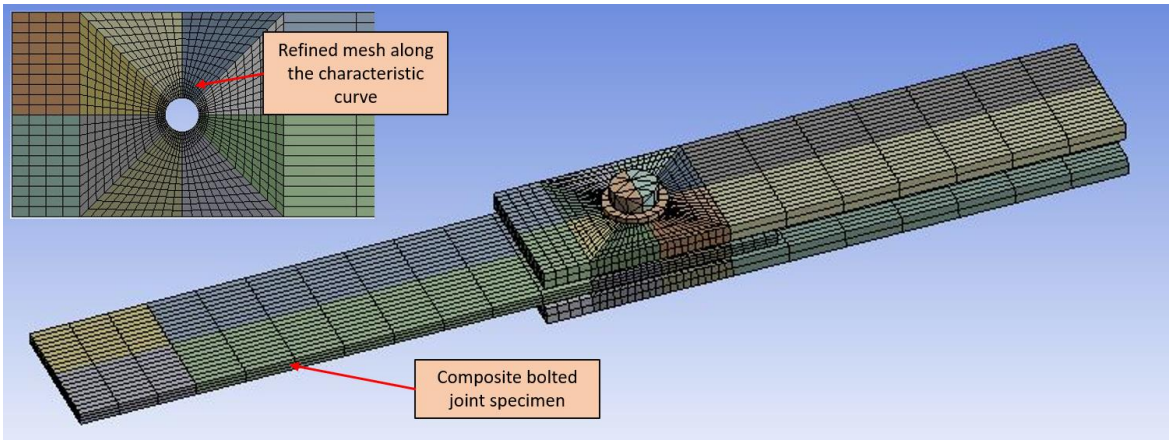

Fig. 5.24 The meshing of composite bolted joint specimen

Figure 5.25 shows the progressive damage contour plots of a particular composite joint specimen. With the gradual increase in applied load, the damage initiates at the hole

boundary and progresses radially towards the free edge of the joint specimen. The damage contour plots clearly show the effect of bolt pretension on the joint specimen. With the increase in torque value, the damage is distributed over a wide area instead of going straight towards the free edge. The failure in the joint is measured when the damage status is greater than or equal to 1 on any point of the characteristic curve.

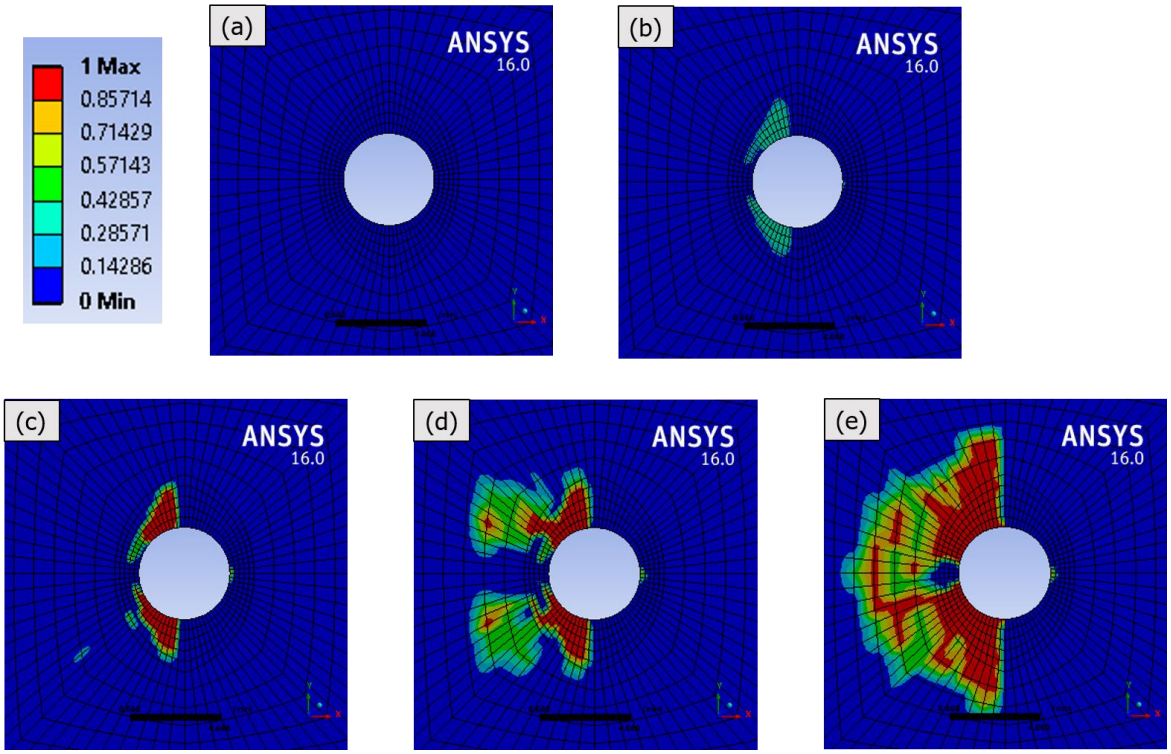

Fig. 5.25 Progressive damage contour plots of composite bolted joint specimen with bolt torque of 4 Nm at (a) 20%, (b) 40%, (c) 60%, (d) 80% and (e) 100% of applied load

In Fig. 5.26, the experimentally obtained progressive damage is compared with the numerically obtained progressive damage showing similar trends at 4 Nm bolt torque in neat configuration specimen.

The numerically predicted ultimate failure loads of the composite joint specimens are shown in Fig. 5.27. Comparing experimentally obtained ultimate failure loads with numerically predicted values shows a good correlation between the results. It was found that hygrothermal aging conditions have a severe impact on the ultimate failure loads of the joint specimens. Whereas, the bolt pretension has shown an increase in ultimate failure loads at higher torques. Incorporating MWCNTs in the joint specimens shows higher predicted ultimate failure loads than the neat composite bolted joint specimens.

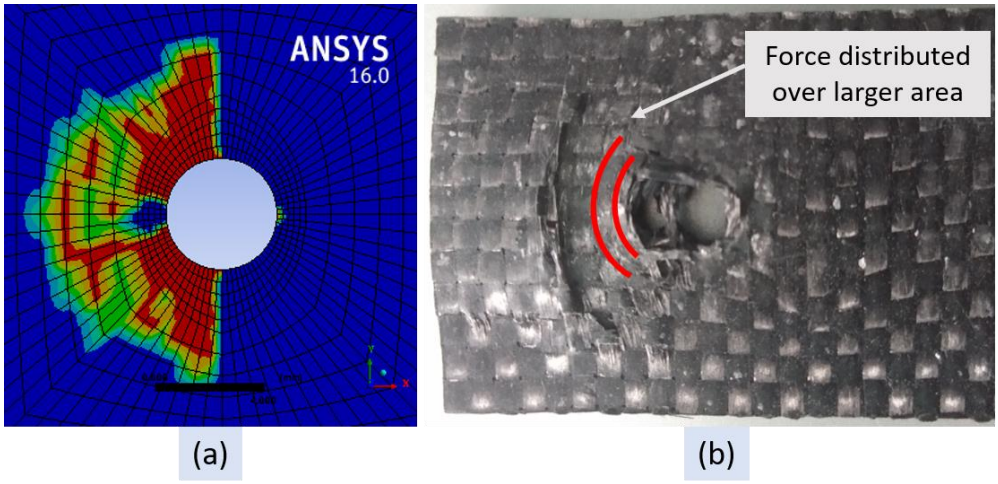

Fig. 5.26 Damage plots obtained at 4 Nm bolt torque for neat configuration (a) numerical and (b) experimental

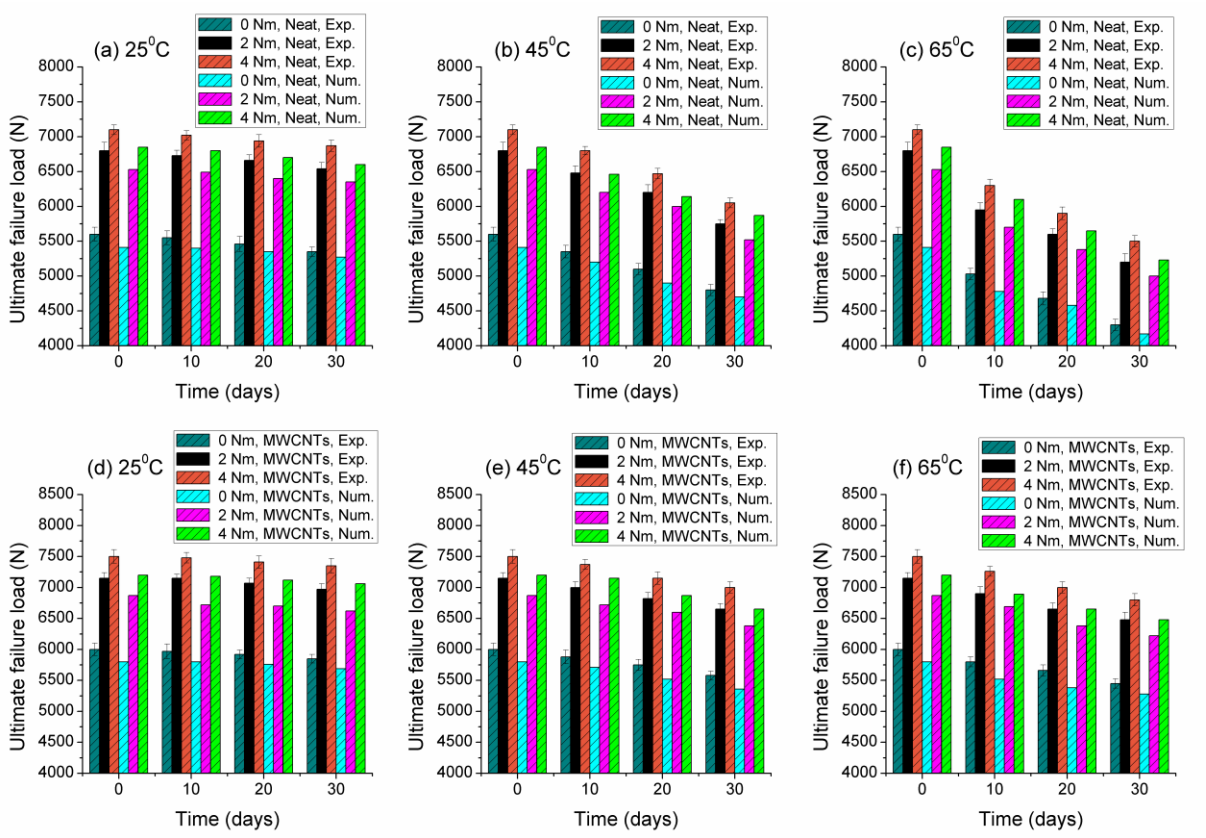

Fig. 5.27 Numerically predicted ultimate failure loads obtained after different hygrothermal aging conditions

5.4 Closure

The present chapter deals with the hygrothermal aging of bolted joints prepared from carbon fiber/epoxy composite laminates. The studies were performed on the composite materials prepared using two different processes, EB curing process and the thermal curing process.

The optimized 0.3 wt.% of MWCNTs nanofiller content was used to improve the mechanical properties of the composite material. The bolt torque in the range of 0 to 4 Nm was applied on the bolted joints. The increasing bolt torque facilitated the distribution of the stresses over a wider area and increased the ultimate failure load as well as stiffness of the joint.

To investigate the performance of joints under hygrothermal aging conditions, three different conditions *i.e.*, 25 ^{o}C, 45 ^{o}C and 65 ^{o}C for the duration of 10, 20 and 30 days, respectively, were considered. The composite specimens under higher water temperatures (45 ^{o}C and 65 ^{o}C) for 30 days have shown the significant degradation. However, at lower water temperature (25 ^{o}C), no significant degradation was observed in the composite specimens. Under aging conditions, the water absorption tendency was higher in neat composite specimens than MWCNTs added composite specimens. Similarly, in the aging process, specimens prepared with the addition of MWCNTs nanofiller have shown good mechanical strength retention than neat composite specimens. A strong correlation between the water temperature, aging duration and the ultimate failure load of the joint was observed. With the increase in immersion time and water temperature, the ultimate failure load values decreased. The bolted joint with MWCNTs added configuration had shown higher ultimate failure loads retention than the joints with neat configuration.

Progressive damage analysis was performed using characteristic curve method along with Hashin damage criteria. A good correlation was obtained between the experimental and numerical results.

To further investigate the joints on environmental aging, the next chapter is concentrated on the performance of bolted joints under accelerated aging conditions *i.e.*, ultraviolet (UV) radiations, moisture and high temperatures.

Chapter 6
Performance of Bolted Joints under Accelerated Aging Environment

In numerous applications, FRP composite based bolted joints have concerns about their long-term durability under harsh environmental conditions, such as ultraviolet (UV) radiation, moisture, elevated temperature, alkalinity and fire [189-191]. From the literature [147-149, 164, 165], it is noted that the combined action of UV radiation, moisture and elevated temperature accelerates the degradation of polymeric materials. So, the present work investigates the performance of carbon fiber/epoxy composite joints under accelerated weathering conditions to evaluate the bearing failure loads of the composite joints. The investigations were carried out on the neat and optimized 0.3 wt.% of MWCNTs added composite materials prepared using two different processes, EB curing process and thermal curing process. The addition of MWCNTs nanofiller tends to slow down the photochemical degradation and also acts as a mechanical barrier against the seepage of water through the polymer matrix. The composite bolted joint specimens were designed as per ASTM D5961 standard having geometric parameters, width to diameter ratio (W/D) and edge to diameter ratio (E/D) fixed to 6 and 5, respectively. The effect of bolt torque applied at different levels (0, 2 and 4 Nm) was also examined.

6.1 Accelerated weathering conditions

The combined cyclic exposure of UV radiation, moisture and the temperature was given to the neat and 0.3 wt.% of MWCNTs added composite specimens as per procedure given in section 2.2.4.2. For uniform exposure at both sides, the specimens were turned over every 24 h. At different intervals of aging exposure, the composite specimens were taken out and were analyzed for physical, chemical, thermal and mechanical characteristics.

6.1.1 Bolted joint under accelerated aging conditions

The bolted joint specimens prepared from the neat and 0.3 wt.% of MWCNTs added carbon fiber/epoxy composite laminates were exposed to the aging environment in the accelerated weathering chamber for different durations. After aging, the bolted joint specimens were clamped into the fixture through fasteners and given a tightening bolt torque using a calibrated torque wrench. Three different bolt tightening torques (0, 2 and 4 Nm) were used for the bolted joints before testing. The testing fixture was prepared as per ASTM D5961,

which consists of steel plates and fasteners (shoulder bolts (M4), lock nuts and washers). The specification of the components of testing fixture is given in Table 2.6. Five joint specimens for each configuration were tested under tensile loading before and after the aging process on the Zwick Roell make UTM machine having a capacity of 10 kN at a crosshead speed of 2 mm/min. The UTM setup along with the bolted joint specimen is shown in Fig. 2.6.

6.2 Results and discussion

The following section provides the results obtained after accelerated weathering conditioning of the bolted joint specimens prepared from EB cured and thermally cured composite laminates.

6.2.1 Bolted joints prepared from EB cured composites

6.2.1.1 FTIR analysis

The FTIR analysis of EB cured neat and 0.3 wt.% of MWCNTs added composite specimens was performed before and after exposure to different accelerated aging conditions. The ATR-FTIR spectra of the carbonyl regions and the hydroxyl regions for neat and 0.3 wt.% of MWCNTs added composite specimens are shown in Figs. 6.1 and 6.2.

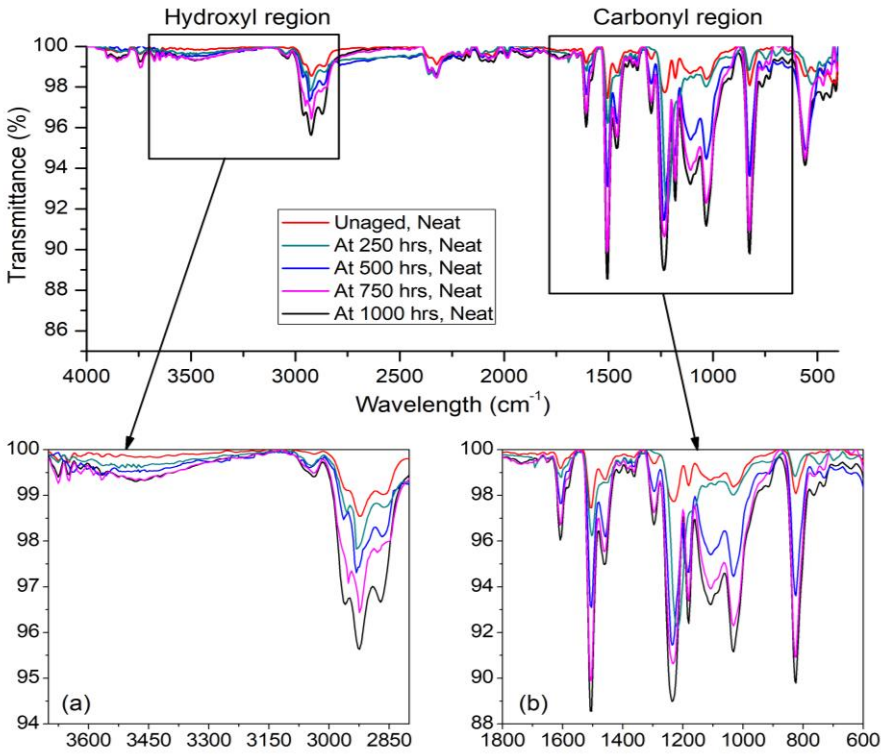

Fig. 6.1 ATR-FTIR spectra of neat configurations showing changes in (a) hydroxyl region and (b) carbonyl region for unaged and accelerated aged specimens

Previous research have found that carboxyl and hydroxyl groups were produced due to hydrogen abstraction from the polymer backbone and degradative oxidation reactions following chain scission [214]. In Fig. 6.1 (b) (carbonyl region), the peaks at 1653 cm^{-1} signify the carbonyl stretching vibrations, at 1716 cm^{-1} was related to the ester groups, at 1510 cm^{-1} was related to N-H stretching, at 1435 cm^{-1} was related to fluorenone type structure, at 1010, 1155 and 1215 cm^{-1} was related to the 1,4-distributed benzenes, at 925 cm^{-1} was related to the diphenyl ketone group and at 850, 765 and 680 cm^{-1} was related to the aromatic C-H out of plane vibration of two adjacent hydrogens [215], which were higher as compared to the MWCNTs added composite specimens under similar conditions as shown in Fig. 6.2 (b).

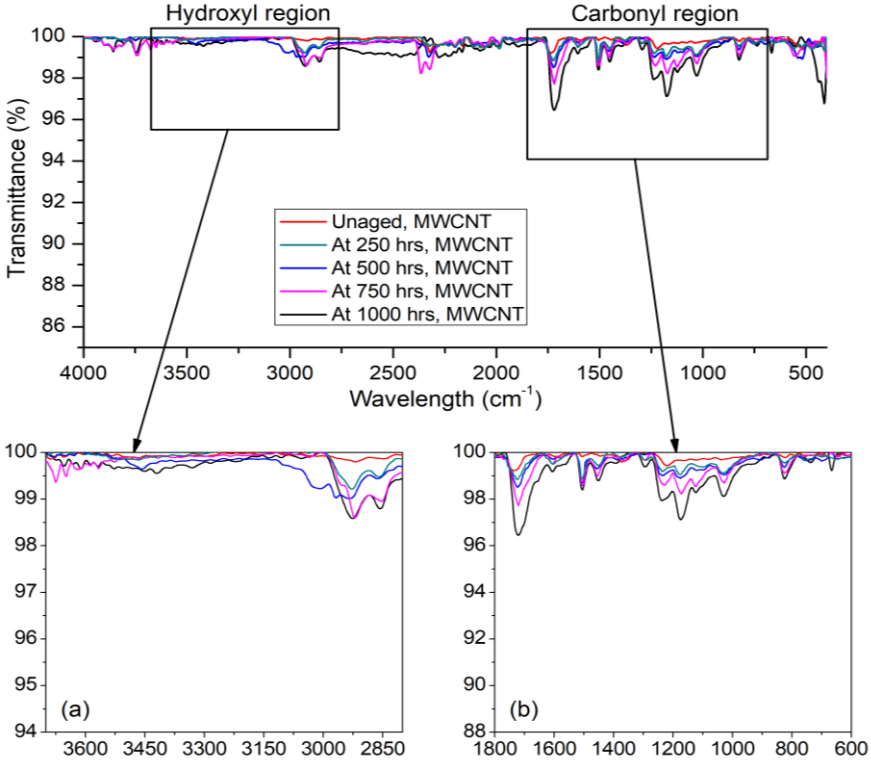

Fig. 6.2 ATR-FTIR spectrums of 0.3 wt.% of MWCNTs added configurations showing changes in (a) hydroxyl region and (b) carbonyl region for unaged and accelerated aged specimens

According to the intensity of each group, several carbonyl categories (diphenyl ketone, fluorenone, esters) were formed, illustrating the deterioration via chain scission reaction and the formation of low molecular products after exposure to UV radiation. Figures 6.1 (a) and 6.2 (a) represents the hydroxyl region of neat and MWCNTs added specimens showing the

change in the hydroxyl group spectrum from 3700 cm^{-1} to 2800 cm^{-1}. The peaks at 3440 cm^{-1} attributed to O-H stretching of carboxylic acid and at 2935 and 2860 cm^{-1} related to the C-H stretching of the monomer units. The higher peaks in the hydroxyl region attributed to the moisture absorption during the condensation exposure step. The results from Fig. 6.2 (a) revealed that moisture absorption is lower in MWCNTs added specimens during aging as compared to the neat composite specimens (Fig. 6.1 (a)).

6.2.1.2 Thermogravimetric analysis

Typical thermograms of the neat and 0.3 wt.% of MWCNTs added composite specimens are shown in Figs. 6.3 and 6.4. The thermal stability at each aging condition in terms of the onset temperature (T_{onset}), maximum decomposition temperature (T_{max}) and residual mass for both neat and 0.3 wt.% of MWCNTs added configuration are summarized in Table 6.1. The results revealed that the specimens before and after exposure show a one-stage decomposition process independent of the exposure time, whereas the amount of residue at 630 ^{o}C strictly depends on the exposure time [180]. It can be seen from Table 6.1 that for unaged, 0.3 wt.% of MWCNTs added specimen have a higher onset temperature at 330.8 ^{o}C as compared to that of the neat specimen (300.7 ^{o}C). With the increase in accelerated aging time, a significant drop in the onset temperature was observed, which was more in neat specimens (257.5 ^{o}C) than 0.3 wt.% of MWCNTs added specimens (315.2 ^{o}C).

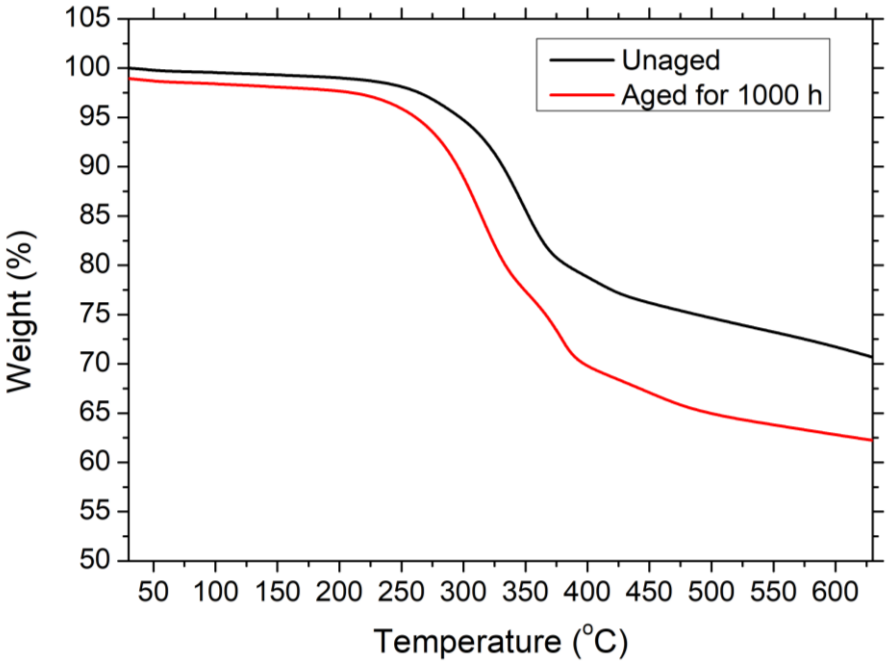

Fig. 6.3 TGA thermograms of neat composite specimens before and after accelerated aging

For short aging exposure, no changes were observed in the weight loss for both neat and MWCNTs configurations. The T_{max} of the neat specimens decreased with exposure time from 368.7 ºC to 349.2 ºC, while for MWCNTs specimens it decreased from 387.6 ºC to 381.9 ºC. In terms of percent residue, the unaged MWCNTs composite specimens have more residue of 74.5% at 630 ºC, in comparison to that of neat composite specimens (71.2%).

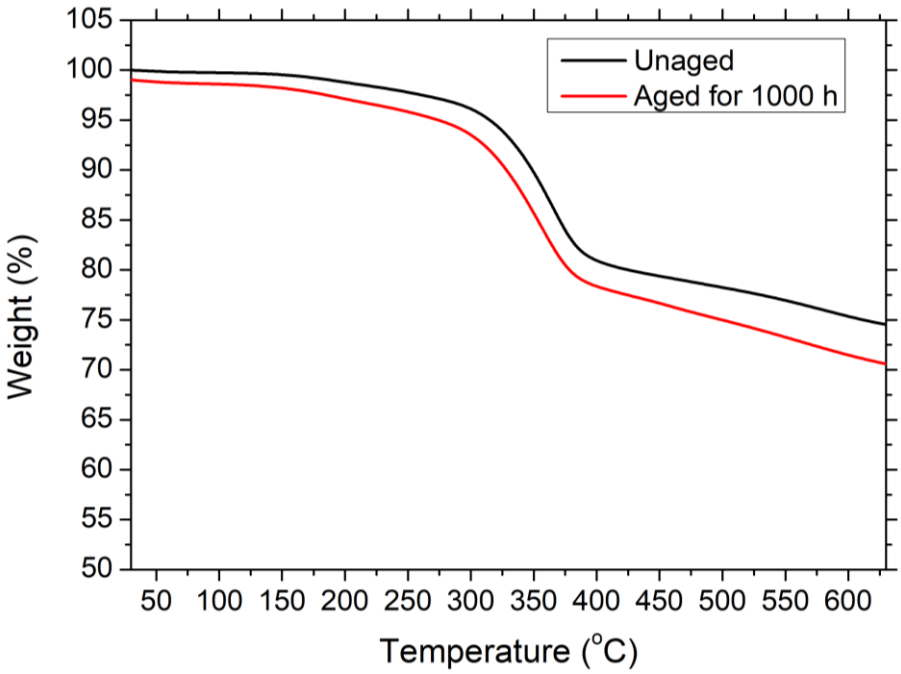

Fig. 6.4 TGA thermograms of 0.3 wt.% of MWCNTs added composite specimens before and after accelerated aging

Table 6.1 TGA results of neat and 0.3 wt.% of MWCNTs added composite specimens before and after accelerated aging

Exposure time (h)	Neat specimens			0.3 wt.% of MWCNTs added specimens		
	T_{onset} (ºC)	T_{max} (ºC)	Residue (%)	T_{onset} (ºC)	T_{max} (ºC)	Residue (%)
Unaged	300.7	368.7	71.2	330.8	387.6	74.5
250	299.4	364.3	70.8	329.8	385.1	74.2
500	283.1	358.2	67.9	324.5	383.9	73.6
750	269.7	353.0	64.7	320.7	382	72.3
1000	257.5	349.2	62.4	315.2	381.9	71.7

Evidently, this trend continued after 1000 h of accelerated aging exposure, although the amount of residue drops significantly. The enhancement of thermal stability of 0.3 wt.% of

MWCNTs added composite specimens after aging is due to the multiple points of covalent bonding between the aliphatic epoxy and the MWCNTs [180].

6.2.1.3 Effect of accelerated aging on the mechanical properties of the nanocomposites

The mechanical strength and modulus properties (in tension, compression and shear) of neat and 0.3 wt.% of MWCNTs added composite specimens were determined before and after exposure to 1000 h accelerated aging environment and the results are presented in Figs. 6.5 (a)-(c). Five specimens for each configuration were tested and average results were plotted in the form of bar graphs (strength) and blue lines (modulus) in Fig. 6.5. The bar graphs and symbols on blue lines for unaged composite specimens revealed that the MWCNTs added specimens had significantly higher tensile strength, tensile modulus, compressive strength, compressive modulus, shear strength and shear modulus by 15.4%, 6.7%, 20.2%, 11%, 23.9% and 20%, respectively, in comparison with the neat specimens. It was found that under all aging conditions, the strength and modulus properties of MWCNTs added specimens were well above the neat composite specimens. Upto 250 h of aging, there was an increase in the strength and modulus properties for both neat and MWCNTs added specimens which indicate that exposure to UV radiations, moisture and temperature under this condition attributed to a stiffening effect due to crosslinking formation in the epoxy matrix [171]. Another cause for improvement is the presence of unreacted cationic photoinitiator under UV radiations and temperature that increases the degree of cure in the composite specimens.

After 250 h of aging, the reduction in the strength and modulus properties began which directed towards the initiation of degradation mechanism as seen from results after 500, 750 and 1000 h of aging (Fig. 6.5). It can be said that in this phase epoxy degradation was more prominent than the relative stiffening effect. The combined effect of UV radiation and condensation at elevated temperature accelerates the degradation mechanism in number of ways. At higher aging durations, the diffusion of chemical agents and moisture increases because of the pathways provided by the microcracks developed on the surface due to UV exposure. Another mechanism is the enhancement of photo-oxidation reactions due to the presence of moisture. In the condensation cycle, the soluble photo-oxidation reaction products were removed due to the exposure of surface to UV radiation which set up a new surface on which further degradation occurs [23]. Furthermore, the epoxy swelling due to absorbed moisture, plasticization, chain scission reactions and thermally induced microcracks is the source of deterioration in the composite specimens.

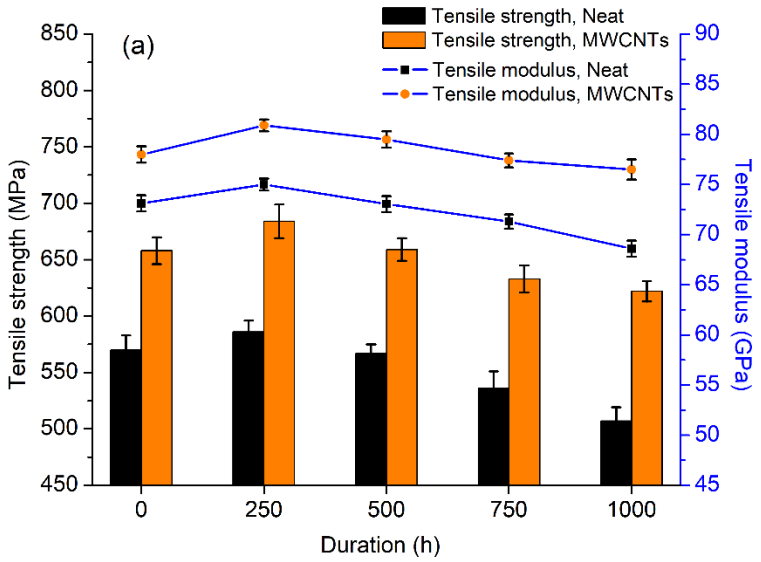
(a)
Tensile strength, Neat
Tensile strength, MWCNTs
Tensile modulus, Neat
Tensile modulus, MWCNTs
Tensile strength (MPa)
Tensile modulus (GPa)
Duration (h)
850
800
750
700
650
600
550
500
450
90
85
80
75
70
65
60
55
50
45
0
250
500
750
1000

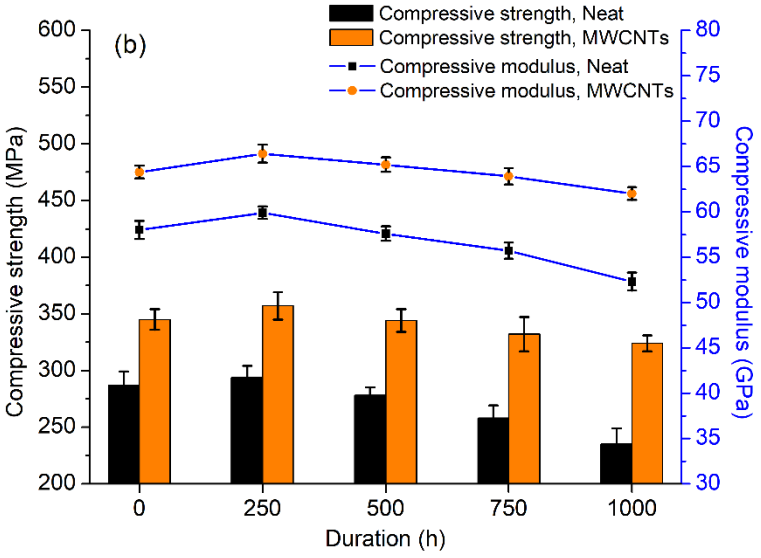
(b)
Compressive strength, Neat
Compressive strength, MWCNTs
Compressive modulus, Neat
Compressive modulus, MWCNTs
Compressive strength (MPa)
Compressive modulus (GPa)
Duration (h)
600
550
500
450
400
350
300
250
200
80
75
70
65
60
55
50
45
40
35
30
0
250
500
750
1000

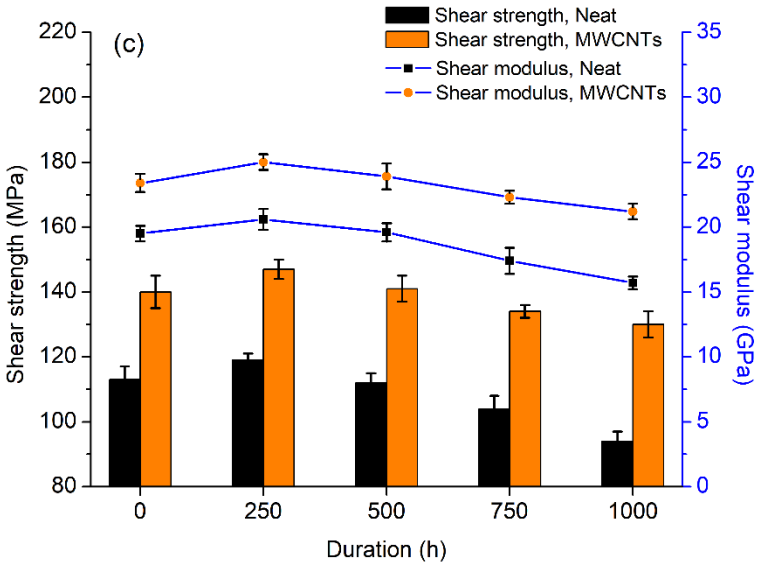
(c)
Shear strength, Neat
Shear strength, MWCNTs
Shear modulus, Neat
Shear modulus, MWCNTs
Shear strength (MPa)
Shear modulus (GPa)
Duration (h)
220
200
180
160
140
120
100
80
35
30
25
20
15
10
5
0
0
250
500
750
1000

Fig. 6.5 Strength and modulus properties of EB cured neat and MWCNTs added nanocomposites (a) tensile, (b) compressive and (c) shear

For improved perception, the strength retention graphs of neat and MWCNTs added composite specimens, before and after aging are presented in Fig. 6.6. The MWCNTs added composite specimen results in a higher strength retention rate, as more steep slopes (showing the rate of degradation) can be seen in the neat composite specimens as compared to MWCNTs added composite specimens. It was found that in aging time of 250 h, there was a slight increase in tensile, compressive and shear strength of 4%, 3.4% and 5.2%, respectively for MWCNTs added composite specimens and 2.8%, 2.4% and 4.3%, respectively for neat composite specimens as compared to unaged specimens. After 250 h, the mechanical properties got reduced and in 1000 h of aging time, the tensile, compressive and shear strength retentions in MWCNTs added composite specimens were 94.5%, 93.8% and 93% respectively. Correspondingly, for neat composite specimens, these were 89%, 82% and 83.5%, respectively. The results revealed that MWCNTs added composite specimens show less degradation than the neat composite specimens. This is due to the high aspect ratio of the MWCNTs that tends to create the wall against the UV radiation and produces a tortuosity effect which allows the moisture to follow prolonged paths. Also, the formation of good MWCNTs/polymer interfacial bonding and excellent barrier properties tends to restrict the interfacial debonding [161].

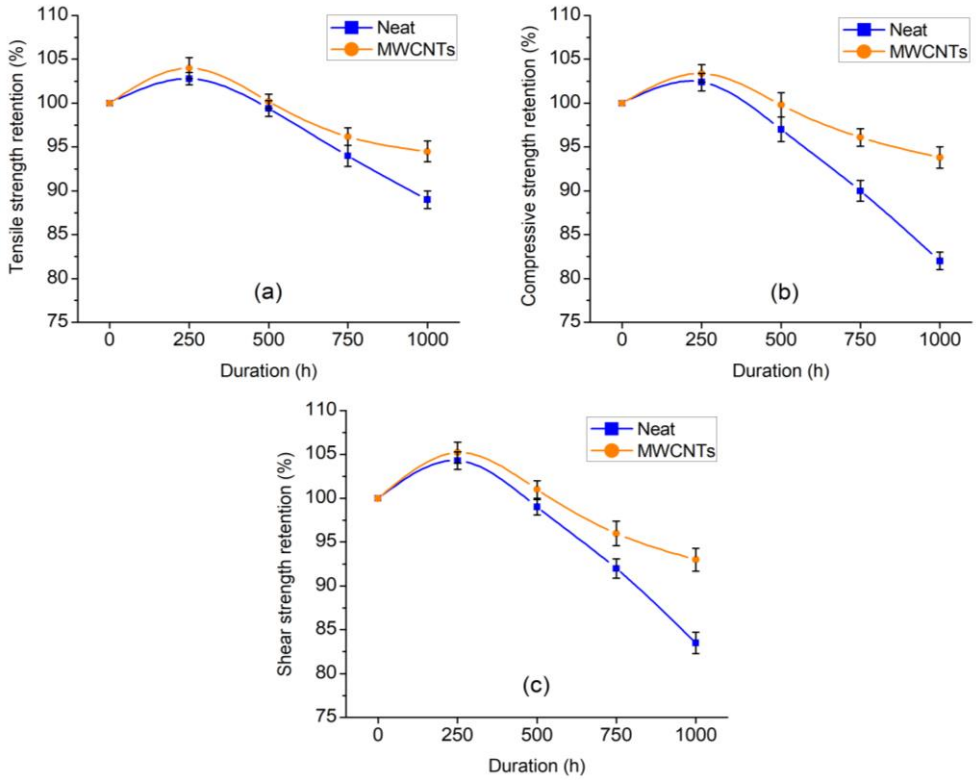

Fig. 6.6 Strength retentions of EB cured neat and MWCNTs added nanocomposites (a) tensile strength, (b) compressive strength and (c) shear strength

6.2.1.4 SEM micrographs

For material morphological investigations, SEM images were taken before and after the accelerated aging process on the surface of neat and MWCNTs added composite specimens and on the tensile fractured specimens of both configurations.

The surface micrographs of neat and 0.3 wt.% of MWCNTs added composite specimens before and after exposure to accelerated aging conditions are shown in Fig. 6.7. It was found that before exposure to aging conditions, unaged composite specimens had homogenous surfaces and there was no degradation and microcracks observed on the surfaces of neat and MWCNTs added specimens.

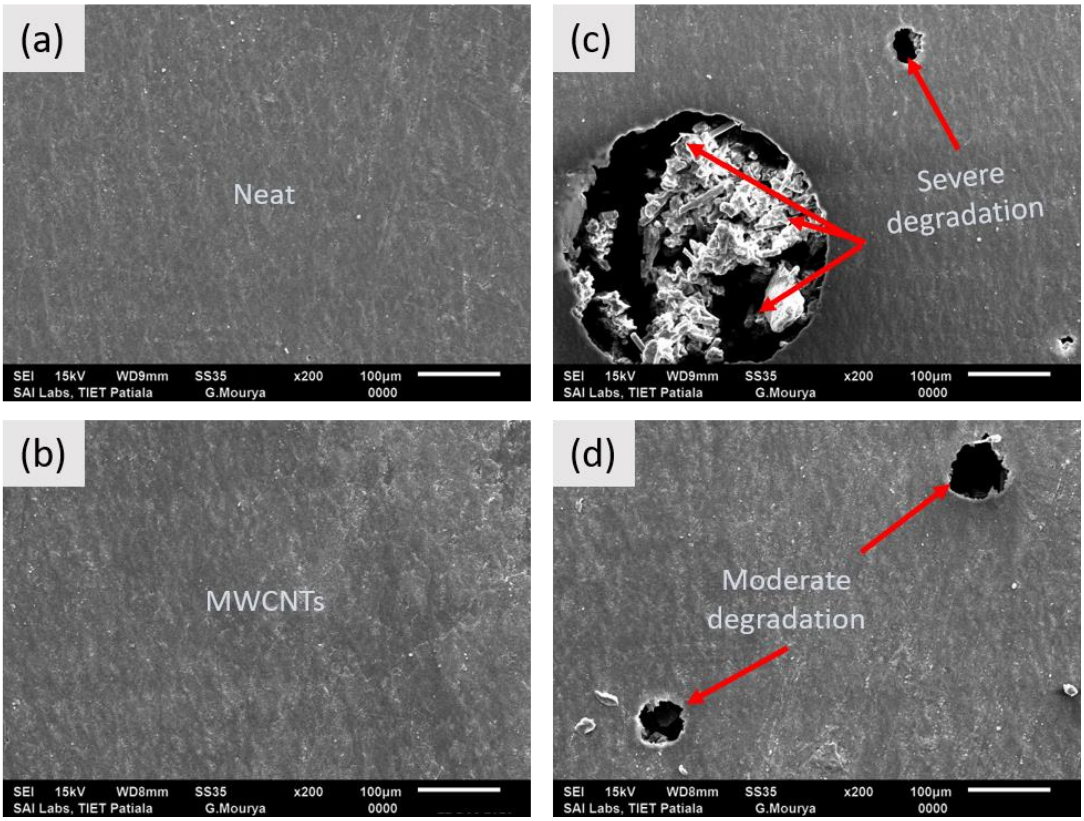

Fig. 6.7 Surface morphology of neat composite specimens (a) unaged, (b) after 1000 h of accelerated aging and MWCNTs added composite specimens (c) unaged and (d) after 1000 h of accelerated aging

The SEM micrographs for a fractured surfaces of neat and 0.3 wt.% of MWCNTs added composite specimens before and after the aging conditioning are shown in Fig. 6.8. Generally, fiber pull-out, matrix cracking, fracture of fiber and debonding are the general failure mechanisms of the FRP composites [216].

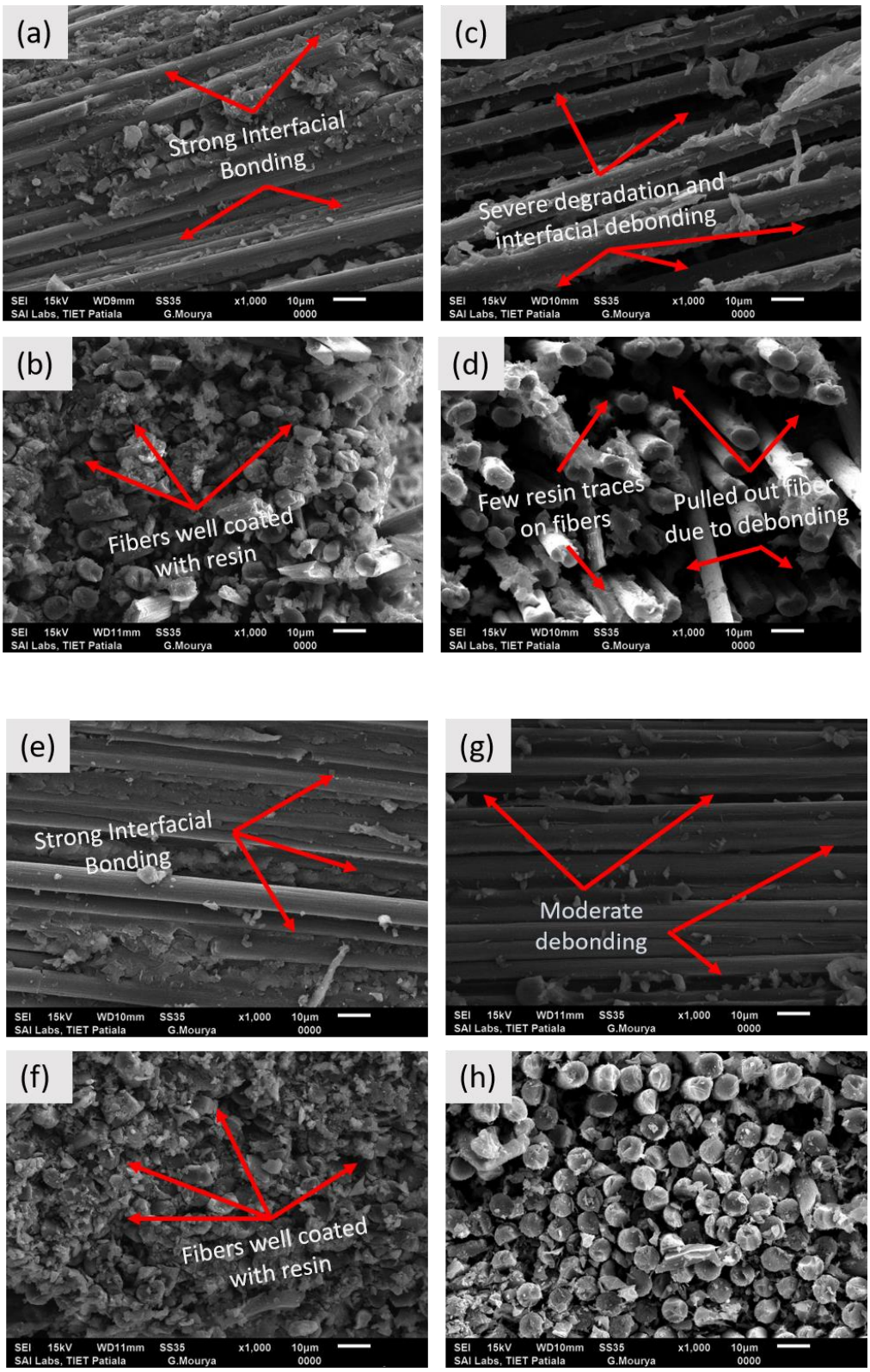

Fig. 6.8 SEM micrographs obtained from tensile fracture specimens of neat composite specimens (a),(b) unaged and (c),(d) aged for 1000 h and MWCNTs added composite specimens (e),(f) unaged, (g),(h) aged for 1000 h

For unaged neat and MWCNTs composite specimens, the dominant failure mechanism is the fiber fracture as shown in Figs. 6.8 (a)-(b) and (e)-(f), which promotes the excellent mechanical properties of the material. The generation of this failure mechanism is due to the applied tensile stress. Under tension, the failure of material with an increased level of fiber fracture showed the excellent interfacial bonding between the fiber and the epoxy matrix, which in turn required higher tensile stress for material failure. Therefore, higher mechanical properties can be obtained with more fiber fracture.

In neat composites (Fig. 6.8 (c)-(d)), after 1000 h of aging exposure, severe degradation was observed showing the fiber pull out and matrix cracking failure mechanisms. Large fiber pull-out in tensile fractured surface indicated the poor interfacial bonding between the fiber and the epoxy matrix. Consequently, composites showed lower mechanical properties due to less effective stress transfer. This is due to the increased crosslinking (by exposure to UV radiation) that leads to embrittlement and creates microcracks which result in debonding at the fiber/matrix interface. The widening of microcracks accelerates the degradation rate by exposing the new surface to UV radiations and increased moisture diffusion [175].

It can be seen that after 1000 h of aging (Fig. 6.8 (c)-(d)), the surface morphology of pulled-out fibers changes from wavelike to relatively smooth i.e., less adhesion of the resin to fibers. The accelerated weathering effect leads to interphase shrinkage due to crosslinking of an epoxy matrix which weakens the interfacial bonding between epoxy and fibers [215]. For similar exposure to 1000 h (Fig. 6.8 (g)-(h)), MWCNTs added fractured composites have shown less degradation than neat fractured composites. This is because incorporating MWCNTs produces a tortuosity effect which forces water molecules to follow prolonged paths and reduces moisture absorption rate. Moreover, the UV resistant property and hydrophobic nature of MWCNTs helps to counter the degradation upto some extent under the effect of UV radiation and moisture. Besides this, MWCNTs have a high specific surface area, that helps in improving the interfacial properties countering the aging effect [57].

6.2.1.5 Performance of bolted joints under accelerated aging conditions

Figures 6.9 and 6.10 show the tensile testing results for unaged and accelerated aged EB cured composite bolted joint specimens of neat and 0.3 wt.% of MWCNTs configurations, respectively at different bolt torques. As can be seen from Figs 6.9 and 6.10, the curves for bearing response start with a linear movement and after reaching the first failure load, it continues moving in a zig-zag pattern showing the bearing mode of failure. The highest peak of a curve in the graphs is taken as the ultimate failure load for a particular condition. The

mechanism of bearing failure in bolted joints undergoes different stages before final failure. In each stage, a set of shear cracks were produced in hand tightening bolt torque (0 Nm) through washers. This is due to the damage growth in individual plies of the joint specimen. The generated shear cracks propagate towards the outer surface of the specimens as lateral constraints prevent the inward growth of shear cracks which opposes delamination. Furthermore, the damaged material was supported by these lateral constraints that provides the additional failure load even after significant damage has occurred under the washers.

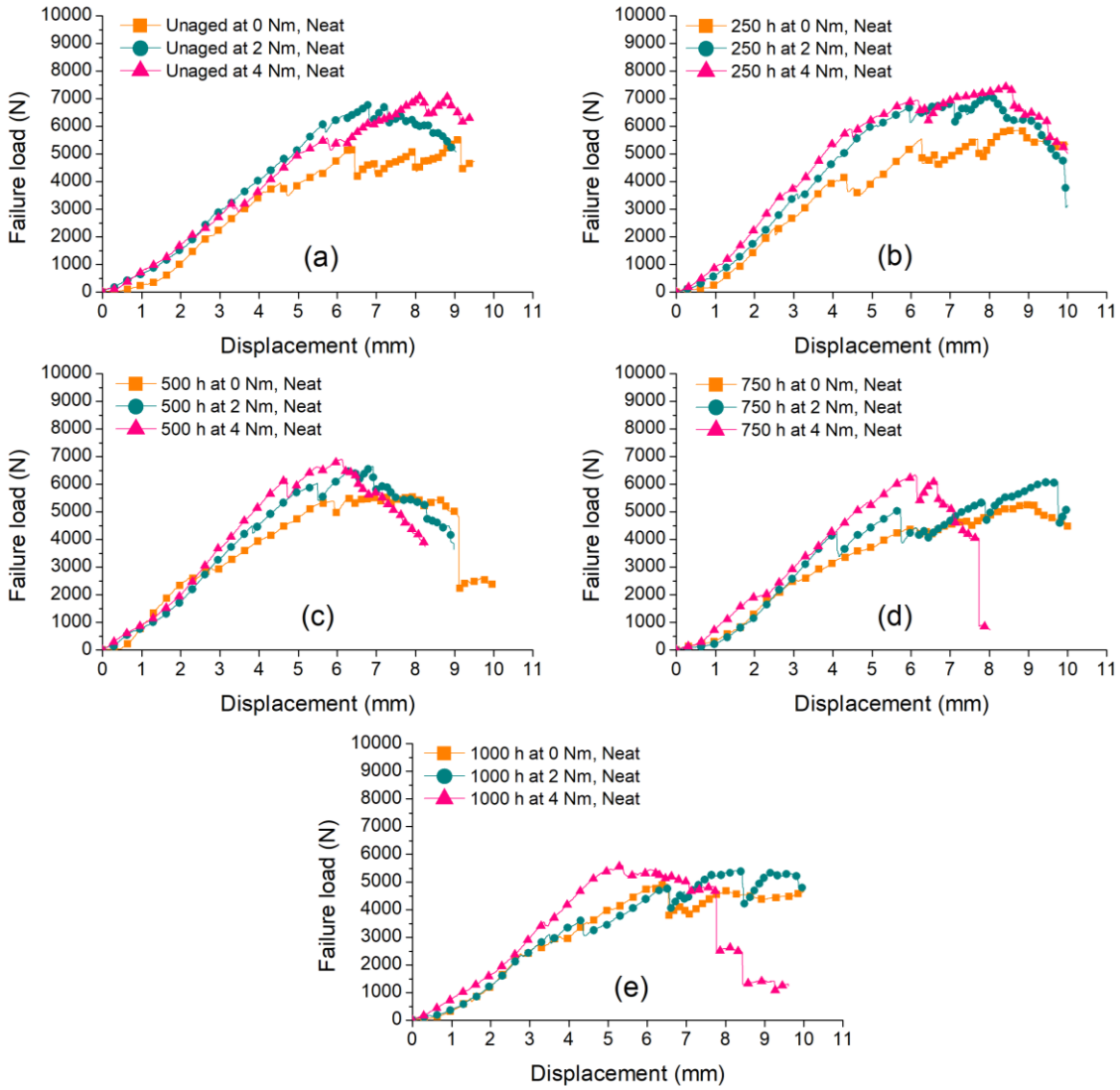

Fig. 6.9 Load vs. displacement graphs for EB cured neat composite bolted joint specimens (a) unaged, (b) 250 h, (c) 500 h, (d) 750 h and (e) 1000 h of accelerated environmental aging

With increase in load, the propagation and accumulation of damage continued in the joint specimen. Proceeding from the first set, a second set of shear cracks was formed. This shear crack growth mechanism continued until the damage propagated beyond the washers. At

this point, joints loses its capacity to withstand higher failure loads due to the absence of lateral supports.

But in the case of higher bolt torques (2 and 4 Nm), the shear crack formation was hindered as transverse expansion of damaged material was restrained. Although bolt torque does not alter the nature of the bearing failure mechanism under lateral constraints but hinders the material damage from formation of visible shear cracks. Hence, the increase in the ultimate failure load in bolted joints at higher bolt torques attributed to the frictional forces between the washers and the specimens [67].

The load vs. displacement curves (Figs 6.9 and 6.10) revealed that the ultimate failure load values decreased with an increase in cyclic exposure of UV radiation and condensation at higher temperatures. It was observed that with varying bolt torque from 0 to 2 Nm and 2 to 4 Nm, the slope of the curves shows increasing trends. This was due to the increased lateral compressive forces through washers which increase the joint stiffness. But with increased exposure time under an accelerated environment, the slope of the curves decreases and varying bolt torques become less effective. The epoxy swelling due to absorbed moisture, plasticization, chain scission reactions and thermally induced microcracks are the source for degradation at severe aging exposures. The reduction of slope in the load vs displacement curves shows that the neat joint configurations (Fig. 6.9) were more susceptible to the accelerated environment than the MWCNTs added joint configurations (Fig. 6.10). The hydrophobic nature of MWCNTs counterattack the water absorption and UV resistant properties that resist UV damage upto some extent. The bridging effect between the fibers and the epoxy matrix maintains the joint stiffness.

The comparison of neat and MWCNTs added composite bolted joint specimens, unaged and accelerated aged, at different bolt torques are plotted as bar graphs shown in Fig. 6.11.

It was found that at all aging conditions, the ultimate failure load values in MWCNTs joint specimens were on the higher side as compared to neat joint specimens. Moreover, the ultimate failure load values increased drastically at 250 h of aging exposure (Fig 6.11 (a and b)) in both neat and MWCNTs added joint specimens. The increased values attributed to the fact that exposure to UV radiations, moisture and temperature under this condition give rise to a stiffening effect due to crosslinking formation in the epoxy matrix [171]. Another cause of improvement is the presence of unreacted cationic photoinitiator under UV radiations and temperature that increases the degree of cure in the joint specimens.

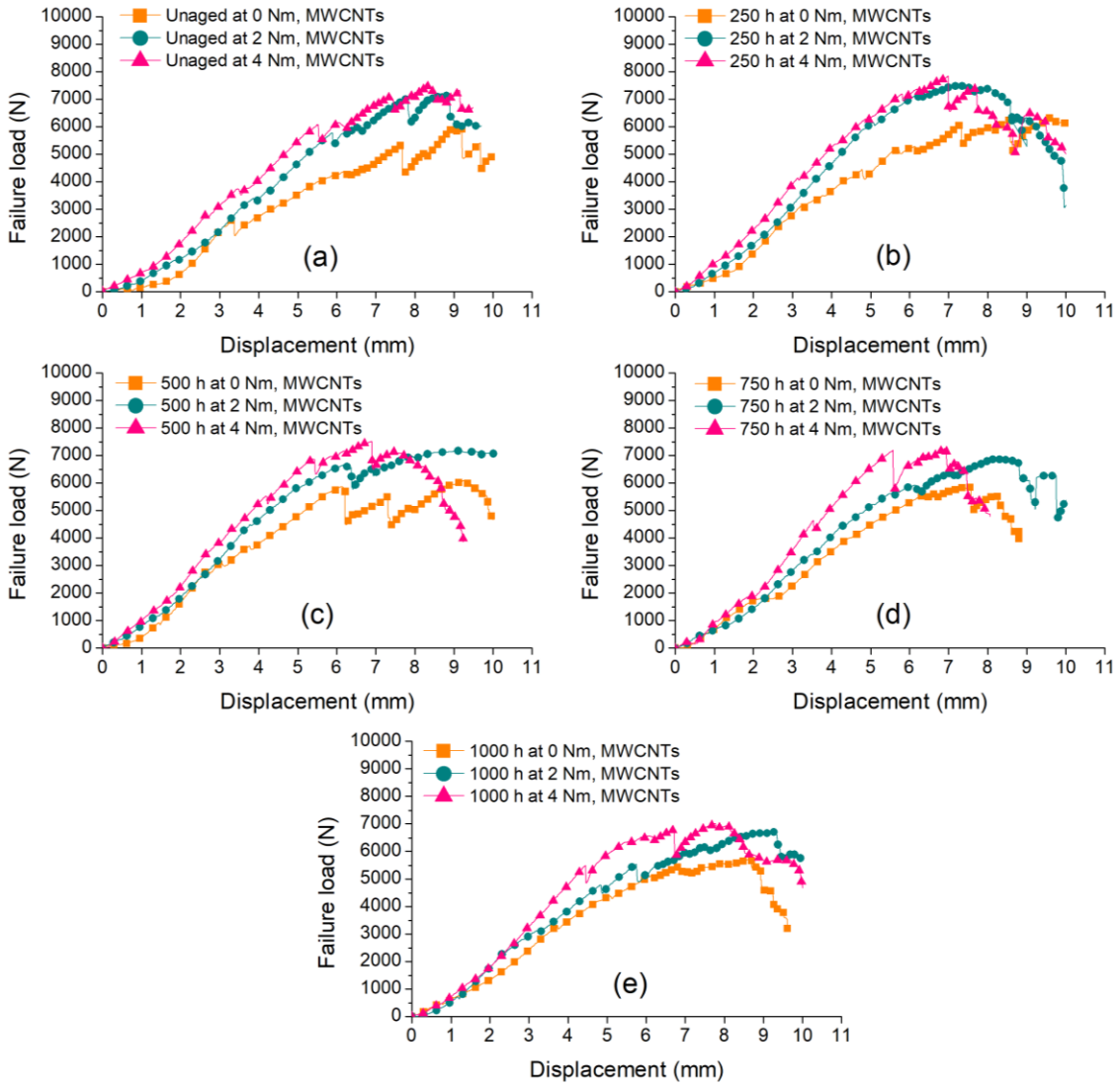

Fig. 6.10 Load vs. displacement graphs for EB cured MWCNTs added composite bolted joint specimens (a) unaged, (b) 250 h, (c) 500 h, (d) 750 h and (e) 1000 h of accelerated environmental aging

It can be seen from Fig. 6.11 that there was a significant loss in the ultimate failure load values after 250 h of aging exposure due to severe degradation in the neat composite joint specimens. During 250 to 1000 h of aging exposure, the relative stiffening effects lag behind the other degradation factors (such as plasticization, epoxy swelling and photo-oxidation reactions) that deteriorate the joint specimens and were further responsible for lower ultimate failure loads. Another reason was the excessive embrittlement that gives rise to generation of microcracks under cyclic exposure at elevated temperatures. The excellent barrier properties and good resistance towards UV radiation of MWCNTs nanofiller help the joint specimens to withstand higher ultimate failure loads than neat joint specimens after longer exposure.

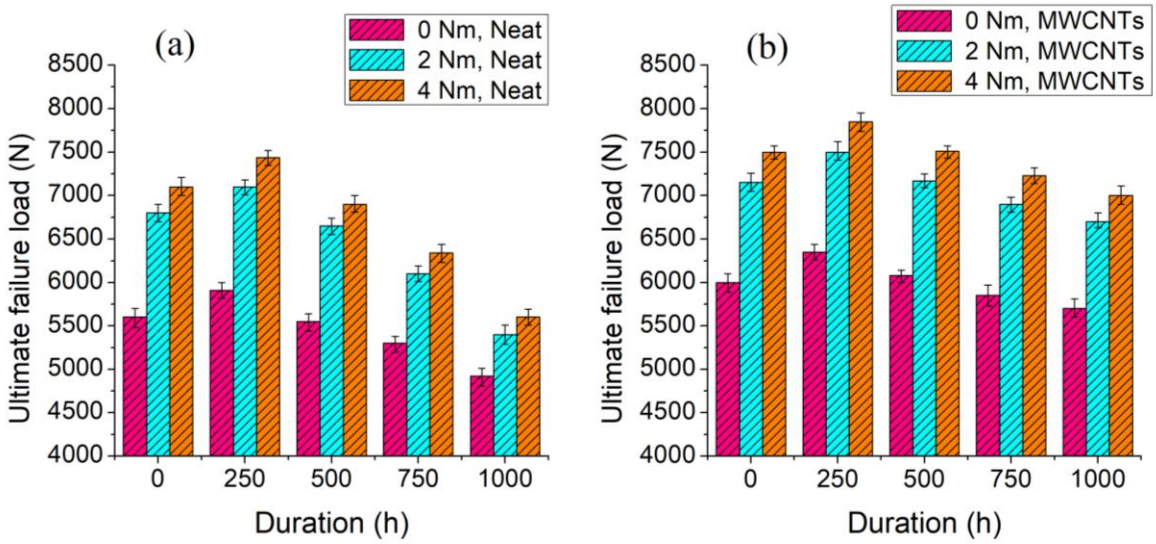

Fig. 6.11 Bar graphs showing ultimate failure loads of EB cured unaged and aged joint specimens at different bolt torques (a) neat and (b) MWCNTs added configurations

The bolt torque contribution can also be seen from Fig. 6.11, which reflects towards positive aspects of using bolt torque under accelerated conditions. It was found that for 0, 2 and 4 Nm bolt torques, the overall increase in ultimate failure loads at 250 h of aging exposure was 5.5%, 4.4% and 4.8%, respectively for neat joint specimens. Correspondingly, for MWCNTs added joint specimens, the overall increase in ultimate failure loads at 250 h of aging exposure was 5.8%, 4.9% and 4.9%, respectively. Similarly, the overall decrease in ultimate failure loads in neat joint specimens for 0, 2 and 4 Nm bolt torques at 1000 h of aging exposure were 12.1%, 20.6% and 21.1%, respectively. Correspondingly, for MWCNTs added joint specimens, the overall decrease in ultimate failure loads at 1000 h of aging exposure was 5.0%, 6.3% and 6.7%, respectively. The results show that in neat joint specimens, the ultimate failure load retention ability was less at higher bolt torques after the aging process as compared to MWCNTs added joint specimens.

6.2.1.6 Statistical Analysis

Response surface methodology (RSM) technique was applied on the bolted composite joint using a central composite design to optimize the output response which has a dependency on the different control parameters. Using RSM statistical approach, 26 runs were conducted for analysis. In the present work, failure load is taken as an output response for two continuous and one categorical control parameters. Continuous factors used are duration (P) and torque (Q) while the categorical factor used is material (M). The experimental data obtained through analysis of variance (ANOVA) is given in Table 6.2. ANOVA is a

collection of statistical data used to verify the differences in means among the different groups.

Table 6.2 ANOVA table

Source	DF	Adj SS	Adj MS	F-Value	P-Value	Contribution (%)
Model	8	12836613	1604577	128.16	0.0001	98.36
Linear	3	9701962	3233987	258.30	0.0001	74.34
Duration, P	1	1944075	1944075	155.27	0.0001	14.89
Torque, Q	1	5018133	5018133	400.79	0.0001	38.45
Material, M	1	2739754	2739754	218.82	0.0001	21.01
Square	2	2511359	1255679	100.29	0.0001	19.24
$P \times P$	1	772150	772150	61.67	0.0001	5.91
$Q \times Q$	1	782511	782511	62.50	0.0001	5.99
2-Way interaction	3	623292	207764	16.59	0.0001	4.77
$P \times Q$	1	130050	130050	10.39	0.0005	0.99
$P \times R$	1	452408	452408	36.13	0.0001	3.46
$Q \times R$	1	40833	40833	3.26	0.0089	0.31
Error	17	212849	12521			1.63
Lack-of-fit	9	201289	22365	15.48	0.0001	1.54
Pure error	8	11560	1445			0.08
Total	25	13049462				

This statistical approach confirms the model's significance at P-value < 0.050. It can be seen from Table 6.2 that factors P, Q, M, $P \times P$, $Q \times Q$, $P \times Q$ and $M \times M$ are the significant terms for output response (failure load). Therefore, these factors are taken as the input factors for the output response. The R^2 value is determined to examine the correctness of the statistical model. For the present model, the R^2 value is 0.9615, the model can describe 98.36% variation in the failure loads. The contribution of the factors, duration (P), torque (Q) and material (M) are 14.89%, 38.45% and 21.01%, respectively.

The regression Eqs (6.1) and (6.2) are used to predict the failure loads in neat and MWCNTs added composite material joints.

$$Failure\ load\ (Neat) = 5719.9 + (0.557 \times P) + (734.3 \times Q) - (0.001496 \times P \times P) - (94.1 \times Q \times Q) - (0.1275 \times P \times Q) \quad (6.1)$$

$$Failure\ load\ (MWCNT) = 5864.2 + (1.334 \times P) + (792.6 \times Q) - (0.001496 \times P \times P) - (94.1 \times Q \times Q) - (0.1275 \times P \times Q) \quad (6.2)$$

To check the difference between experimental and predicted results, a validation test has been performed through Eqs (6.1) and (6.2). The results obtained through the validation test on composite joints are shown in Table 6.3.

The validation test has been conducted for six trials with extended control factor *i.e.,* torque (Q) for 3 Nm and 5 Nm values in 0, 500 and 750 h aging durations randomly. It was found that the percentage error between the experimental and predicted values is less than 5%. The individual consequence of input factors on failure loads is explained through the surface plots as shown in Fig. 6.12. It is visualized that the bearing load capacity decreases with higher aging time. At a shorter duration, the effect of UV exposure and temperature imposes the crosslinking in the epoxy matrix which further results in a relative stiffening effect and increases the performance of the bolted joints. But at longer durations, cyclic exposure degrades the structural properties of the composites due to debonding of fiber-matrix and epoxy swelling which reduces the performance of bolted joints. As compared to neat composite joints, the ultimate failure loads are higher in MWCNTs added composite joints at different aging durations. Addition of MWCNTs into the epoxy act as a link between fiber and the matrix which enhances the interfacial bonding strength. Debonding is the consequence of the different volumetric expansion of fiber and epoxy matrix due to moisture absorption that creates localized stresses in the material, which is more severe in accelerated aging conditions. The addition of MWCNTs hinders the moisture absorption and also maintains the interfacial bonding of the composite material. Therefore, it helps in improving the bearing load capacity of the composite joints.

Table 6.3 Validation test for bolted joint configurations

Duration, P (h)	**Torque, Q (Nm)**	**Material, M**	**Experimental load (N)**	**Predicted load (N)**	**% error**
500	3	Neat	6720	6789	1.03
750	5	Neat	6410	6137	4.2
0	3	Neat	7050	7075	0.35
500	3	MWCNTs	7370	7497	1.72
750	5	MWCNTs	7400	7156	3.29
0	3	MWCNTs	7380	7395	0.20

From Fig. 6.12, it is also observed that ultimate failure loads increase with the increase in bolt torque values for both neat and MWCNTs added composite joints. The addition of MWCNTs in the composites improves the bolt torque efficiency even at longer aging durations in comparison to neat composites. In comparison to the MWCNTs added

composites, the bonding between matrix and the fiber was loosened due to UV irradiation, moisture and temperature effect in the neat composites, which resulted in severe degradation. In such conditions, even the applied torque is not capable of maintaining the joint stiffness and thus the improvement in failure load is reduced. The comparison of slopes at 1000 h in surface plots of neat and MWCNTs added composites shows the contribution of bolt torque, where bolt torque effect is on the higher side for MWCNTs added composites than the neat composites.

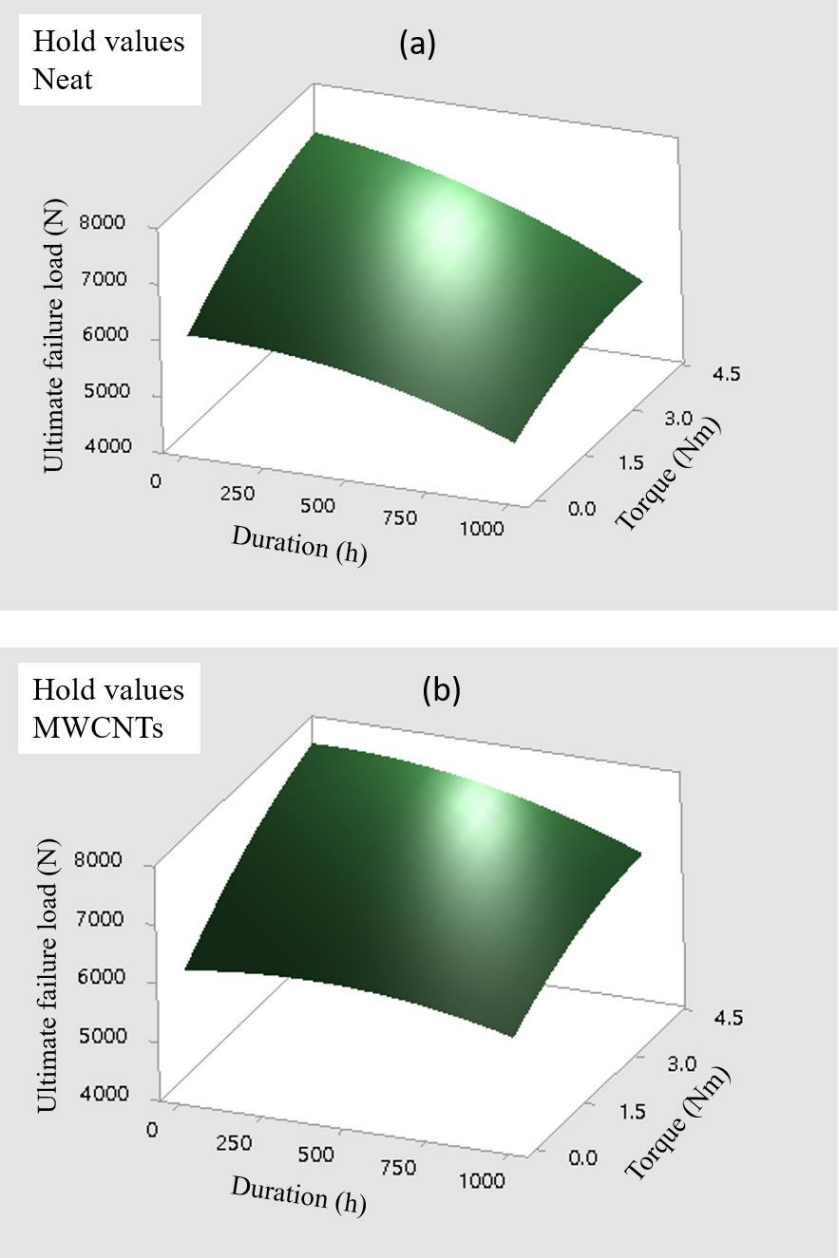

Fig. 6.12 Surface plots indicating ultimate failure loads for (a) neat composite joints (b) MWCNTs added composite joints

6.2.2 Bolted joints prepared from thermally cured composites

The thermally cured composite laminates and their bolted joints were characterized before and after the aging process and results obtained are described in the following subsections.

6.2.2.1 FTIR analysis

The results obtained through FTIR analysis of thermally cured neat and MWCNTs added composite specimens, before and after the aging process are shown in Figs 6.13 and 6.14. The change in the ATR-FTIR spectra (change in peaks) revealed the changes in chemical structure after aging conditions.

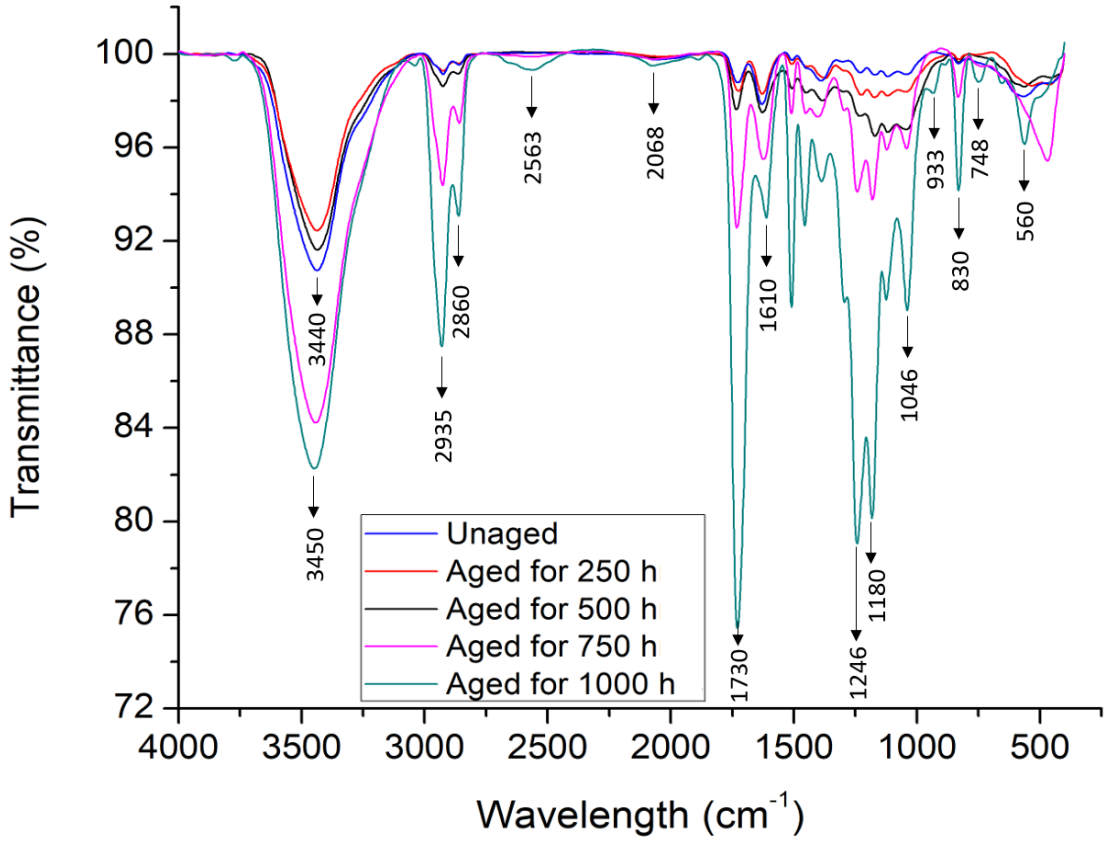

Fig. 6.13 ATR-FTIR spectra of thermally cured neat composite specimens, unaged and aged

In Fig. 6.13, the broad peaks at 3440 cm^{-1} correspond to O-H stretching of carboxylic acids and the peaks at 2860 and 2935 cm^{-1} are related to the C-H stretching of the monomer units. The results show that a chemical change occurred due to the accelerated aging process [173]. The aldehyde or ketone C=O stretching at 1730 cm^{-1}, ether C-O-C stretching at 1246 and 1180 cm^{-1} and C-N stretching at 1046 cm^{-1} indicate that these bonds in the epoxy matrix are influenced by the accelerated aging. The results show that the possible change is obtained

through the peak at 830 cm^{-1} of symmetric bending of N-H. The increase of peaks in the C=O group at different aging durations indicates photooxidation of aromatic esters linkage units [169].

The shift of the O-H band from 3440 to 3450 cm^{-1} at accelerated aging is attributed to the fact that there is redistribution in the arrangement of a hydroxyl group. Comparing Figs 6.13 and 6.14, it is observed that the peaks for MWCNTs added composite specimens show lesser deviation than the neat composite samples at different aging durations. The region of 3670-3100 cm^{-1} represents the O-H group. The increase in this region after aging relates to the presence of O–H due to the absorption of moisture during the condensation cycle. The peaks around 1800-1600 cm^{-1} are attributed to carbonyl (C=O) stretching, which is attributed to the oxidation of epoxy during UV and temperature exposure in the chamber. The peaks between 1300-1100 cm^{-1} occur due to the oxidation process, like the formation of C–O bonds [217, 218]. These increases lead to cross-linking and excessive brittleness, which have opposite effects.

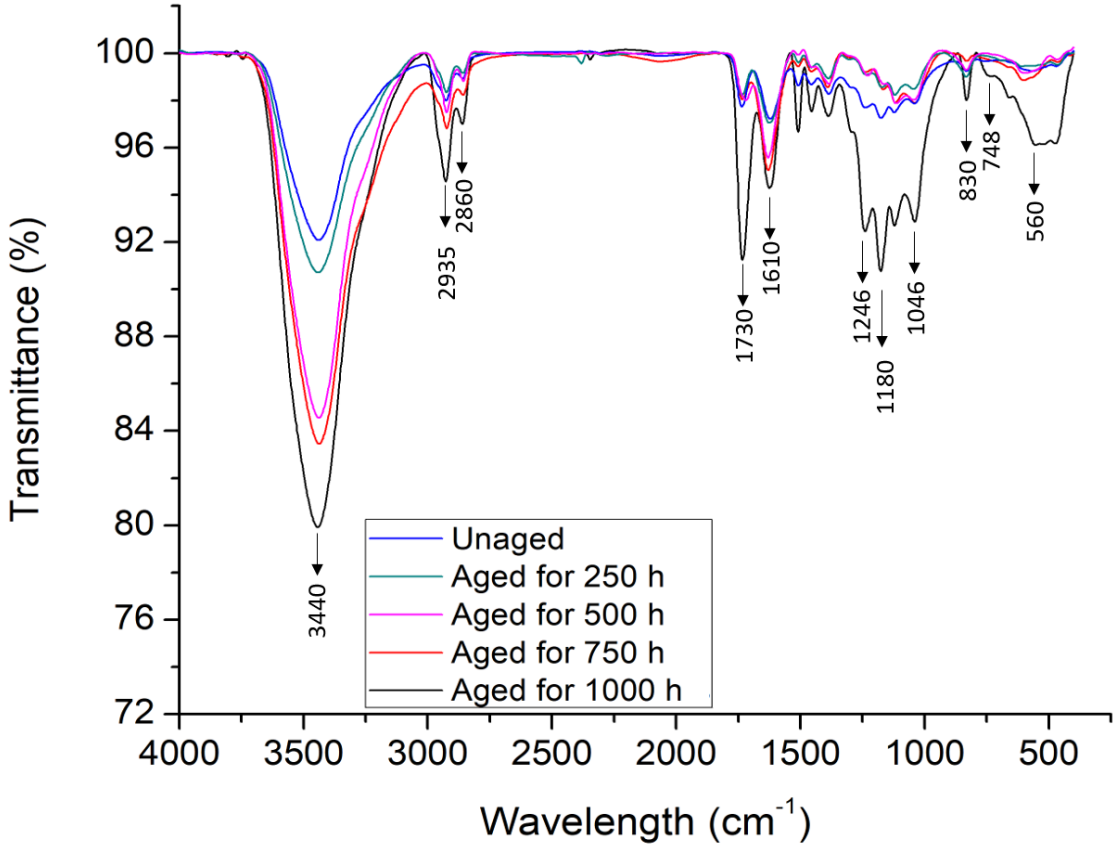

Fig. 6.14 ATR-FTIR spectra of thermally cured MWCNTs added composite specimens, unaged and aged

It can be concluded that the basic difference between the neat and MWCNTs specimens is the amount of moisture absorbed (represented by the O-H group), oxidation of epoxy during UV and temperature exposure (represented by C=O stretching and formation of C-O bonds) before and after the aging process. It was seen that the oxidation process after aging was more severe in the case of neat composite specimens as compared to MWCNTs composite specimens.

6.2.2.2 Mechanical properties

The thermally cured composite specimens were characterized for their tensile, compression and shear properties after exposure to an accelerated aging environment, results are summarized in Table 6.4. The tensile, compressive and shear strength retentions in the neat and with 0.3 wt.% of MWCNTs added specimens at different aging exposures are shown in Fig. 6.15. It was found that the aging exposures significantly affect the strength properties of the thermally cured composite specimens even more than EB cured composite specimens. The degradation occurred because of epoxy swelling, moisture absorption, formation of microcracks and photooxidation at the surface (due to UV exposure).

Table 6.4 Mechanical properties of thermally cured composite specimens under accelerated aging conditions

S. No.	Duration (h)	Tensile strength (MPa) (± SD*)		Compressive strength (MPa) (± SD*)		Shear strength (MPa) (± SD*)	
		Neat	MWCNTs	Neat	MWCNTs	Neat	MWCNTs
1	0	606 ± 09	680 ± 10	315 ± 10	371 ± 10	125 ± 05	153 ± 06
2	250	617 ± 11	698 ± 12	321 ± 08	383 ± 07	130 ± 04	160 ± 04
3	500	585 ± 10	671 ± 11	301 ± 10	364 ± 11	119 ± 06	150 ± 05
4	750	552 ± 09	656 ± 10	258 ± 11	339 ± 09	108 ± 05	142 ± 04
5	1000	513 ± 11	635 ± 10	220 ± 15	327 ± 12	90 ± 05	133 ± 03

***SD = Standard deviation**

The mechanical strength retentions of 93.4% in tension, 88.2% in compression and 87% in shear were observed after aging of 1000 h in specimens prepared with 0.3 wt.% of MWCNTs content, whereas, under similar conditions, 84.7% in tension, 70.1% in compression and 72% in shear were observed in neat composite specimens.

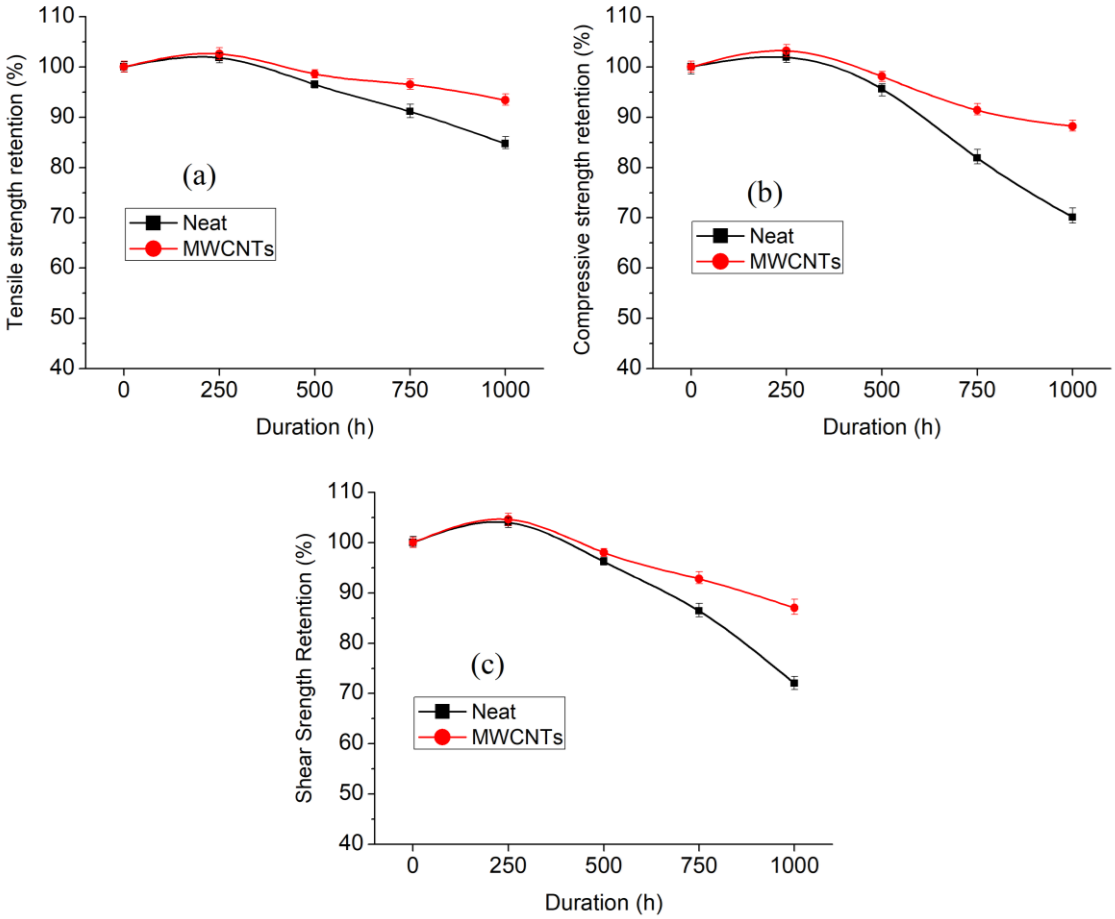

Fig. 6.15 Mechanical strength retention of thermally cured unaged and aged composite specimens for 0, 250, 500, 750 and 1000 h (a) tensile, (b) compressive and (c) shear strength

6.2.2.3 SEM images

The fractured tensile specimens of thermally cured neat and MWCNTs added configurations after different aging exposures were analyzed through SEM images as shown in Fig. 6.16. SEM micrographs shown in Fig. 6.16 (a and c) for neat and MWCNTs added unaged composite specimens illustrate good adhesion between the epoxy matrix and the carbon fiber, with the fibers that pulled out, were well coated with resin. It was observed that even after fracture, carbon fibers were firmly placed at their positions. From Fig. 6.16 (b), the neat composite specimens aged for 1000 h revealed more pulled out fibers due to fiber-matrix debonding, microcracks formation and epoxy loss in some areas that lead to a reduction in mechanical properties. For similar aging conditions, the SEM micrographs for MWCNTs added fractured composite specimens are shown in Fig. 6.16 (d) representing less degradation of the epoxy matrix.

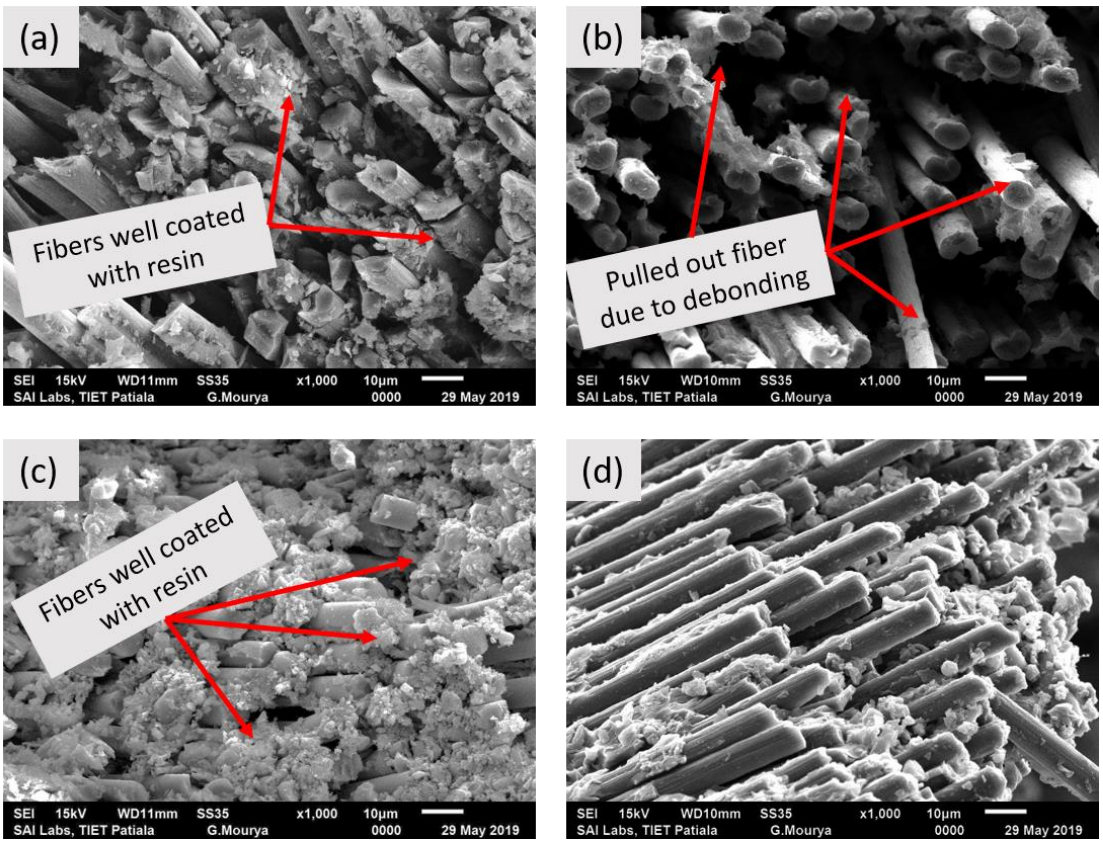

Fig. 6.16 SEM micrographs obtained from tensile fracture specimens of neat composite specimens (a) unaged and (b) aged for 1000 h and MWCNTs added composite specimens (c) unaged, (d) aged for 1000 h

6.2.2.4 Performance of bolted joints under accelerated aging conditions

Five joint specimens of each configuration after accelerated aging conditions were tested and the average results are plotted in Fig. 6.17 and 6.18. The trends in load vs. displacement graphs of thermally cured bolted joints are similar to the EB cured bolted joints showing an increasing trend of the failure loads up to 250 h of aging, beyond which it decreases with an increase in the accelerated aging exposures.

It is seen from Fig. 6.17 (a) that the joint possesses higher failure loads with an increase in bolt torque from 0 to 4 Nm. Also, the unaged joint configuration shows more bolt torque effectiveness than the aged joint configuration as can be seen in Fig. 6.17 (a)-(e). On the other hand, the joints prepared from MWCNTs composites show higher failure load values for similar bolt torques and aging conditions as shown in Fig. 6.18 (a)-(e).

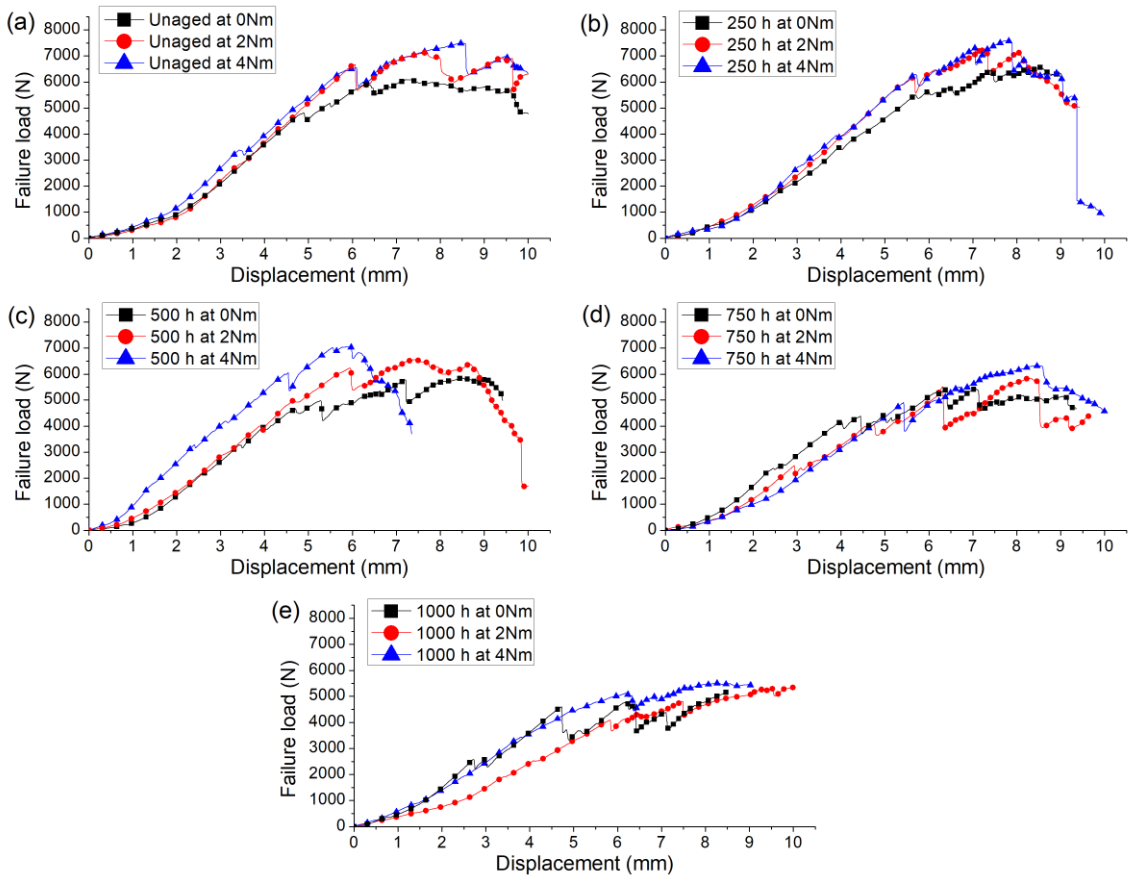

Fig. 6.17 Load vs. displacement graphs for thermally cured neat composite joint specimens (a) unaged, (b) aged for 250 h, (c) aged for 500 h, (d) aged for 750 h and (e) aged for 1000 h

The ultimate failure loads of thermally cured neat composite material for aged and unaged joint specimens at different bolt torque values are shown in Fig. 6.19 (a). It can be observed from the bar graphs that for the joint at 0 Nm bolt torque, there is 7.7% increase in the failure load for 250 h of exposure and 3.9%, 10.5% and 14.9% decrease in the failure load for 500, 750 and 1000 h of exposure. The bolt torque of 2 Nm showed 1.3% increase and 8%, 17.9%, 25% decrease in the failure loads for the corresponding exposures. An increase of 1.2% and a decrease of 5.9%, 15.6% and 26.4% in the failure load for similar exposure time with 4 Nm bolt torque was observed.

The ultimate failure loads of MWCNTs added composite material, for aged and unaged joint specimens at different bolt torques are shown in Fig. 6.19 (b). It can be observed from the bar graphs that for the joint at 0 Nm bolt torque, there is 9.7% increase in the failure load for 250 h of exposure and 2.2%, 8.3%, 9.7% of the decrease in the failure load for 500, 750 and 1000 h of exposure. The bolt torque of 2 Nm showed 1.3% increase and 2.5%, 7.1%, 10.4% decrease in the failure loads for the corresponding exposures. An increase of 4.7%

and a decrease of 0.7%, 4.79%, 7.9% in the failure loads for similar exposure time for 4 Nm bolt torque was observed.

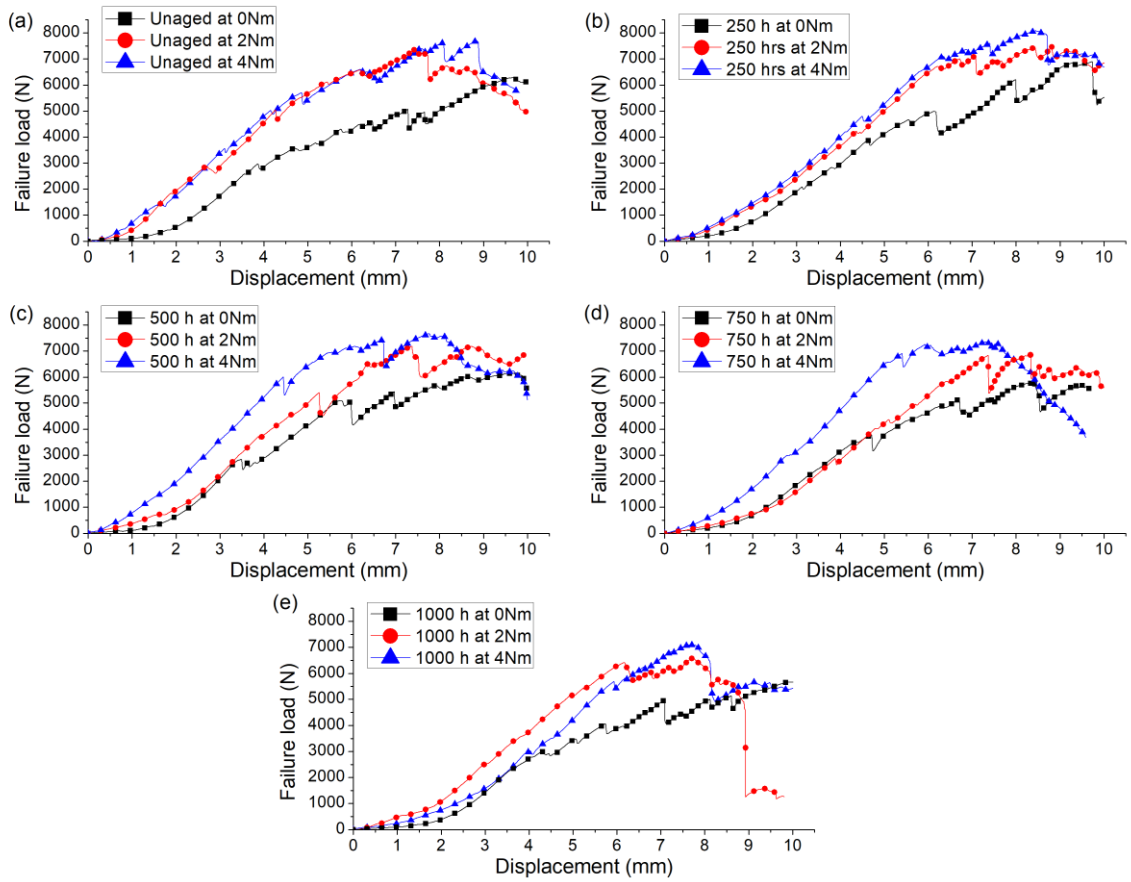

Fig. 6.18 Load vs. displacement graphs for thermally cured MWCNTs added composite joint specimens (a) unaged, (b) aged for 250 h, (c) aged for 500 h, (d) aged for 750 h and (e) aged for 1000 h

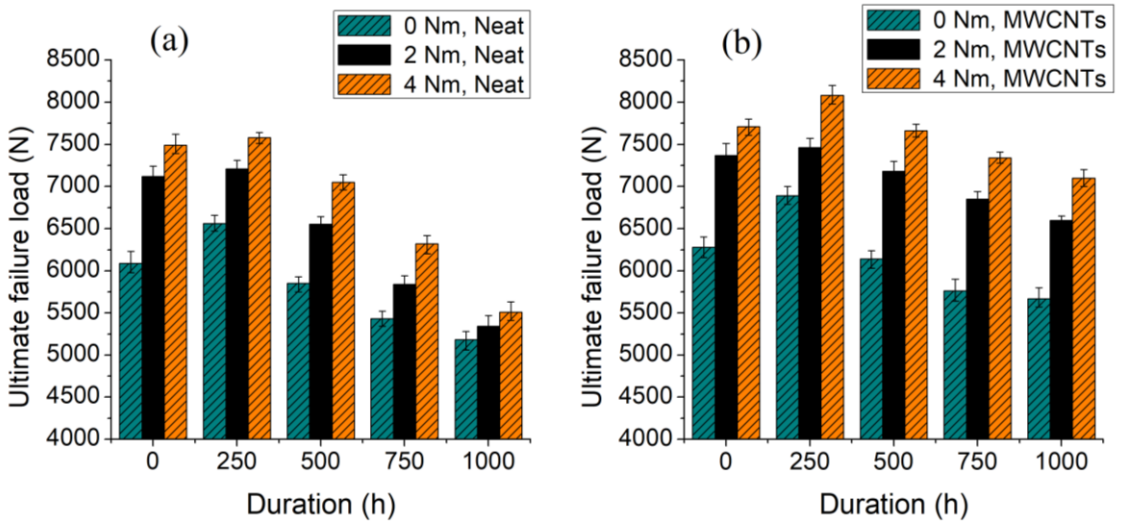

Fig. 6.19 Ultimate failure loads at different bolt torques (a) neat composite joints and (b) MWCNTs added composite joints

6.3 Numerical analysis

To predict the failure loads and failure modes in the composite bolted joint specimens, the finite element analysis was performed using the static structural module in ANSYS software. In-situ properties of the EB cured composite specimens (before and after accelerated aging exposures) were considered for numerical analysis. The progressive damage analysis was performed on the different bolted joint configurations using the characteristic curve method along with Hashin damage criteria.

The radius of characteristic curve was determined using Eq.(5.6) as discussed in Section 5.3. For damage progression in the bolted joint specimen, the Hashin damage criteria was implemented. Hashin damage criteria works upon the equations of fiber and the matrix failure in tensile and compressive loads, as shown in Table 4.2.

6.3.1 Loads and boundary conditions

The boundary conditions, applied loads and contact regions are the same as shown in Fig. 5.23 in Section 5.3.1. The meshing is done using the multizone mesh method with all quad elements. A refined mesh is used in the region around the hole boundary to increase the accuracy of results. The analysis has been done in two steps. Firstly, the bolt pretension is given to the joint specimen and secondly, the tensile load is applied while the given bolt pretension is locked.

The progressive damage contour plots of an unaged neat composite bolted joint specimen at 0 Nm and 4 Nm bolt torque are shown in Figs 6.20 and 6.21. With the gradual increase in applied load, the damage initiates at the hole boundary and progresses radially towards the free edge of the joint specimen.

At 0 Nm bolt torque (Fig. 6.20), the damage spreads in the narrow zone and travel towards the free edge, showing less effect of the bolt torque as there were no lateral constraints. But at 4 Nm bolt torque (Fig. 6.21), the damage was distributed over a wide area instead of going straight towards the free edge, showing that lateral constraints tend to control the damage propagation and distributed the loads in the washer's contact area. The failure in the joint is measured when the damage status is '1' or above on any point of the characteristic curve.

Figure 6.22 represents the comparison of numerically predicted progressive failure damage with the experimentally obtained damage showing similar trends at 0 Nm and 4 Nm bolt torque of neat composite specimen.

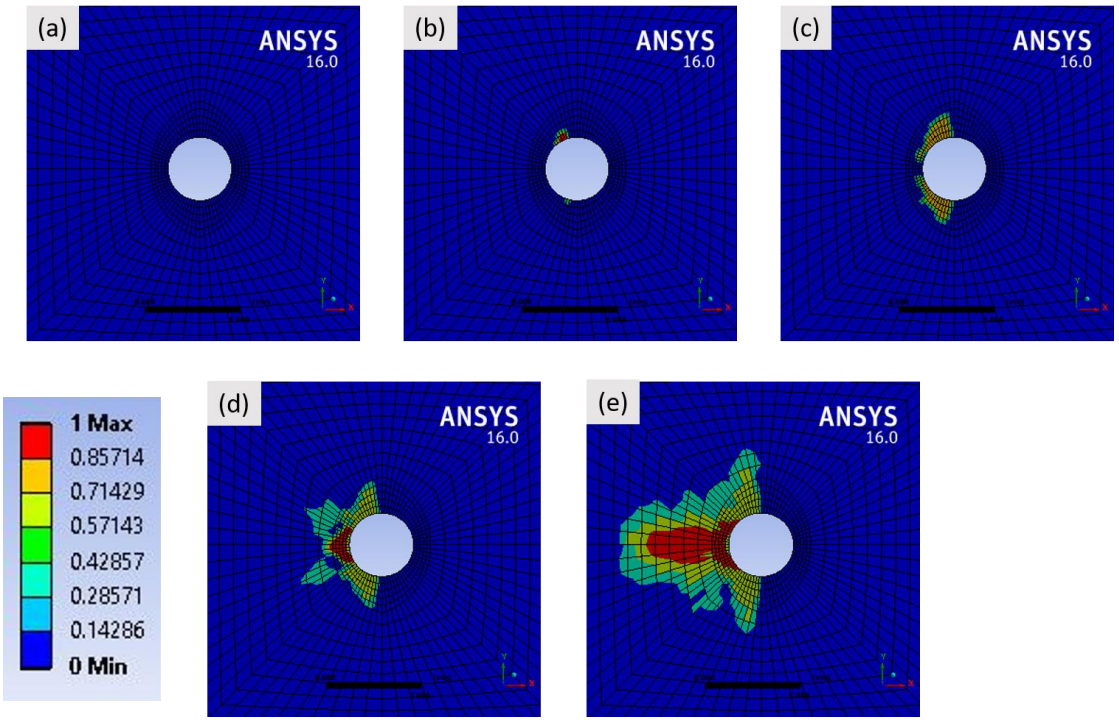

Fig. 6.20 Progressive damage contour plots of unaged neat composite bolted joint specimen with bolt torque of 0 Nm at (a) 20%, (b) 40%, (c) 60%, (d) 80% and (e) 100% of applied load

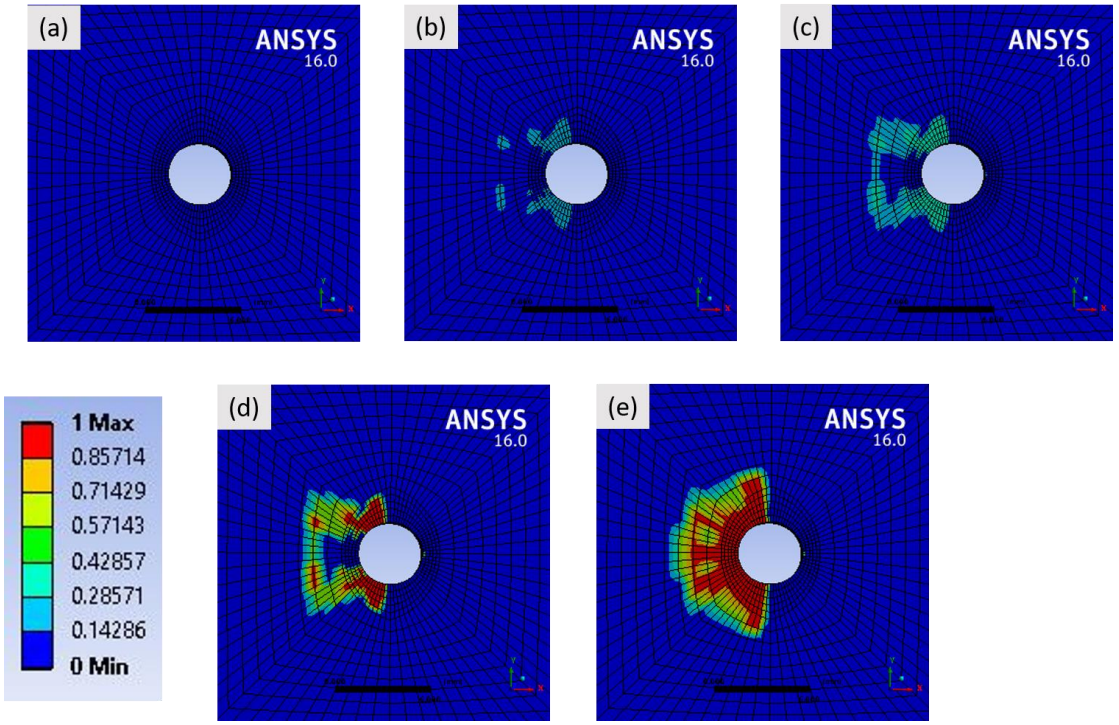

Fig. 6.21 Progressive damage contour plots of unaged MWCNTs added composite bolted joint specimen with bolt torque of 4 Nm at (a) 20%, (b) 40%, (c) 60%, (d) 80% and (e) 100% of applied load

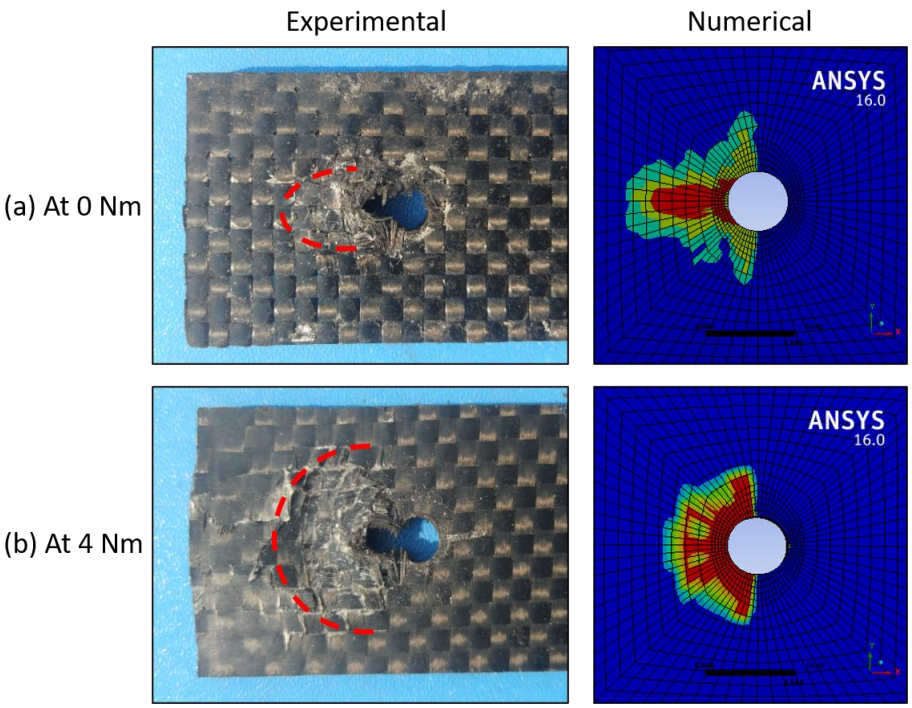

Fig. 6.22 Numerical and experimentally obtained damage plots for unaged neat bolted joint configuration at (a) 0 Nm and (b) 4 Nm

The ultimate failure loads for neat and MWCNTs added composite specimens under the accelerated aging condition at different bolt torques were determined numerically and are shown in Fig. 6.23. These were compared with the experimentally obtained results and found a good correlation between them.

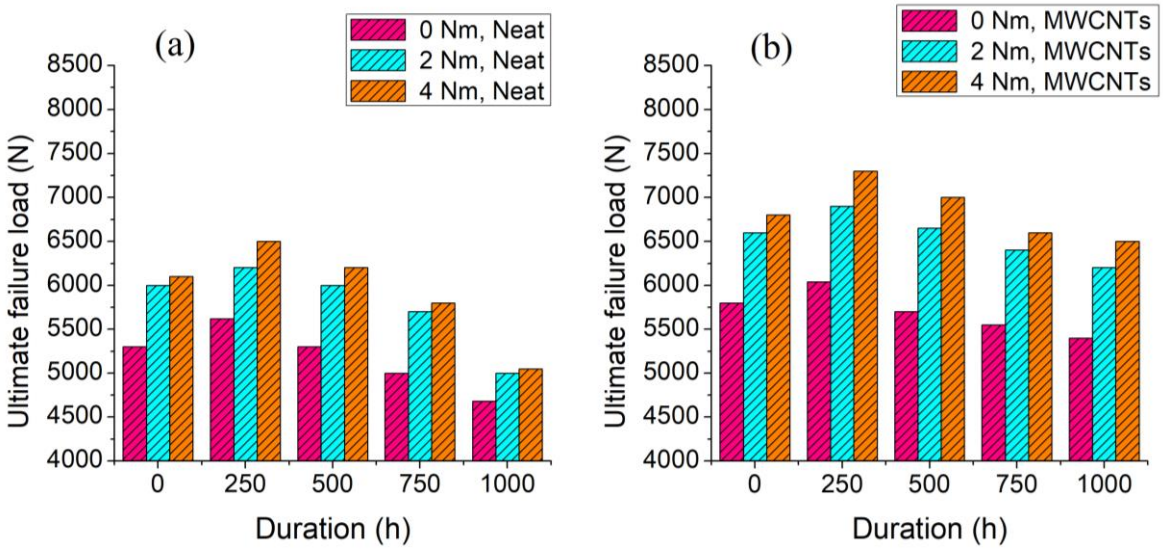

Fig. 6.23 Numerically predicted ultimate failure loads under accelerated aging for 0, 250, 500, 750 and 1000 h (a) neat composites and (b) MWCNTs added composites at different bolt torques

6.4 Closure

The present chapter deals with the accelerated aging of bolted joints prepared from carbon fiber/epoxy composite laminates. The studies were performed on the composite materials prepared using two different processes, EB curing process and the thermal curing process. The optimized 0.3 wt.% of MWCNTs nanofiller content was used to improve the mechanical properties of the composite material. The bolt torques in the range of 0 to 4 Nm was applied on the bolted joints. The increasing bolt torque facilitated the distribution of the stresses over a wider area and increased the ultimate failure load as well as stiffness of the joint.

To investigate the performance of joints under accelerated aging conditions, the combined cyclic exposure of UV radiations, moisture and temperature was given to the composite specimens for 0, 250, 500, 750 and 1000 h. At 250 h of accelerated aging, a slight increase in mechanical strength and modulus properties was noticed due to relative stiffening effect and reaction of unreacted cationic photoinitiator molecules under UV radiation. However, after 250 h of exposure, the reduction in the strength and modulus properties began which directed towards the initiation of degradation in the material due to moisture absorption, the photo-oxidation reactions. The specimens made from MWCNTs nanofiller have shown good mechanical strength retention than that of neat composite specimens. The ultimate failure load values of the bolted joints are affected due to accelerated weathering conditions. The exposure of 1000 h, significantly degraded the failure loads of the bolted joints. However, the bolted joint with MWCNTs added configuration have shown higher retention of ultimate failure loads than the joints with neat configuration.

Progressive damage analysis was performed using characteristic curve method along with Hashin damage criteria. A good correlation was obtained between the experimental and numerical results.

The next chapter gives the conclusions and recommendations for further scope of the research work.

Chapter 7
Conclusions and Recommendations for Future Work

This chapter is mainly oriented on the mainstreams obtained through the electron beam (EB) cured carbon fiber/epoxy composite laminates and its mechanical joints.

7.1 Conclusions

The optimum content of MWCNTs in the composite material is found to be 0.3 wt.% showing maximum strength properties with both curing processes. In EB cured composite material, the addition of 0.3 wt.% of MWCNTs increased the tensile, compressive and shear strength by 15.43%, 20.20% and 23.89%, respectively. Correspondingly, for thermally cured composite material, the increase was 12.21%, 17.77% and 22.40%, respectively.

The failure modes for EB cured pin joint specimens showed dependency on the W/D and E/D ratios. Net-tension and shearing failure modes occur at lower values of E/D and W/D. Sudden failure is seen in these failure modes. The bearing failure mode occurs at $E/D \geq 3$ and $W/D \geq 3$ which is the desired mode of failure, as strength of joints is higher in the bearing mode. Ultimate failure loads in the joint specimens increases with increase in W/D and E/D ratios. The addition of optimized 0.3 wt.% of MWCNTs content have shown improvement in ultimate failure loads of the pin joints. Reportedly, a maximum improvement of 14.3% and 15.3% has been seen in the failure loads for EB cured and thermally cured pin joint composites at W/D=5 and E/D=5, respectively. The numerically predicted ultimate failure loads are within 10% of acceptable difference with the experimental results, providing good correlation between each other.

The immersion of EB cured composite laminates and its joints into water at elevated temperatures (45 ^{o}C and 65 ^{o}C), for duration of 30 days significantly reduces the performance of composite material. However, at lower water temperature (25 ^{o}C), no significant reduction is noticed in the composite material. The elevated temperatures for prolonged duration contribute to inducing the water intake kinetics. The neat composite specimens are more susceptible to the water absorption specially at higher temperatures. Incorporating MWCNTs nanofiller lowers the water absorption rate. With addition of MWCNTs, the water absorption rate and corrected diffusion coefficient are reduced by 20.5% and 28.9% at 25 ^{o}C, 23.7% and 22.3% at 65 ^{o}C after aging for 30 days in composite specimens.

The tensile and flexural strength retention of hygrothermally aged EB cured neat composite specimens at 25 ^{o}C, 45 ^{o}C and 65 ^{o}C, after 30 days are 97.5%, 92%, 87.3% and 95%, 89%, 80.5%, respectively. However, under similar conditions, the tensile and flexural strength retentions for MWCNTs added composite specimens are 98.8%, 96.4%, 93.2% and 98%, 94.5%, 92%, respectively.

SEM micrographs show excellent fiber/epoxy interfacial bonding even after fracture at 25^{o}C of water aging temperature. At elevated water temperatures (45 ^{o}C and 65 ^{o}C), SEM micrographs reveal the severe degradation (microcracks, debonding and delamination) in neat composite specimens due to water absorption whereas MWCNTs added composite specimens show good resistance towards the deterioration with moderate degradation.

The ultimate failure loads of EB cured composite bolted joint specimens are enormously affected by hygrothermal aging at higher water temperatures and aging times. After 30 days, the overall reduction in ultimate failure loads of EB cured neat composite bolted joints at 0 Nm bolt torque are 4.5%, 14.3% and 23.2% at 25 ^{o}C, 45 ^{o}C and 65 ^{o}C, respectively. For similar conditions, the reduction in ultimate failure loads for MWCNTs composite bolted joints are 2.5%, 7.0% and 9.2%, respectively.

The increasing bolt torques have positive effect on the ultimate failure loads for both neat and MWCNTs configurations. But at higher water temperature (65^{o}C), the bolt torque efficiency for neat configuration gets reduced from 88.73% to 77.46% after hygrothermal aging of 30 days. However, incorporating MWCNTs in the specimens shows good bolt torque efficiency at higher water temperature (65^{o}C), upto 91% after hygrothermal aging of 30 days.

The accelerated aging, shows an impact on the properties of EB cured composite bolted joints. On aging for 250 h, the EB cured neat composite specimen shows a slight increase in tensile, compressive and shear strength by 2.8%, 2.4% and 4.3%, respectively. Correspondingly, EB cured, MWCNTs added composite specimens shows improvement by 4%, 3.4% and 5.2%, respectively, as compared to unaged specimens. After 250 h, the mechanical properties get reduced and after aging for 1000 h, the tensile, compressive and shear strength retentions for EB cured neat composite specimens are 89%, 82% and 83.5% respectively. Correspondingly, the EB cured MWCNTs added composite specimens show higher strength retention of 94.5%, 93.8% and 93%, respectively.

The chemical structural changes have been detected through FTIR results showing higher peaks in carbonyl region (600 to 1800 cm^{-1}) and hydroxyl region (2800 to 3700 cm^{-1}) for EB cured neat composite specimens as compared to MWCNTs added composite specimens.

The results from the assessment of the performance of bolted joints shows that failure loads of EB cured unaged composite bolted joint specimens for MWCNTs added configurations is 7.14% higher than that in neat configurations. The composite bolted joints are enormously affected by accelerated weathering condition after long exposure time. After 1000 h of aging exposure (at 0 Nm bolt torque), the overall reduction in ultimate failure load is 12.1% for neat joint specimens, whereas in MWCNTs joint specimens the reduction of 5% is noticed after exposure for 1000 h. Bolt torque gave a positive effect on the performance of joints. It is concluded that as compared to aged specimens, the bolt torque effect is more prominent in unaged specimens. But at higher exposure time (1000 h) under accelerated environment, the bolt torque effectiveness for neat configuration gets reduced by 13%. Moreover, incorporating MWCNTs in the specimens shows good bolt torque effectiveness and shows reduction of only 2.19% even after longer exposure time of 1000 h, under similar conditions. Bolt torque efficiency is less affected by the accelerated aging exposures in MWCNTs joints specimens as compared to neat joint specimens.

The progressive damage analysis with characteristic curve method was used to predict the ultimate failure loads of bolted joints exposed to hygrothermal aging and accelerated aging conditions. The numerically predicted results have shown good correlation with the experimental ones.

7.2 Recommendations for future work

The present work can be extended in the following ways:

(a) Other different curing method like microwave curing, UV curing and VARTM can be used for the preparation of composite materials.

(b) Studies can be extended to natural fibers such as jute, cotton, flax and kenaf in place of synthetic fibers.

(c) The durability studies can be performed in other environmental aging conditions.

References

[1] Bilgen S. Structure and environmental impact of global energy consumption. Renewable and Sustainable Energy Reviews. 2014;38:890-902.

[2] Ehsani M, Gao Y, Longo S, Ebrahimi K. Modern electric, hybrid electric and fuel cell vehicles. Boca Raton, USA: CRC Press; 2018.

[3] Sonnenschein R, Gajdosova K, Holly I. FRP composites and their using in the construction of bridges. Procedia Engineering. 2016;161:477-482.

[4] Soutis C. Fibre reinforced composites in aircraft construction. Progress in Aerospace Sciences. 2005;41:143-151.

[5] Pathak H, Burela RG, Singh A, VirSingh I. Thermo-elastic failure simulation of 3-D orthotropic composites by XFEM. AIP Conference Proceedings: AIP Publishing LLC; 2015. p. 360006.

[6] Soutis C. Introduction: Engineering requirements for aerospace composite materials. Polymer Composites in the Aerospace Industry: Elsevier; 2015. p. 1-18.

[7] Pendhari SS, Kant T, Desai YM. Application of polymer composites in civil construction: A general review. Composite Structures. 2008;84:114-124.

[8] Jacob A. Carbon fibre and cars–2013 in review. Reinforced Plastics. 2014;58:18-19.

[9] Rubino F, Nistico A, Tucci F, Carlone P. Marine application of fiber reinforced composites: a review. Journal of Marine Science and Engineering. 2020;8:26.

[10] Selvam JDR, Dinaharan I, Philip SV, Mashinini P. Microstructure and mechanical characterization of in situ synthesized AA6061/(TiB_2+ Al_2O_3) hybrid aluminum matrix composites. Journal of Alloys and Compounds. 2018;740:529-535.

[11] Mallick PK. Fiber-reinforced composites: materials, manufacturing and design: CRC Press; 2007.

[12] Jones RM. Mechanics of composite materials: CRC Press; 1998.

[13] Sen R, Mullins G. Application of FRP composites for underwater piles repair. Composites Part B: Engineering. 2007;38:751-758.

[14] Cao S, Zhis W, Wang X. Tensile properties of CFRP and hybrid FRP composites at elevated temperatures. Journal of Composite Materials. 2009;43:315-330.

[15] Natarajan V, Gangarao HV, Shekar V. Fatigue response of fabric-reinforced polymeric composites. Journal of Composite Materials. 2005;39:1541-1559.

[16] Chohan JS, Boparai KS, Singh R, Hashmi M. Manufacturing techniques and applications of polymer matrix composites: a brief review. Advances in Materials and Processing Technologies. 2020:1-11.

[17] Jiang X, Kolstein H, Bijlaard F, Qiang X. Effects of hygrothermal aging on glass-fibre reinforced polymer laminates and adhesive of FRP composite bridge: Moisture diffusion characteristics. Composites Part A: Applied Science and Manufacturing. 2014;57:49-58.

[18] Ray B. Temperature effect during humid aging on interfaces of glass and carbon fibers reinforced epoxy composites. Journal of Colloid and Interface Science. 2006;298:111-117.

[19] Dao B, Hodgkin J, Krstina J, Mardel J, Tian W. Accelerated aging versus realistic aging in aerospace composite materials. V. The effects of hot/wet aging in a structural epoxy composite. Journal of Applied Polymer Science. 2010;115:901-910.

[20] Ladhari A, Daly HB, Belhadjsalah H, Cole KC, Denault J. Investigation of water absorption in clay-reinforced polypropylene nanocomposites. Polymer Degradation and Stability. 2010;95:429-439.

[21] Pramoda K, Liu T. Effect of moisture on the dynamic mechanical relaxation of polyamide-6/clay nanocomposites. Journal of Polymer Science Part B: Polymer Physics. 2004;42:1823-1830.
[22] Alessi S, Conduruta D, Pitarresi G, Dispenza C, Spadaro G. Hydrothermal ageing of radiation cured epoxy resin-polyether sulfone blends as matrices for structural composites. Polymer Degradation and Stability. 2010;95:677-683.
[23] Kumar BG, Singh RP, Nakamura T . Degradation of carbon fiber-reinforced epoxy composites by ultraviolet radiation and condensation. Journal of Composite Materials. 2002;36:2713-2733.
[24] Nair A, Joseph R. Eco-friendly bio-composites using natural rubber (NR) matrices and natural fiber reinforcements. Chemistry, Manufacture and Applications of Natural Rubber: Elsevier; 2014. p. 249-283.
[25] Agarwal BD, Broutman LJ, Chandrashekhara K. Analysis and performance of fiber composites: John Wiley & Sons; 2006.
[26] Chalmers D. Experience in design and production of FRP marine structures. Marine Structures. 1991;4:93-115.
[27] Chung DD, Chung D. Carbon fiber composites: Elsevier; 2012.
[28] Singh TJ, Samanta S. Characterization of kevlar fiber and its composites: A review. Materials Today: Proceedings. 2015;2:1381-1387.
[29] Tang LG, Kardos JL. A review of methods for improving the interfacial adhesion between carbon fiber and polymer matrix. Polymer Composites. 1997;18:100-113.
[30] Ebewele RO. Polymer science and technology: CRC press; 2000.
[31] Dang ZM, Yuan JK, Zha JW, Zhou T, Li ST, Hu GH. Fundamentals, processes and applications of high-permittivity polymer–matrix composites. Progress in Materials Science. 2012;57:660-723.
[32] Brandrup J, Immergut EH, Grulke EA, Abe A, Bloch DR. Polymer handbook: Wiley New York; 1999.
[33] Chung DD. Carbon composites: composites with carbon fibers, nanofibers and nanotubes: Butterworth-Heinemann; 2016.
[34] Boisse P. Advances in composites manufacturing and process design: Woodhead Publishing; 2015.
[35] Balasubramanian K, Sultan MT, Rajeswari N. Manufacturing techniques of composites for aerospace applications. Sustainable Composites for Aerospace Applications: Elsevier; 2018. p. 55-67.
[36] Elkington M, Bloom D, Ward C, Chatzimichali A, Potter K. Hand layup: understanding the manual process. Advanced Manufacturing: Polymer & Composites Science. 2015;1:138-151.
[37] Abliz D, Duan Y, Steuernagel L, Xie L, Li D, Ziegmann G. Curing methods for advanced polymer composites-a review. Polymers and Polymer Composites. 2013;21:341-348.
[38] Howell JR, Menguc MP, Siegel R. Thermal radiation heat transfer: CRC Press; 2010.
[39] Mitschang P. Manufacturing of thermoplastic fiber-reinforced polymer composites. Wiley Encyclopedia of Composites. 2011:1-15.
[40] Mezeix L, Seman A, Nasir M, Aminanda Y, Rivai A, Castanie B, Olivier P, Ali KM. Spring-back simulation of unidirectional carbon/epoxy flat laminate composite manufactured through autoclave process. Composite Structures. 2015;124:196-205.
[41] Spadaro G, Alessi S, Dispenza C, Sabatino MA, Pitarresi G, Tumino D, Przbytniak G. Radiation curing of carbon fibre composites. Radiation Physics and Chemistry. 2014;94:14-17.

[42] Singh A, Saunders CB, Barnard JW, Lopata VJ, Kremers W, McDougall TE, Chung M, Tateishi M. Electron processing of fibre-reinforced advanced composites. Radiation Physics and Chemistry. 1996;48:153-170.
[43] Weeton JW, Thomas KL, Peters DM. Engineers guide to composite materials. American Society of Metals; 1987.
[44] Saunders CB, Lopata V, Kremers W, McDougall T, Tateishi M, Singh A. Electron curing of fiber-reinforced composites; recent developments. Advanced Materials: Performance Through Technology Insertion. 1993;38:1681-1691.
[45] Beziers D, Perilleux P, Grenie Y. Composite structures obtained by ionization curing. Radiation Physics and Chemistry. 1996;48:171-177.
[46] Chappas WJ, Devney BG, Olding RP, McLaughlin WL. EB curing of maritime composite structures. Radiation Physics and Chemistry. 1999;56:417-427.
[47] Lopata VJ, Saunders CB, Singh A, Janke CJ, Wrenn GE, Havens SJ. Electron-beam-curable epoxy resins for the manufacture of high-performance composites. Radiation Physics and Chemistry. 1999;56:405-415.
[48] Weeton JW, Thomas KL, Peters DM. Engineers guide to composite materials. American Society of Metals, Metals Park, OH. 1987.
[49] Iverson SL, Saunders CB, McDougall TE, Kremers W, Lopata VJ, Singh A, Kerluke D. Radiation curable composites: environmental advantages. International Symposium on Applications of Isotopes and Radiation in Conservation of the Environment, Karlsruhe, Germany. 1992.
[50] Koo JH. Polymer nanocomposites: McGraw-Hill Professional Publications.; 2006.
[51] Kornmann X, Rees M, Thomann Y, Necola A, Barbezat M, Thomann R. Epoxy-layered silicate nanocomposites as matrix in glass fibre-reinforced composites. Composites Science and Technology. 2005;65:2259–2268.
[52] Haque A, Shamsuzzoha M, Hussain F, Dean D. S_2-glass/epoxy polymer nanocomposites: manufacturing, structures, thermal and mechanical properties. Journal of Composite Materials. 2003;37:1821–1837.
[53] Quaresimin M, Varley RJ. Understanding the effect of nano-modifier addition upon the properties of fibre reinforced laminates. Composites Science and Technology. 2008;68:718–726.
[54] Xu Y, Hoa SV. Mechanical properties of carbon fiber reinforced epoxy/clay nanocomposites. Composites Science and Technology. 2008;68:854–861.
[55] Karthikeyan S, Vijayaraghavan L, Madhavan S, Almeida A. Study on the mechanical properties of heat-treated electroless NiP coatings reinforced with Al_2O_3 nano particles. Metallurgical and Materials Transactions A. 2016;47:2223-2231.
[56] Afkham Y, Khosroshahi RA, Rahimpour S, Aavani C, Brabazon D, Mousavian RT. Enhanced mechanical properties of in situ aluminium matrix composites reinforced by alumina nanoparticles. Archives of Civil and Mechanical Engineering. 2018;18:215-226.
[57] Rathore DK, Prusty RK, Kumar DS, Ray BC. Mechanical performance of CNT-filled glass fiber/epoxy composite in in-situ elevated temperature environments emphasizing the role of CNT content. Composites Part A: Applied Science and Manufacturing. 2016;84:364-376.
[58] Njuguna J, Pielichowski K, Desai S. Nanofiller-reinforced polymer nanocomposites. Polymers for Advanced Technologies. 2008;19:947-959.
[59] Su DH. Application of fiber reinforced composites for sports instruments. Applied Mechanics and Materials: Trans Tech Publ; 2014. p. 4256-4259.

[60] Thoppul SD, Finegan J, Gibson RF. Mechanics of mechanically fastened joints in polymer–matrix composite structures–a review. Composites Science and Technology. 2009;69:301-329.
[61] Ducept F, Davies P, Gamby D. Mixed mode failure criteria for a glass/epoxy composite and an adhesively bonded composite/composite joint. International Journal of Adhesion and Adhesives. 2000;20:233-244.
[62] Choi JH, Ban CS, Kweon JH. Failure load prediction of a mechanically fastened composite joint subjected to a clamping force. Journal of Composite Materials. 2008;42:1415-1429.
[63] Irisarri FX, Laurin F, Carrere N, Maire JF. Progressive damage and failure of mechanically fastened joints in CFRP laminates–Part I: Refined Finite Element modelling of single-fastener joints. Composite Structures. 2012;94:2269–2277.
[64] Asgari MF. Experimental and numerical failure analysis of adhesive composite joints. International Journal of Aerospace Engineering. 2012;2012:1–10.
[65] Ahn HS, Kweon JH, Choi JH. Failure of unidirectional-woven composite laminated pin-loaded joints. Journal of Reinforced Plastics and Composites. 2005;24:735-752.
[66] Atas C. Bearing strength of pinned joints in woven fabric composites with small weaving angles. Composite Structures. 2009;88:40-45.
[67] Wang HS, Hung CL, Chang FK. Bearing failure of bolted composite joints. Part I: experimental characterization. Journal of Composite Materials. 1996;30:1284-1313.
[68] Pisano AA, Fuschi P, De Domenico D. A layered limit analysis of pinned-joints composite laminates: Numerical versus experimental findings. Composites Part B: Engineering. 2012;43:940–952.
[69] Aktas A. Failure analysis of serial pinned joints in composite materials. 2011.
[70] Abdullah M, Abdullah A, Hassan M, Samad Z. Bearing strength and progressive failure analysis of the punched hole of CFRP under tensile loading. The International Journal of Advanced Manufacturing Technology. 2018;97:2163-2171.
[71] Aktas A, Husnu DM. An experimental and numerical investigation of strength characteristics of carbon-epoxy pinned-joint plates. Composites Science and Technology. 2004;64:1605-1611.
[72] Tian W, Hodgkin J. Long-term aging in a commercial aerospace composite sample: Chemical and physical changes. Journal of Applied Polymer Science. 2010;115:2981-2985.
[73] Dao B, Hodgkin J, Krstina J, Mardel J, Tian W. Accelerated ageing versus realistic ageing in aerospace composite materials. IV. Hot/wet ageing effects in a low temperature cure epoxy composite. Journal of Applied Polymer Science. 2007;106:4264-4276.
[74] Kishi H, Shi YB, Huang J, Yee AF. Shear ductility and toughenability study of highly cross-linked epoxy/polyethersulphone. Journal of Materials Science. 1997;32:761-771.
[75] Swier S, Van Mele B. Reaction-induced phase separation in polyethersulfone-modified epoxy-amine systems studied by temperature modulated differential scanning calorimetry. Thermochimica Acta. 1999;330:175-187.
[76] Berejka AJ, Cleland M, Galloway R, Gregoire O. X-ray curing of composite materials. Nuclear Instruments and Methods in Physics Research Section B: Beam Interactions with Materials and Atoms. 2005;241:847-849.
[77] Endruweit A, Ruijter W, Johnson MS, Long AC. Transmission of ultraviolet light through reinforcement fabrics and its effect on ultraviolet curing of composite laminates. Polymer Composites. 2008;29:818-829.

[78] Nishitsuji D, Marinucci G, Evora M, Silva L. Cationic concentration effects on electron beam cured of carbon-epoxy composites. Radiation Physics and Chemistry. 2010;79:306-309.
[79] Saunders C, Lopata V, Kremers W, Chung M, Singh A, Kerluke D. Electron curing of fibre-reinforced composites: an industrial application for high-energy accelerators. Radiation Physics and Chemistry. 1995;46:991-994.
[80] Ahad IU, Budner B, Korczyc B, Fiedorowicz H, Bartnik A, Kostecki J, Burdynska S, Brabazon D. Polycarbonate polymer surface modication by extreme ultraviolet (EUV) radiation. Acta Physica Polonica A. 2014;125:924-928.
[81] Castro AS, Kim RY, Rice BP. Electron beam cure of composites for aerospace structures. Evolving Technologies for the Competitive Edge. 1997;42:487-497.
[82] Parrot P, His S, Boursereau F. Improved epoxy resins cured by electron beam irradiation. 44th International SAMPE Symposium. 1999;44:1254.
[83] Abrams F, Tolle TB. An analysis of E-beam potential in aerospace composite manufacturing. Evolving Technologies for the Competitive Edge. 1997;42:548-557.
[84] Glauser T, Johansson M, Hult A. A comparison of radiation and thermal curing of thick composites. Macromolecular Materials and Engineering. 2000;274:25-30.
[85] Sui G, Zhang ZG, Chen CQ, Zhong WH. Analyses on curing process of electron beam radiation in epoxy resins. Materials Chemistry and Physics. 2003;78:349-357.
[86] Crivello JV, Walton TC, Malik R. Fabrication of epoxy matrix composites by electron beam induced cationic polymerization. Chemistry of Materials. 1997;9:1273-1284.
[87] Janke CJ, Norris RE, Yarborough K, Havens SJ, Lopata VJ. Critical parameters for electron beam curing of cationic epoxies and property comparison of electron beam cured cationic epoxies versus thermal cured resins and composites. Oak Ridge National Lab., TN (United States); 1997.
[88] Singh A. Radiation processing of carbon fibre-reinforced advanced composites. Nuclear Instruments and Methods in Physics Research Section B: Beam Interactions with Materials and Atoms. 2001;185:50-54.
[89] Berejka AJ, Eberle C. Electron beam curing of composites in North America. Radiation Physics and Chemistry. 2002;63:551-556.
[90] Janke C, Wheeler D, Saunders C. Electron beam curing of polymer matrix composites. Oak Ridge Y-12 Plant, TN (United States); 1998.
[91] Norris RE, Schulz MD. Selection of materials to be utilized in fabrication tooling for electron-beam curing of composites. Society for the Advancement of Material and Process Engineering. 1996:890-900.
[92] Janke C. A cooperative R&D program on interfacial properties of electron beam cured composites. 3 Electron Beam Curing of Composites Workshop Proceedings (c/o Dave Howell, ORNL, orcmtcmt@ mailhub ornl gov); 1999.
[93] Glauser T, Johansson M, Hult A. Electron-beam curing of thick thermoset composites: Effect of temperature and fiber. Macromolecular Materials and Engineering. 2000;274:20-24.
[94] Zhang Z, Liu Y, Huang Y, Liu L, Bao J. The effect of carbon-fiber surface properties on the electron-beam curing of epoxy-resin composites. Composites Science and Technology. 2002;62:331-337.
[95] Nishi Y, Mizutani A, Uchida N. Electron beam strengthening for carbon fiber-reinforced composite materials. Journal of Thermoplastic Composite Materials. 2004;17:289-302.
[96] Cleland MR. Electron beam materials irradiators. Industrial Accelerators And Their Applications. World Scientific; 2012. p. 87-137.

[97] Vautard F, Fioux P, Vidal L, Dentzer J, Schultz J, Nardin M, Defoort B. Influence of an oxidation of the carbon fiber surface by boiling nitric acid on the adhesion strength in carbon fiber-acrylate composites cured by electron beam. Surface and Interface Analysis. 2013;45:722-741.
[98] Zsigmond B, Halasz L, Czvikovszky T. Electron beam processing of carbon fibre reinforced braided composites. Radiation Physics and Chemistry. 2003;67:441-445.
[99] Crivello JV. UV and electron beam-induced cationic polymerization. Nuclear Instruments and Methods in Physics Research Section B: Beam Interactions with Materials and Atoms. 1999;151:8-21.
[100] Sui G, Zhong WH, Yang XP. The revival of electron beam irradiation curing of epoxy resin materials characterization and supportive cure studies. Polymers for Advanced Technologies. 2009;20:811-817.
[101] Nishitsuji DA, Marinucci G, Evora MC, e Silva LGDA. Study of electron beam curing process using epoxy resin system. Nuclear Instruments and Methods in Physics Research Section B: Beam Interactions with Materials and Atoms. 2007;265:135-138.
[102] Sui G, Zhang ZG, Liang ZY, Chen CQ. Dynamic mechanical studies on epoxy resins cured by electron beam radiation. Materials Science and Engineering: A. 2003;342:28-37.
[103] Raghavan J. Evolution of cure, mechanical properties and residual stress during electron beam curing of a polymer composite. Composites Part A: Applied Science and Manufacturing. 2009;40:300-308.
[104] Pitarresi G, Alessi S, Tumino D, Nowicki A, Spadaro G. Interlaminar fracture toughness behavior of electron-beam cured carbon-fiber reinforced epoxy–resin composites. Polymer Composites. 2014;35:1529-1542.
[105] Vautard F, Fioux P, Vidal L, Schultz J, Nardin M, Defoort B. Influence of the carbon fiber surface properties on interfacial adhesion in carbon fiber–acrylate composites cured by electron beam. Composites Part A: Applied Science and Manufacturing. 2011;42:859-867.
[106] Raghavan J, Baillie MR. Electron beam curing of polymer composites. Polymer Composites. 2000;21:619-629.
[107] Alessi S, Dispenza C, Fuochi P, Corda U, Lavalle M, Spadaro G. E-beam curing of epoxy-based blends in order to produce high-performance composites. Radiation Physics and Chemistry. 2007;76:1308-1311.
[108] Alessi S, Dispenza C, Spadaro G. Thermal properties of E-beam cured epoxy/thermoplastic matrices for advanced composite materials. Macromolecular Symposia: Wiley Online Library; 2007. p. 238-243.
[109] Quinn W, Matthews F. The effect of stacking sequence on the pin-bearing strength in glass fibre reinforced plastic. Journal of Composite Materials. 1977;11:139-145.
[110] Okutan B, Karakuzu R. The strength of pinned joints in laminated composites. Composites Science and Technology. 2003;63:893-905.
[111] VirSingh I, Shedbale A, Mishra B. Material property evaluation of particle reinforced composites using finite element approach. Journal of Composite Materials. 2016;50:2757-2771.
[112] Aluko O. An analytical method for failure prediction of composite pinned joints. Proceedings of the World Congress on Engineering. 2011. p. 978–988.
[113] Irisarri F-, Laurin F, Carrere N, Maire JF. Progressive damage and failure of mechanically fastened joints in CFRP laminates–Part I: Refined finite element modelling of single-fastener joints. Composite Structures. 2012;94:2269-2277.

[114] Turan K, Gur M, Kaman MO. Progressive failure analysis of pin-loaded unidirectional carbon-epoxy laminated composites. Mechanics of Advanced Materials and Structures. 2014;21:98-106.
[115] Olmedo A, Santiuste C, Barbero E. An analytical model for predicting the stiffness and strength of pinned-joint composite laminates. Composites Science and Technology. 2014;90:67-73.
[116] Bakhshan H, Afrouzian A, Ahmadi H, Taghavimehr M. Progressive failure analysis of fiber-reinforced laminated composites containing a hole. International Journal of Damage Mechanics. 2018;27:963-978.
[117] Khashaba U, Sebaey T, Selmy A. Experimental verification of a progressive damage model for composite pinned-joints with different clearances. International Journal of Mechanical Sciences. 2019;152:481-491.
[118] Karakuzu R, Gülem T, İçten BM. Failure analysis of woven laminated glass–vinylester composites with pin-loaded hole. Composite Structures. 2006;72:27-32.
[119] Karakuzu R, Caliskan CR, Aktas M, Icten BM. Failure behavior of laminated composite plates with two serial pin-loaded holes. Composite Structures. 2008;82:225-234.
[120] Karakuzu R, Taylak N, Icten BM, Aktas M. Effects of geometric parameters on failure behavior in laminated composite plates with two parallel pin-loaded holes. Composite Structures. 2008;85:1-9.
[121] Aktas A, İmrek H, Cunedioğlu Y. Experimental and numerical failure analysis of pinned-joints in composite materials. Composite Structures. 2009;89:459-466.
[122] Pisano A, Fuschi P, De Domenico D. Failure modes prediction of multi-pin joints FRP laminates by limit analysis. Composites Part B: Engineering. 2013;46:197-206.
[123] Sen F, Pakdil M, Sayman O, Benli S. Experimental failure analysis of mechanically fastened joints with clearance in composite laminates under preload. Materials & Design. 2008;29:1159-1169.
[124] Othman A, Jadee KJ. Specific bearing strength of bolted composite joint with different glass fiber reinforcement. ARPN Journal of Engineering and Applied Science. 2016;11:12039-12044.
[125] Giannopoulos IK, Doroni DD, Kourousis KI, Yasaee M. Effects of bolt torque tightening on the strength and fatigue life of airframe FRP laminate bolted joints. Composites Part B: Engineering. 2017;125:19-26.
[126] Choi JI, Hasheminia SM, Chun H-J, Park JC, Chang HS. Failure load prediction of composite bolted joint with clamping force. Composite Structures. 2018;189:247-255.
[127] Mandal B, Chakrabarti A. Numerical failure assessment of multi-bolt FRP composite joints with varying sizes and preloads of bolts. Composite Structures. 2018;187:169-178.
[128] Murthy AV, Dattaguru B, Narayana H, Rao A. Stress and strength analysis of pin joints in laminated anisotropic plates. Composite Structures. 1991;19:299-312.
[129] Zhai Y, Li D, Li X, Wang L, Yin Y. An experimental study on the effect of bolt-hole clearance and bolt torque on single-lap, countersunk composite joints. Composite Structures. 2015;127:411-419.
[130] Khashaba U, Sallam H, Al-Shorbagy A, Seif M. Effect of washer size and tightening torque on the performance of bolted joints in composite structures. Composite Structures. 2006;73:310-317.
[131] Kim SY, Kim D. Interference-fit effect on improving bearing strength and fatigue life in a pin-loaded woven carbon fiber-reinforced plastic laminate. Journal of Engineering Materials and Technology. 2019;141:021006.

[132] Nilsson S. Increasing strength of graphite/epoxy bolted joints by introducing an adhesively bonded metallic insert. Journal of Composite Materials. 1989;23:642-650.
[133] Mara V, Haghani R, Al-Emrani M. Improving the performance of bolted joints in composite structures using metal inserts. Journal of Composite Materials. 2016;50:3001-3118.
[134] Singh K, Saini J, Bhunia H. Effect of metallic inserts on the strength of pin joints prepared from glass fiber reinforced composites. Defence Science Journal. 2017;67:592-600.
[135] Bagotia N, Choudhary V, Sharma D. Synergistic effect of graphene/multiwalled carbon nanotube hybrid fillers on mechanical, electrical and EMI shielding properties of polycarbonate/ethylene methyl acrylate nanocomposites. Composites Part B: Engineering. 2019;159:378-388.
[136] Panwar A, Choudhary V, Sharma D. A review: polystyrene/clay nanocomposites. Journal of Reinforced Plastics and Composites. 2011;30:446-459.
[137] Choudhary V, Gupta A. Polymer/carbon nanotube nanocomposites. Carbon Nanotubes-Polymer Nanocomposites. 2011;2011:65-90.
[138] Kiran R, Kumar A, Chauhan VS, Kumar R, Vaish R. Engineered carbon nanotubes reinforced polymer composites for enhanced thermoelectric performance. Materials Research Express. 2017;4:105002.
[139] Aly M, Hashmi M, Olabi A, Messeiry M, Hussain A, Abadir E. Effect of nano-clay and waste glass powder on the properties of flax fibre reinforced mortar. Journal of Engineering and Applied Science. 2011;6:19-28.
[140] Asi O. An experimental study on the bearing strength behavior of Al_2O_3 particle filled glass fiber reinforced epoxy composites pinned joints. Composite Structures. 2010;92:354-363.
[141] Singh M, Saini J, Bhunia H. Investigation on failure modes for pin joints made from unidirectional glass–epoxy nanoclay laminates. Fatigue & Fracture of Engineering Materials & Structures. 2016;39:320-334.
[142] Sekhon M, Saini J, Singla G, Bhunia H. Influence of nanoparticle fillers content on the bearing strength behavior of glass fiber-reinforced epoxy composites pin joints. Proceedings of the Institution of Mechanical Engineers, Part L: Journal of Materials: Design and Applications. 2017;231:641-656.
[143] Singh M, Bhunia H, Saini JS. Effect of ply orientation on strength and failure mode of pin jointed unidirectional glass-epoxy nanoclay laminates. Defence Science Journal. 2015;65:489-499.
[144] Tüzemen MC, Salamcı E, Avci A. Enhancing mechanical properties of bolted carbon/epoxy nanocomposites with carbon nanotube, nanoclay and hybrid loading. Composites Part B: Engineering. 2017;128:146-154.
[145] Shuaeib F, Benyounis K, Hashmi M. Material behavior and performance in Environments of extreme pressure and temperatures. 2017.
[146] Aly M, Hashmi M, Olabi A, Messeiry M. Durability of waste glass flax fiber reinforced mortar. AIP Conference Proceedings: American Institute of Physics; 2011. p. 241-246.
[147] Boer P, Holliday L, Kang THK. Independent environmental effects on durability of fiber-reinforced polymer wraps in civil applications: a review. Construction and Building Materials. 2013;48:360-370.
[148] Sciolti MS, Frigione M, Aiello MA. Wet lay-up manufactured FRPs for concrete and masonry repair: influence of water on the properties of composites and on their epoxy components. Journal of Composites for Construction. 2010;14:823-833.

[149] Bazli M, Ashrafi H, Oskouei AV. Experiments and probabilistic models of bond strength between GFRP bar and different types of concrete under aggressive environments. Construction and Building Materials. 2017;148:429-443.
[150] Gonon P, Sylvestre A, Teysseyre J, Prior C. Combined effects of humidity and thermal stress on the dielectric properties of epoxy-silica composites. Materials Science and Engineering: B. 2001;83:158-164.
[151] Maggana C, Pissis P. Water sorption and diffusion studies in an epoxy resin system. Journal of Polymer Science Part B: Polymer Physics. 1999;37:1165-1182.
[152] De'Nève B, Shanahan M. Water absorption by an epoxy resin and its effect on the mechanical properties and infra-red spectra. Polymer. 1993;34:5099-5105.
[153] Zheng Q, Morgan R. Synergistic thermal-moisture damage mechanisms of epoxies and their carbon fiber composites. Journal of Composite Materials. 1993;27:1465-1478.
[154] Alessi S, Pitarresi G, Spadaro G. Effect of hydrothermal ageing on the thermal and delamination fracture behaviour of CFRP composites. Composites Part B: Engineering. 2014;67:145-153.
[155] Hong B, Xian G, Wang Z. Durability study of pultruded carbon fiber reinforced polymer plates subjected to water immersion. Advances in Structural Engineering. 2018;21:571-579.
[156] Xin H, Liu Y, Mosallam A, Zhang Y, Wang C. Hygrothermal aging effects on flexural behavior of pultruded glass fiber reinforced polymer laminates in bridge applications. Construction and Building Materials. 2016;127:237-247.
[157] Chow W, Abu BA, Mohd IZ. Water absorption and hygrothermal aging study on organomontmorillonite reinforced polyamide 6/polypropylene nanocomposites. Journal of Applied Polymer Science. 2005;98:780-790.
[158] Firdosh S, Murthy HN, Pal R, Angadi G, Raghavendra N, Krishna M. Durability of GFRP nanocomposites subjected to hygrothermal ageing. Composites Part B: Engineering. 2015;69:443-451.
[159] Glaskova T, Aniskevich A. Moisture absorption by epoxy/montmorillonite nanocomposite. Composites Science and Technology. 2009;69:2711-2715.
[160] Nayak RK, Mahato KK, Ray BC. Water absorption behavior, mechanical and thermal properties of nano TiO_2 enhanced glass fiber reinforced polymer composites. Composites Part A: Applied Science and Manufacturing. 2016;90:736-747.
[161] Prusty RK, Rathore DK, Ray BC. Water-induced degradations in MWCNT embedded glass fiber/epoxy composites: An emphasis on aging temperature. Journal of Applied Polymer Science. 2018;135:45987.
[162] Rubio-González C, José-Trujillo E, Rodríguez-González JA, Mornas A, Talha A. Low-velocity impact behavior of glass fiber-MWCNT/polymer laminates exposed to seawater and distilled water aging. Polymer Composites. 2020;41:2181-2197.
[163] Lee JH, Rhee KY, Lee JH. Effects of moisture absorption and surface modification using 3-aminopropyltriethoxysilane on the tensile and fracture characteristics of MWCNT/epoxy nanocomposites. Applied Surface Science. 2010;256:7658–7667.
[164] Shokrieh MM, Bayat A. Effects of ultraviolet radiation on mechanical properties of glass/polyester composites. Journal of Composite Materials. 2007;41:2443-2455.
[165] Cabral FS, Correia J, Rodrigues M, Branco F. Artificial accelerated ageing of GFRP pultruded profiles made of polyester and vinylester resins: characterisation of physical–chemical and mechanical damage. Strain. 2012;48:162-173.
[166] Roy P, Surekha P, Rajagopal C, Chatterjee S, Choudhary V. Accelerated aging of LDPE films containing cobalt complexes as prooxidants. Polymer Degradation and Stability. 2006;91:1791-1799.

[167] Bazli M, Ashrafi H, Jafari A, Zhao XL, Gholipour H, Oskouei AV. Effect of thickness and reinforcement configuration on flexural and impact behaviour of GFRP laminates after exposure to elevated temperatures. Composites Part B: Engineering. 2019;157:76-99.
[168] Mouzakis DE, Zoga H, Galiotis C. Accelerated environmental ageing study of polyester/glass fiber reinforced composites (GFRPCs). Composites Part B: Engineering. 2008;39:467-475.
[169] Stewart A, Douglas EP. Accelerated testing of epoxy-FRP composites for civil infrastructure applications: property changes and mechanisms of degradation. Polymer Reviews. 2012;52:115-141.
[170] Yan L, Chouw N, Jayaraman K. Effect of UV and water spraying on the mechanical properties of flax fabric reinforced polymer composites used for civil engineering applications. Materials & Design. 2015;71:17-25.
[171] Batista NL, de Faria MCM, Iha K, de Oliveira PC, Botelho EC. Influence of water immersion and ultraviolet weathering on mechanical and viscoelastic properties of polyphenylene sulfide-carbon fiber composites. Journal of Thermoplastic Composite Materials. 2015;28:340-356.
[172] Nicholas J, Mohamed M, Dhaliwal G, Anandan S, Chandrashekhara K. Effects of accelerated environmental aging on glass fiber reinforced thermoset polyurethane composites. Composites Part B: Engineering. 2016;94:370-378.
[173] Barbosa AP, Fulco AP, Guerra ES, Arakaki FK, Tosatto M, Costa MC, Melo JD. Accelerated aging effects on carbon fiber/epoxy composites. Composites Part B: Engineering. 2017;110:298-306.
[174] Panaitescu I, Koch T, Archodoulaki VM. Accelerated aging of a glass fiber/polyurethane composite for automotive applications. Polymer Testing. 2019;74:245-256.
[175] Bazli M, Jafari A, Ashrafi H, Zhao X-L, Bai Y, Raman RS. Effects of UV radiation, moisture and elevated temperature on mechanical properties of GFRP pultruded profiles. Construction and Building Materials. 2020;231:117137.
[176] Woo RS, Chen Y, Zhu H, Li J, Kim JK, Leung CK. Environmental degradation of epoxy–organoclay nanocomposites due to UV exposure. part I: Photo-degradation. Composites Science and Technology. 2007;67:3448-3456.
[177] Woo RS, Zhu H, Leung CK, Kim JK. Environmental degradation of epoxy-organoclay nanocomposites due to UV exposure: part II residual mechanical properties. Composites Science and Technology. 2008;68:2149-2155.
[178] Chang L, Chow W. Accelerated weathering on glass fiber/epoxy/organo-montmorillonite nanocomposites. Journal of Composite Materials. 2010;44:1421-1434.
[179] Chiang CL, Chou HY, Shen MY. Effect of environmental aging on mechanical properties of graphene nanoplatelet/nanocarbon aerogel hybrid-reinforced epoxy/carbon fiber composite laminates. Composites Part A: Applied Science and Manufacturing. 2020;130:105718.
[180] Awad SA, Fellows CM, Mahini SS. Effects of accelerated weathering on the chemical, mechanical, thermal and morphological properties of an epoxy/multi-walled carbon nanotube composite. Polymer Testing. 2018;66:70-77.
[181] Zhang J, Rowland J. Damage modeling of carbon-fiber reinforced polymer composite pin-joints at extreme temperatures. Composite Structures. 2012;94:2314-2325.

[182] Soykok IF, Sayman O, Ozen M, Korkmaz B. Failure analysis of mechanically fastened glass fiber/epoxy composite joints under thermal effects. Composites Part B: Engineering. 2013;45:192-199.
[183] Soykok IF, Sayman O, Pasinli A. Effects of hot water aging on failure behavior of mechanically fastened glass fiber/epoxy composite joints. Composites Part B: Engineering. 2013;54:59-70.
[184] Jojibabu P, Ram GJ, Deshpande AP, Bakshi SR. Effect of carbon nano-filler addition on the degradation of epoxy adhesive joints subjected to hygrothermal aging. Polymer Degradation and Stability. 2017;140:84-94.
[185] Fang H, Bai Y, Liu W, Qi Y, Wang J. Connections and structural applications of fibre reinforced polymer composites for civil infrastructure in aggressive environments. Composites Part B: Engineering. 2019;164:129-143.
[186] Soutis C. Carbon fiber reinforced plastics in aircraft construction. Materials Science and Engineering: A. 2005;412:171-176.
[187] Godara A, Mezzo L, Luizi F, Warrier A, Lomov SV, Van Vuure AW, Gorbatikh L, Moldenaers P, Verpoest I. Influence of carbon nanotube reinforcement on the processing and the mechanical behaviour of carbon fiber/epoxy composites. Carbon. 2009;47:2914-2923.
[188] Sun G, Liu Z, Chen G. Dispersion of pristine multi-walled carbon nanotubes in common organic solvents. Nano. 2010;5:103-109.
[189] Lopresto V, Langella A, Papa I. Interaction of water with carbon fiber reinforced polymer laminates under dynamic loading conditions. Journal of Materials Engineering and Performance. 2019;28:3220-3227.
[190] Panda BP, Mohanty S, Nayak SK. Polyolefin nanocomposites with enhanced photostability weathering effect on morphology and mechanical properties. Journal of Materials Engineering and Performance. 2014;23:3229-3244.
[191] Javier C, Smith T, LeBlanc J, Shukla A. Effect of prolonged ultraviolet radiation exposure on the blast response of fiber reinforced composite plates. Journal of Materials Engineering and Performance. 2019;28:3174-3185.
[192] Tsuda T, Ogasawara T, Deng F, Takeda N. Direct measurements of interfacial shear strength of multi-walled carbon nanotube/PEEK composite using a nano-pullout method. Composites Science and Technology. 2011;71:1295-1300.
[193] Hashin Z. Analysis of composite materials-a survey. 1983.
[194] Lessard LB, Shokrieh MM. Two-dimensional modeling of composite pinned-joint failure. Journal of Composite Materials. 1995;29:671-697.
[195] Dano ML, Gendron G, Picard A. Stress and failure analysis of mechanically fastened joints in composite laminates. Composite Structures. 2000;50:287-296.
[196] Camanho P, Bowron S, Matthews F. Failure mechanisms in bolted CFRP. Journal of Reinforced Plastics and Composites. 1998;17:205-233.
[197] Bal S, Saha S. Mechanical performances of hygrothermally conditioned CNT/epoxy composites using seawater. Journal of Polymer Engineering. 2017;37:633-645.
[198] Grammatikos SA, Evernden M, Mitchels J, Zafari B, Mottram JT, Papanicolaou GC. On the response to hygrothermal aging of pultruded FRPs used in the civil engineering sector. Materials & Design. 2016;96:283-295.
[199] Nayak RK, Ray BC. Influence of seawater absorption on retention of mechanical properties of nano-TiO_2 embedded glass fiber reinforced epoxy polymer matrix composites. Archives of Civil and Mechanical Engineering. 2018;18:1597-1607.
[200] Wang M, Xu X, Ji J, Yang Y, Shen J, Ye M. The hygrothermal aging process and mechanism of the novolac epoxy resin. Composites Part B: Engineering. 2016;107:1-8.

[201] Park SY, Choi WJ, Choi CH, Choi HS. An experimental study into aging unidirectional carbon fiber epoxy composite under thermal cycling and moisture absorption. Composite Structures. 2019;207:81-92.
[202] Ramirez FA, Carlsson LA. Modified single fiber fragmentation test procedure to study water degradation of the fiber/matrix interface toughness of glass/vinylester. Journal of Materials Science. 2009;44:3035-3042.
[203] Rao R, Balasubramanian N, Chanda M. Factors affecting moisture absorption in polymer composites part I: Influence of internal factors. Journal of Reinforced Plastics and Composites. 1984;3:232-245.
[204] Awaja F, Moon JB, Gilbert M, Zhang S, Kim CG, Pigram PJ. Surface molecular degradation of selected high performance polymer composites under low earth orbit environmental conditions. Polymer Degradation and Stability. 2011;96:1301-1309.
[205] Shimokawa T, Katoh H, Hamaguchi Y, Sanbongi S, Mizuno H, Nakamura H, Asagumo R, Tamura H. Effect of thermal cycling on microcracking and strength degradation of high-temperature polymer composite materials for use in next-generation SST structures. Journal of Composite Materials. 2002;36:885-895.
[206] Chow W, Teoh J, Lim L. Mechanical and hygrothermal aging study on polystyrene/organo-montmorillonite nanocomposites. Polymer-Plastics Technology and Engineering. 2008;47:1040-1045.
[207] Alkhatib M, Mamun A, Akbar I. Application of response surface methodology (RSM) for optimization of color removal from POME by granular activated carbon. International Journal of Environmental Science and Technology. 2015;12:1295-1302.
[208] Myers RH, Montgomery DC anderson-Cook CM. Response surface methodology: process and product optimization using designed experiments: John Wiley & Sons; 2016.
[209] Costa ML, Almeida SFMD, Rezende MC. Hygrothermal effects on dynamic mechanical snalysis and fracture behavior of polymeric composites. Materials Research. 2005;8:335-340.
[210] Zulfli NM, Bakar AA, Chow W. Mechanical and water absorption behaviors of carbon nanotube reinforced epoxy/glass fiber laminates. Journal of Reinforced Plastics and Composites. 2013;32:1715-1721.
[211] Abdel-Magid B, Ziaee S, Gass K, Schneider M. The combined effects of load, moisture and temperature on the properties of E-glass/epoxy composites. Composite Structures. 2005;71:320-326.
[212] Ellyin F, Maser R. Environmental effects on the mechanical properties of glass-fiber epoxy composite tubular specimens. Composites Science and Technology. 2004;64:1863-1874.
[213] Chang FK, Scott RA, Springer GS. Strength of mechanically fastened composite joints. Journal of Composite materials. 1982;16:470-494.
[214] Puglia D, Valentini L, Kenny J. Analysis of the cure reaction of carbon nanotubes/epoxy resin composites through thermal analysis and Raman spectroscopy. Journal of Applied Polymer Science. 2003;88:452-458.
[215] Niu YF, Yang Y, Gao S, Yao JW. Mechanical mapping of the interphase in carbon fiber reinforced poly (ether-ether-ketone) composites using peak force atomic force microscopy: Interphase shrinkage under coupled ultraviolet and hydro-thermal exposure. Polymer Testing. 2016;55:257-260.
[216] de Souza Rios A, de Amorim Junior WF, de Moura EP, de Deus EP, de Andrade Feitosa JP. Effects of accelerated aging on mechanical, thermal and morphological

behavior of polyurethane/epoxy/fiberglass composites. Polymer Testing. 2016;50:152-163.
[217] Kumar A, Commereuc S, Verney V. Ageing of elastomers: a molecular approach based on rheological characterization. Polymer Degradation and Stability. 2004;85:751-757.
[218] Jelle BP, Nilsen TN. Comparison of accelerated climate ageing methods of polymer building materials by attenuated total reflectance Fourier transform infrared radiation spectroscopy. Construction and Building Materials. 2011;25:2122-2132.

List of Publications

Publications from present work in peer reviewed (SCI) journals

1. **Mohit Kumar**, J. S. Saini, H. Bhunia and S. Ray Chowdhury. The effect of radiation curing on mechanical joints prepared from carbon nanotubes added carbon/epoxy laminates. Polymer Composites. 2020:41;4260-4276. **IF- 3.171**
2. **Mohit Kumar**, J. S. Saini, H. Bhunia and S. Ray Chowdhury. Behavior of mechanical joints prepared from EB cured CFRP nanocomposites subjected to hygrothermal aging under bolt preloads. Applied Composite Materials. 2021:28;271-296. **IF- 2.181**
3. **Mohit Kumar**, J. S. Saini and H. Bhunia. Performance of mechanical joints prepared from carbon fiber reinforced polymer nanocomposites under accelerated environmental aging. Journal of Materials Engineering and Performance. 2020:29;7511-7525. **IF- 1.819**
4. **Mohit Kumar**, J. S. Saini and H. Bhunia. Investigations on the strength of mechanical joints prepared from carbon fiber laminates with addition of carbon nanotubes. Journal of Mechanical Science and Technology. 2020:34;1059-1070. **IF- 1.734**
5. **Mohit Kumar**, J.S. Saini and H. Bhunia. Investigations on MWCNT embedded carbon/ epoxy composite joints subjected to hygrothermal aging under bolt preloads. Fibers and Polymers. 2021. **IF- 2.153**
   DOI: https://doi.org/10.1007/s12221-021-0834-z
6. **Mohit Kumar**, J. S. Saini, H. Bhunia and S. Ray Chowdhury. Aging of bolted joints prepared from EB cured MWCNT based nanocomposites with variable torques. Polymer Composites. 2021. **IF- 3.171**
   DOI: https://doi.org/10.1002/pc.26119

Publications under review

1. **Mohit Kumar**, J. S. Saini, H. Bhunia and K. Singh. Comparison of different failure criteria in numerical modelling of polymer composites. Journal of Composite Materials. **IF- 2.591**